

Self-Healing Polymer Composites

Post, Wouter

DOI

[10.4233/uuid:00e46bd1-eef8-4411-8626-fbd902749904](https://doi.org/10.4233/uuid:00e46bd1-eef8-4411-8626-fbd902749904)

Publication date

2017

Document Version

Final published version

Citation (APA)

Post, W. (2017). *Self-Healing Polymer Composites*. [Dissertation (TU Delft), Delft University of Technology]. <https://doi.org/10.4233/uuid:00e46bd1-eef8-4411-8626-fbd902749904>

Important note

To cite this publication, please use the final published version (if applicable).
Please check the document version above.

Copyright

Other than for strictly personal use, it is not permitted to download, forward or distribute the text or part of it, without the consent of the author(s) and/or copyright holder(s), unless the work is under an open content license such as Creative Commons.

Takedown policy

Please contact us and provide details if you believe this document breaches copyrights.
We will remove access to the work immediately and investigate your claim.

Self-Healing Polymer Composites

Proefschrift

ter verkrijging van de graad van doctor
aan de Technische Universiteit Delft,
op gezag van de Rector Magnificus prof. ir. K.C.A.M. Luyben
voorzitter van het College voor Promoties
in het openbaar te verdedigen op vrijdag 24 november 2017 om 12:30 uur

door

Wouter POST

Master of Science in Chemical Engineering
University of Twente
geboren te Heemskerk, Nederland

Dit proefschrift is goedgekeurd door:

Promotor: Prof. dr. ir. S. van der Zwaag

Copromotor: Dr. S.J. García Espallargas

Samenstelling promotiecommissie:

| | |
|--------------------------------|-------------------------------|
| Rector Magnificus | voorzitter |
| Prof. dr. ir. S. van der Zwaag | Technische Universiteit Delft |
| Dr. S.J. García Espallargas | Technische Universiteit Delft |

Onafhankelijke leden:

| | |
|-----------------------------|--|
| Prof. dr. V. Michaud | École Polytechnique Fédérale de Lausanne, Zwitserland |
| Prof. dr. J.P. Dear | Imperial College London, Verenigd Koninkrijk |
| Prof. dr. K. van den Abeele | Katholieke Universiteit Leuven, België |
| Prof. dr. ir. R. Akkerman | Universiteit Twente |
| Prof. dr. ir. R. Benedictus | Technische Universiteit Delft |

Reserve lid:

| | |
|-----------------------------|-------------------------------|
| Prof. dr. ir. K.M.B. Jansen | Technische Universiteit Delft |
|-----------------------------|-------------------------------|

Het onderzoek dat in dit onderzoek wordt beschreven is onderdeel van het EU FP7 programma onder het ALAMSA project en projectnummer 314768.



Gedrukt door: ProefschriftMaken || www.proefschriftmaken.nl

ISBN: 978-94-6295-811-1

Alle rechten voorbehouden. Niets uit deze uitgave mag worden verveelvoudigd, of openbaar gemaakt worden, in enige vorm of op enige wijze, hetzij elektronisch, mechanisch, door printouts, kopieën, of op welke manier dan ook, zonder voorafgaande schriftelijke toestemming van de auteur.

Table of contents

Chapter 1 - Introduction

| | |
|---|---|
| 1.1. Introduction | 2 |
| 1.2. Types of healing in polymer composites | 3 |
| 1.2.1. Extrinsic healing | 3 |
| 1.2.2. Intrinsic healing | 4 |
| 1.3. Characterization of self-healing polymer composites..... | 6 |
| 1.4. Challenges and future prospects | 7 |
| 1.5. Scope and thesis outline..... | 7 |
| References..... | 9 |

Chapter 2 - Self-healing glass fibre-reinforced polymer composites based on montmorillonite reinforced compartmented alginate fibres

| | |
|---|----|
| 2.1. Introduction | 16 |
| 2.2. Materials and Methods..... | 18 |
| 2.2.2. Spinning of compartmented fibres | 18 |
| 2.2.3. Composite production | 19 |
| 2.2.4. Fibre characterization | 20 |
| 2.2.5. Composite characterization and healing | 20 |
| 2.2.5.1. Mechanical characterization..... | 20 |
| 2.2.5.2. Non-destructive healing evaluation | 21 |
| 2.3. Results & Discussion | 22 |
| 2.3.1. Fibre characterization | 22 |
| 2.3.1.1. Fibre tensile properties | 22 |
| 2.3.1.2. Vacuole lateral compression properties | 24 |
| 2.3.2. Composite characterization | 26 |
| 2.3.2.1. Interlaminar fracture properties..... | 26 |

| | |
|------------------------------------|----|
| 2.3.2.2. Flexural properties | 30 |
| 2.4. Conclusion..... | 33 |
| References | 33 |

Chapter 3 - Self-repair of structural and functional composites with intrinsically self-healing polymer matrices: A review

| | |
|---|----|
| 3.1. Introduction | 38 |
| 3.2. Intrinsically self-healing matrix polymers..... | 40 |
| 3.2.1.Heat triggered self-healing | 41 |
| 3.2.2.Photochemical triggered self-healing | 44 |
| 3.2.3.Electrically triggered self-healing..... | 45 |
| 3.2.4.Moisture triggered self-healing | 45 |
| 3.3. Structural composites containing an intrinsically self-healing polymer matrix...45 | |
| 3.3.1.Stiffness recovery | 46 |
| 3.3.2.Strength recovery | 49 |
| 3.4. Functional Polymer Composites | 52 |
| 3.4.1.Electrically conductive polymer composites..... | 52 |
| 3.4.2.Electromagnetic polymer composites | 54 |
| 3.4.3.Electromechanical polymer composites..... | 55 |
| 3.4.4.Magnetic polymer composites..... | 57 |
| 3.4.5.Thermally conductive polymer composites..... | 59 |
| 3.5. Conclusion | 61 |
| References | 62 |

Chapter 4 - Moderate temperature healing in a glass fibre reinforced composite with a disulphide containing organic-inorganic epoxy matrix

| | |
|-------------------------|----|
| 4.1. Introduction | 74 |
| 4.2. Experimental..... | 76 |
| 4.2.1.Materials | 76 |

| | |
|---|----|
| 4.2.2. Resin and GFRPs production | 76 |
| 4.2.2.1. Resin preparation..... | 76 |
| 4.2.3. Composite processing | 77 |
| 4.2.4. Characterization methods | 77 |
| 4.2.4.1. Matrix characterization | 77 |
| 4.2.4.2. GFRP composite characterization | 78 |
| 4.3. Results & discussion..... | 80 |
| 4.3.1. Polymer matrix optimisation..... | 80 |
| 4.3.2. Composite characterization | 82 |
| 4.3.2.1. Flexural properties | 82 |
| 4.3.2.2. Interlaminar fracture properties | 85 |
| 4.3.2.3. Low-velocity impact properties | 87 |
| 4.4. Conclusion..... | 89 |
| References..... | 90 |
| Supplementary Information..... | 94 |

Chapter 5 - Healing of Early Stage Fatigue Damage in Ionomer/Fe₃O₄ Nanoparticle Composites

| | |
|--|-----|
| 5.1. Introduction | 100 |
| 5.2. Materials and Methods | 102 |
| 5.2.1. Materials..... | 102 |
| 5.2.2. Mechanical Testing | 102 |
| 5.2.3. Thermomechanical Testing | 103 |
| 5.2.4. Thermally Induced Healing Process and Evaluation | 104 |
| 5.3. Results..... | 104 |
| 5.3.1. Thermal and Thermomechanical Analysis..... | 104 |
| 5.3.2. Effect of Temperature Post-Treatment after Static and Dynamic Loading | 108 |
| 5.4. Discussion | 113 |
| 5.5. Conclusions | 116 |

| | |
|---------------------------------|-----|
| References | 117 |
| Supplementary Information | 120 |

Chapter 6 - Non-destructive monitoring of delamination healing of a CFRP composite with a thermoplastic ionomer interlayer

| | |
|--|-----|
| 6.1. Introduction | 126 |
| 6.2. Material and methods | 128 |
| 6.2.1. Materials | 128 |
| 6.2.2. Ionomer-CFRP laminate production | 128 |
| 6.2.3. Healing treatment | 129 |
| 6.2.4. Characterization | 129 |
| 6.2.4.1. Thermomechanical analysis of the ionomer film | 129 |
| 6.2.4.2. Ultrasonic NDT analysis | 130 |
| 6.2.4.3. Mechanical characterization of the pristine and healed composites ... | 131 |
| 6.3. Results | 131 |
| 6.3.1. Thermomechanical properties of the ionomer interlayer | 131 |
| 6.3.2. Non-destructive characterization | 133 |
| 6.3.2.1. C-scanning techniques | 133 |
| 6.3.2.2. Local defect resonance scanning | 138 |
| 6.3.3. Destructive characterization by compression testing | 141 |
| 6.4. Discussion | 142 |
| 6.5. Conclusion | 145 |
| References | 146 |
| Supplementary information | 150 |

| | |
|----------------------|------------|
| Summary | 153 |
|----------------------|------------|

| | |
|---------------------------|------------|
| Samenvatting | 157 |
|---------------------------|------------|

| | |
|------------------------------|------------|
| Acknowledgments | 161 |
|------------------------------|------------|

| | |
|-------------------------------|------------|
| Curriculum Vitae | 165 |
|-------------------------------|------------|

| | |
|-----------------------------------|------------|
| List of publications | 167 |
|-----------------------------------|------------|

Chapter 1

Introduction

1.1. Introduction

In the last decades the use of structural lightweight materials in aerospace, automotive and renewable energy applications has increased rapidly. In this respect, one of the biggest progressions of the past decades is the development of fibre- and particle reinforced polymer composites. These materials consist of a polymer matrix that is reinforced with high performance fibres or particles. As such, composite materials can be obtained that have specific strengths and moduli that cannot easily be matched by classical monolytical structural materials such as aluminium alloys and steel. Both thermoplastic and thermoset polymers are frequently used as polymer matrix and continuous carbon, aramid and glass fibres as well as chopped glass, carbon nanotubes and metallic particles are the most commonly found filler materials [1-3].

However, a clear disadvantage of polymer composite materials is that they are known to have many complex and non-easily detectable damage modes compared to single phase materials. Examples of these damage modes are delamination, interface debonding, fibre fracture and matrix micro-cracking. The combination of this multitude of damage modes and the complex internal structure of fibre reinforced composites makes that damage detected and damage-tailored repair of composite components is a very complicated and therefore expensive process and in the case of composites based on thermoset matrix polymers even impossible. Because of these complications, the demand is growing for polymer composites that are capable of repairing themselves when locally damaged, thereby increasing the overall lifetime of the construction to which they belong [4, 5].

This demand for easy repair and lifetime extension has contributed to the fact that the first examples of engineered self-healing materials can be found within the field of composite materials. Pioneering work was performed by Dry and her student Sottos who visually showed the potential of composite healing by embedding glass fibres with a liquid healing agent into an epoxy based polymer [6, 7]. Following this work, White, Sottos et al. [8] subsequently reported the autonomic restoration of cracks in a thermoset polymer matrix. To this end, they encapsulated a liquid healing agent within microcapsules that rupture upon intrusion of a crack in the matrix polymer, allowing the reactive liquid to flow into the crack. As the thermoset matrix phase was doped with a catalyst which polymerizes the healing agent within several minutes, the healing agent flowing into the crack due to capillary forces is turned from a liquid into a well-adhering solid, thereby restoring the load bearing capacity of the thermoset product. Following these landmark contributions, the amount of studies on the development of self-healing composites (and self-healing materials in general) increased rapidly over the past two decades [5].

1.2. Types of healing in polymer composites

1.2.1. Extrinsic healing

Generally, all self-healing strategies can be divided into either extrinsic or intrinsic healing. In extrinsic healing materials, a discrete healing entity (either in particulate, fibrous or planar form), is incorporated within a conventional, non-healable, matrix material. The oldest and still most common approach of extrinsic healing in polymers is based on the dispersion of liquid containing particles in the matrix phase. In the case of polymer composite matrices, many different types of healing agent have been reported of which DCPD, thiol/isocyanate and epoxy/amine are the most prominent examples [8-12]. As the success of the load bearing recovery requires the autonomous transition of the healing agent from the liquid state to the solid state via a crosslinking reaction, very often two different reactive agents, brought together at the appropriate ratio, are needed to complete the healing event. To facilitate the natural interaction of both components in this crosslinking reaction researchers developed binary healing capsules that contain both reactive components in separate layers within the same capsule [13]. Another common approach is the use of encapsulated solvent that partially dissolves or plasticizes the polymer matrix, thereby creating the necessary mobility for healing to take place [14-17].

The most profound disadvantage of capsule based healing systems is that per capsule only a small quantity of healing agent can be delivered to the damaged site and therefore only a small part of the open crack can be mechanically healed. Additionally, the non-uniform dispersion of capsules was found to lead to difficulties in the fibre reinforced composite processing process [18, 19]. To cope with these problems continuous hollow fibres filled with a liquid healing agent have been used. The Bond research team at Bristol University showed the full potential of this concept [20-22], which subsequently evolved to the development of bioinspired interconnected vascular systems [23-26]. However, a negative effect of these complex interconnected networks is that, in the case of a slowly reacting healing agent, a single damage event with a crack opening up to the outside environment can lead to bleeding and depletion of a large volume of healing agent. On the other hand, a premature reaction can lead to irreversible blocking of the supply channels and an effective destruction of the concept. In both cases a second damage event on a different location not too far apart from the first damage site can no longer be repaired as the healing agent is no longer present. A solution to this issue can be found in the biological design of plants which possess non-continuous tubular compartments that are capable of local healing events [27]. Following this approach, Mookhoek et al. developed alginate based compartmented fibres which contain vacuoles filled with healing agent distributed along the fibre backbone. Upon

a damage event localized healing occurs without consuming an excess of healing agent. As a result multiple local damage healing events can take place within the same material [28]. Using the concept of compartmented fibres, solvent induced healing of thermoplastic polymers was shown by Prajer et al.[29]. In this work, the multiple healing of local damage events was visualized by flexural testing and non-destructive x-ray tomography. Notwithstanding this proof of concept for thermoplastic composites the healing of thermoset composites using compartmented fibres has not yet been demonstrated. This can mainly be attributed to the complexity of the encapsulation chemistry and the mismatch in mechanical response of the relatively tough fibres and brittle epoxy networks.

1.2.2. Intrinsic healing

An intrinsic shortcoming of all extrinsic healing systems is that a once healed damaged site can never be healed a second time. This clear disadvantage can be overcome by using materials with intrinsic healing capabilities, i.e. materials which by their very nature and architecture have an in-build tendency to rebond when their surfaces are brought into contact again. In the case of polymers, intrinsic self-healing polymers depend on the presence of reversible moieties, either supramolecular or covalent of nature, built into the polymer structure. Given the reversible nature of the bond formation, local damage restoration can theoretically be infinitely repeated. In the majority of the intrinsic healing polymer systems reported an external stimulus such as heat is required, but polymers that heal upon the exposure to an electrical current, light or moisture have been reported as well [4, 30]. Besides the recovery of mechanical properties such as stiffness and strength, there are many studies that report on the repair of functional properties. Examples of functional healing can be the repair of electrical [31, 32], thermal [33], magnetic [34], electromechanical [35, 36] and corrosion protection [37, 38] properties.

Over the past decade the number of self-healing polymers based on supramolecular interactions has increased exponentially and some of them even approached a commercial status [39-41]. However, because of the presence of a large number of weaker reversible bonds the vast majority of these polymers possess rather low mechanical properties making them unsuitable to be used in structural composites. An exemption to this trend is given by the class of thermoplastic ionomers. These polymers are relatively stiff and strong due to the presence of (reversible) ionic clusters within their polymer architecture. The most famous example of ionomer healing can be found in their ability to autonomously heal ballistic impact events [42-45]. Upon projectile penetration, the combination of induced deformation and temperature rise is directly converted to induce both a shape memory and a hole sealing effect [46, 47]. Another common strategy to combine supramolecular

healing strategies with adequate mechanical properties for structural applications is the immiscible blending of thermoplastic polymers (providing the healing potential) with thermosets (providing the mechanical rigidity). Upon crack formation, the blend can be heated to a level at which the thermoplastic phase melts and flows into the damaged site. Subsequently, upon cooling to temperatures below the thermoplastic melting temperature, the mechanical properties are partially restored [48, 49].

As covalent bonds are per definition stronger than supramolecular bonds, polymers that use reversible covalent bonds as their healing mechanism are considered more optimal for the use as matrix material in intrinsic self-healing fibre reinforced polymer composites with non-trivial mechanical properties. The most well-known example of reversible crosslinking for self-healing purposes is by using Diels-Alder chemistry which is the thermoreversible cycloaddition of a diene and an alkene. This form of reversible chemistry is of particular interest for healing of thermoset composite materials as these reversible moieties are highly compatible with conventional epoxy matrices [50-53]. However, the high temperature range (120-140°C) at which the reversible crosslinking generally occurs is a clear disadvantage for commercial applications.

A less-investigated form of reversible covalent crosslinking for composite applications is the use of the thermally induced disulphide exchange reaction. In this healing mechanism two pairs of disulphide bonds can exchange their covalent S-S bond upon a moderate thermal stimulus of 60-80°C [54, 55]. Polymers with di- or tetrasulfide bridges in their backbone have proven to be good candidates for the development of self-healing coatings and rubbers [56, 57]. To make disulphide based intrinsic healing suitable for structural applications, several strategies to employ these functional groups into epoxy based materials have been developed. A recent study reported on an epoxy resin in which the amine hardener contains the disulphide functionality. The resulting thermoset has properties within the range of conventional epoxy matrices and can be fully reprocessed and recycled at high temperatures (>200°C) and high pressures (>200 bar) [58]. A more elegant approach was reported by Abdollah Zadeh et al. who developed a hybrid thermoset that consists of a di- and tetra sulphide modified epoxy network to initiate reversible crosslinking while the mechanical integrity was boosted by inorganic clusters within the polymer network [59]. As such, coatings and particulate composites capable of healing under mild conditions (70°C and 1 bar) were developed [38, 60]. However, the mechanical properties (Young's modulus <100 MPa) of these thermosets are still considered insufficient for application in structural composites. As such, the challenge remains to develop a thermoset matrix polymer with good mechanical properties that is capable of healing under mild conditions and can be used in the production of fibre reinforced composite products of realistic dimensions under industrially acceptable conditions.

1.3. Characterization of self-healing polymer composites

Along with the growing number of new self-healing polymer systems came an increasing number of methods to quantify the restorative behaviour of their mechanical properties. The most traditional approach to determine the mechanical recovery of the polymer matrix is by tensile testing. In this method the mechanical response (i.e. Young's modulus, ultimate strength) of an undamaged and a damaged-then-healed specimen (having either a simple rectangular shape or that of a conventional tensile testing sample) are compared with each other [39, 60]. In such an approach no effort is made to monitor the efficiency of the healing phenomena at the formerly broken interface. An alternative and more realistic approach is to determine the crack propagation resistance of the pristine and healed polymer matrices. For soft polymer matrices this can be done by using the J-integral approach. A recent study by Grande et al. shows that this method gives a better reflection of the healed polymer interface than conventional tensile testing [61]. For the quantification of the fracture toughness of relatively brittle polymers, such as epoxy thermosets, the most widely acknowledged approach is the tapered double cantilever beam test. The main advantages of this test method are that the fractured interfaces can easily be repositioned towards each other and constant monitoring of the crack development is not required to calculate the fracture toughness [8, 62].

In most cases, the mechanical recovery of particle reinforced composites can be characterized with a similar approach as for the polymer matrix [60]. However, fibre reinforced composites are generally characterized by conventional composite characterization techniques that focus on damage formation within the polymer matrix. The most prominent examples are 3- or 4 point bending, interlaminar fracture testing and low-velocity impact testing, of which the latter one is ideally followed by compression testing [63-67]. Furthermore, the healing of fatigue induced damage was already reported in several studies for extrinsic self-healing composites [26, 68-70]. However, the healing behaviour of intrinsically healing polymers after fatigue is a still relatively unexplored field [35].

Destructive testing has become the conventional approach for the characterization of self-healing materials. However, in doing so the healing effect will be undone and therefore destructive quantification cannot be used in actual applications. For this reason, it is crucial that the self-healing behaviour of polymer composites can be monitored with non-destructive testing (NDT) methods. Although the superior value of non-destructive healing evaluation seems evident, the majority of studies that investigate the self-healing behaviour of composite materials focus on destructive testing and the involvement of NDT is limited to a couple of a studies only [20, 29, 71-74].

1.4. Challenges and future prospects

Within the past decade the development of self-healing fibre reinforced composites progressed slowly towards actual applications. However, several challenges still need to be overcome before industrial adaptation can be achieved routinely. For intrinsic healing polymer composites the main challenge lies within creating the appropriate balance between acceptable mechanical properties and a high healing potential. Another important, more practical, issue can be found in the method that is used to trigger the healing event within the composite structure. In the majority of studies on intrinsic healing polymers, the intended energy input has to be delivered by physically heating the entire sample. This poses a large disadvantage for structural applications and therefore new strategies need to be developed that allow the energy input to be delivered locally from within the structure. In this respect, one approach is to make the polymer matrix susceptible to inductive heating so that, once a damaged site has been identified, it can be repaired by applying a localized inductive field [75-77].

Another factor that will move the field of self-healing composites to a level of industry readiness can be found in combining self-healing behaviour with other smart polymer functionalities. The most prominent examples of such functionalities are the shape memory effect and self-sensing damage detection. Both have been reported separately or even in a combination with self-healing [78, 79]. However, it is believed that full integration of these three functionalities (healing, shape memory and damage sensing) without sacrificing the mechanical properties will open the door for full industrial adaptation. Still, even when all these conditions are met, it is not expected that in the coming future all structural composites will be replaced by self-healing counterparts. The focus will have to be on those applications that truly benefit from an improved lifetime and which are hard or even impossible to manually repair. As such, the emerging ocean based wind turbine industry could very well serve as one of the early adapters of this technology.

1.5. Scope and thesis outline

This thesis aims to contribute to the closure of the gap that exists between the academic concept of structural self-healing composites and its fully implemented industrial application. As such, each chapter targets one of the scientific issues that are currently preventing the industrial acceptance of self-healing polymer composites.

Chapter 2 is devoted to a more extended 'proof of concept' of healing of glass-fibre reinforced thermoset composites using the compartmented fibre technology. In the first part of this chapter, the potential of enhancing the mechanical properties of the alginate fibres by the addition of montmorillonite clay is reported. In the second

part, the effect of different epoxy-thiol based healing agents configurations on the healing of glass fibre reinforced composites locally containing compartmented alginate fibres is studied.

Chapter 3 gives an overview of the many different approaches to intrinsic structural and functional healing that have been reported in the literature in recent years. This literature study aims to address the question whether the underlying optimisation criteria for structural healing are different from those for functional healing.

Chapter 4 reports on the development of an intrinsic healing glass fibre reinforced polymer composite based on a disulphide-containing organic-inorganic thermoset matrix. The intention of the work is to demonstrate whether a combination of decent mechanical properties and healing at moderate temperatures can be obtained for fibre reinforced polymer composites that are manufactured via conventional composite processing routes.

Chapter 5 reports on the healing of early stage fatigue damage that is formed within ionomer/ Fe_3O_4 nanoparticle composites. This work targets to demonstrate that fatigue induced microcracks can be repaired upon localized heating of ferromagnetic particles in the polymer matrix by applying an alternating magnetic field. In addition, the different healing phases of the ionomer that govern both the closure and the sealing of fatigue induced microcracks are investigated separately in order to identify a temperature window for each phase of the early stage damage recovery in these polymer systems.

Chapter 6 presents a comparative study on carbon fibre reinforced polymer composites with an ionomer interlayer in which artificial delaminations of various sizes and at different locations were introduced. Aim of the work is to identify the effectiveness of the selected acoustic NDT techniques during the various stages of the healing process. Furthermore a correlation is made between the reduction in the delaminated zone as observed by the various NDT techniques and the recovery in compressive strength of the as- produced and healed samples.

References

1. Agarwal, B.D., Broutman, L.J., and Chandrashekhara, K., *Analysis And Performance Of Fiber Composites*. Third Edition ed. 2006: John Wiley & Sons.
2. Chung, D.D.L., *Composite Materials*. 2nd ed. Engineering Materials and Processes. 2010: Springer London.
3. Soutis, C., *Fibre reinforced composites in aircraft construction*. Progress in Aerospace Sciences, 2005. 41(2): p. 143-151.
4. Zhong, N. and Post, W., *Self-repair of structural and functional composites with intrinsically self-healing polymer matrices: A review*. Composites Part A: Applied Science and Manufacturing, 2015. 69(0): p. 226-239.
5. van der Zwaag, S., *An Introduction to Material Design Principles: Damage Prevention versus Damage Management*, in *Self-Healing Materials an Alternative Approach to 20 Centuries of Materials Science*, S. van der Zwaag, Editor. 2007.
6. Dry, C.M. and Sottos, N.R. *Passive smart self-repair in polymer matrix composite materials*. 1993.
7. Dry, C., *Procedures developed for self-repair of polymer matrix composite materials*. Composite Structures, 1996. 35(3): p. 263-269.
8. White, S.R., Sottos, N.R., Geubelle, P.H., Moore, J.S., Kessler, M.R., Sriram, S.R., Brown, E.N., and Viswanathan, S., *Autonomic healing of polymer composites*. Nature, 2001. 409(6822): p. 794-797.
9. McIlroy, D.A., Blaiszik, B.J., Caruso, M.M., White, S.R., Moore, J.S., and Sottos, N.R., *Microencapsulation of a reactive liquid-phase amine for self-healing Epoxy composites*. Macromolecules, 2010. 43(4): p. 1855-1859.
10. Hillewaere, X.K.D. and Du Prez, F.E., *Fifteen chemistries for autonomous external self-healing polymers and composites*. Progress in Polymer Science, 2015. 49-50: p. 121-153.
11. Hillewaere, X.K.D., Teixeira, R.F.A., Nguyen, L.T.T., Ramos, J.A., Rahier, H., and Du Prez, F.E., *Autonomous self-healing of epoxy thermosets with thiol-isocyanate chemistry*. Advanced Functional Materials, 2014. 24(35): p. 5575-5583.
12. Neuser, S., Chen, P.W., Studart, A.R., and Michaud, V., *Fracture toughness healing in epoxy containing both epoxy and amine loaded capsules*. Advanced Engineering Materials, 2014. 16(5): p. 581-587.
13. Mookhoek, S.D., Blaiszik, B.J., Fischer, H.R., Sottos, N.R., White, S.R., and van der Zwaag, S., *Peripherally decorated binary microcapsules containing two liquids*. Journal of Materials Chemistry, 2008. 18(44): p. 5390-5394.
14. Mookhoek, S.D., Mayo, S.C., Hughes, A.E., Furman, S.A., Fischer, H.R., and van der Zwaag, S., *Applying SEM-based X-ray microtomography to observe self-healing in solvent encapsulated thermoplastic materials*. Advanced Engineering Materials, 2010. 12(3): p. 228-234.
15. Manfredi, E., Cohades, A., Richard, I., and Michaud, V., *Assessment of solvent capsule-based healing for woven E-glass fibre-reinforced polymers*. Smart Materials and Structures, 2015. 24(1).

16. Neuser, S., Michaud, V., and White, S.R., *Improving solvent-based self-healing materials through shape memory alloys*. Polymer, 2012. 53(2): p. 370-378.
17. Jones, A.R., Blaiszik, B.J., White, S.R., and Sottos, N.R., *Full recovery of fiber/matrix interfacial bond strength using a microencapsulated solvent-based healing system*. Composites Science and Technology, 2013. 79: p. 1-7.
18. Kessler, M.R., Sottos, N.R., and White, S.R., *Self-healing structural composite materials*. Composites Part A: Applied Science and Manufacturing, 2003. 34(8): p. 743-753.
19. Kessler, M.R. and White, S.R., *Self-activated healing of delamination damage in woven composites*. Composites Part A: Applied Science and Manufacturing, 2001. 32(5): p. 683-699.
20. Pang, J.W.C. and Bond, I.P., *A hollow fibre reinforced polymer composite encompassing self-healing and enhanced damage visibility*. Composites Science and Technology, 2005. 65(11-12): p. 1791-1799.
21. Pang, J.W.C. and Bond, I.P., *'Bleeding composites' - Damage detection and self-repair using a biomimetic approach*. Composites Part A: Applied Science and Manufacturing, 2005. 36(2 SPEC. ISS.): p. 183-188.
22. Trask, R.S. and Bond, I.P., *Biomimetic self-healing of advanced composite structures using hollow glass fibres*. Smart Materials and Structures, 2006. 15(3): p. 704-710.
23. Toohey, K.S., Sottos, N.R., Lewis, J.A., Moore, J.S., and White, S.R., *Self-healing materials with microvascular networks*. Nature Materials, 2007. 6(8): p. 581-585.
24. Toohey, K.S., Hansen, C.J., Lewis, J.A., White, S.R., and Sottos, N.R., *Delivery of two-part self-healing chemistry via microvascular networks*. Advanced Functional Materials, 2009. 19(9): p. 1399-1405.
25. Trask, R.S. and Bond, I.P., *Bioinspired engineering study of Plantae vasculues for self-healing composite structures*. Journal of the Royal Society Interface, 2010. 7(47): p. 921-931.
26. Luterbacher, R., Trask, R.S., and Bond, I.P., *Static and fatigue tensile properties of cross-ply laminates containing vasculues for self-healing applications*. Smart Materials and Structures, 2015. 25(1).
27. McCulloh, K.A., Sperry, J.S., and Adler, F.R., *Water transport in plants obeys Murray's law*. Nature, 2003. 421(6926): p. 939-942.
28. Mookhoek, S.D., Fischer, H.R., and van der Zwaag, S., *Alginate fibres containing discrete liquid filled vacuoles for controlled delivery of healing agents in fibre reinforced composites*. Composites Part A: Applied Science and Manufacturing, 2012. 43(12): p. 2176-2182.
29. Prajer, M., Wu, X., García, S.J., and van der Zwaag, S., *Direct and indirect observation of multiple local healing events in successively loaded fibre reinforced polymer model composites using healing agent-filled compartmented fibres*. Composites Science and Technology, 2015. 106(0): p. 127-133.

30. García, S.J., *Effect of polymer architecture on the intrinsic self-healing character of polymers*. European Polymer Journal, 2014. 53(0): p. 118-125.
31. Wang, C., Wu, H., Chen, Z., McDowell, M.T., Cui, Y., and Bao, Z., *Self-healing chemistry enables the stable operation of silicon microparticle anodes for high-energy lithium-ion batteries*. Nat Chem, 2013. 5(12): p. 1042-1048.
32. Palleau, E., Reece, S., Desai, S.C., Smith, M.E., and Dickey, M.D., *Self-Healing Stretchable Wires for Reconfigurable Circuit Wiring and 3D Microfluidics*. Advanced Materials, 2013. 25(11): p. 1589-1592.
33. Lafont, U., Moreno-Belle, C., Van Zeijl, H., and van der Zwaag, S., *Self-healing thermally conductive adhesives*. Journal of Intelligent Material Systems and Structures, 2014. 25(1): p. 67-74.
34. Zhang, Y., Yang, B., Zhang, X., Xu, L., Tao, L., Li, S., and Wei, Y., *A magnetic self-healing hydrogel*. Chemical Communications, 2012. 48(74): p. 9305-9307.
35. James, N.K., Lafont, U., van der Zwaag, S., and Groen, W.A., *Piezoelectric and mechanical properties of fatigue resistant, self healing PZT-ionomer composites*. Smart Materials and Structures, 2014. 23(5): p. 055001
36. Tee, B.C.K., Wang, C., Allen, R., and Bao, Z., *An electrically and mechanically self-healing composite with pressure- and flexion-sensitive properties for electronic skin applications*. Nature Nanotechnology, 2012. 7(12): p. 825-832.
37. Abdolah Zadeh, M., van der Zwaag, S., and García, S.J., *Adhesion and Long-Term Barrier Restoration of Intrinsic Self-Healing Hybrid Sol-Gel Coatings*. ACS Applied Materials and Interfaces, 2016. 8(6): p. 4126-4136.
38. Abdolah Zadeh, M., van der Zwaag, S., and García, S.J., *Assessment of healed scratches in intrinsic healing coatings by AC/DC/AC accelerated electrochemical procedure*. Surface and Coatings Technology, 2016. 303(Part B): p. 396-405.
39. Susa, A., Bose, R.K., Grande, A.M., van der Zwaag, S., and García, S.J., *Effect of the Dianhydride/Branched Diamine Ratio on the Architecture and Room Temperature Healing Behavior of Polyetherimides*. ACS Applied Materials and Interfaces, 2016. 8(49): p. 34068-34079.
40. Sijbesma, R.P., Beijer, F.H., Brunsveld, L., Folmer, B.J.B., Hirschberg, J.H.K.K., Lange, R.F.M., Lowe, J.K.L., and Meijer, E.W., *Reversible polymers formed from self-complementary monomers using quadruple hydrogen bonding*. Science, 1997. 278(5343): p. 1601-1604.
41. Cordier, P., Tournilhac, F., Soulié-Ziakovic, C., and Leibler, L., *Self-healing and thermoreversible rubber from supramolecular assembly*. Nature, 2008. 451(7181): p. 977-980.
42. Varley, R.J. and van der Zwaag, S., *Towards an understanding of thermally activated self-healing of an ionomer system during ballistic penetration*. Acta Materialia, 2008. 56(19): p. 5737-5750.
43. Varley, R.J. and van der Zwaag, S., *Autonomous damage initiated healing in a thermo-responsive ionomer*. Polymer International, 2010. 59(8): p. 1031-1038.

44. Post, W., Bose, R., García, S., and van der Zwaag, S., *Healing of Early Stage Fatigue Damage in Ionomer/Fe₃O₄ Nanoparticle Composites*. *Polymers*, 2016. 8(12): p. 436.
45. Wang, C.H., Sidhu, K., Yang, T., Zhang, J., and Shanks, R., *Interlayer self-healing and toughening of carbon fibre/epoxy composites using copolymer films*. *Composites Part A: Applied Science and Manufacturing*, 2012. 43(3): p. 512-518.
46. Kalista Jr, S.J. and Ward, T.C., *Thermal characteristics of the self-healing response in poly(ethylene-co-methacrylic acid) copolymers*. *Journal of the Royal Society Interface*, 2007. 4(13): p. 405-411.
47. Kalista Jr, S.J., Ward, T.C., and Oyetunji, Z., *Self-healing of poly(ethylene-co-methacrylic acid) copolymers following projectile puncture*. *Mechanics of Advanced Materials and Structures*, 2007. 14(5): p. 391-397.
48. Luo, X., Ou, R., Eberly, D.E., Singhal, A., Viratyaporn, W., and Mather, P.T., *A thermoplastic/thermoset blend exhibiting thermal mending and reversible adhesion*. *ACS Applied Materials and Interfaces*, 2009. 1(3): p. 612-620.
49. Cohades, A., Manfredi, E., Plummer, C.J.G., and Michaud, V., *Thermal mending in immiscible poly(ϵ -caprolactone)/epoxy blends*. *European Polymer Journal*, 2016. 81: p. 114-128.
50. Chen, X., Dam, M.A., Ono, K., Mal, A., Shen, H., Nutt, S.R., Sheran, K., and Wudl, F., *A thermally re-mendable cross-linked polymeric material*. *Science*, 2002. 295(5560): p. 1698-1702.
51. Peterson, A.M., Jensen, R.E., and Palmese, G.R., *Thermoreversible and remendable glass-polymer interface for fiber-reinforced composites*. *Composites Science and Technology*, 2011. 71(5): p. 586-592.
52. Coope, T.S., Turkenburg, D.H., Fischer, H.R., Luterbacher, R., Van Bracht, H., and Bond, I.P., *Novel Diels-Alder based self-healing epoxies for aerospace composites*. *Smart Materials and Structures*, 2016. 25(8).
53. Dello Iacono, S., Martone, A., Filippone, G., Acierno, D., Zarrelli, M., Giordano, M., and Amendola, E. *Insight on mendable resin made by combining Diels-Alder epoxy adducts with DGEBA*. in *AIP Conference Proceedings*. 2016.
54. Canadell, J., Goossens, H., and Klumperman, B., *Self-healing materials based on disulfide links*. *Macromolecules*, 2011. 44(8): p. 2536-2541.
55. Pepels, M., Filot, I., Klumperman, B., and Goossens, H., *Self-healing systems based on disulfide-thiol exchange reactions*. *Polymer Chemistry*, 2013. 4(18): p. 4955-4965.
56. Hernández, M., Grande, A.M., Dierkes, W., Bijleveld, J., van der Zwaag, S., and García, S.J., *Turning Vulcanized Natural Rubber into a Self-Healing Polymer: Effect of the Disulfide/Polysulfide Ratio*. *ACS Sustainable Chemistry and Engineering*, 2016. 4(10): p. 5776-5784.
57. Lafont, U., Van Zeijl, H., and van der Zwaag, S., *Influence of cross-linkers on the cohesive and adhesive self-healing ability of polysulfide-based thermosets*. *ACS Applied Materials and Interfaces*, 2012. 4(11): p. 6280-6288.

58. Ruiz de Luzuriaga, A., Martin, R., Markaide, N., Rekondo, A., Cabanero, G., Rodriguez, J., and Odriozola, I., *Epoxy resin with exchangeable disulfide crosslinks to obtain reprocessable, repairable and recyclable fiber-reinforced thermoset composites*. Materials Horizons, 2016. 3(3): p. 241-247.
59. Abdolazadeh, M., C. Esteves, A.C., van der Zwaag, S., and García, S.J., *Healable dual organic-inorganic crosslinked sol-gel based polymers: Crosslinking density and tetrasulfide content effect*. Journal of Polymer Science, Part A: Polymer Chemistry, 2014. 52(14): p. 1953-1961.
60. Zhong, N., Garcia, S.J., and van der Zwaag, S., *The effect of filler parameters on the healing of thermal conductivity and mechanical properties of a thermal interface material based on a self-healable organic-inorganic polymer matrix*. Smart Materials and Structures, 2016. 25(8).
61. Grande, A.M., García, S.J., and van der Zwaag, S., *On the interfacial healing of a supramolecular elastomer*. Polymer, 2015. 56: p. 435-442.
62. Blaiszik, B.J., Kramer, S.L.B., Olugebefola, S.C., Moore, J.S., Sottos, N.R., and White, S.R., *Self-healing polymers and composites*, in *Annual Review of Materials Research*. 2010. p. 179-211.
63. Sordo, F. and Michaud, V., *Processing and damage recovery of intrinsic self-healing glass fiber reinforced composites*. Smart Materials and Structures, 2016. 25(8).
64. Cohades, A. and Michaud, V., *Thermal mending in E-glass reinforced poly(ϵ -caprolactone)/epoxy blends*. Composites Part A: Applied Science and Manufacturing, 2017. 99: p. 129-138.
65. Williams, G.J., Bond, I.P., and Trask, R.S., *Compression after impact assessment of self-healing CFRP*. Composites Part A: Applied Science and Manufacturing, 2009. 40(9): p. 1399-1406.
66. Patel, A.J., Sottos, N.R., Wetzel, E.D., and White, S.R., *Autonomic healing of low-velocity impact damage in fiber-reinforced composites*. Composites Part A: Applied Science and Manufacturing, 2010. 41(3): p. 360-368.
67. Norris, C.J., Bond, I.P., and Trask, R.S., *Healing of low-velocity impact damage in vascularised composites*. Composites Part A: Applied Science and Manufacturing, 2013. 44(1): p. 78-85.
68. Brown, E.N., White, S.R., and Sottos, N.R., *Retardation and repair of fatigue cracks in a microcapsule toughened epoxy composite - Part II: In situ self-healing*. Composites Science and Technology, 2005. 65(15-16 SPEC. ISS.): p. 2474-2480.
69. Jones, A.S., Rule, J.D., Moore, J.S., Sottos, N.R., and White, S.R., *Life extension of self-healing polymers with rapidly growing fatigue cracks*. Journal of the Royal Society Interface, 2007. 4(13): p. 395-403.
70. Neuser, S. and Michaud, V., *Fatigue Response of Solvent-Based Self-Healing Smart Materials*. Experimental Mechanics, 2014. 54(2): p. 293-304.
71. Norris, C.J., Meadway, G.J., O'Sullivan, M.J., Bond, I.P., and Trask, R.S., *Self-healing fibre reinforced composites via a bioinspired vasculature*. Advanced Functional Materials, 2011. 21(19): p. 3624-3633.
72. Tabaković, A., Post, W., Cantero, D., Copuroglu, O., Garcia, S.J., and Schlangen, E., *The reinforcement and healing of asphalt mastic mixtures by*

- rejuvenator encapsulation in alginate compartmented fibres*. Smart Materials and Structures, 2016. 25(8).
73. Van Stappen, J., Bultreys, T., Gilabert, F.A., Hillewaere, X.K.D., Gómez, D.G., Van Tittelboom, K., Dhaene, J., De Belie, N., Van Paepegem, W., Du Prez, F.E., and Cnudde, V., *The microstructure of capsule containing self-healing materials: A micro-computed tomography study*. Materials Characterization, 2016. 119: p. 99-109.
74. Bekas, D.G., Baltzis, D., Tsirka, K., Exarchos, D., Matikas, T., Meristoudi, A., Pispas, S., and Paipetis, A.S., *Self-healing polymers: Evaluation of self-healing process via non-destructive techniques*. Plastics, Rubber and Composites, 2016. 45(4): p. 147-156.
75. Adzima, B.J., Kloxin, C.J., and Bowman, C.N., *Externally triggered healing of a thermoreversible covalent network via self-limited hysteresis heating*. Advanced Materials, 2010. 22(25): p. 2784-2787.
76. Corten, C.C., Urban, M.W., and Shelby, F., *Repairing polymers using an oscillating magnetic field*. Advanced Materials, 2009. 21(48): p. 5011-5015.
77. Duenas, T., Enke, A., Chai, K., Castellucci, M., Sundaresan, V.B., Wudl, F., Murphy, E.B., Mal, A., Alexandar, J.R., Corder, A., and Ooi, T.K., *Smart self-healing material systems using inductive and resistive heating*, in *ACS Symposium Series*. 2010. p. 45-60.
78. Swait, T.J., Rauf, A., Grainger, R., Bailey, P.B.S., Lafferty, A.D., Fleet, E.J., Hand, R.J., and Hayes, S.A., *Smart composite materials for self-sensing and self-healing*. Plastics, Rubber and Composites, 2012. 41(4-5): p. 215-224.
79. Rodriguez, E.D., Luo, X., and Mather, P.T., *Linear/network poly(ϵ -caprolactone) blends exhibiting shape memory assisted self-healing (SMASH)*. ACS Applied Materials and Interfaces, 2011. 3(2): p. 152-161.

Chapter 2

Self-healing glass fibre-reinforced polymer composites based on montmorillonite reinforced compartmented alginate fibres

This chapter is to be submitted as:

W. Post, E. Jeoffroy, S. J. García, S. van der Zwaag; *Self-healing glass fibre-reinforced polymer composites based on montmorillonite reinforced compartmented alginate fibres*, Polymer Composites

2.1. Introduction

Over the past decades, fibre reinforced polymer composites (FRPCs) have emerged as a lightweight alternative for aluminium alloys and steel in structural applications. However, compared to these conventional materials, FRPCs are more susceptible to complex and hard to detect damage modes such as matrix microcracking, interface debonding and delamination. As the repair of this large number of damage modes leads to complicated repair procedures, the demand for FRPCs that can repair themselves after being locally damaged has grown in recent years [1-4].

Such self-repairing materials can be divided into intrinsic and extrinsic systems [5]. Intrinsically healing polymers, in which the polymer nature and architecture is responsible for healing, can undergo multiple healing cycles, but are currently limited to the healing of small scale damage [6]. Extrinsic healing systems have discrete healing agents embedded within their structure that generally allow the singular healing of larger damages [7]. On top of that, extrinsic healing systems are generally fully autonomous whereas intrinsic systems most often require an external stimulus (e.g. a heat treatment from the nearby environment) to facilitate healing [8]. As the most frequent damage modes in FRPCs exceed the micron-sized damage level and fully autonomous systems are preferred from a commercial point of view, the initial focus within the field of self-healing polymer composites has been on the development of extrinsic self-healing polymeric systems.

Extrinsic self-healing strategies can generally be divided into three different liquid healing agent carrier concepts: i) microencapsulation [9-12], ii) hollow fibres [1, 3, 13] and iii) vascular networks [14-16]. However, all these concepts have to overcome several practical disadvantages before application in FRPCs becomes feasible. Microcapsules have only a limited amount of healing agent available and tend to cluster around resin rich pockets, which are located in between the plies of the reinforcing fibres, during processing which reduces their healing capacity. Hollow fibre and vascular systems on the other hand risk using a large portion of healing liquid upon a first damage event, thereby depleting healing agent from undamaged areas. Additionally, the chemical reaction responsible for healing may propagate into the repair fibres that are located in undamaged regions of the composite. These two issues will prevent secondary healing events to take place thereby effectively negating the full potential of the concept.

A bio-inspired solution for these issues can be found in the non-continuous tubular compartments of plants, which can locally heal macroscale damage events [17]. Following this concept, Mookhoek et al. developed compartmented alginate fibres with vacuoles of liquid healing agent distributed along the fibre backbone. In doing so they showed that is possible to evenly distribute relatively large volumes of healing agent throughout the polymer matrix [18, 19]. The general concept of the

compartmented fibre technology and its advantages over hollow fibre and vascular network systems is depicted in Figure 2.1.

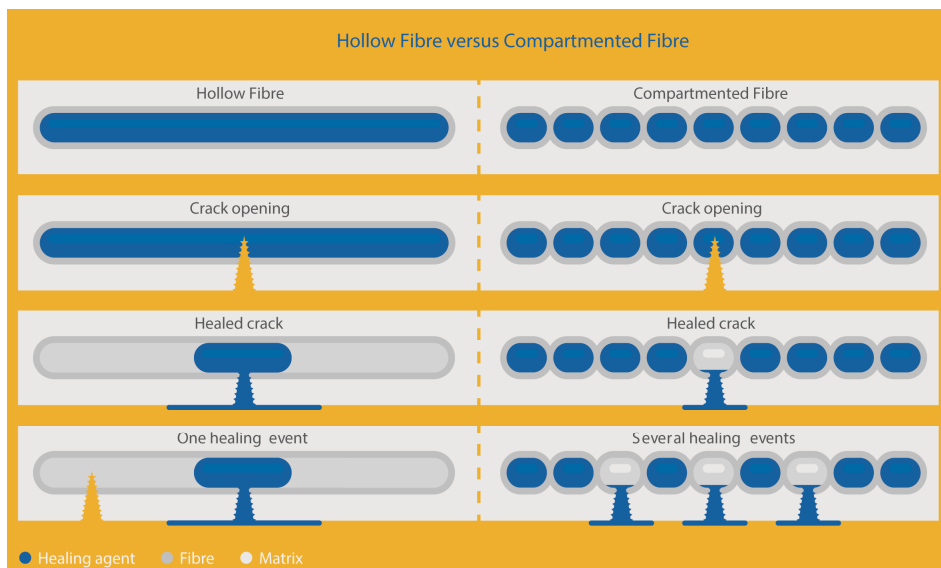


Figure 2.1 Graphical overview of the compartmented fibre concept versus the hollow fibre concept, which clearly shows the capability of multiple healing events in the same polymer matrix.

In a follow-up study by Prajer et al. the multiple healing of a thermoplastic matrix by encapsulated solvent was quantified by mechanical flexural testing and non-destructive x-ray tomography [20]. Notwithstanding this proof of concept for thermoplastic composites, the healing of thermoset matrices for FRPCs by compartmented fibres has yet to be demonstrated. This can mainly be attributed to the complexity of the encapsulation chemistry and the mismatch in mechanical response of the relatively flexible alginate fibres and the rigid and brittle FRPCs. The first issue, the encapsulation chemistry, will require a deviation from 'classical healing agents' due to the fact that the most reactive (and thereby effective) liquid agents react with the bio-based alginate fibres. As such, less reactive compounds in combination with a catalyst need to be selected [21, 22]. The second challenge, the misalignment between the compartmented fibres and their intended applications, could be resolved by enhancing the mechanical properties of the alginate fibres by doping with inorganic fillers. In this respect, one of the most promising approaches is the addition of layered silicates to the alginate spinning dope. These layered silicates can either intercalate or exfoliate within the biopolymer architecture thereby having a profound effect on the mechanical properties already at low concentrations [23-25]. Montmorillonite (MMT) is one of the most investigated layered silicates for polymer modification and was shown to be capable of modifying alginate film properties within multiple applications [26-28].

This study investigates the feasibility of using compartmented fibres for the healing of epoxy based FRPCs by focussing on two distinctly different aspects. The first part of this study focusses on the potential of enhancing the mechanical properties of the alginate fibres by the addition of montmorillonite (MMT) clay particles in order to match the specific damage behaviour of commercial epoxy based FRPCs. In the second part of this work a proof of concept of healing by compartmented fibres in glass fibre reinforced polymer (GFRP) composites with different types of epoxy-and thiol based healing agents is shown. Model GFRP composites are prepared and their healing behaviour is characterized with both destructive and non-destructive characterization techniques.

2.2. Materials and Methods

2.2.1. Materials

Alginic acid sodium salt (powder), Poly(ethylene-alt-maleic anhydride), Pentaerythritol tetrakis-(3-mercaptopropionate) (>95%), 2,4,6-Tris (dimethylaminomethyl)-phenol and Calcium chloride hexahydrate (98%) from hereon called sodium alginate, PEMA, Tetrathiol, DMP-30 and CaCl_2 respectively were all purchased from Sigma Aldrich. Commercially available montmorillonite (Cloisite Na⁺ (MMT) from hereon called MMT was purchased from Southern Clay Products Inc., Rockwood. Epikote™ Resin 04908 and Epikure™ Curing Agent 04908 were purchased from Hexion Specialty Chemicals. All chemicals were used as received without further purification. The selected glass fibre reinforcement was a woven HexForce® 7581 Fibre Glass Fabric , with a nominal areal weight of 303 g.m⁻² and a fabric thickness of 0.23 mm purchased from Hexcel.

2.2.2. Spinning of compartmented fibres

Compartmented fibres were spun from an emulsion of healing agent and a solution of 6 wt.% sodium alginate in de-ionized water based on a methodology that is described in previous work [18, 20]. In order to reinforce the fibres, the sodium alginate solution was mixed with a 3 wt.% MMT solution for 24 hours at 300 rpm using a magnetic stirrer following the approach reported by Zlopasa et al.[27]. In this way solutions were prepared with 0, 10 and 20 wt.% of MMT relative to the amount of sodium alginate. Epikote resin, Tetrathiol and a 50/50 wt.% mixture of these components were used as healing agent. A dye was used to colour the healing agent in order to improve its visibility within the fibre compartments. To obtain a homogeneous dispersion of healing agent within the sodium alginate solution a 2.3 wt.% PEMA solution in water was mixed with the healing agent. The healing agent/PEMA ratio was 60/40 by weight. The sodium alginate solution was then added to the healing agent/PEMA solution to obtain an emulsion with a final sodium alginate/healing agent ratio of 57/43 by weight. The emulsion was manually

stirred for 20 seconds in order to obtain dispersed spheres of healing agent with a diameter in the range of 0.5-2.0 mm within the alginate solution.

The emulsion was then spun via a wet spinning technique using a plunger-based lab scale wet spinning line. With a rate of $1.93 \text{ cm}^3/\text{min}$ the emulsion was extruded through a spinneret with a single 1.5 mm long capillary with 0.5 mm diameter. The emulsion was extruded directly (i.e. no air gap) into a 0.8 m long coagulation bath containing a 0.45 M CaCl_2 solution in water. A clear overview of the fibre spinning process is given in Figure 2.2. Fibres were collected on Teflon rolls that were placed on a filament winder with take up speeds of 19.7, 29.5 and 39.3 m/min resulting in draw ratios of 2, 3 and 4 respectively. The filament winder was set so that a spacing of approximately 0.5 mm was maintained between each fibre. The fibre containing Teflon rolls were then cut and positioned horizontally so that the fibres were straightened and dried for 24 hours under ambient conditions.

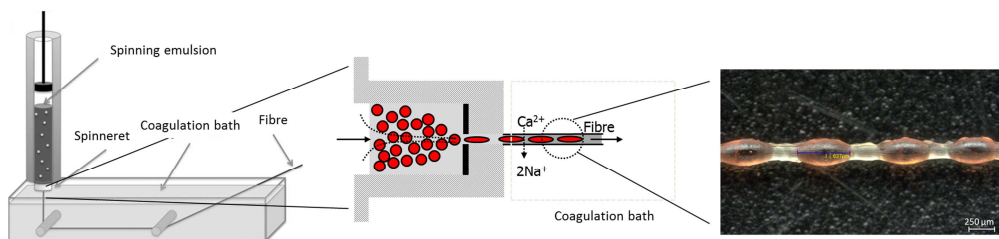


Figure 2.2 Overview of the compartmented fibre spinning process[18]

2.2.3. Composite production

Composites with three types of alginate fibres (10 wt.% MMT and a draw ratio of 2) were prepared:

- No healing agent: pure alginate fibres without encapsulated liquid
- 1 healing agent: compartmented fibres containing a mixture of Epikote and Tetrathiol (50/50 wt.%).
- 2 healing agents: compartmented fibres with either Epikote or Tetrathiol encapsulated.

The glass fibre fabric was cut into pieces of 150x200 mm and these were subsequently stacked in a $[0/90]_{2s}$ lay-up. In between one of the glass fibre fabric layers, 4 layers of alginate fibres were placed. One layer of fibres consists out of one batch of fibres spun on a Teflon roll with a fixed spacing of approximately 0.5 mm. For the composites containing 2 healing agents, 2 layers of Epikote filled and 2 layers of Tetrathiol filled fibres were used. The compartmented fibres were located either in between ply 1 and 2 for composites prepared for 4 point bending

experiments and in between ply 2 and 3 for composites prepared for double cantilever beam fracture testing. For the latter set of composites a Teflon film of 15 mm was inserted to serve as a notch in the fracture experiments.

After stacking, the composites were impregnated with the Epikote/Epikure resin (100/30 ratio by weight) using the hand lay-up method. To increase the reactivity of the healing agents upon fibre rupture, 1 wt.% of DMP-30 catalyst was added to the resin mixture. After 1 minute of manual stirring the resin was degassed for 20 minutes. The layers of glass fibre fabric and compartmented fibres were then impregnated layer by layer with the resin. After impregnation, bleeder material was placed to absorb the excess of resin and a vacuum bag is used to apply a constant absolute pressure of 100 mbar for 24 hours in which the product was cured. No additional post-curing was performed.

2.2.4. Fibre characterization

Uniaxial tensile tests were performed on the prepared fibres with a Zwick mechanical testing machine (model 1455) fitted with a 10N load cell. Experiments were performed at room temperature with a constant crosshead speed of 2 mm/min. A minimum of 10 fibres was tested per test condition. Vacuole lateral compression tests were performed using a custom-made microcompression instrument based on the setup of Keller and Sottos [10] and consists of a DC motor actuator and controller (M-230.25 DC and C-863 Mercury, Physik Instrumente, Germany) equipped with a 30 g load cell. The vacuoles were compressed at a rate of 1 $\mu\text{m/s}$. A minimum of 8 vacuoles was tested per test condition.

2.2.5. Composite characterization and healing

2.2.5.1. Mechanical characterization

Mode I opening of DCB specimens was performed based on the guidelines depicted in ASTM D5528. A Zwick mechanical testing machine (model 1455) equipped with a 20 kN load cell was used. Using a constant crosshead speed of 5 mm/min, crack growth was induced in between the 2nd and 3rd ply of the GFRP composite. The experiment was terminated when a final displacement of 60 mm was achieved. After creation of the initial opening, the samples were unloaded and the composites were left to heal for 10 days under ambient conditions while applying a minimal pressure (<0.1 bar) perpendicular to the crack plane to ensure contact between the damaged interfaces. After healing the specimen were retested following the same testing procedure as for the pristine samples.

In order to determine the potential of the compartmented fibre concept to undergo multiple damaging and healing events on different locations in the composite an adaptation of the flexural off-axis test described by Prajer et al. was implemented

[20]. As such, 4 point bending experiments were performed according to ASTM D7264 using a Zwick mechanical testing machine (model 1455) equipped with a 20 kN load cell. Specimen were cut into coupons of 15x100 mm with the alginate fibres aligned along the length of the specimen. The prepared coupons were then tested via 4 point bending using a span of 40 mm (span to depth 1:32) with the alginate fibres located at the tension side of the composites. A constant cross-head speed of 5mm/min was applied until a maximum strain of 2.0% was reached. Subsequently the flexural stress was calculated using equation (2.1) [29]:

$$\sigma_f = \left(\frac{3PL}{4bd^2} \right) \quad (2.1)$$

where σ_f is the flexural stress (MPa), L is the support span (mm), d is the depth of beam (mm), P is the measured load at a given point (N) and b is the beam thickness (mm). The flexural strain was calculated using equation (2.2) [29]:

$$\varepsilon_f = \frac{4.36Dd}{L^2} * 100 \quad (2.2)$$

where ε_f is the flexural strain (%) and D is the mid-span deflection (mm). The flexural modulus (E_B) was then calculated as the slope of the linear section of the stress-strain curve within the 0.5-1.0% strain range. After the initial test, healing was allowed under similar conditions as for the DCB mode I opening experiments. After healing the specimen were retested following the same approach but the position of the specimen was shifted (20 mm off-axis) compared to the first loading event so that a loading profile is obtained that ensures loading of both healed and non-healed regions.

2.2.5.2. Non-destructive healing evaluation

Air-coupled C-scanning (ACU) was carried out on manually healed specimen thereby simulating the healing process. The applied frequency was 200 kHz. Ultrasonic transducers with a focus distance of 38 mm and a focus spot size of 2 mm were set in transmission mode. The transducers were powered with 10 periods of carrier frequency and rectangular bursts of 200 V amplitude. The data acquisition unit included a 14-bit A/D converter with 5 MHz sampling frequency and 40 dB maximum amplification. Scanning steps of 1 mm along the x and the y-axes were performed with a scanning speed of 20 mm/s. Additionally, μ -Computed X-Ray tomography was performed on a composite panel damaged by Mode I DCB and healed under ambient conditions for 10 days using a ZEISS Xradia 520 Versa 3D X-ray microscope with a spatial resolution of 0.7 μ m.

2.3. Results & Discussion

2.3.1. Fibre characterization

To study the effect of MMT doping on the mechanical properties of the compartmented fibres, both the tensile properties of the fibres and the lateral compression properties of the vacuoles were investigated.

2.3.1.1. Fibre tensile properties

Figure 2.3 shows the representative stress-strain curves of compartmented fibres (containing vacuoles filled with Epikote resin) with MMT contents of 0, 10 and 20 wt.%. From this figure it can be seen that both the Young's modulus and the ultimate tensile strength (UTS) increase as the concentration of MMT clay particles is increased while the strain at break is unaffected. These trends are more quantitatively shown in Figure 2.4. All fibres were spun with an as-spun draw ratio of 3. As is expected for fibres spun with a non-optimized lab scale line, the results show a high level of scatter. This is more accurately reflected by the linearized Weibull distributions of the ultimate strength that show a rather low Weibull modulus of less than 3.5 for all sets of fibres [30].

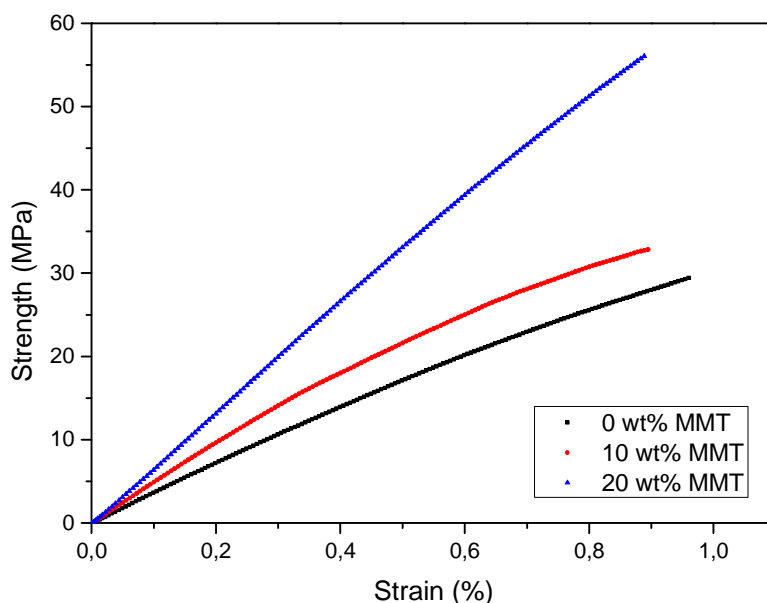


Figure 2.3 Representative tensile behaviour for compartmented fibres with different levels of MMT doping

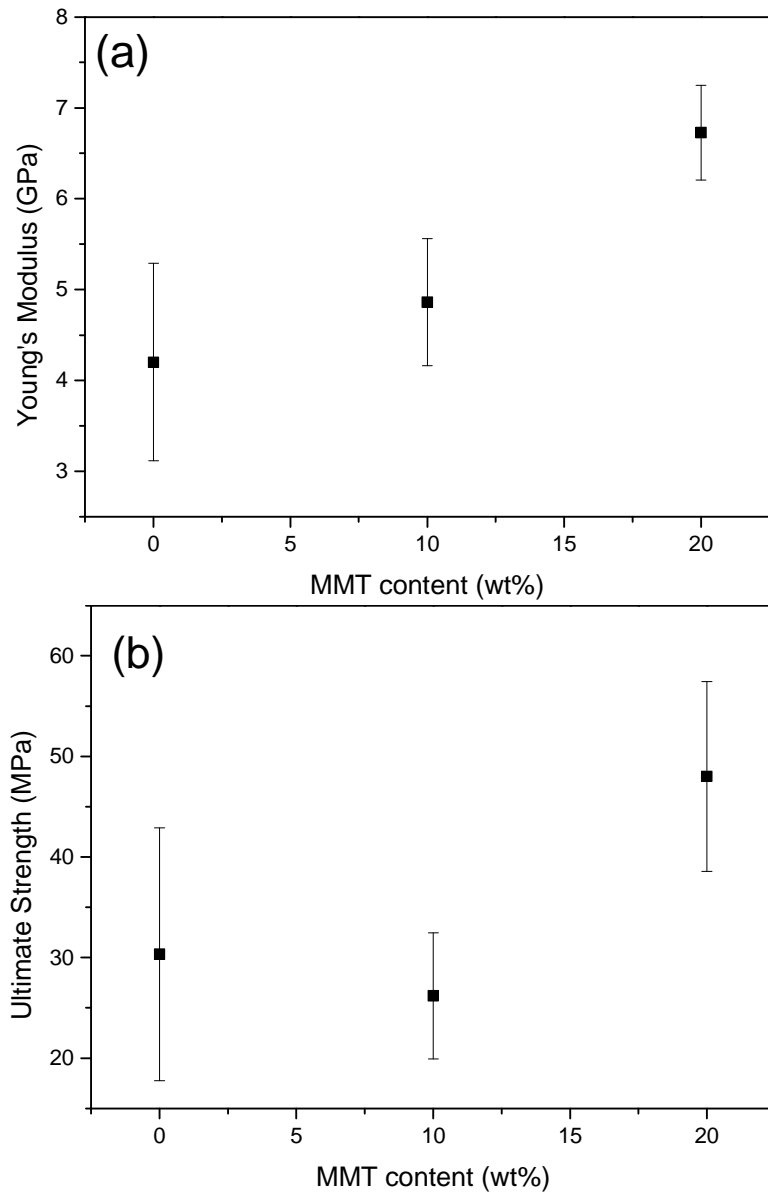


Figure 2.4 Young's modulus (a) and ultimate strength (b) dependency of compartmented fibres with different levels of MMT doping

To optimize the self-healing potential of compartmented fibres in polymer composites, it is required that the damage behaviour of the fibres can be modified so that it matches the mechanical properties of the matrix to be healed. Commercial epoxies typically have a Young's modulus of 3-6 GPa, a UTS of 35-100 MPa and a strain at break of 1-6% which is of the same order of the magnitude as the properties of the compartmented fibres developed [31]. The results from Figure 2.3

and Figure 2.4 therefore show that addition of compartmented fibres will not lower the mechanical properties and that by varying the MMT concentration in the spin dope it is possible to match the damage characteristics of a specific epoxy network.

However, ideally the compartmented fibres would also contribute to the load-bearing properties of fibre reinforced polymer composites and as such the Young's modulus has to match that of reinforcing fibres instead of the matrix material. It is found that the Young's moduli of the compartmented fibres are comparable to those typically found for natural fibres such as cotton or flax [31]. However, there is still a difference of 3 orders of magnitude compared to the moduli of high performance (E-glass/carbon) which implies that the mechanical properties of the compartmented fibres need to be significantly enhanced before they can contribute to the overall properties of structural composite materials. Zlopasa et al. found that the modulus of alginate films can be drastically increased when higher levels of MMT doping, up to 80 wt.% are used [27]. However, as it was found that with increasing MMT concentration the coagulation speed decreases, it was impossible to spin high quality fibres with MMT concentrations higher than 20 wt.% with the parameters used in this study. A similar trend was found for the effect of the draw ratio. It is expected that these problems can be partially resolved by increasing the residence time within the coagulation medium, but no further investigations on this matter were performed in this study.

2.3.1.2. Vacuole lateral compression properties

Figure 2.5 shows the representative lateral compression curves of compartmented fibre alginate vacuoles with 0, 10 and 20 wt.% MMT. The y-axis of Figure 2.5 shows the displacement over the initial diameter of the vacuole as was previously described by Keller and Sottos [10]. The results indicate that loading the alginate with 10 wt.% MMT slightly increases both the strength at break and the compression modulus of the vacuole compared to the non-doped alginate vacuoles. However, a clear drop in the lateral compressive properties can be observed for the vacuoles containing 20 wt.% of MMT. This effect is more clearly observed in Figure 2.6 in which the normalized compression modulus is given for each investigated concentration of MMT. The selected modulus is the relative slope of the measured force in the region where $d/D=0.1-0.15$. In addition, Table 2.1 gives an overview of the dimensional details and maximum compressive force measured for the fibres produced with the three MMT concentrations.

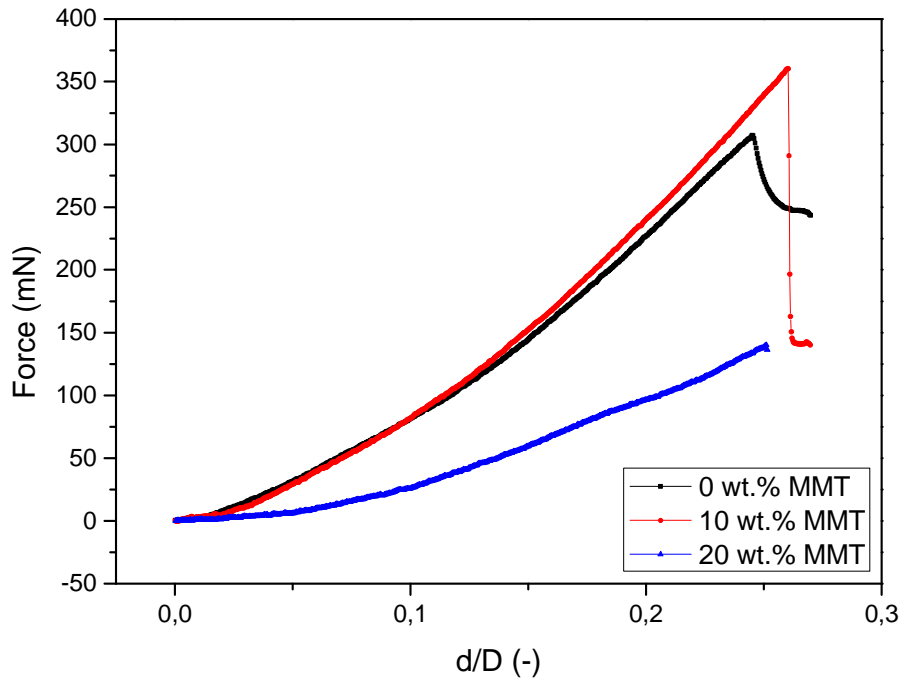


Figure 2.5 Representative force-displacement relations for lateral compression of vacuoles with different levels of MMT doping.

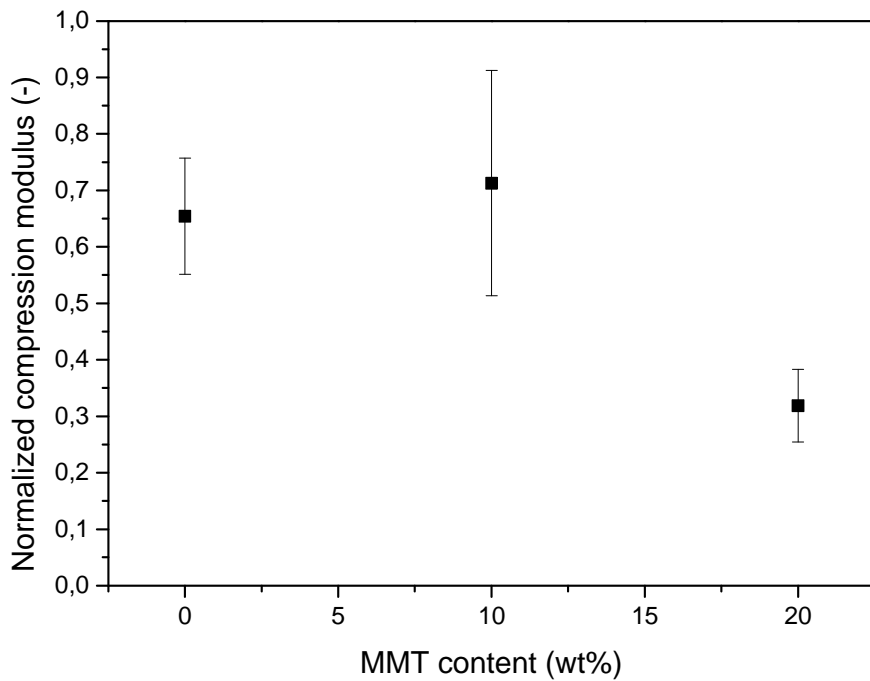


Figure 2.6 Compression modulus dependency of vacuoles with different levels of MMT doping.

Table 2.1 Overview of properties of capsules tested in lateral compression mode

| MMT wt. % | Diameter (mm) | Length (mm) | Volume (mm ³) | Max Force (mN) |
|-----------|---------------|-------------|---------------------------|----------------|
| 0 | 0,22±0,01 | 0,40±0,10 | 0,19±0,05 | 295,6±159 |
| 10 | 0,23±0,03 | 0,46±0,08 | 0,22±0,08 | 399,5±193 |
| 20 | 0,23±0,02 | 0,58±0,15 | 0,28±0,08 | 238,7±114 |

Upon comparing the vacuole lateral compression data with the fibre tensile results, a clear difference is observed for the fibres/vacuoles loaded with 20 wt.% MMT. Where high levels of MMT increase the tensile modulus, the opposite effect is observed for the compressive behaviour of the vacuoles. A possible explanation for this can be found in the difference in length of the vacuoles tested. As can be seen from Table 2.1, the average length of the 20 wt.% MMT vacuoles is higher than those with 10 and 0 wt.% MMT. It can be anticipated that the lateral compressive load profile will gradually change as the vacuole moves from a spherical to a conical shape (i.e. the effect of the liquid phase becomes more dominant) and that for this the longer vacuoles for geometrical reasons give rise to a lower compression modulus and maximum force. However, with the high scatter in the compression data and since the current fibre spinning process holds many parameters (e.g. vacuole wall thickness) that lie beyond the scope of this study, it is impossible to draw firm conclusions on this matter.

2.3.2. Composite characterization

To investigate the potential of compartmented fibres for the healing of high performance thermoset composites, model GFRPs containing alginate fibres without healing agent, one healing agent and two healing agents were prepared. These composites were then characterized via interlaminar fracture testing and flexural testing.

2.3.2.1. Interlaminar fracture properties

Delaminations were introduced within the compartmented fibre rich interface of the model GFRP composites via Mode I opening. Figure 2.7 shows the load-displacement curves of a pristine specimen and the three selected compartmented fibre configurations after 10 days of healing. From these results it can be clearly observed that the system with only one healing agent shows partial recovery of the interlaminar fracture properties. It is interesting to note that the fracture behaviour has changed compared to the pristine specimen. While the undamaged specimen shows a classical laminate fracture pattern containing multiple peak loads, the

healed specimen has a more gradual load development upon re-opening of the crack. This is attributed to the nature of the healed thiol-epoxy interface, which gives rise to a relatively soft polymer interlayer compared to the original amine-epoxy network.

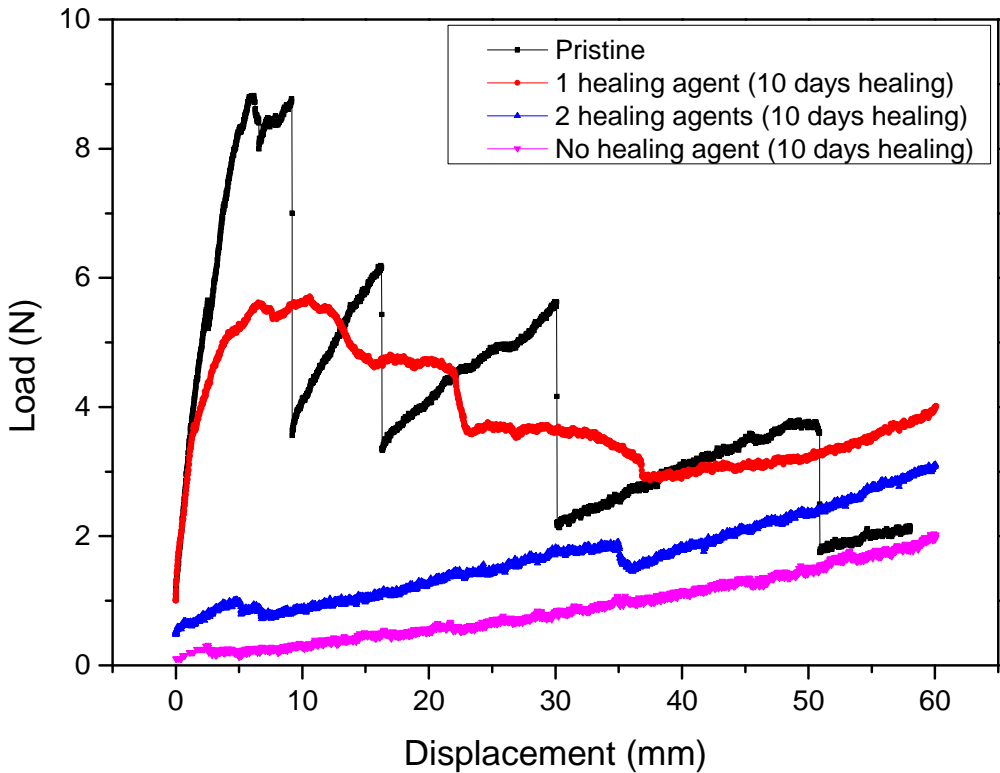


Figure 2.7 Mode I DCB opening of model GFRP composites with three different compartmented fibre configurations that were all damaged and then healed for 10 days.

In comparison to the single healing agent containing GFRP, the system with two healing agents shows only very minor recovery of mechanical integrity and an almost identical response as the non-healing specimen. The absence of healing in this composite can be readily explained by the additional healing conditions that need to be met. For adequate healing in this system, the rupture of two vacuoles from different compartmented fibres is required to trigger liquid release which should be followed by the proper mixing of these components. A potential solution to assist the mixing of two reactive components can be found in the development of binary capsule systems, but till this date no studies were reported on converting this approach to the compartmented fibre concept [12]. As this key limitation is not present in a system with only one healing agent, the results in Figure 2.7 clearly indicate that autonomous healing in a single agent system is more promising.

However, although the tertiary amine catalyst which is dispersed in the matrix is required for healing within an acceptable timeframe, it has to be stressed that the current single agent system will eventually cure even without catalyst intervention. As such, the investigated system is unsuitable for usage in actual self-healing applications with realistic deployment times.

To support the explanation provided for the recovery of the interlaminar fracture properties, x-ray micro-tomography scanning was performed. Figure 2.8 shows the cross-section of a composite with compartmented fibres containing the mixed epoxy/thiol healing agent configuration that was fractured in Mode I and healed for 10 days. The scan shows a clear distinction between the GFRP plies, the epoxy polymer and the compartmented alginate fibres. More interestingly, the figure shows that the induced crack propagated through several of the compartments and that these compartments released their healing agents into crack plane upon rupture. However, the damaged interface was not fully covered with healing agent and therefore complete recovery of the damaged interface is not expected. This observation corresponds with the partial healing that was observed during the mechanical evaluation depicted in Figure 2.7. Finally, the tomography image shows the presence of undamaged vacuoles, which indicates that a second healing event on a different location within the composite can still take place. This is a clear advantage compared to the more conventional interconnected fibre and vascular healing systems.

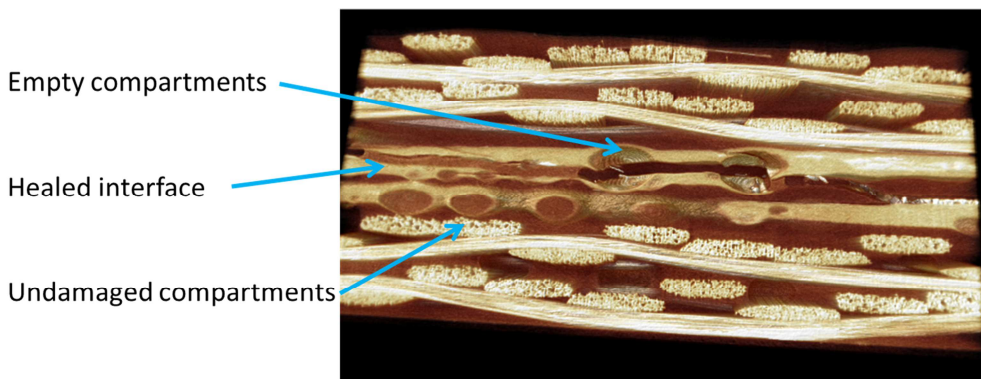


Figure 2.8 X-ray μ CT scan through the crack plane of a model GFRP composite with a single healing agent phase containing compartmented fibre interlayer. The specimen was healed for 10 days after Mode I opening.

Although the x-ray micro tomography scans show that the crack is partially filled, it does not give qualitative information on whether the liquid mixture was just present or was actually cured and therefore whether the healing event was really successful from a load bearing perspective. To contribute to the development of methods to measure healing non-destructively (for a more detailed study see Chapter 6 of this

thesis), a case study with air-coupled ultrasound (ACU) C-scanning was performed on GFRP composites. These composites were manually treated with different healing conditions by external healing agent injection analogous to the method used by Keller et al. [32]. Figure 2.9 shows the ACU C-scans of three different GFRP composites prior to Mode I opening and after treatments with no healing agent, a non-curing epoxy monomer, and a curing epoxy-thiol mixture respectively.

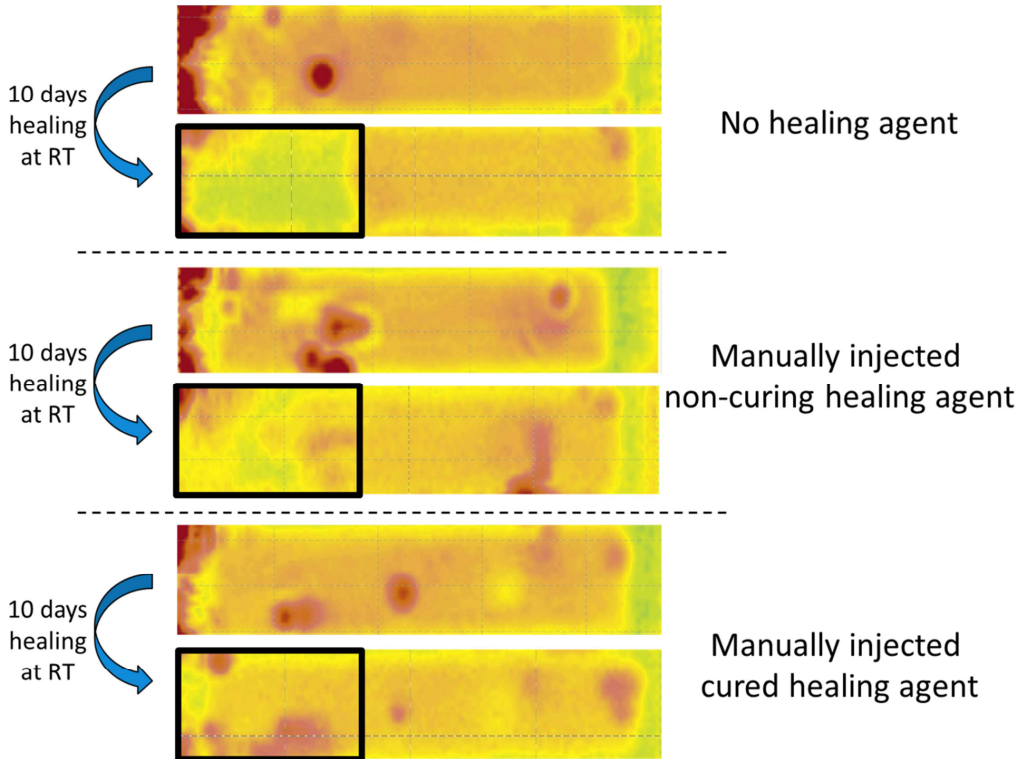


Figure 2.9 Model air-coupled ultrasound C-scanning investigation of the healing of Mode I crack opening of a specimen which after the initial damage was manually treated with no healing agent, a non-curing healing agent and a curing healing agent.

These results show that there is a clear difference in the level of transmission between an interface without healing agent and a cured healing agent. Based on these results it might seem reasonable to assume that the restoration of the ACU transmission level is accompanied with the mechanical restoration of the interface. However, the transmission level of the wetted, but non-healed, interface is comparable to the cured interface. At the same time, Figure 2.10 shows that the fracture response upon retesting is similar to that of the specimen without healing agent. These results therefore show that more extensive non-destructive characterization is required to confirm that a crack filled with healing agent is de

facto restored. As such, C-scanning techniques might not be the most appropriate approach to evaluate healing behaviour in extrinsic polymer systems.

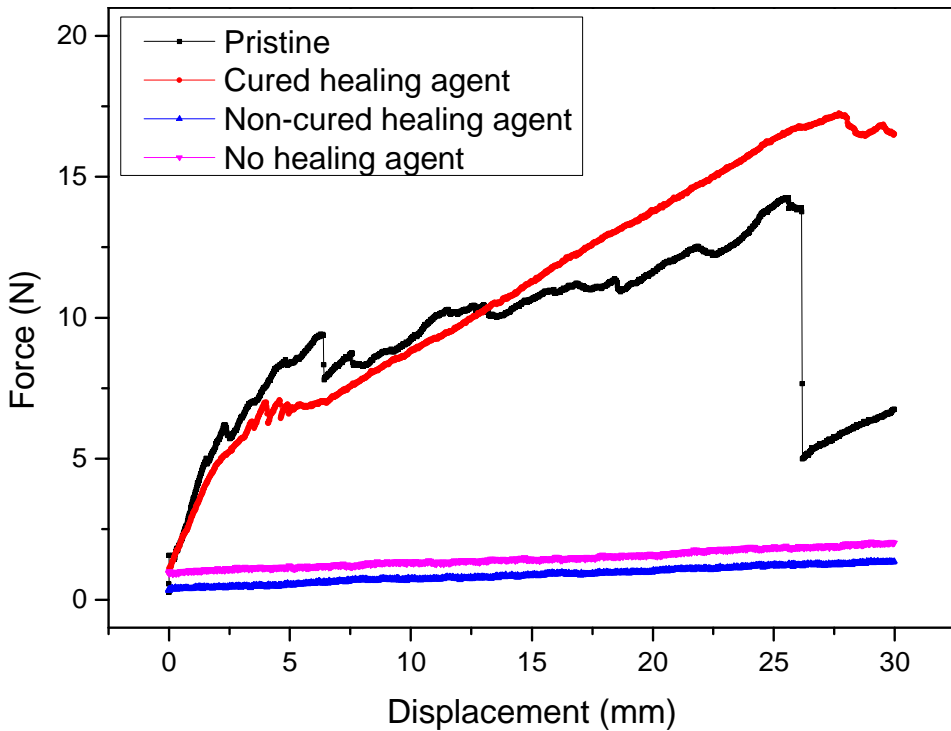


Figure 2.10 Load-displacement curves of the Mode I DCB opening of model GFRP composites which were manually treated to different healing conditions.

2.3.2.2. *Flexural properties*

The potential of compartmented fibre containing GFRPs to undergo multiple damage and healing events at different locations is evaluated by off-axis 4 point bending. Figure 2.11 and Figure 2.12 show the effect of autonomous healing on the ultimate flexural strength and flexural modulus of the different healing configurations used throughout this study. Non-healed and healed specimen were re-tested within a 2 hour and 10 day timeframe respectively.

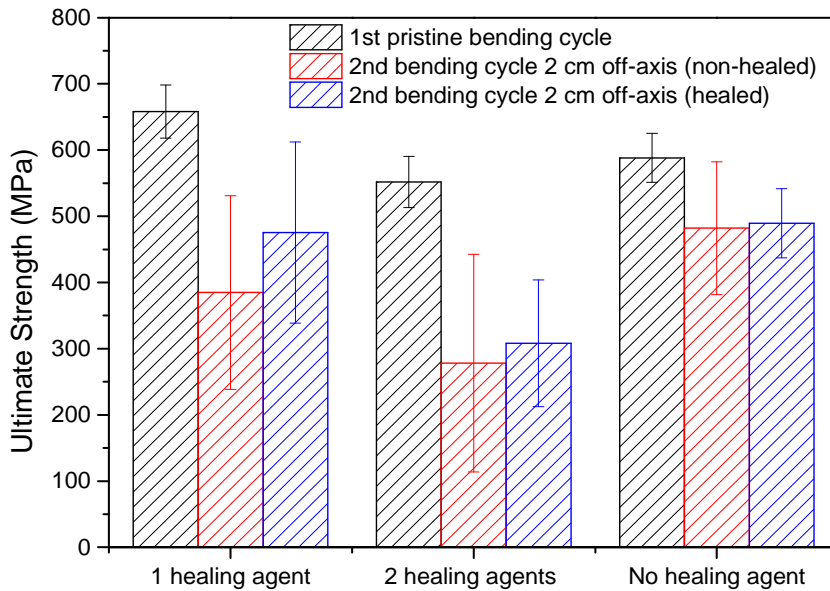


Figure 2.11 Ultimate strength of GFRP composites with different types of alginate fibres. Non-healed specimen are tested within a 2 hour time frame whereas healed specimen were given 10 days healing time.

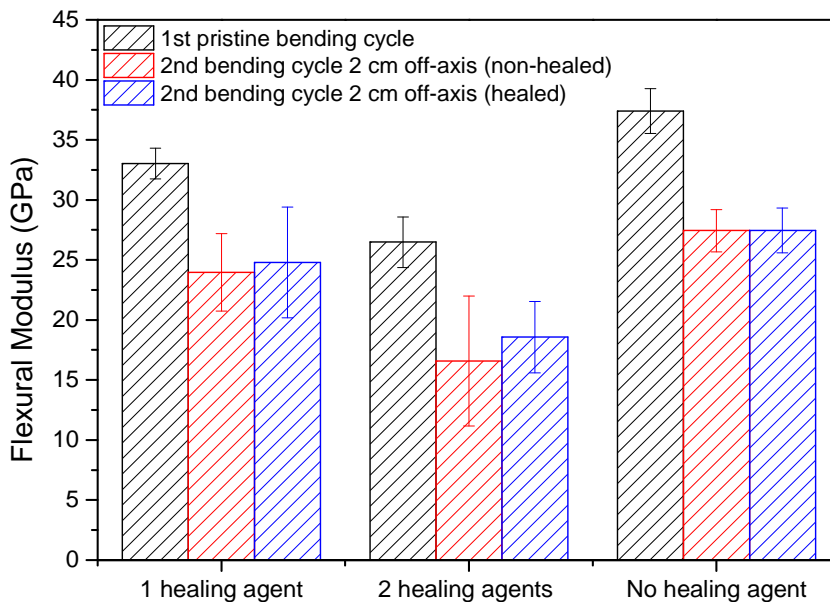


Figure 2.12 Flexural modulus of GFRP composites with different types of alginate fibres. Non-healed specimen are tested within a 2 hour time frame whereas healed specimen were given 10 days healing time.

The results of the pristine tests show that both the flexural strength and modulus are comparable to that of commercial GFRP composites and that the incorporation of the compartmented fibres does not have a negative effect on their initial performance. When healing is considered, it is shown that the increase in flexural strength after healing is larger for the composites with a single healing agent than for those with two healing agents. As expected, the specimen without healing agent show no difference in strength between retesting after 2 hours or 10 days. These observations are in line with the results obtained for the recovery of the interlaminar fracture properties. However, the relative level of healing in these experiments is much lower compared to the healing showed in Figure 2.7. This can be explained by the fact that during the flexural testing procedure both the matrix and the non-healable glass fibre fabric are damaged whereas the interlaminar fracture testing localized the damage within the matrix.

Compared to healing of strength observed in Figure 2.11, Figure 2.12 shows only a minimal recovery of the flexural modulus for both healing agent configurations. This is attributed to the fact that the composite modulus is mainly governed by the much stiffer glass fibres and as such the repair of the matrix is less reflected in this parameter. Although both the strength and modulus show a certain degree of repair, it can also be observed that the obtained levels of healing result in values that are below those obtained for the 2nd bending cycle of the “no healing agent” configuration. This indicates that the levels of healing obtained do not outweigh the loss in damage tolerance. Furthermore it has to be noted that for the majority of the model composites, ultimate failure during the 2nd bending cycle still occurred within the initially damaged region of the composite and therefore does not lead to a second healing event as no new vacuoles were ruptured during the process. Altogether, these results therefore show that the incorporation of compartmented fibres might not be the appropriate approach for the autonomous healing of flexural damage events in high performance FRPCs.

2.4. Conclusion

The feasibility of using compartmented alginate fibres as healing agent carriers for the autonomous self-repair of GFRP composites is investigated. First it is shown that the fibre tensile properties can be improved by an increased level of MMT clay doping. As such, the mechanical properties of the compartmented fibres can be modified to match those of the selected epoxy matrices. The second part of this study shows a proof of concept of compartmented fibre healing in model GFRP composites. A thiol-epoxy based healing chemistry is selected and a one- and a two healing agent configuration are compared. Interlaminar fracture and off-axis flexural bending experiments show that a one agent configuration is highly favourable over a system with two agents. Furthermore, the mechanical characterization showed that the compartmented fibre technology should focus on the healing of matrix damage only as the loss of mechanical integrity upon glass fibre fracture cannot be overcome. Even with an assumed significant further improvement in fibre properties and healing efficiency there is a serious concern whether the loss in initial properties and damage resistance of high quality fibre reinforced composites is sufficiently compensated by the intended self-healing ability.

References

1. Dry, C., *Procedures developed for self-repair of polymer matrix composite materials*. Composite Structures, 1996. 35(3): p. 263-269.
2. White, S.R., Sottos, N.R., Geubelle, P.H., Moore, J.S., Kessler, M.R., Sriram, S.R., Brown, E.N., and Viswanathan, S., *Autonomic healing of polymer composites*. Nature, 2001. 409(6822): p. 794-797.
3. Trask, R.S. and Bond, I.P., *Biomimetic self-healing of advanced composite structures using hollow glass fibres*. Smart Materials and Structures, 2006. 15(3): p. 704-710.
4. Kirkby, E.L., Rule, J.D., Michaud, V.J., Sottos, N.R., White, S.R., and Månson, J.A.E., *Embedded shape-memory alloy wires for improved performance of self-healing polymers*. Advanced Functional Materials, 2008. 18(15): p. 2253-2260.
5. Zhong, N. and Post, W., *Self-repair of structural and functional composites with intrinsically self-healing polymer matrices: A review*. Composites Part A: Applied Science and Manufacturing, 2015. 69(0): p. 226-239.
6. García, S.J., *Effect of polymer architecture on the intrinsic self-healing character of polymers*. European Polymer Journal, 2014. 53(0): p. 118-125.
7. White, S.R., Moore, J.S., Sottos, N.R., Krull, B.P., Santa Cruz, W.A., and Gergely, R.C.R., *Restoration of large damage volumes in polymers*. Science, 2014. 344(6184): p. 620-623.
8. Blaiszik, B.J., Kramer, S.L.B., Olugebefola, S.C., Moore, J.S., Sottos, N.R., and White, S.R., *Self-healing polymers and composites*, in *Annual Review of Materials Research*. 2010. p. 179-211.

9. Brown, E.N., White, S.R., and Sottos, N.R., *Retardation and repair of fatigue cracks in a microcapsule toughened epoxy composite - Part II: In situ self-healing*. Composites Science and Technology, 2005. 65(15-16 SPEC. ISS.): p. 2474-2480.
10. Keller, M.W. and Sottos, N.R., *Mechanical Properties of Microcapsules Used in a Self-Healing Polymer*. Experimental Mechanics, 2006. 46(6): p. 725-733.
11. Manfredi, E., Cohades, A., Richard, I., and Michaud, V., *Assessment of solvent capsule-based healing for woven E-glass fibre-reinforced polymers*. Smart Materials and Structures, 2015. 24(1).
12. Mookhoek, S.D., Blaiszik, B.J., Fischer, H.R., Sottos, N.R., White, S.R., and van der Zwaag, S., *Peripherally decorated binary microcapsules containing two liquids*. Journal of Materials Chemistry, 2008. 18(44): p. 5390-5394.
13. Pang, J.W.C. and Bond, I.P., *A hollow fibre reinforced polymer composite encompassing self-healing and enhanced damage visibility*. Composites Science and Technology, 2005. 65(11-12): p. 1791-1799.
14. Luterbacher, R., Coope, T.S., Trask, R.S., and Bond, I.P., *Vascular self-healing within carbon fibre reinforced polymer stringer run-out configurations*. Composites Science and Technology, 2016. 136: p. 67-75.
15. Norris, C.J., Meadway, G.J., O'Sullivan, M.J., Bond, I.P., and Trask, R.S., *Self-healing fibre reinforced composites via a bioinspired vasculature*. Advanced Functional Materials, 2011. 21(19): p. 3624-3633.
16. Toohey, K.S., Sottos, N.R., Lewis, J.A., Moore, J.S., and White, S.R., *Self-healing materials with microvascular networks*. Nature Materials, 2007. 6(8): p. 581-585.
17. McCulloh, K.A., Sperry, J.S., and Adler, F.R., *Water transport in plants obeys Murray's law*. Nature, 2003. 421(6926): p. 939-942.
18. Mookhoek, S.D., Fischer, H.R., and van der Zwaag, S., *Alginate fibres containing discrete liquid filled vacuoles for controlled delivery of healing agents in fibre reinforced composites*. Composites Part A: Applied Science and Manufacturing, 2012. 43(12): p. 2176-2182.
19. Mookhoek, S.D., Fischer, H.R., and van der Zwaag, S., *A numerical study into the effects of elongated capsules on the healing efficiency of liquid-based systems*. Computational Materials Science, 2009. 47(2): p. 506-511.
20. Prajer, M., Wu, X., García, S.J., and van der Zwaag, S., *Direct and indirect observation of multiple local healing events in successively loaded fibre reinforced polymer model composites using healing agent-filled compartmented fibres*. Composites Science and Technology, 2015. 106(0): p. 127-133.
21. Billiet, S., Hillewaere, X.K.D., Teixeira, R.F.A., and Du Prez, F.E., *Chemistry of crosslinking processes for self-healing polymers*. Macromolecular Rapid Communications, 2013. 34(4): p. 290-309.
22. Hillewaere, X.K.D. and Du Prez, F.E., *Fifteen chemistries for autonomous external self-healing polymers and composites*. Progress in Polymer Science, 2015. 49-50: p. 121-153.

23. Pavlidou, S. and Papaspyrides, C.D., *A review on polymer-layered silicate nanocomposites*. Progress in Polymer Science, 2008. 33(12): p. 1119-1198.
24. Sinha Ray, S. and Okamoto, M., *Polymer/layered silicate nanocomposites: a review from preparation to processing*. Progress in Polymer Science, 2003. 28(11): p. 1539-1641.
25. Bershtein, V., Fainleib, A., Egorova, L., Gusakova, K., Grigoryeva, O., Kirilenko, D., Konnikov, S., Ryzhov, V., Yakushev, P., and Lavrenyuk, N., *The impact of ultra-low amounts of amino-modified MMT on dynamics and properties of densely cross-linked cyanate ester resins*. Nanoscale Research Letters, 2015. 10(1): p. 165.
26. Bhat, S.D. and Aminabhavi, T.M., *Novel sodium alginate-Na+MMT hybrid composite membranes for pervaporation dehydration of isopropanol, 1,4-dioxane and tetrahydrofuran*. Separation and Purification Technology, 2006. 51(1): p. 85-94.
27. Zlopasa, J., Norder, B., Koenders, E.A.B., and Picken, S.J., *Origin of highly ordered sodium alginate/montmorillonite bionanocomposites*. Macromolecules, 2015. 48(4): p. 1204-1209.
28. Boguń, M. and Rabiej, S., *The influence of fiber formation conditions on the structure and properties of nanocomposite alginate fibers containing tricalcium phosphate or montmorillonite*. Polymer Composites, 2010. 31(8): p. 1321-1331.
29. *Standard Test Method for Flexural Properties of Unreinforced and Reinforced Plastics and Electrical Insulating Materials by Four-Point Bending*. 2017, ASTM International.
30. van der Zwaag, S., *The Concept of Filament Strength and the Weibull Modulus*. 1989.
31. Ku, H., Wang, H., Pattarachaiyakoo, N., and Trada, M., *A review on the tensile properties of natural fiber reinforced polymer composites*. Composites Part B: Engineering, 2011. 42(4): p. 856-873.
32. Kessler, M.R., Sottos, N.R., and White, S.R., *Self-healing structural composite materials*. Composites Part A: Applied Science and Manufacturing, 2003. 34(8): p. 743-753.

Chapter 3

Self-repair of structural and functional composites with intrinsically self-healing polymer matrices: A review

This chapter has been published as:

Zhong, N. and **W. Post**, *Self-repair of structural and functional composites with intrinsically self-healing polymer matrices: A review*. Composites Part A: Applied Science and Manufacturing, Volume 69, February 2015, Pages 226-239

3.1. Introduction

Over the last decades the amount of studies reporting on polymer composite functionality and mechanical properties has grown significantly. Polymer composites showing for example thermal and electrical properties can be found in daily life in communication, lightning and aerospace applications [1, 2]. Although the field of multifunctional polymer composites is increasing rapidly, researchers are far away from reaching the diversity in functionalities that nature has established in its composites over the past millions of years. Wood is one of nature's finest examples of a multifunctional fibrous composite material. This well-known material consists of parallel hollow tubular cells reinforced by spirally wound cellulosic fibrils embedded in a hemicellulose and lignin matrix. The helix angle of the spiral fibrils is responsible for a variety of mechanical properties such as wood stiffness and toughness, whereas the hollow tubular cells are capable of transporting nutrients from the soil to the top parts of a tree [3]. Also skeleton bones deliver optimal mechanical properties due to a smart combination of material selection and material shaping [4].

Besides a variety of mechanical and functional properties, wood and bone possess the capability to self-repair damage that is inflicted to their components [5]. Since both structural and functional polymer composites show a drop in performance when subjected to a certain cyclic or impact loading due to the formation of cracks or delamination, a bio-inspired system that autonomously restores the material properties is considered tremendously valuable. Therefore, in the past two decades, the self-healing capacity has inspired many researchers to design polymer composites that are capable of healing damage rather than preventing it [6, 7]. This field was pioneered by Dry who included hollow glass fibers containing liquid adhesive in a concrete matrix. The liquid agent is released upon local fracture, wets the crack surface and crosslinks thereby partially restoring the load bearing capacity [8, 9]. White et al. showed the recovery of tensile strength of an epoxy material by embedding polymeric microcapsules filled with crosslinkable liquid oligomer into the polymer matrix with dispersed Grubbs catalyst [10]. However, since it is quite challenging to obtain a uniform distribution of healing agent using particulate containers, Bond et al. developed a self-healing fiber reinforced composite by introducing glass fibers filled with healing agent. The resulting composite was capable of restoring a significant amount of its original flexural strength [11].

At the pioneering start of the field of self-healing composites, the employed healing strategies are extrinsic (i.e. are due to the inclusion of discrete entities containing the healing agents in an otherwise non-self-healing surroundings) and therefore in principle only a single healing event can occur at the same damaged site. This concept was further improved by Toohey et al. who developed a bio-inspired

vascular system capable of repeated healing of an epoxy coating. The healing strategy, however, still relies on the inclusion of external healing agent [12]. In more recent years, the intrinsically self-healing route (i.e. the architecture of the polymer is such that local damage can be restored upon a mild proper trigger by the reformation of reversible chemical bonds) was shown as an attractive alternative. Due to the reversible character of the chemical bonds involved in the healing (and breaking) process, intrinsically self-healing polymers can theoretically lead to an infinite amount of healing cycles as no external healing agents are required. However, where extrinsic healing systems are capable of healing polymers with large scale damages up to 35 mm as was recently reported by White et al.[13], intrinsic healing strategies are reported to be well suited for healing small scale damages, but restoration of larger damages remains a challenge because the contact between the failed surfaces is often lost. The intrinsic healing process depends on the ability of the matrix to acquire local mobility upon the stimulation of an external stimulus, such as temperature, light induction, electrical current and moisture exposure. Therefore, in contrast with their extrinsic counterparts, intrinsic healing materials are generally not fully autonomous. Intrinsic healing systems will require the input of extra energy which in some cases can be supplied by the damage event itself (e.g. impact damage in ionomers [14, 15]). Alternatively, damage has to be detected by a sensor or the composite has to be exposed periodically to its healing trigger. Still, the implementation of theoretically infinitely repeatable intrinsic healing in polymer composites is considered as a valuable addition to the development of materials that are designed to mend damage rather than preventing it [7, 16, 17].

The majority of studies that cover the intrinsic healing of polymer composites reported on the healing of structural properties (i.e. properties related to load bearing behavior, such as stiffness, strength and failure strain), whereas the field of general self-healing polymer functionality (including healing of non-mechanical properties such as thermal conduction, electrical conduction and magnetic shielding etc.) is emerging only in the last couple of years. However, damage (upon fatigue or impact loading) in either the polymer matrix (cracks) or at the matrix-filler interface (delamination) is responsible for a decrease in the properties of both structural and functional polymer composites, because the filler material is no longer capable of transferring its specific properties towards the matrix material. (In structural composites, reinforcing fibers and particles are customarily referred to as the 'reinforcement', while in functional composites, the added fibers or particles are referred to as 'filler'. In order to maintain consistency of text, in this review we only use the term 'filler' to refer to the non-continuous non-polymer constituent in the composite.) Therefore healing strategies in both types of composites can be similar and will be most effective in the form of a polymer matrix capable of restoring either

itself or the matrix-filler interface. For this reason the development of polymer matrices that can intrinsically heal themselves or restore the adhesive properties at the composite interface is considered to be a major challenge within the field of self-healing polymers. This review aims to give an overview of the progress that is made on intrinsic matrix healing of both structural and functional properties in polymer composites. Firstly, the current developments in intrinsic polymer matrix healing are discussed, grouped by the triggering mechanism for the healing process. Secondly, the general concepts and influence of filler materials on structural composite properties (stiffness, strength) and their healing capabilities is covered. Finally, a similar approach is used to analyze the self-healing potential of functional (electrical, electromagnetic, electromechanical, magnetic and thermal) polymer based composites.

3.2. Intrinsically self-healing matrix polymers

In structural and functional composites, polymers, such as polyester, polyimide, polyurethane, epoxy or silicone rubber, are used as matrix because of their ability to bind and preserve the location of the filling materials, their low density, chemical inertness, low cost and versatility in fabrication methods. Traditionally polymer based composite systems were composed such that a maximum resistance to local mechanical, thermo-mechanical or chemo-mechanical degradation is obtained. Very often the optimization focused on creating a lasting chemo-mechanical bond between the polymer matrix and the fillers. This conventional optimization damage, virtually always starting in the polymer matrix or at the matrix-particle interface, was treated as an irrecoverable event. However, with the advent of intrinsically self-healing polymers, i.e. polymers which can restore mechanical bonding with itself or a different material due to reformation of chemical bonds under the appropriate stimulus (see Figure 3.1 and Figure 3.2), the design concepts for composites have changed significantly and irreversibly. Below, we describe the range of self-healing polymers and group them according to the trigger they need to heal cracks and interfacial delamination.

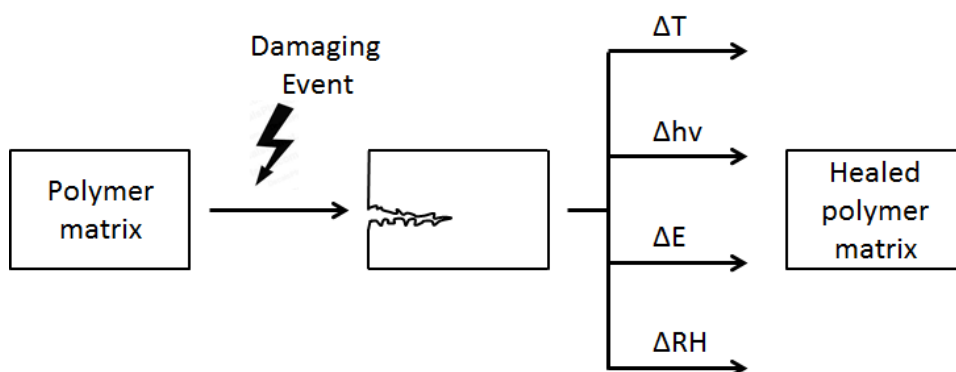


Figure 3.1 Schematic representation of intrinsic self-sealing by external stimuli; thermal, photochemical, electrical and moisture activation.

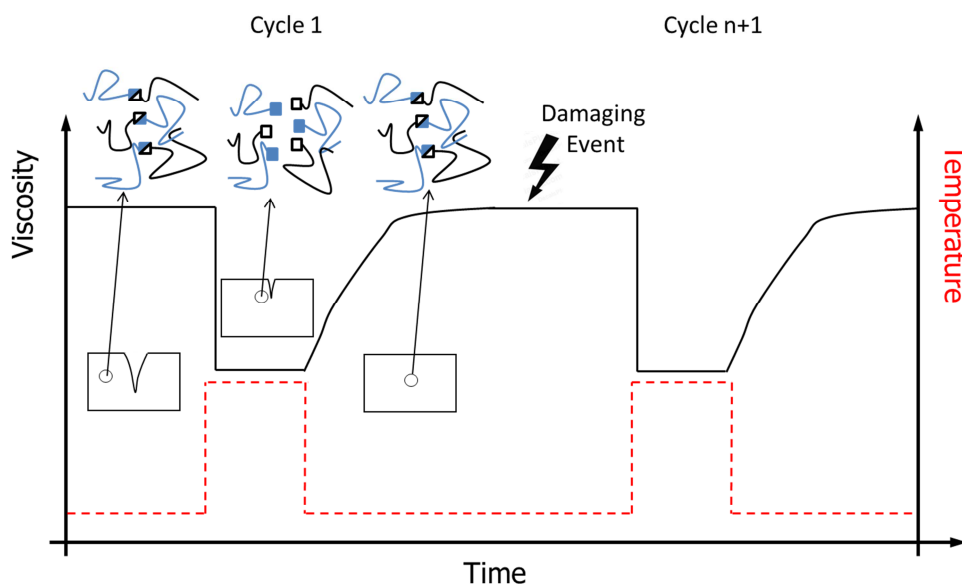


Figure 3.2 General concept of matrix healing using intrinsic healing concepts. The figure shows a sudden drop in viscosity upon heating linked to local temporary network mobility necessary for flow and damage repair. Upon cooling the local properties (e.g. viscosity) are restored to initial values so the material can be further used. The figure also shows the multiple healing events possible with intrinsic healing concepts [7].

3.2.1. Heat triggered self-healing

Intrinsic self-healing polymers based on heat triggered reversible reactions have been studied extensively, because it is relatively practical to apply heat as stimulus compared to other stimuli such as light, electrical fields or moisture. Among the thermally activated self-healing polymers, the Diels-Alder/retro-Diels-Alder reaction (DA/rDA) has received most of the attention. The Diels-Alder reaction is a reversible

reaction that takes place between a conjugated diene and a substituted alkene, usually termed the dienophile to form a substituted cyclohexene system. The DA/rDA reaction can be used as healing mechanism in multiple polymer systems (e.g. polyamide, polyethylene and epoxies) and can be used to heal both the matrix and the matrix-filler interface. The latter one is schematically depicted in Figure 3.3. The healing temperature ranges from 100°C to 150°C and the healing times were reported in the range of 10 minutes to 2 hours [18-26].

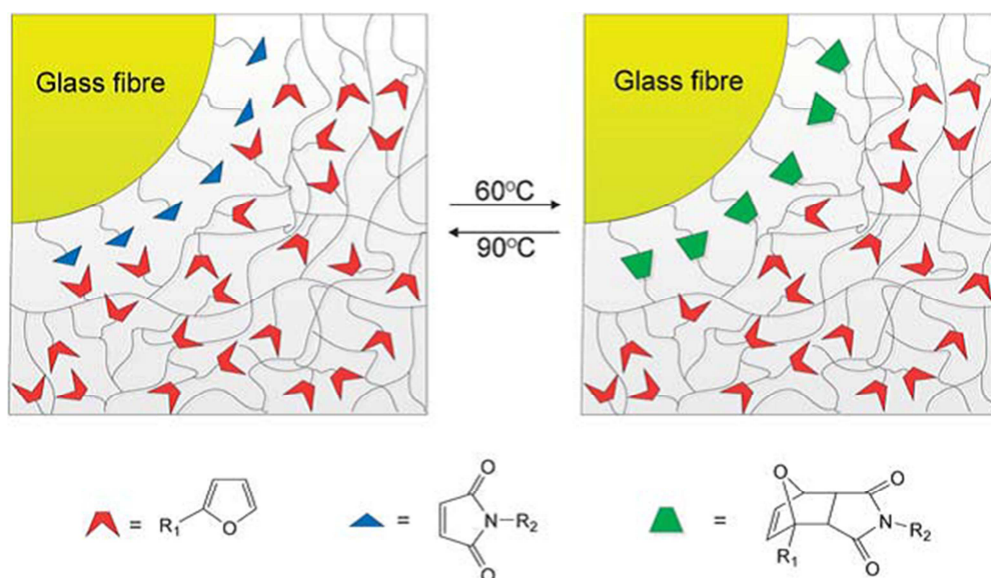


Figure 3.3 Self-healing of composite strength via a reversible Diels-Alder reaction at the fiber-matrix interface. Glass fibers are functionalized with maleimide functionalized groups (blue figures) and placed in a furan group (red figures) containing polymer network. The resulting composite is capable of thermoreversible interface healing resulting in restoration of stress transfer between fibers and matrix [27, 28].

A second type of thermally activated self-healing was introduced by Canadell et al. who used remendable disulfide chemistry in a covalently cross-linked rubber [29]. In their work, an epoxy resin containing disulfide groups was cross-linked with a tetrafunctional thiol in a base-catalyzed addition reaction. Upon fracture, the mechanical properties of this material can be fully restored by re-contacting the fractured surfaces while heating at 60°C for 1h. A more recent study showed that the dominant healing mechanism is based on the thiol-disulfide exchange and that reaction is highly pH dependent [30]. An advantage of using disulfide chemistry as self-healing mechanism is that healing can be achieved at moderate temperatures, while keeping a reasonable level of bond strength.

Another example of self-healing by a thermal stimulus is the radical exchange reaction of alkoxyamine units that can be used to prepare a thermodynamic polymer

cross-linking system [31, 32]. Based on this mechanism, Yuan et al. developed self-healing polystyrene with alkoxyamine side chains which function as cross-linker. In this system, fission and radical recombination of C-ON bonds takes place among alkoxyamine moieties when a thermal stimulus is applied. The healing efficiency of this system reaches values of 75.9% by heating upon 130°C for 2.5 hours [33].

Besides the aforementioned thermally triggered covalent self-healing systems, matrices can use supramolecular interactions, such as hydrogen bonding and π - π interactions, as a mechanism for intrinsic healing. In healing systems based on hydrogen bonding, mending will occur already at room temperature when the functional groups are brought into effective contact with each other. However, the healing efficiency decreases with increasing waiting time between the damage event and mending because the free hydrogen bonds can rearrange and associate with one another at the fractured surface instead of those on the other side of the crack. Moreover, the elevation of the healing temperature can increase the molecular dynamics and accelerate the equilibrium, thereby decreasing the healing time [34-40].

A second system capable of supramolecular healing is based on π -electron-poor receptors and π -electron-rich pyrenyl end-groups. Here, the healing mechanism involves two steps. The first step is the disruption of the intermolecular π - π stacking cross-links upon an increased temperature. The second step is the rearrangement of chains and reformation of π - π stacking cross-links when the temperature is lowered. The healing temperature is reported to be around 100°C with healing time more than 2 hours [41-43].

Ionomers are another class of thermally activated supramolecular self-healing polymers that possess the ability to heal ballistic impact damage. In ionomers, ionic metal salts are bonded to the polymer backbone creating electrostatic interactions. The local heat that is released upon impact enables these bonds to reform and thereby heal the material. Studies on ionomer healing focused on the autonomous healing after high speed ballistic impact [44, 45] and on the stimulated self-healing after quasi static damage production [46-49].

Heat triggered self-healing polymers are excellent candidates as matrix material in polymer composites that can easily be exposed to a heat source. The heat triggered matrix material should be selected on the basis of the nominal working temperature of the desired application and the thermal fluctuations during product use. Hence, for some applications, it may be practically impossible to apply a proper thermal healing treatment and systems based on a different healing trigger might be more appropriate. Three other types of self-healing stimuli are presented below.

3.2.2. Photochemical triggered self-healing

Besides thermal activation, self-healing behavior can be triggered by photochemical reactions. Based on photochemical [2+2] cycloaddition of cinnamoyl groups, Chung et al. developed a self-healing polymer from 1,1,1-tris-(cinnamoyloxymethyl)ethane, which is a photo-cross-linkable cinnamate monomer [50]. In their study, healing was conducted by photoirradiation ($\lambda > 280$ nm) for 10 minutes. More recently, Ling et al. and Oya et al. continued this line of research by synthesizing novel self-healing polymers based on [2+2] photocycloaddition [51, 52].

Another example of photochemically triggered healing was reported by Ghosh et al. who developed a self-healing oxetane-substituted chitosan polyurethane [53]. Upon fracture, four-membered oxetane rings open up thereby creating two reactive ends. When the crack plane is exposed to ultraviolet light ($\lambda=302$ nm), chitosan chain scission occurs, which forms crosslinks between the reactive oxetane ends and repairs the network in less than 1 hour.

Amamoto et al. showed two novel studies on self-healing polymers by photoinduced reshuffling of disulphide bonds. First, they introduced self-healing in poly(*n*-butyl acrylate) by including repeatable trithiocarbonate units [54]. These polymers are capable of healing macroscopic cracks almost completely after UV irradiation ($\lambda=330$ nm) for 48 hours. In a second study, they reported on macroscopic self-healing crosslinked polyurethanes based on radical reshuffling of thiuram disulfide units under the stimulation of visible light at room temperature [55].

Moreover, photochemical self-healing in metallosupramolecular polymers were reported by Burnworth et al.. Their low-molecular-mass polymers possess ligand end groups that are non-covalently linked through metal-ion binding [56]. Samples were healed by exposure to UV light leading to a temporary disengagement of the metal-ligand bonds.

Polymers that heal upon a photochemical trigger have a potential healing time that ranges from minutes to days, which can be advantageous over heat triggered polymers which generally need at least several hours for proper healing. Therefore, photochemical triggered self-healing polymers can be a good choice as matrix material when fast healing is required. However, due to light scattering at matrix-filler interfaces the penetration depth of light into a composite will be limited and the approach will be restricted to very thin, sheet like composite structures.

3.2.3. Electrically triggered self-healing

Matrix healing upon electrical stimulus was proposed by Chuo et al. who prepared an electrically triggered self-healing polymeric material based on the complexation reaction between ferrocene modified poly(glycidylmethacrylate) and β -cyclodextrin groups [57]. A knife-cut crack on the surface of this sample mends almost completely after an electrical treatment of 9V for 24 hours followed by a resting period at room temperature for another 24 hours. The healing efficiency can be improved by an additional thermal treatment (85°C, 24 h) after the electrically induced repairing process. Although the number of studies on this topic is rather limited, self-healing based on electric stimuli has a great potential in electronic applications, because the healing will be instigated while the component is still functioning.

3.2.4. Moisture triggered self-healing

Another stimulus that triggers self-healing in polymers was reported by Zhang et al.[58]. They synthesized an isocyanate containing methacrylate monomer copolymer system that repairs macroscopic cracks after a relative humidity treatment (95% at 30°C) of 12 hours and serves as a protecting fluorine-containing monomer component. Healing is based on a zipper-like healing mechanism in which the isocyanate groups on both sides of the crack within the effective contact areas are coupled by reacting with environmental water. This process can be gradually extended to the ineffectively contacted areas which ultimately results in full closure and healing of the crack.

Taking the different self-healing stimuli into account, it is clear that heat triggered intrinsic self-healing is currently the most developed strategy. However, based on the actual application of a polymer composite, a different healing mechanism might be more appropriate in order to reduce the healing time or to create a system that heals while functioning.

3.3. Structural composites containing an intrinsically self-healing polymer matrix

Structural composites are optimized to give desirable mechanical properties, in particular (specific) stiffness and mechanical strength. The strength and stiffness of such composites depends on the properties of the constituent phases (polymer matrix and inorganic filler), their volume fraction and their configuration. To realize their full potential a perfect bonding between the matrix and the filler particles is required. As the inorganic fillers are based on strong irreversible (non-self-healing) covalent bonds, any self-healing has to come from the polymer matrix which (in

principle) can restore the integrity of the matrix as well that of the interfacial bond. Below we demonstrate how the principal mechanical properties are to be affected by a self-healing polymer matrix.

3.3.1. Stiffness recovery

The stiffness of a material is defined by the ratio between stress and strain (Young's modulus or modulus of elasticity) at the elastic regime of a tensile experiment and describes the resistance to elastic deformation of a material. To improve the typical low stiffness of polymers either particles or fibers of a high modulus material are integrated into the polymer matrix [2, 59, 60].

In particulate reinforced composites, the first factor that affects the stiffness is the weight percentage of the added particles. An increasing concentration of stiff particles in a polymer matrix improves the stiffness since the rigidity of fillers is much higher than that of matrix. This effect was described in many studies such as the work of Zhu et al. on polyimide/silica particle composites [61-65]. The polymer composite stiffness is less clearly affected by a change in particle size. For particles with sizes in the micrometer scale, the Young's modulus does not change with increasing diameter [63], but for nanometer-sized particles an increase in stiffness is observed when the average particle size is decreased [62]. Besides the particle size, the interfacial adhesion between the particles and the matrix has little effect on the stiffness as well. Since values for the stiffness are determined at relatively low deformation, there is insufficient dilation for interfacial adhesion parameters to have an effect on the Young's modulus [61, 64].

Besides adding particles, long continuous or short discontinuous fibers can also be used to increase the stiffness of a polymer matrix. The elastic modulus of common reinforcement fibers (glass, aramid, carbon) is typically a hundred times higher than that of conventionally used polymer matrices [60]. Based on the volume fraction of the fibers in the matrix, the overall stiffness of fiber reinforced polymer composites can be estimated by the 'rule of mixture':

$$E_c = \eta_L \eta_0 V_f E_f + (1 - V_f) E_m \quad (3.1)$$

where E_c , E_f and E_m are the stiffness of the composite, fiber and matrix respectively, V_f is the volume fraction of the fiber and η_L and η_0 are the length efficiency and orientation factor respectively [66]. The fiber orientation factor has a value ranging from 0.2 (for randomly distributed fibers) till 1 (for unidirectional fibers). The length efficiency factor η_L depends on the critical fiber length (L_c) of the filler material which is described by:

$$L_c = \frac{\sigma_f d_f}{2\tau} \quad (3.2)$$

where σ_f is the maximum fiber stress (or ultimate fiber strength), d_f is the fiber diameter and τ is the interfacial shear stress which can be regarded as a measure for the interfacial adhesion between filler and matrix. When the fiber length is below L_c , η_L has a value near zero and the filler material does not contribute to the composite stiffness. The value for η_L increases with increasing fiber length up till the point where the fiber length is ten times L_c and η_L has a value of 1. At this level, an increase in interfacial adhesion does no longer adds to the composite stiffness. For this reason the interfacial adhesion has only a small effect on the stiffness of continuous fiber reinforced polymers. However, the effect of interfacial adhesion on short fiber reinforced composite stiffness is significant. A graphical description of the effect of interfacial adhesion on the composite stiffness is presented in Figure 3.4. In the case of complete debonding the fillers do not carry any load and the stiffness of the composite decreases with increasing filler content. In the case of perfect bonding, the stiffness of the composite increases with filler content according to the physical limit given by equation 3.1. In the case of partial debonding intermediate stiffness values are obtained. Several studies described interfaces that are modified to improve the adhesion between fiber and matrix which show higher elastic moduli than their unmodified counterparts [60, 67, 68]. A study by Thomason et al. on continuous glass fiber reinforced polyimides shows that the composite stiffness is unaffected by changes in the fiber diameter because the fiber length greatly exceeds the L_c [69].

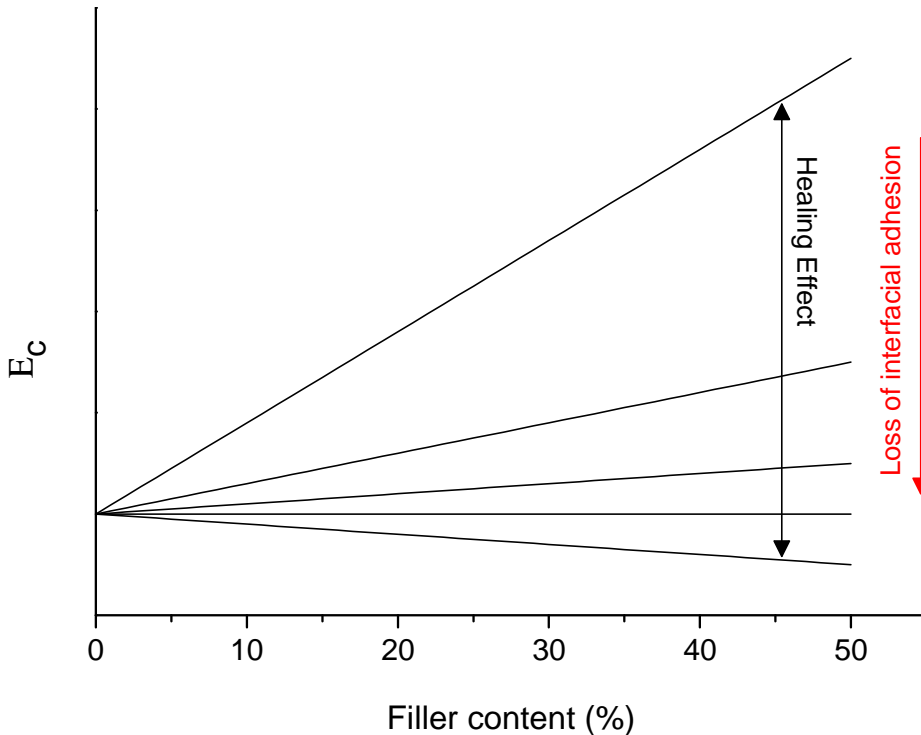


Figure 3.4 Graphical representation of the relation between filler content, interfacial adhesion and the elastic modulus in a short discontinuous fiber reinforced polymer composite material. The relation is plotted for various values of τ resulting in values for η_L ranging from 0 to 1 which directly shows the range of stiffness that can be healed by restoring the fiber-matrix interface. A similar model could be composed for the strength of a polymer composite.

Fatigue and impact damage are the most occurring types of damage in real-life applications of particulate and short fiber reinforced polymer composites. Fatigue damage results in cracks splitting either part of the polymer matrix or the matrix-filler interface and damage upon impact ranges from barely visible impact damage (microcracks or delamination) to large scale breakage like target penetration [7, 70]. In short fiber reinforced polymer composites the damage will initiate at the interface resulting in a reduction of τ and η_L leading to a drop in composite stiffness. Figure 3.4 shows the stiffness range that can potentially be recovered by healing of the interfacial adhesion between filler and matrix. To repair the composite's damage and regain its structural properties, the focus should therefore be on healing the matrix and the composite interface which results in restoring the initial values of τ and η_L . Because of the small effect of interfacial adhesion on the stiffness of continuous fiber reinforced composites, healing of the filler-matrix interface does not contribute significantly to the recovery of the stiffness for these types of composites.

Studies that report on stiffness regeneration include the work of Yoshie et al. who reported on the recovery of tensile moduli of a self-mending polymer based on the

Diels-Alder chemistry between anthracene and maleimide at both room temperature (17%) and 100°C (46%) [71]. Secondly, recovery rates of Young's moduli of almost 100% were reported by Amamoto et al. who designed a polyurethane that heals using radical reshuffling of thiuram disulphide bonds under ambient conditions (Figure 3.5) [55]. A third example of stiffness regeneration was shown in the study of Zako and Takano. They developed a composite blend material that consists of a rigid polymer matrix in which melt processable thermosetting epoxy particles are introduced. Specimens were damaged and healed at 120°C. After healing the stiffness of the composite material was fully recovered [72]. The self-healing matrices described in the cited studies are considered good candidates for stiffness regeneration in particulate and short fiber reinforced composites. However, their influence on the healing of the filler-matrix interface is yet to be shown in future studies. For the recovery of stiffness in continuous fiber reinforced composites alternative strategies need to be considered. Furthermore, due to the reversible nature of the relatively weak chemical bonds in the matrix polymer, the polymer matrix has a tendency to flow when exposed to mechanical loads for long periods of time. So the dynamic nature of the self-healing polymer will restrict the use of such composites for continuously loaded structures.

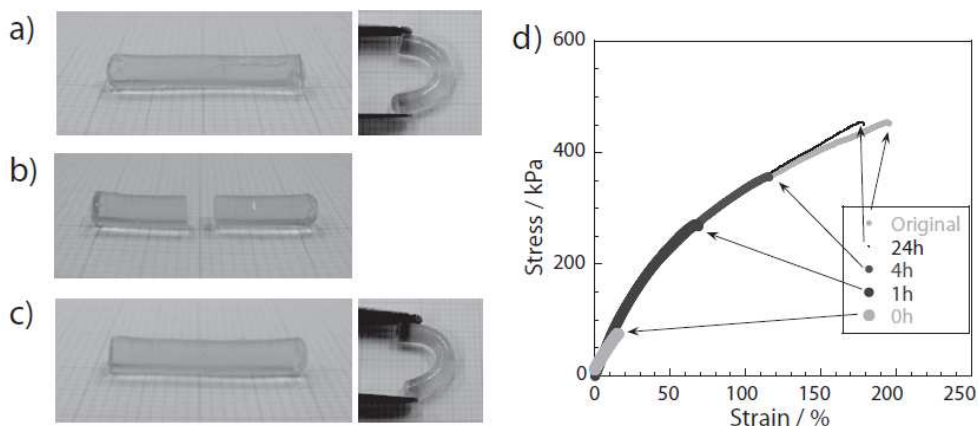


Figure 3.5 Recovery of structural properties in a self-healing polymer matrix using photochemical reversible thiuram disulfide bonds. The polymer matrix is displayed prior cutting and self-healing (a), after cutting (b) and after 24h of self-healing (c). (d) shows a stress, strain curve in which the regeneration of mechanical properties is plotted at different stages of the self-healing process [55].

3.3.2. Strength recovery

The strength of a material can be described by several parameters. The tensile strength is defined as the maximum stress that a material can sustain under tensile loading and is also called the ultimate strength. The stress at fracture and the stress above which plastic deformation occurs are called the breaking strength and yield

strength respectively [2]. In line with polymer stiffness improvement, the polymer composite strength can be increased by introducing particles or fibers that have much higher strength values than the matrix.

The strength of micro and nano-particulate composites is mainly determined by the effectiveness of the stress transfer between the matrix and the particles [59]. As for composite stiffness, the strength depends on the weight percentage of filler that is present in the matrix. However, no clear trend can be derived from literature as studies show that an increase in filler concentration can initially improve the composite strength while it is reduced upon further increase of particle concentration [59]. This is exemplified by the work of Zhu et al. who reported on polyimide films with silica fillers that show an increase in tensile strength up to a silica weight fraction of 10% [65]. However, a decline of tensile strength is observed upon further increase of the silica concentration. This can be explained by the fact that the particle cluster size increases together with the weight fraction which suppresses the strength of the composite, since, in contrast to stiffness, there is a clear relation between the size of added micro- and nanoparticles and the strength of a polymer composite. Generally, a decrease in particle size will lead to an increase in tensile strength as is shown for epoxy/silica composites by Nakamura et al. [73]. A final crucial parameter is the strength of the interfacial particle/matrix adhesion which determines the stress transfer between the components. For polymer composites containing very well-bonded particles, the addition of particles will result into a higher material strength. Poorly adhered particles, however, have an ineffective stress transfer and therefore do not contribute to the reinforcement of the matrix which leads to a decrease in strength. This phenomenon was quantified by Zhang et al. who showed the effect of interfacial adhesion in polypropylene/silica nano-composites on the material's strength by treating the particles with various monomers [74, 75].

Short and continuous reinforcing fibers with high elastic moduli (carbon, aramid, glass) are used to enhance the strength of a polymer composite in a similar fashion as is described for stiffness modification. Therefore, the 'rule of mixture' can also be used to approach the strength of a composite based on the volume fraction of the fibers:

$$\sigma_c = \eta_L \eta_0 V_f \sigma_f + (1 - V_f) \sigma_m \quad (3.3)$$

where σ_c , σ_f and σ_m are the strength of the composite, fibers and matrix respectively. For strength, the length efficiency factor, η_L , is again related to the critical thickness L_c , as is described by equation 3.2. Therefore a similar graphical relation between the strength, volume fraction and interfacial adhesion, similar to that depicted in

Figure 3.4 could be composed. Such a graph would indicate that the interfacial adhesion between fiber and polymer also has a large effect on the strength of short fiber reinforced composites. However, for continuous fiber reinforced composites, this effect is much less. Additionally, delamination between fiber and matrix can have a significant effect on the crack-growth resistance and may therefore even increase the ultimate strength of a polymer composite [67, 76].

As is described for stiffness, the strength of short fiber reinforced composites will drop upon interfacial failure due to a reduction of effective stress transfer resulting from cracks and delamination in the matrix or at the interface. Therefore, studies on strength healing of these composites should also focus on the recovery of η_L and τ by intrinsic restoration of the polymer matrix or the matrix-filler interface. For this purpose mainly intrinsic covalent healing strategies, containing either thermo reversible or photo reversible chemistries, are used [27]. Healing of the strength of epoxy-amine thermoset composites by the addition of thermally reversible cross-linking gel based on Diels-Alder chemistry was reported by Peterson et al. [25]. Recovery of strength can be achieved by direct application of the gel (37%) and by incorporation as a secondary particulate phase (21%) [77]. A more recent study described strength recovery (41% healing efficiency) in an actual continuous glass fiber reinforced composite at the fiber-polymer interface by coating with DA functional groups (Figure 3.3) which results in restoration of stress transfer capacity between matrix and fiber [28]. A second thermo reversible route is the incorporation of disulphide bonds in epoxy thermosets which leads to the recovery of the material's tensile strength (>90%) [29] or adhesive strength (100%)[78].

Alternatively, self-healing of structural properties by photoreversible chemistry was introduced by Chung et al. in 2004, however, the healing efficiency was rather low [50]. Later, Ling et al. managed to achieve tensile strength recoveries up to 100% by embedding coumarin groups in the main chains of a polyurethane network [52, 79].

Instead of using covalent healing chemistry Hayes et al. showed the recovery of strength by blending conventional thermosets with thermoplastic material. Their study showed that including 20 wt.% of thermoplastic material results in a regain of 70% of the virgin properties of the matrix [80]. More recent, Luo et al. showed a strength recovery of more than 100% in a polymerization-induced phase separated thermoset/thermoplastic blend that is capable of differential expansive bleeding [81].

Similar to the studies that reported on stiffness recovery, the healing capabilities of majority of the matrices discussed was not yet investigated in actual composite materials. However, the work of Peterson et al. is an indication that the restoration of interfacial properties can actually lead to strength healing in both short and

continuous fiber reinforced polymer composites. However, since the interfacial adhesion between matrix and filler has a larger effect for particulate or short fiber reinforced composites, it is expected that the development of such composites will be easier.

3.4. Functional Polymer Composites

Polymer based composites are also widely used as functional materials such as electrically conductive materials, electromagnetic interference shielding materials, electromechanical materials, magnetic materials or thermally conductive materials. Like structural polymer composites their properties generally (but not always) rely on the absence of damage in the polymer matrix and the absence of interfacial delamination. The opportunities for restoration of functional properties due to a self-healing polymer matrix are addressed below. The potential options are grouped according to the functional character of the composite.

3.4.1. Electrically conductive polymer composites

Electrically conductive polymer composites consist of a non-conductive polymer matrix and electrically conductive fillers and are widely used in various commercial applications due to their light weight, high manufacturability, corrosion resistance and good electrical conductivity [82-89].

To analyze the electrical conductivity of filler-loaded polymer composites, the percolation theory is usually used. When the content of fillers is below the percolation threshold, a long-range connection of fillers does not exist, leading to a very low electrical conductivity. While above the percolation threshold, the electrical conductivity increases significantly due to the formation of a long-range filler connection. When the percolation threshold for a material with a fixed filler concentration is reduced an increase in electrical conductivity is observed. According to the statistic percolation theory [90], the percolation threshold is inversely proportional to the particle aspect ratio. Therefore carbon nanotubes are promising candidates as electrically conductive fillers. This is exemplified by the work of Sandler et al. who reported percolation thresholds below 0.01% in a carbon nanotube/epoxy system [82]. Additionally, the work of Bilotti et al. showed that a further reduction of percolation threshold can be achieved by the addition of secondary nano-fillers [91].

Other systems using graphite, carbon black and carbon fibers as fillers are also investigated and research focuses on improving the processability and reducing the costs. An effective strategy that can be applied to these systems is to form a double percolation phenomenon by localizing fillers at the interface or within one of the

phases of an immiscible polymer blend [92, 93]. Furthermore, processing conditions will affect the particle alignment and the electrical conductivity of composites. For example, Kitajima et al. fabricated anisotropic electrically conductive polymer composites by applying a strong magnetic field to orient fillers [94]. The resulting composites showed much higher electrical conductivity along the direction of the magnetic field.

When micro- or macro-cracks are formed in the system, the connection of fillers may break down. Since the electrical conductivity of composites depends on the connection of fillers, this leads to a full or at least significant decrease of electrical conductivity and unexpected failure of electronic devices. These problems can be overcome by introducing an intrinsic self-healing polymer matrix that can heal the crack and restore the connection of fillers. Following this concept, Li et al. fabricated electrically conductive self-healing films by depositing Ag nanowires on top of healable polyelectrolyte multilayer films consisting of a layer-by-layer assembled branched poly(ethylenimine) and poly(acrylic acid)-hyaluronic acid blend [95]. Cuts can be autonomically repaired when water is sprayed on the films thereby recovering the electrical conductivity. A second example electrical conductivity healing was given by Tee et al.. They prepared an electrically and mechanically self-healing composite consisting of a supramolecular polymeric hydrogen-bonding network with self-healing ability filled with chemically compatible micro-nickel particles with nanoscale surface features [96]. The result showed a full recovery of electrical conductivity within 1 minute at room temperature upon complete fracture (as shown in Figure 3.6).

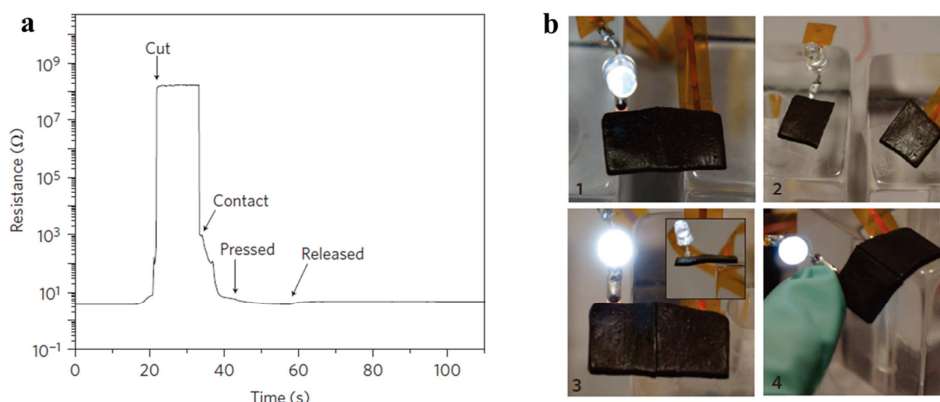


Figure 3.6 Electrical conductivity healing characterization of self-healing composite. (a) Resistance measurement shows electrical conductivity healing at room temperature. (b) Demonstration of the healing process using an LED in series with a self-healing composite conductor. 1, undamaged; 2, completely severed (open circuit); 3, electrical healing (inset shows conductor being self-supporting); 4, healed film being flexed to show its mechanical healing after only 5 min at room temperature [96].

Self-healing of electrical properties in stretchable wires was reported by Palteau et al. who combined the self-healing Reverlink polymer produced by Arkema with liquid metal [97]. In their experiment, 2D or 3D structures were made after cutting a straight sample. The self-healing polymer provided the mechanical recovery and helped to re-align the liquid metal channel. Once re-aligned, the liquid metal components merged together and formed a conductive channel again. Self-healing wires are particularly important for the growing field of stretchable electronics in which electronic components may undergo significant deformation and lead to unexpected failure. In addition, these self-healing structures offer a simple method to rewire circuits.

Another example of self-healing electrically conductive polymer composite was reported by Wang et al.. They fabricated silicon micro-particle (SiMP) anodes for high-energy lithium-ion batteries, which are coated with a self-healing polymer composite consisting of a randomly branched hydrogen-bonding polymer matrix and carbon black nanoparticles [98]. The self-healing conductive composite coatings assist to heal the cracks, which are generated during the cycling process, and as such extends the cycle life ten times longer than state-of-the-art anodes made from SiMPs while still retaining a high capacity.

3.4.2. Electromagnetic polymer composites

All electrical and electronic devices emit electromagnetic signals, which can interfere with the operational properties of either the emitting equipment or any other equipment around it. To overcome this problem, the equipment can be shielded by electromagnetic interference (EMI) shielding materials. The first generation of EMI shielding materials were made of metals, but in recent years electrically conducting polymer composites have gained popularity for EMI shielding applications. EMI shielding polymer composites are lightweight, resistant to corrosion, flexible, and cost less than metals. The most important property of EMI shielding materials is the shielding effectiveness (SE). According to Simon's equation [99]:

$$SE(\text{dB}) = 50 + 10 \log_{10} \left(\frac{1}{\rho f} \right) + 1.7t \left(\frac{f}{\rho} \right)^{\frac{1}{2}} \quad (3.4)$$

where ρ is the volume resistivity in $\Omega \cdot \text{cm}$, f is the frequency in MHz, and t is the thickness in cm, the EMI SE is higher when the electrical resistivity is lower. As discussed in section 4.1, the electrical conductivity can be restored after damage by introducing a self-healing polymer matrix to electrically conducting composites. Subsequently, the EMI shielding property can recover.

3.4.3. *Electromechanical polymer composites*

Polymers that possess the ability to convert electrical into mechanical energy or vice versa are used in composite materials for numerous applications, such as sensors, actuators and energy harvesting. The functionality of these so called electromechanical composites can be found either in the polymer matrix or in the added filler material. The driving force behind electromechanical polymer matrices can be electronic (driven by an electric field or Coulomb forces) or ionic (involving diffusion or mobility of ions). Electronically driven polymers operate at room temperature and show a rapid electroactive response (ms range), but the required voltages are high (± 200 MV/m). Ionic electroactive polymers already operate at low voltage levels (< 5 MV/m), but this is combined with a relatively slow response (in the order of seconds) [100, 101].

One of the most common electronically activated electromechanical functionalities is the piezoelectric effect. Piezoelectricity is found only in noncentrosymmetric materials and it is called ferroelectricity when such a material exhibits spontaneous polarization. Among the few polymers that show ferroelectric behavior, poly(vinylidene fluoride)(PVDF) and its copolymers have shown to have the best overall electroactive properties. Therefore PVDF is used in the majority of the research and industrial applications that involve piezoelectric polymers [102]. Another class of electronically driven polymers is that of the dielectric elastomers. This group of polymers includes silicones and acrylics with rubberlike properties such as low tensile strength and high deformability [103]. Studies of Pelrine et al. describe high strain rates ($> 100\%$) for both silicone and acrylic polymers [104, 105].

Ionic electroactive polymers are used for the production of ionomeric polymer-metal composites (IPMC). IPMCs bend at low voltages due to an ionomer that provides mobility of positive ions between a fixed network of negative ions on metal clusters. Two types of ionomers are typically used for the production of IPMCs, being Nafion (DuPont) and Flemion (Asahi Glass). Both ionomers consist of a tetrafluoroethylene backbone with a sidechain containing a negative sulfonate end group that is responsible for ion mobility. The majority of follow-up research in this field is based on these two commercial ionomers [106, 107]. Recent studies describe the influence of the ionomer sidechains [108] and the effects of softening and heating processes [109]. A second class of ionic electroactive polymers are conducting polymers. Their electromechanical response is based on the reversible insertion and expulsion of ions that occurs during redox cycling which induces a considerable volume change of the polymer. Frequently used conducting polymers are polyaniline, polypyrrole and polythiophenes [110, 111].

Besides using an electroactive polymer as matrix material, composites with electrochemical properties can be developed by adding functional fillers to a conventional matrix. These fillers range from inorganic metallic fibers to organic polymer particles. A common strategy is to enhance a matrix with semi-crystalline ferroelectric ceramic particles (0-3 composites) or fibers (1-3 composites) of which lead zirconate titanate (PZT) is the most frequently used example. These composites typically have a high electromechanical sensitivity, high pressure tolerance and good acoustical impedance [112]. Another strategy that increases the electromechanical performance of non-electroactive polymers is the addition of highly conductive fillers such as metal powders (e.g. aluminium and nickel) and carbon based materials which changes the composite resistivity value with several orders of magnitude [103]. Many recent studies describe the high potential of carbon nanotubes (CNTs), however, many problems will have to be overcome before they will be used in industrial applications [113]. Another recent study describes the combination of PZT and aluminium particles in an electromechanical epoxy based material [114].

Since both electromechanical polymers and self-healing polymers are able to regain a previously adapted form it seems a logical step to combine these two material functionalities into one material. However, the amount of studies that report on the regeneration of electromechanical properties after fracture is rather limited. Still, Soroushian et al. report on the piezo-driven self-healing of fiber reinforced polymer composites. Here, the mechanical energy that is released upon fracture, is converted into electrical energy by the PVDF based matrix. Healing of the composite is then achieved by an electrochemical reaction at the fiber-matrix interface [115]. A second study, that shows self-healing of electrical (as mentioned in chapter 4.1) and electromechanical properties was performed by Tee et al. Their piezoresistive polymer composite with tactile pressure- and flexion bending sensitive properties can be used in electronic skin applications (Figure 3.7). The healing is based on supramolecular hydrogen bonding with high healing efficiencies, whereas the piezoresistive behavior is generated by adding μNi particles to the polymer matrix. This resulted in an almost full recovery of the composite functionality, however, the mechanical properties were not fully restored [96]. A final option that can be employed to prepare self-healing electromechanical composites could be through the use of ionomers. Since ionomers possess both electromechanical and self-healing properties, they are ideal candidates to serve as matrix material for multifunctional materials. Recently, James et al were the first to report a self-healing piezoelectric PZT-ionomer based polymer. They showed that the loss of sensorial functionality after high cyclic tensile fatigue can be partially recovered by thermal healing at 70°C [116].

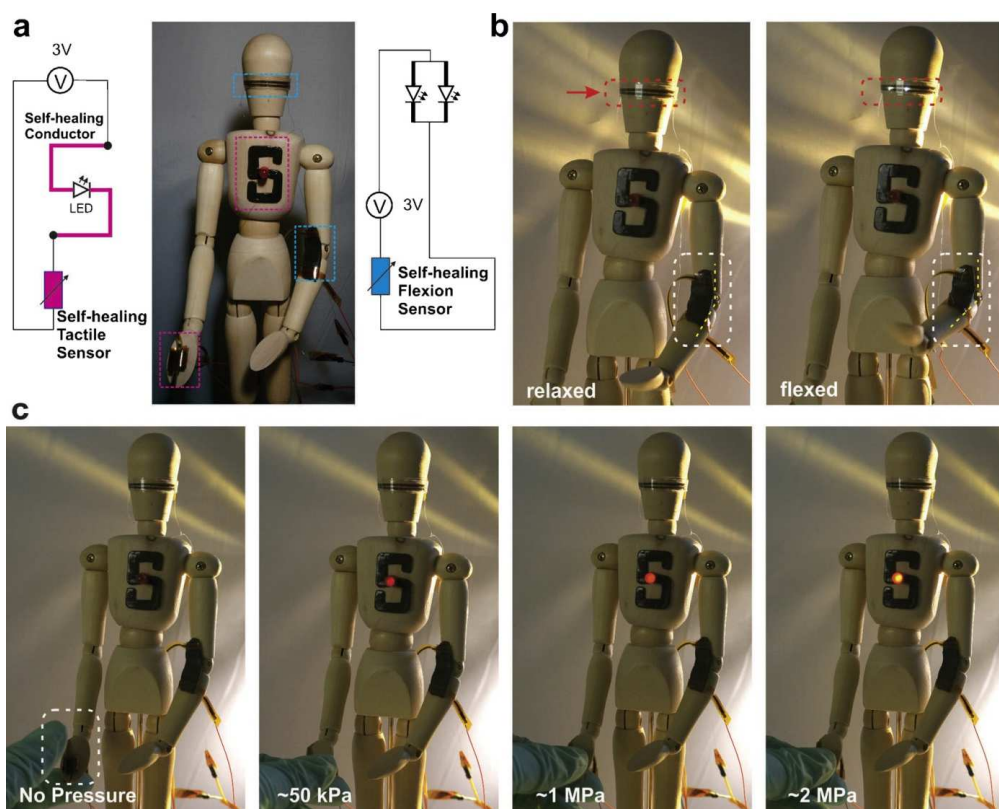


Figure 3.7 Example of piezoresistive recovery in a fully articulated wooden mannequin. (a) A self-healing flexion and a self-healing tactile sensor were mounted on the elbow and palm of the mannequin respectively. LEDs in the eye and body region are used to transduce mechanical deformation into visible light. (b) shows the LED lights up with increasing elbow flexion. (c) shows LED lightening with increasing palm tactile pressure [96].

3.4.4. Magnetic polymer composites

Magnetic polymer composites generally contain magnetic powders, such as Fe_3O_4 , CoFe_2O_4 , strontium ferrite and nickel [117-120], whereas epoxies, polyurethanes and polyimides are often selected as matrix material [118, 121, 122]. Although they possess inferior magnetic properties compared to cast or sintered magnets, they have various advantages, such as a higher manufacturability and the possibility to produce complicated small and thin shapes with high precision. Therefore they are widely used for various applications, such as electronic and communications instruments, household tools and audio equipment[123]. Self-healing in magnetic polymer composites could be achieved by substituting conventional with intrinsically self-healing matrices, thereby creating more reliable and longer-lasting materials.

Magnetic gels are highly elastic hydrogels with magnetic fillers and they are an important group of magnetic polymer composites, which could greatly benefit from the self-healing effect. Controlled by the action of external magnetic fields, magnetic gels can perform elongation, contraction and coiling actions (as shown in Figure 3.8), which makes them suitable for actuator applications such as artificial muscles [124-126]. In these kinds of applications, the material will undergo significant deformation which may lead to unexpected failure. The mechanical damage can potentially be undone by introducing self-healing hydrogels, which are well developed [127-129], as polymer matrix in magnetic gels. This concept is exemplified by a study of Zhang et al.. They mixed Fe_3O_4 nanoparticles into a chitosan solution and subsequently added synthetic telechelic difunctional polyethylene glycol into the ferrofluid. The result is that a magnetic self-healing hydrogel can be fabricated quickly and straightforward at room temperature within less than 2 minutes. The resulting composite is capable of regenerating itself after multiple complete fractures under the influence of an external magnetic field [130].

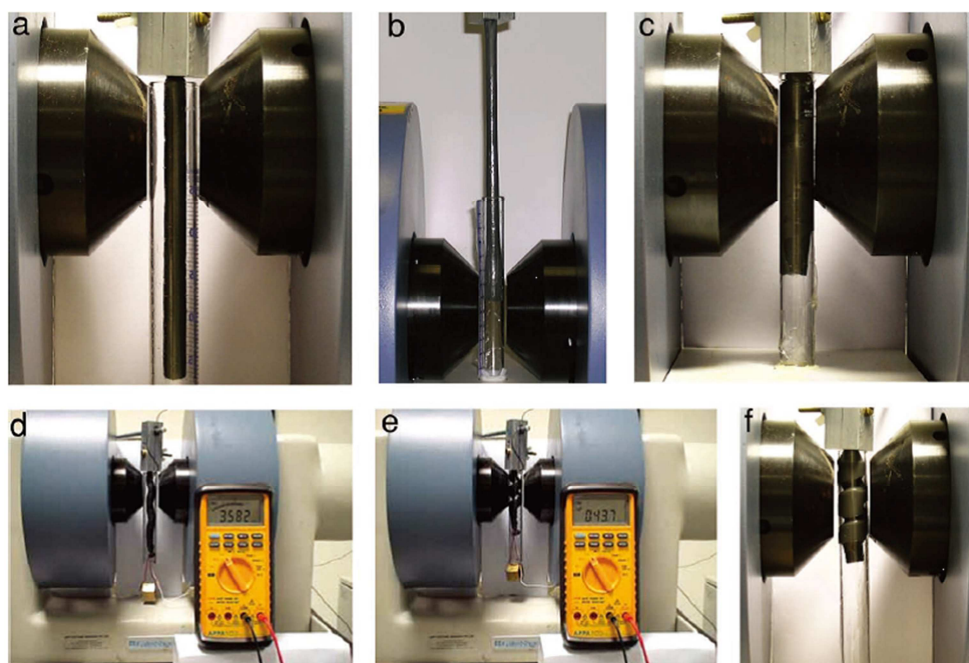


Figure 3.8 Performance of magnetic gel (20 wt.% Fe in silicone) controlled by external magnetic fields. (a) Relaxed mode without magnetic field; (b) elongation mode; (c) contraction mode; (d) and (e) coiling mode, the ohmmeter shows the resistance change of the sample during coiling process; (f) hybrid mode at $B = 1\text{ T}$ [126].

3.4.5. Thermally conductive polymer composites

Thermally conductive polymer composites, consisting of a polymeric matrix and high thermally conductive fillers, such as carbon fibers, carbon nanotubes, aluminum oxide, zinc oxide, silicon carbide, boron nitride and metal powders, are widely used as thermal interface materials (TIMs), which play a key role in thermal management of the electronic industry [131-135].

Both modelling and experimental results indicate that the formation of thermally conductive chains leads to an increase in thermal conductivity of composites. For example, Devpura et al proposed a model on percolation phenomenon based thermal conductivity [136]. On the other hand, an experimental study by Hu et al. described the addition of carbon nanotubes into a silicone composite filled with spherical nickel particles [137]. They found out that even small quantities of carbon nanotubes can effectively improve the heat conduction performance of the composites by forming carbon nanotube-nickel sphere chains. Their work shows that a large increase in the thermal conductivity can be obtained by percolation phenomena, which is also justified in many recent studies [138-140]. Upon crack formation the thermally conductive chains can be cut off, which leads to a significant decrease in the thermal conductivity of the composite.

The adhesion at the interface between the polymer matrix and the fillers is essential to the thermal conductivity of composites. Many studies showed that the surface treatment with coupling agent can improve the matrix-filler interfacial adhesion, which increases the thermal conductivity of composites [141-143]. Thermal boundary resistance (R_b) is a measure of an interface's resistance to thermal flow. Every et al. built a thermal conductivity model of spherical particle loaded composite material which took R_b into account, as shown in equation 4.2 [144],

$$(1 - V)^3 = \left(\frac{\lambda_m}{\lambda_c} \right)^{(1+2\alpha)/(1-\alpha)} \times \left[\frac{\lambda_c - \lambda_f(1 - \alpha)}{\lambda_m - \lambda_f(1 - \alpha)} \right]^{3/(1-\alpha)} \quad (3.5)$$

in which λ_c , λ_m and λ_f are the thermal conductivity of composite material, matrix and filler, respectively, V is the volume fraction of filler, α is a non-dimensional parameter with reference to the boundary resistance, which is defined by equation 4.3,

$$\alpha = \frac{2R_b\lambda_m}{d} \quad (3.6)$$

in which d is the diameter of filler. When $\lambda_f \gg \lambda_m$, equation 4.2 can be deduced to

$$\frac{\lambda_c}{\lambda_m} = \frac{1}{(1 - V)^{3(1-\alpha)/(1+2\alpha)}} \quad (3.7)$$

If crack formation occurs at the matrix-filler interface, the boundary resistance will increase significantly leading to a decrease of the composite's thermal conductivity, as shown schematically in Figure 3.9. As in its reference figure for mechanical stiffness (Figure 3.4), Figure 9 shows that upon full delamination the properties of the composite decrease with filler fraction and reach a value well below that of the matrix. Only for the case of perfect interface heat transfer, the properties of the composite increase with the filler content to reach values that are substantially above that of the polymer matrix.

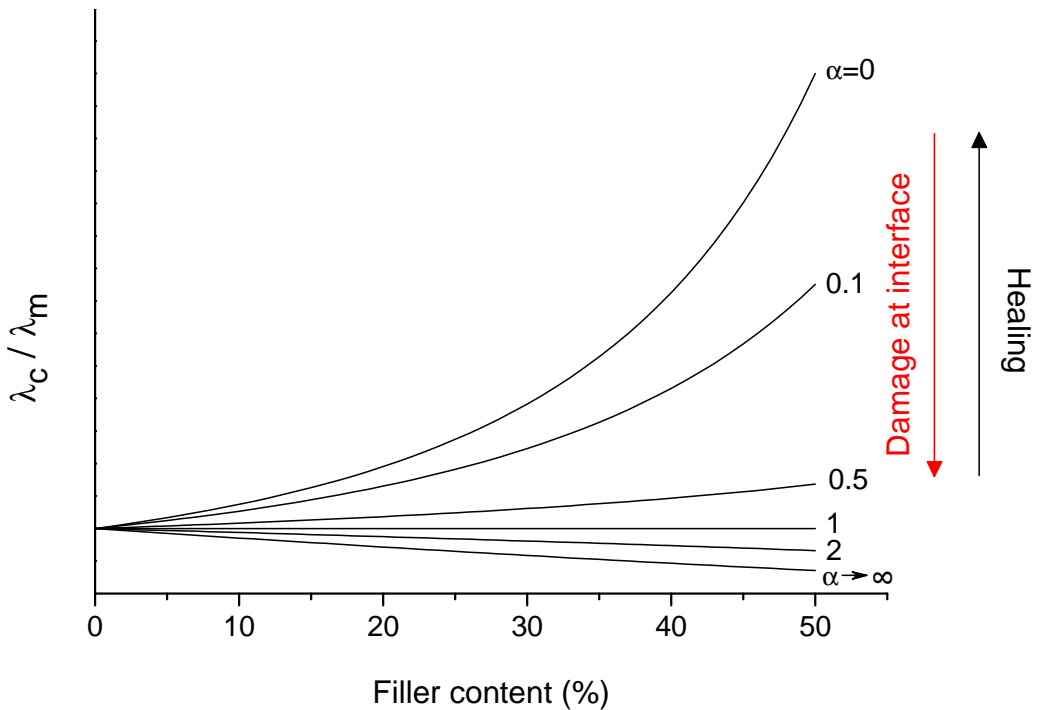


Figure 3.9 Graphical representation of the relation between filler content, thermal boundary resistance and the thermal conductivity of spherical particle loaded composite material. The relation is plotted for various values of R_b resulting in values for α ranging from 0 to ∞ which directly shows the range of thermal conductivity that can be healed by restoring the fiber-matrix interface.

Interfacial failure is a key failure mechanism in the use of Thermal Interface Materials (TIMs), which are composites designed to mechanically and thermally connect a heat source and component to minimize a potential temperature rise of the entire structure, hence TIMs and the components contacted to them usually have a mismatch in coefficient of thermal expansion (CTE) which leads to mechanical stress. After some thermal cycles, CTE mismatch may induce

delamination between components and TIMs, which leads to an increase in thermal contact resistance and subsequent failure of the whole device [145-147].

In general, the functionality of TIMs will be damaged in three ways: cracks cutting off the thermally conductive chains, cracks separating matrix and fillers and delamination between components and TIMs. To introduce cohesive and adhesive self-healing ability to TIMs could be an effective way to solve this problem. Although much work has been done on both self-healing polymers and TIMs, only a few attempts have been made to fabricate self-healing TIMs. Lafont et al. prepared TIMs consisting of boron nitride or graphite particles and two types of self-healing polysulphide-based thermoset matrices [148]. The composites exhibit recovery of both cohesion and adhesion properties under a mild healing temperature (65°C). After multiple healing cycles, most of the samples show full recovery of initial adhesive strength. On the other hand, the samples behave differently on cohesion recovery: 20-100% recovery can be achieved depending on filler concentration, filler type and matrix type.

Since thermally conductive polymer composites invariably will be exposed to a range of temperatures during use, heat triggered self-healing polymers are the most appropriate matrix materials. In the case of unexpected local failure of thermally conductive polymer composites, the resulting change in the temperature in the region surrounding the crack or the delamination can trigger the healing process and allow the thermally conductive polymer composites to recover their original performance thus increasing the reliability of the device. Although the development of self-healing thermally conductive polymer composites is still in its infancy, it is expected that self-healing thermally conductive polymer composites have real potential applications in the electronics and lighting industry [149].

3.5. Conclusion

This review gives the first overview on the emerging field of self-healing behaviour of composite materials. In polymer based composite materials, the damages in the matrix or at the matrix-filler interface lead to the loss of both structural and functional properties. By applying intrinsic self-healing polymer as matrix, those damages can be healed upon the stimulation of an external stimulus and subsequently both structural and functional properties can be partially or even fully restored.

As described, the majority of recent studies regarding self-healing composite materials focus on the restoration of structural properties, such as stiffness and strength. Research into the self-healing of functional properties (electrical, electromagnetic, electromechanical, magnetic and thermal conductive) is still in its

early stage development. However, as the demand for functional polymer composites is increasing, it is expected that the focus of researchers will broaden to the development of materials that are capable of healing both structural and functional properties in the upcoming years.

References

1. Gibson, R.F., *A review of recent research on mechanics of multifunctional composite materials and structures*. Composite Structures, 2010. 92(12): p. 2793-2810.
2. Chung, D.D.L., *Composite Materials*. 2nd ed. Engineering Materials and Processes. 2010: Springer London.
3. Eadie, L. and Ghosh, T.K., *Biomimicry in textiles: Past, present and potential. An overview*. Journal of the Royal Society Interface, 2011. 8(59): p. 761-775.
4. Olszta, M.J., Cheng, X., Jee, S.S., Kumar, R., Kim, Y.Y., Kaufman, M.J., Douglas, E.P., and Gower, L.B., *Bone structure and formation: A new perspective*. Materials Science and Engineering R: Reports, 2007. 58(3-5): p. 77-116.
5. Bauer, G. and Speck, T., *Restoration of tensile strength in bark samples of Ficus benjamina due to coagulation of latex during fast self-healing of fissures*. Annals of botany, 2012. 109(4): p. 807-811.
6. van der Zwaag, S., *An Introduction to Material Design Principles: Damage Prevention versus Damage Management*, in *Self-Healing Materials an Alternative Approach to 20 Centuries of Materials Science*, S. van der Zwaag, Editor. 2007.
7. van der Zwaag, S., Grande, A.M., Post, W., Garcia, S.J., and Bor, T.C., *Review of current strategies to induce self-healing behaviour in fibre reinforced polymer based composites*. Materials Science and Technology, 2014. 30(13a): p. 1633-1641.
8. Dry, C., *Procedures developed for self-repair of polymer matrix composite materials*. Composite Structures, 1996. 35(3): p. 263-269.
9. Dry, C.M. and Sottos, N.R. *Passive smart self-repair in polymer matrix composite materials*. 1993.
10. White, S.R., Sottos, N.R., Geubelle, P.H., Moore, J.S., Kessler, M.R., Sriram, S.R., Brown, E.N., and Viswanathan, S., *Autonomic healing of polymer composites*. Nature, 2001. 409(6822): p. 794-797.
11. Pang, J.W.C. and Bond, I.P., *A hollow fibre reinforced polymer composite encompassing self-healing and enhanced damage visibility*. Composites Science and Technology, 2005. 65(11-12): p. 1791-1799.
12. Toohey, K.S., Sottos, N.R., Lewis, J.A., Moore, J.S., and White, S.R., *Self-healing materials with microvascular networks*. Nat Mater, 2007. 6(8): p. 581-585.
13. White, S.R., Moore, J.S., Sottos, N.R., Krull, B.P., Santa Cruz, W.A., and Gergely, R.C.R., *Restoration of large damage volumes in polymers*. Science, 2014. 344(6184): p. 620-623.

14. Kalista, S.J., Ward, T.C., and Oyetunji, Z., *Self-Healing of Poly(Ethylene-co-Methacrylic Acid) Copolymers Following Projectile Puncture*. Mechanics of Advanced Materials and Structures, 2007. 14(5): p. 391-397.
15. John Varley, R. and van der Zwaag, S., *Development of a quasi-static test method to investigate the origin of self-healing in ionomers under ballistic conditions*. Polymer Testing, 2008. 27(1): p. 11-19.
16. Billiet, S., Hillewaere, X.K.D., Teixeira, R.F.A., and Du Prez, F.E., *Chemistry of crosslinking processes for self-healing polymers*. Macromolecular Rapid Communications, 2013. 34(4): p. 290-309.
17. García, S.J., *Effect of polymer architecture on the intrinsic self-healing character of polymers*. European Polymer Journal, 2014. 53(0): p. 118-125.
18. Zhang, Y., Broekhuis, A.A., and Picchioni, F., *Thermally Self-Healing Polymeric Materials: The Next Step to Recycling Thermoset Polymers?* Macromolecules, 2009. 42(6): p. 1906-1912.
19. Kavitha, A.A. and Singha, N.K., *"Click Chemistry" in Tailor-Made Polymethacrylates Bearing Reactive Furfuryl Functionality: A New Class of Self-Healing Polymeric Material*. ACS Applied Materials & Interfaces, 2009. 1(7): p. 1427-1436.
20. Canary, S.A. and Stevens, M.P., *Thermally reversible crosslinking of polystyrene via the furan-maleimide Diels-Alder reaction*. Journal of Polymer Science Part A: Polymer Chemistry, 1992. 30(8): p. 1755-1760.
21. Liu, Y.-L., Hsieh, C.-Y., and Chen, Y.-W., *Thermally reversible cross-linked polyamides and thermo-responsive gels by means of Diels-Alder reaction*. Polymer, 2006. 47(8): p. 2581-2586.
22. Magana, S., Zerroukhi, A., Jegat, C., and Mignard, N., *Thermally reversible crosslinked polyethylene using Diels-Alder reaction in molten state*. Reactive and Functional Polymers, 2010. 70(7): p. 442-448.
23. Tian, Q., Rong, M.Z., Zhang, M.Q., and Yuan, Y.C., *Synthesis and characterization of epoxy with improved thermal remendability based on Diels-Alder reaction*. Polymer International, 2010. 59(10): p. 1339-1345.
24. Bai, N., Saito, K., and Simon, G.P., *Synthesis of a diamine cross-linker containing Diels-Alder adducts to produce self-healing thermosetting epoxy polymer from a widely used epoxy monomer*. Polymer Chemistry, 2013. 4(3): p. 724-730.
25. Pratama, P.A., Peterson, A.M., and Palmese, G.R., *The role of maleimide structure in the healing of furan-functionalized epoxy-amine thermosets*. Polymer Chemistry, 2013. 4(18): p. 5000-5006.
26. Du, P., Liu, X., Zheng, Z., Wang, X., Joncheray, T., and Zhang, Y., *Synthesis and characterization of linear self-healing polyurethane based on thermally reversible Diels-Alder reaction*. RSC Advances, 2013. 3(35): p. 15475-15482.
27. Zhang, M.Q. and Rong, M.Z., *Intrinsic self-healing of covalent polymers through bond reconnection towards strength restoration*. Polymer Chemistry, 2013. 4(18): p. 4878-4884.
28. Peterson, A.M., Jensen, R.E., and Palmese, G.R., *Thermoreversible and remendable glass-polymer interface for fiber-reinforced composites*. Composites Science and Technology, 2011. 71(5): p. 586-592.

29. Canadell, J., Goossens, H., and Klumperman, B., *Self-healing materials based on disulfide links*. *Macromolecules*, 2011. 44(8): p. 2536-2541.
30. Pepels, M., Filot, I., Klumperman, B., and Goossens, H., *Self-healing systems based on disulfide-thiol exchange reactions*. *Polymer Chemistry*, 2013. 4(18): p. 4955-4965.
31. Higaki, Y., Otsuka, H., and Takahara, A., *A Thermodynamic Polymer Cross-Linking System Based on Radically Exchangeable Covalent Bonds*. *Macromolecules*, 2006. 39(6): p. 2121-2125.
32. Otsuka, H., Aotani, K., Higaki, Y., Amamoto, Y., and Takahara, A., *Thermal Reorganization and Molecular Weight Control of Dynamic Covalent Polymers Containing Alkoxyamines in Their Main Chains*. *Macromolecules*, 2007. 40(5): p. 1429-1434.
33. Yuan, C.e., Rong, M.Z., Zhang, M.Q., Zhang, Z.P., and Yuan, Y.C., *Self-Healing of Polymers via Synchronous Covalent Bond Fission/Radical Recombination*. *Chemistry of Materials*, 2011. 23(22): p. 5076-5081.
34. Sijbesma, R.P., Beijer, F.H., Brunsveld, L., Folmer, B.J.B., Hirschberg, J.H.K.K., Lange, R.F.M., Lowe, J.K.L., and Meijer, E.W., *Reversible Polymers Formed from Self-Complementary Monomers Using Quadruple Hydrogen Bonding*. *Science*, 1997. 278(5343): p. 1601-1604.
35. Park, T., Zimmerman, S.C., and Nakashima, S., *A Highly Stable Quadruply Hydrogen-Bonded Heterocomplex Useful for Supramolecular Polymer Blends*. *Journal of the American Chemical Society*, 2005. 127(18): p. 6520-6521.
36. Cordier, P., Tournilhac, F., Soulie-Ziakovic, C., and Leibler, L., *Self-healing and thermoreversible rubber from supramolecular assembly*. *Nature*, 2008. 451(7181): p. 977-980.
37. Montarnal, D., Tournilhac, F., Hidalgo, M., and Leibler, L., *Epoxy-based networks combining chemical and supramolecular hydrogen-bonding crosslinks*. *Journal of Polymer Science Part A: Polymer Chemistry*, 2010. 48(5): p. 1133-1141.
38. Colquhoun, H.M., *Self-repairing polymers: Materials that heal themselves*. *Nat Chem*, 2012. 4(6): p. 435-436.
39. Li, G., Wie, J.J., Nguyen, N.A., Chung, W.J., Kim, E.T., Char, K., Mackay, M.E., and Pyun, J., *Synthesis, self-assembly and reversible healing of supramolecular perfluoropolyethers*. *Journal of Polymer Science Part A: Polymer Chemistry*, 2013. 51(17): p. 3598-3606.
40. Zhang, A., Yang, L., Lin, Y., Yan, L., Lu, H., and Wang, L., *Self-healing supramolecular elastomers based on the multi-hydrogen bonding of low-molecular polydimethylsiloxanes: Synthesis and characterization*. *Journal of Applied Polymer Science*, 2013. 129(5): p. 2435-2442.
41. Greenland, B.W., Burattini, S., Hayes, W., and Colquhoun, H.M., *Design, synthesis and computational modelling of aromatic tweezer-molecules as models for chain-folding polymer blends*. *Tetrahedron*, 2008. 64(36): p. 8346-8354.

42. Burattini, S., Colquhoun, H.M., Greenland, B.W., and Hayes, W., *A novel self-healing supramolecular polymer system*. Faraday Discussions, 2009. 143: p. 251-264.
43. Burattini, S., Greenland, B.W., Merino, D.H., Weng, W., Seppala, J., Colquhoun, H.M., Hayes, W., Mackay, M.E., Hamley, I.W., and Rowan, S.J., *A Healable Supramolecular Polymer Blend Based on Aromatic π - π Stacking and Hydrogen-Bonding Interactions*. Journal of the American Chemical Society, 2010. 132(34): p. 12051-12058.
44. Kalista Jr, S.J. and Ward, T.C., *Thermal characteristics of the self-healing response in poly(ethylene-co-methacrylic acid) copolymers*. Journal of the Royal Society Interface, 2007. 4(13): p. 405-411.
45. Kalista Jr, S.J., Ward, T.C., and Oyetunji, Z., *Self-healing of poly(ethylene-co-methacrylic acid) copolymers following projectile puncture*. Mechanics of Advanced Materials and Structures, 2007. 14(5): p. 391-397.
46. Varley, R.J., Shen, S., and van der Zwaag, S., *The effect of cluster plasticisation on the self healing behaviour of ionomers*. Polymer, 2010. 51(3): p. 679-686.
47. Varley, R.J. and van der Zwaag, S., *Autonomous damage initiated healing in a thermo-responsive ionomer*. Polymer International, 2010. 59(8): p. 1031-1038.
48. Varley, R.J. and van der Zwaag, S., *Towards an understanding of thermally activated self-healing of an ionomer system during ballistic penetration*. Acta Materialia, 2008. 56(19): p. 5737-5750.
49. Varley, R.J. and van der Zwaag, S., *Development of a quasi-static test method to investigate the origin of self-healing in ionomers under ballistic conditions*. Polymer Testing, 2008. 27(1): p. 11-19.
50. Chung, C.-M., Roh, Y.-S., Cho, S.-Y., and Kim, J.-G., *Crack Healing in Polymeric Materials via Photochemical [2+2] Cycloaddition*. Chemistry of Materials, 2004. 16(21): p. 3982-3984.
51. Oya, N., Sukarsaatmadja, P., Ishida, K., and Yoshie, N., *Photoinduced mendable network polymer from poly(butylene adipate) end-functionalized with cinnamoyl groups*. Polym J, 2012. 44(7): p. 724-729.
52. Ling, J., Rong, M.Z., and Zhang, M.Q., *Coumarin imparts repeated photochemical remendability to polyurethane*. Journal of Materials Chemistry, 2011. 21(45): p. 18373-18380.
53. Ghosh, B. and Urban, M.W., *Self-Repairing Oxetane-Substituted Chitosan Polyurethane Networks*. Science, 2009. 323(5920): p. 1458-1460.
54. Amamoto, Y., Kamada, J., Otsuka, H., Takahara, A., and Matyjaszewski, K., *Repeatable Photoinduced Self-Healing of Covalently Cross-Linked Polymers through Reshuffling of Trithiocarbonate Units*. Angewandte Chemie, 2011. 123(7): p. 1698-1701.
55. Amamoto, Y., Otsuka, H., Takahara, A., and Matyjaszewski, K., *Self-Healing of Covalently Cross-Linked Polymers by Reshuffling Thiuram Disulfide Moieties in Air under Visible Light*. Advanced Materials, 2012. 24(29): p. 3975-3980.

56. Burnworth, M., Tang, L., Kumpfer, J.R., Duncan, A.J., Beyer, F.L., Fiore, G.L., Rowan, S.J., and Weder, C., *Optically healable supramolecular polymers*. *Nature*, 2011. 472(7343): p. 334-337.
57. Chuo, T.-W., Wei, T.-C., and Liu, Y.-L., *Electrically driven self-healing polymers based on reversible guest–host complexation of β -cyclodextrin and ferrocene*. *Journal of Polymer Science Part A: Polymer Chemistry*, 2013. 51(16): p. 3395-3403.
58. Zhang, Z., Hu, Y., Liu, Z., and Guo, T., *Synthesis and evaluation of a moisture-promoted healing copolymer*. *Polymer*, 2012. 53(14): p. 2979-2990.
59. Fu, S.Y., Feng, X.Q., Lauke, B., and Mai, Y.W., *Effects of particle size, particle/matrix interface adhesion and particle loading on mechanical properties of particulate-polymer composites*. *Composites Part B: Engineering*, 2008. 39(6): p. 933-961.
60. Ku, H., Wang, H., Pattarachaiyakoo, N., and Trada, M., *A review on the tensile properties of natural fiber reinforced polymer composites*. *Composites Part B: Engineering*, 2011. 42(4): p. 856-873.
61. Dekkers, M.E.J. and Heikens, D., *The effect of interfacial adhesion on the tensile behavior of polystyrene–glass-bead composites*. *Journal of Applied Polymer Science*, 1983. 28(12): p. 3809-3815.
62. Mishra, S., Sonawane, S.H., and Singh, R.P., *Studies on characterization of nano CaCO₃ prepared by the in situ deposition technique and its application in PP-nano CaCO₃ composites*. *Journal of Polymer Science, Part B: Polymer Physics*, 2005. 43(1): p. 107-113.
63. Spanoudakis, J. and Young, R.J., *Crack propagation in a glass particle-filled epoxy resin - Part 1 Effect of particle volume fraction and size*. *Journal of Materials Science*, 1984. 19(2): p. 473-486.
64. Wang, K., Wu, J., Ye, L., and Zeng, H., *Mechanical properties and toughening mechanisms of polypropylene/barium sulfate composites*. *Composites Part A: Applied Science and Manufacturing*, 2003. 34(12): p. 1199-1205.
65. Zhu, Z.K., Yang, Y., Yin, J., and Qi, Z.N., *Preparation and properties of organosoluble polyimide silica hybrid materials by sol-gel process*. *Journal of Applied Polymer Science*, 1999. 73(14): p. 2977-2984.
66. Wang, Z., Ciselli, P., and Peijs, T., *The extraordinary reinforcing efficiency of single-walled carbon nanotubes in oriented poly(vinyl alcohol) tapes*. *Nanotechnology*, 2007. 18(45).
67. Nogueira, C.L., De Paiva, J.M.F., and Rezende, M.C., *Effect of the interfacial adhesion on the tensile and impact properties of carbon fiber reinforced polypropylene matrices*. *Materials Research*, 2005. 8(1): p. 81-89.
68. Shazed, M.A., Suraya, A.R., Rahmanian, S., and Mohd Salleh, M.A., *Effect of fibre coating and geometry on the tensile properties of hybrid carbon nanotube coated carbon fibre reinforced composite*. *Materials & Design*, 2014. 54(0): p. 660-669.

69. Thomason, J.L., *The influence of fibre length, diameter and concentration on the modulus of glass fibre reinforced polyamide 6,6*. Composites Part A: Applied Science and Manufacturing, 2008. 39(11): p. 1732-1738.
70. Agarwal, B.D., Broutman, L.J., and Chandrashekhara, K., *Analysis And Performance Of Fiber Composites*. Third Edition ed. 2006: John Wiley & Sons.
71. Yoshie, N., Saito, S., and Oya, N., *A thermally-stable self-mending polymer networked by Diels-Alder cycloaddition*. Polymer, 2011. 52(26): p. 6074-6079.
72. Zako, M. and Takano, N., *Intelligent material systems using epoxy particles to repair microcracks and delamination damage in GFRP*. Journal of Intelligent Material Systems and Structures, 2000. 10(10): p. 836-841.
73. Nakamura, Y., Yamaguchi, M., Okubo, M., and Matsumoto, T., *Effects of particle size on mechanical and impact properties of epoxy resin filled with spherical silica*. Journal of Applied Polymer Science, 1992. 45(7): p. 1281-1289.
74. Rong, M.Z., Zhang, M.Q., Pan, S.L., Lehmann, B., and Friedrich, K., *Analysis of the interfacial interactions in polypropylene/silica nanocomposites*. Polymer International, 2004. 53(2): p. 176-183.
75. Wu, C.L., Zhang, M.Q., Rong, M.Z., and Friedrich, K., *Silica nanoparticles filled polypropylene: Effects of particle surface treatment, matrix ductility and particle species on mechanical performance of the composites*. Composites Science and Technology, 2005. 65(3-4): p. 635-645.
76. Soutis, C., *Fibre reinforced composites in aircraft construction*. Progress in Aerospace Sciences, 2005. 41(2): p. 143-151.
77. Peterson, A.M., Jensen, R.E., and Palmese, G.R., *Reversibly cross-linked polymer gels as healing agents for epoxy-amine thermosets*. ACS Applied Materials and Interfaces, 2009. 1(5): p. 992-995.
78. Lafont, U., Van Zeijl, H., and van der Zwaag, S., *Influence of cross-linkers on the cohesive and adhesive self-healing ability of polysulfide-based thermosets*. ACS Applied Materials and Interfaces, 2012. 4(11): p. 6280-6288.
79. Ling, J., Rong, M.Z., and Zhang, M.Q., *Photo-stimulated self-healing polyurethane containing dihydroxyl coumarin derivatives*. Polymer (United Kingdom), 2012. 53(13): p. 2691-2698.
80. Hayes, S.A., Jones, F.R., Marshiya, K., and Zhang, W., *A self-healing thermosetting composite material*. Composites Part A: Applied Science and Manufacturing, 2007. 38(4): p. 1116-1120.
81. Luo, X., Ou, R., Eberly, D.E., Singhal, A., Viratyaporn, W., and Mather, P.T., *A thermoplastic/thermoset blend exhibiting thermal mending and reversible adhesion*. ACS Applied Materials and Interfaces, 2009. 1(3): p. 612-620.
82. Sandler, J.K.W., Kirk, J.E., Kinloch, I.A., Shaffer, M.S.P., and Windle, A.H., *Ultra-low electrical percolation threshold in carbon-nanotube-epoxy composites*. Polymer, 2003. 44(19): p. 5893-5899.
83. Gojny, F.H., Wichmann, M.H., Fiedler, B., Kinloch, I.A., Bauhofer, W., Windle, A.H., and Schulte, K., *Evaluation and identification of electrical and*

- thermal conduction mechanisms in carbon nanotube/epoxy composites*. Polymer, 2006. 47(6): p. 2036-2045.
84. Gubbels, F., Blacher, S., Vanlathem, E., Jérôme, R., Deltour, R., Brouers, F., and Teyssie, P., *Design of electrical composites: determining the role of the morphology on the electrical properties of carbon black filled polymer blends*. Macromolecules, 1995. 28(5): p. 1559-1566.
85. Zheng, W. and Wong, S.-C., *Electrical conductivity and dielectric properties of PMMA/expanded graphite composites*. Composites Science and Technology, 2003. 63(2): p. 225-235.
86. Sengupta, R., Bhattacharya, M., Bandyopadhyay, S., and Bhowmick, A.K., *A review on the mechanical and electrical properties of graphite and modified graphite reinforced polymer composites*. Progress in Polymer Science, 2011. 36(5): p. 638-670.
87. Feller, J.F., Linossier, I., and Grohens, Y., *Conductive polymer composites: comparative study of poly(ester)-short carbon fibres and poly(epoxy)-short carbon fibres mechanical and electrical properties*. Materials Letters, 2002. 57(1): p. 64-71.
88. Choi, M.H., Jeon, B.H., and Chung, I.J., *The effect of coupling agent on electrical and mechanical properties of carbon fiber/phenolic resin composites*. Polymer, 2000. 41(9): p. 3243-3252.
89. Kim, W.J., Taya, M., and Nguyen, M.N., *Electrical and thermal conductivities of a silver flake/thermosetting polymer matrix composite*. Mechanics of Materials, 2009. 41(10): p. 1116-1124.
90. Stauffer, D. and Aharony, A., *Introduction to percolation theory*. 1994: CRC press.
91. Bilotti, E., Zhang, H., Deng, H., Zhang, R., Fu, Q., and Peijs, T., *Controlling the dynamic percolation of carbon nanotube based conductive polymer composites by addition of secondary nanofillers: The effect on electrical conductivity and tuneable sensing behaviour*. Composites Science and Technology, 2013. 74(0): p. 85-90.
92. Calberg, C., Blacher, S., Gubbels, F., Brouers, F., Deltour, R., and Jérôme, R., *Electrical and dielectric properties of carbon black filled co-continuous two-phase polymer blends*. Journal of Physics D: Applied Physics, 1999. 32(13): p. 1517.
93. Thongruang, W., Spontak, R.J., and Balik, C.M., *Bridged double percolation in conductive polymer composites: an electrical conductivity, morphology and mechanical property study*. Polymer, 2002. 43(13): p. 3717-3725.
94. Kitajima, S., Matsuda, M., Yamato, M., and Tominaga, Y., *Anisotropic ionic conduction in composite polymer electrolytes filled with clays oriented by a strong magnetic field*. Polym J, 2013. 45(7): p. 738-743.
95. Li, Y., Chen, S., Wu, M., and Sun, J., *Polyelectrolyte Multilayers Impart Healability to Highly Electrically Conductive Films*. Advanced Materials, 2012. 24(33): p. 4578-4582.
96. Tee, B.C.K., Wang, C., Allen, R., and Bao, Z., *An electrically and mechanically self-healing composite with pressure- and flexion-sensitive*

- properties for electronic skin applications*. Nat Nano, 2012. 7(12): p. 825-832.
97. Palleau, E., Reece, S., Desai, S.C., Smith, M.E., and Dickey, M.D., *Self-Healing Stretchable Wires for Reconfigurable Circuit Wiring and 3D Microfluidics*. Advanced Materials, 2013. 25(11): p. 1589-1592.
98. Wang, C., Wu, H., Chen, Z., McDowell, M.T., Cui, Y., and Bao, Z., *Self-healing chemistry enables the stable operation of silicon microparticle anodes for high-energy lithium-ion batteries*. Nat Chem, 2013. 5(12): p. 1042-1048.
99. Simon, R.M., *EMI shielding through conductive plastics*. Polymer-Plastics Technology and Engineering, 1981. 17(1): p. 1-10.
100. Bar-Cohen, Y., *Electroactive polymers as artificial muscles: A review*. Journal of Spacecraft and Rockets, 2002. 39(6): p. 822-827.
101. Bar-Cohen, Y. and Zhang, Q., *Electroactive Polymer Actuators and Sensors*. MRS Bulletin, 2008. 33(03): p. 173-181.
102. Martins, P., Lopes, A.C., and Lanceros-Mendez, S., *Electroactive phases of poly(vinylidene fluoride): Determination, processing and applications*. Progress in Polymer Science, 2013.
103. Vinogradov, A.M. *Accomplishments and future trends in the field of electroactive polymers*. 2008.
104. Pelrine, R., Kornbluh, R., and Kofod, G., *High-strain actuator materials based on dielectric elastomers*. Advanced Materials, 2000. 12(16): p. 1223-1225.
105. Pelrine, R., Kornbluh, R., Pei, Q., and Joseph, J., *High-speed electrically actuated elastomers with strain greater than 100%*. Science, 2000. 287(5454): p. 836-839.
106. Akle, B.J., Leo, D.J., Hickner, M.A., and McGrath, J.E., *Correlation of capacitance and actuation in ionomeric polymer transducers*. Journal of Materials Science, 2005. 40(14): p. 3715-3724.
107. Tiwari, R. and Garcia, E., *The state of understanding of ionic polymer metal composite architecture: A review*. Smart Materials and Structures, 2011. 20(8).
108. Liu, Y., Ghaffari, M., Zhao, R., Lin, J.H., Lin, M., and Zhang, Q.M., *Enhanced electromechanical response of ionic polymer actuators by improving mechanical coupling between ions and polymer matrix*. Macromolecules, 2012. 45(12): p. 5128-5133.
109. Akle, B.J. and Leo, D.J., *Softening and heating effects in ionic polymer transducers: An experimental investigation*. Journal of Intelligent Material Systems and Structures, 2013. 24(10): p. 1266-1277.
110. Bhadra, S., Khastgir, D., Singha, N.K., and Lee, J.H., *Progress in preparation, processing and applications of polyaniline*. Progress in Polymer Science (Oxford), 2009. 34(8): p. 783-810.
111. Barisci, J.N., Lewis, T.W., Spinks, G.M., Too, C.O., and Wallace, G.G., *Conducting polymers as a basis for responsive materials systems*. Journal of Intelligent Material Systems and Structures, 1999. 9(9): p. 723-731.

112. Tressler, J.F., Alkoy, S., and Newnham, R.E., *Piezoelectric sensors and sensor materials*. Journal of Electroceramics, 1998. 2(4): p. 257-272.
113. McClory, C., Chin, S.J., and McNally, T., *Polymer/carbon nanotube composites*. Australian Journal of Chemistry, 2009. 62(8): p. 762-785.
114. Banerjee, S. and Cook-Chennault, K.A., *An investigation into the influence of electrically conductive particle size on electromechanical coupling and effective dielectric strain coefficients in three phase composite piezoelectric polymers*. Composites Part A: Applied Science and Manufacturing, 2012. 43(9): p. 1612-1619.
115. Soroushian, P., Nassar, R.U.D., and Balachandra, A.M., *Piezo-driven self-healing by electrochemical phenomena*. Journal of Intelligent Material Systems and Structures, 2013. 24(4): p. 441-453.
116. James, N.K., Lafont, U., van der Zwaag, S., and Groen, W.A., *Piezoelectric and mechanical properties of fatigue resistant, self healing PZT-ionomer composites*. Smart Materials and Structures, 2014.
117. Ahmad, H., Kumar, K., Rahman, M.A., Rahman, M.M., Miah, M.A.J., Minami, H., and Nuri, M.A., *Preparation and characterization of conducting polyaniline layered magnetic nano composite polymer particles*. Polymers for Advanced Technologies, 2013. 24(8): p. 740-746.
118. Lagorce, L.K. and Allen, M.G., *Magnetic and mechanical properties of micromachined strontium ferrite/polyimide composites*. Microelectromechanical Systems, Journal of, 1997. 6(4): p. 307-312.
119. Munoz Resta, I., Horwitz, G., Mendez Elizalde, M.L., Jorge, G.A., Molina, F.V., and Soledad Antonel, P., *Magnetic and Conducting Properties of Composites of Conducting Polymers and Ferrite Nanoparticles*. Magnetism, IEEE Transactions on, 2013. 49(8): p. 4598-4601.
120. Song, P., Peng, Z., Yue, Y., Zhang, H., Zhang, Z., and Fan, Y., *Mechanical properties of silicone composites reinforced with micron-and nano-sized magnetic particles*. EXPRESS POLYMER LETTERS, 2013. 7(6): p. 546-553.
121. Ramajo, L.A., Cristóbal, A.A., Botta, P.M., Porto López, J.M., Reboredo, M.M., and Castro, M.S., *Dielectric and magnetic response of Fe₃O₄/epoxy composites*. Composites Part A: Applied Science and Manufacturing, 2009. 40(4): p. 388-393.
122. Senthur Pandi, R., Chokkalingam, R., and Mahendran, M., *Thermal and Magnetic studies of Ni-Mn-Ga/PU Polymer Composites*. Indian Journal of Physics, 2012. 86(9): p. 787-790.
123. Gokturk, H.S., Fiske, T.J., and Kalyon, D.M., *Electric and magnetic properties of a thermoplastic elastomer incorporated with ferromagnetic powders*. Magnetism, IEEE Transactions on, 1993. 29(6): p. 4170-4176.
124. Szabó, D. and Zrínyi, M., *MUSCULAR CONTRACTION MIMICED BY MAGNETIC GELS*. International Journal of Modern Physics B, 2001. 15(06n07): p. 557-563.
125. Nguyen, V.Q. and Ramanujan, R.V., *Novel Coiling Behavior in Magnet-Polymer Composites*. Macromolecular Chemistry and Physics, 2010. 211(6): p. 618-626.

126. Nguyen, V.Q., Ahmed, A.S., and Ramanujan, R.V., *Morphing Soft Magnetic Composites*. Advanced Materials, 2012. 24(30): p. 4041-4054.
127. Xu, K., An, H., Lu, C., Tan, Y., Li, P., and Wang, P., *Facile fabrication method of hydrophobic-associating cross-linking hydrogel with outstanding mechanical performance and self-healing property in the absence of surfactants*. Polymer, 2013. 54(21): p. 5665-5672.
128. Kakuta, T., Takashima, Y., Nakahata, M., Otsubo, M., Yamaguchi, H., and Harada, A., *Preorganized Hydrogel: Self-Healing Properties of Supramolecular Hydrogels Formed by Polymerization of Host-Guest-Monomers that Contain Cyclodextrins and Hydrophobic Guest Groups*. Advanced Materials, 2013. 25(20): p. 2849-2853.
129. Hao, X., Liu, H., Xie, Y., Fang, C., and Yang, H., *Thermal-responsive self-healing hydrogel based on hydrophobically modified chitosan and vesicle*. Colloid and Polymer Science, 2013. 291(7): p. 1749-1758.
130. Zhang, Y., Yang, B., Zhang, X., Xu, L., Tao, L., Li, S., and Wei, Y., *A magnetic self-healing hydrogel*. Chemical Communications, 2012. 48(74): p. 9305-9307.
131. Sim, L.C., Ramanan, S.R., Ismail, H., Seetharamu, K.N., and Goh, T.J., *Thermal characterization of Al₂O₃ and ZnO reinforced silicone rubber as thermal pads for heat dissipation purposes*. Thermochimica Acta, 2005. 430(1-2): p. 155-165.
132. Nakamura, A. and Iji, M., *Factors affecting the magnitudes and anisotropies of the thermal and electrical conductivities of poly(L-lactic) acid composites with carbon fibers of various sizes*. Journal of Materials Science, 2011. 46(3): p. 747-751.
133. Fu, S., Song, P., Yang, H., Jin, Y., Lu, F., Ye, J., and Wu, Q., *Effects of carbon nanotubes and its functionalization on the thermal and flammability properties of polypropylene/wood flour composites*. Journal of Materials Science, 2010. 45(13): p. 3520-3528.
134. Wattanakul, K., Manuspiya, H., and Yanumet, N., *Thermal conductivity and mechanical properties of BN-filled epoxy composite: effects of filler content, mixing conditions, and BN agglomerate size*. Journal of Composite Materials, 2011. 45(19): p. 1967-1980.
135. Ren, F., Ren, P.-g., Di, Y.-y., Chen, D.-m., and Liu, G.-g., *Thermal, Mechanical and Electrical Properties of Linear Low-Density Polyethylene Composites Filled with Different Dimensional SiC Particles*. Polymer-Plastics Technology and Engineering, 2011. 50(8): p. 791-796.
136. Devpura, A., Phelan, P.E., and Prasher, R.S. *Percolation theory applied to the analysis of thermal interface materials in flip-chip technology*. in *Thermal and Thermomechanical Phenomena in Electronic Systems, 2000. ITHERM 2000. The Seventh Intersociety Conference on*. 2000.
137. Xuejiao, H., Linan, J., and Goodson, K.E. *Thermal conductance enhancement of particle-filled thermal interface materials using carbon nanotube inclusions*. in *Thermal and Thermomechanical Phenomena in Electronic Systems, 2004. ITHERM '04. The Ninth Intersociety Conference on*. 2004.

138. Kim, B.-W., Park, S.-H., Kapadia, R.S., and Bandaru, P.R., *Evidence of percolation related power law behavior in the thermal conductivity of nanotube/polymer composites*. Applied Physics Letters, 2013. 102(24): p. -.
139. Kwon, S.Y., Kwon, I.M., Kim, Y.-G., Lee, S., and Seo, Y.-S., *A large increase in the thermal conductivity of carbon nanotube/polymer composites produced by percolation phenomena*. Carbon, 2013. 55(0): p. 285-290.
140. Wang, B., Hao, J., and Li, H., *Remarkable improvements in the stability and thermal conductivity of graphite/ethylene glycol nanofluids caused by a graphene oxide percolation structure*. Dalton Transactions, 2013. 42(16): p. 5866-5873.
141. Zhou, W., *Effect of coupling agents on the thermal conductivity of aluminum particle/epoxy resin composites*. Journal of Materials Science, 2011. 46(11): p. 3883-3889.
142. Zengbin, W., Iizuka, T., Kozako, M., Ohki, Y., and Tanaka, T., *Development of epoxy/BN composites with high thermal conductivity and sufficient dielectric breakdown strength part I - sample preparations and thermal conductivity*. Dielectrics and Electrical Insulation, IEEE Transactions on, 2011. 18(6): p. 1963-1972.
143. Zhang, M., Gu, A., Liang, G., and Yuan, L., *Preparation of high thermal conductive aluminum nitride/cyanate ester nanocomposite using a new macromolecular coupling agent*. Polymers for Advanced Technologies, 2012. 23(11): p. 1503-1510.
144. Every, A.G., Tzou, Y., Hasselman, D.P.H., and Raj, R., *The effect of particle size on the thermal conductivity of ZnS/diamond composites*. Acta Metallurgica et Materialia, 1992. 40(1): p. 123-129.
145. Chou, T.-L., Huang, C.-F., Han, C.-N., Yang, S.-Y., and Chiang, K.-N., *Fabrication process simulation and reliability improvement of high-brightness LEDs*. Microelectronics Reliability, 2009. 49(9-11): p. 1244-1249.
146. Longzao, Z., Bing, A., Yiping, W., and Shunhong, L. *Analysis of delamination and darkening in high power LED packaging*. in *Physical and Failure Analysis of Integrated Circuits, 2009. IPFA 2009. 16th IEEE International Symposium on the*. 2009.
147. Lu, G., Yang, S., and Huang, Y. *Analysis on failure modes and mechanisms of LED*. in *Reliability, Maintainability and Safety, 2009. ICRMS 2009. 8th International Conference on*. 2009. IEEE.
148. Lafont, U., Moreno-Belle, C., van Zeijl, H., and van der Zwaag, S., *Self-healing thermally conductive adhesives*. Journal of Intelligent Material Systems and Structures, 2014. 25(1): p. 67-74.
149. Lafont, U., van Zeijl, H., and van der Zwaag, S., *Increasing the reliability of solid state lighting systems via self-healing approaches: A review*. Microelectronics Reliability, 2012. 52(1): p. 71-89.

Chapter 4

Moderate temperature healing in a glass fibre reinforced composite with a disulphide containing organic-inorganic epoxy matrix

This chapter has been published as:

W. Post, A. Cohades, V. Michaud, S. van der Zwaag, S. J. García

Healing of a glass fibre reinforced composite with a disulphide containing organic-inorganic epoxy matrix

Composites, Science and Technology, volume 152, November 2017, pages 85-93

4.1. Introduction

Over the past decades, fibre reinforced polymer composites (FRPCs) have found their way into numerous lightweight structural, automotive and aerospace applications. However, their complex failure behaviour and high susceptibility to impact and fatigue damage makes FRPCs hard to repair after being damaged. As such, it is of high interest to develop FRPCs that can heal themselves multiple times, thereby extending their overall lifetime [1-3]. Thermoset polymer matrices (i.e. polymers having a decent dimensional stability under load) with an intrinsic healing ability (i.e. the healing stems from the polymer architecture itself) are considered to be ideal candidates for the recovery of frequently occurring damage modes in fibre reinforced polymer composites, such as barely visible impact damage, matrix cracking and delaminations [4-6]. Contrary to approaches based on extrinsic self-healing polymeric systems (i.e. polymers with embedded discrete healing agents) [7-10], composites based on intrinsic healing polymers can undergo multiple healing events provided the damage to the reinforcing fibres is not excessive or highly localised [11]. Over the past decade several polymer matrices, with proven intrinsic healing capacity, have been proposed for polymer composites. The most common approach is by using matrices containing reversible Diels Alder moieties which have a high compatibility with conventional epoxy matrices [12-14]. Another approach is the use of thermoplastic ionomers, which are of interest due to their relatively high thermomechanical properties during healing [15-17]. Recently, glass fibre composites were manufactured with the supramolecular polymer Reverlink (from Arkema) which showed healing at room temperature [18]. Another common strategy is the blending of immiscible thermoplastic polymers with epoxy-based thermosets. Upon melting, the thermoplastic phase flows into the damaged region while the thermoset phase ensures the mechanical stability [19-21]. However, all these examples result in composites, which are also marked by either low mechanical properties, high ($>100^{\circ}\text{C}$) healing temperatures, unconventional manufacturing routes or a combination of these undesirable factors.

A promising recent approach to obtain a good combination of adequate mechanical properties and healing at low temperature is the introduction of covalently bonded disulphide groups within a conventional epoxy based network. These systems combine mild healing temperatures ($<100^{\circ}\text{C}$) with relatively high mechanical properties (Young's modulus within the range of 20-200 MPa) and proved to be ideal candidates for the development of self-healing coatings [22-24], rubbers [25] and composites [26, 27]. However, the majority of these polymer systems still have insufficient mechanical properties and their complex chemistries (resulting in high viscosities or fast reactivity) make conventional composite processing impractical for application in structural composites. Additionally, these polymers often require a

healing temperature that is similar to or even higher than their curing temperature. For example, Odrizola et al. developed FRPCs, cured at 150°C, with mechanical properties similar to commercial epoxy composites while the selected repair temperature is 200°C [27]. As a result, it is difficult to decouple healing and post-curing effects. Furthermore the overlap of healing and curing temperatures will ultimately limit the possibility of multiple healing.

In intrinsic healing of polymeric matrices, a high elastic modulus (at room temperature) is generally accompanied by a high healing temperature. Figure 4.1 summarizes the major developments in the field by representing the elastic modulus versus the healing temperature of a wide range of intrinsic healing polymer matrices. The figure includes branched polyetherimide (PEI) elastomers [28], multiphase elastomers [29], supramolecular elastomers [30-32], human skin [33], disulfide based elastomers [25], metallopolymer [34], ionomers [17], Diels-Alder based polymers [35, 36], epoxy-PCL blends [19] and the family of disulfide based epoxy thermosets [24, 26]. For comparison, a selection of engineering thermoplastics at their melting temperatures was added to the figure [37]. Figure 4.1 clearly shows that the current challenge in self-healing polymers lies within the development of systems with a high modulus and low healing temperature in order to reach properties of interest that can compete with commercial high performance polymers.

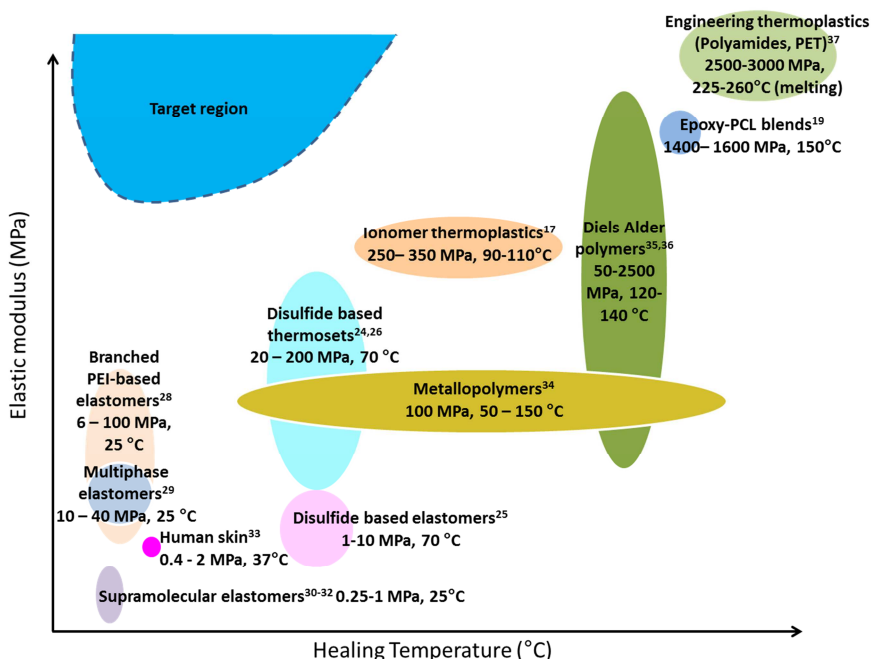


Figure 4.1 Overview of elastic modulus versus healing temperature of a wide range of intrinsic self-healing polymer matrices developed in the past decade.

Figure 4.1 shows that the disulphide based thermosets are among the polymer systems closest to the target region for intrinsic self-healing polymers, thereby indicating that these polymers are a good starting point for the development of self-healing fibre composites with good mechanical properties. This work presents a next step in this direction by introducing a self-healing glass fibre reinforced polymer (GFRP) composite based on an organic-inorganic disulphide containing epoxy thermoset. This polymeric system shows multiple healing upon a short thermal treatment of 70°C and has mechanical properties (20-200 MPa) suitable for coating applications [24, 38]. To allow for processing by conventional composite manufacturing routes the polymer matrix curing kinetics were slowed down by modifying the polymer composition. The effect of the curing conditions on the room temperature stiffness and the matrix network mobility at elevated temperatures was investigated. Subsequently, GFRPs were prepared and their multiple healing capabilities at modest temperatures were evaluated by conventional flexural, fracture and low-velocity impact testing.

4.2. Experimental

4.2.1. Materials

EponTM 828 resin was purchased from Momentive. Ancamine®2500 curing agent was purchased from Air Products. (3-Aminopropyl)trimethoxysilane (97%), Pentaerythritol tetrakis(3-mercaptopropionate) and Triethylamine from hereon called APTS, tetrathiol and TEA respectively, were purchased from Sigma-Aldrich. Bis[3-(triethoxysilyl)propyl]disulfide (99%), from hereon called BDS, was purchased from Capture Chemicals. All chemicals were used as received without further purification. The selected glass fibre reinforcement was a woven twill 2 × 2 E-glass fabric, with a nominal areal weight of 390 g.m⁻², 6 end cm⁻¹ for warp fibres and 6.7 picks cm⁻¹ for weft fibres, fibre diameter of 9 µm yarn thickness of 0.45 mm, warp tex of 68 × 5 and weft tex of 272, from Suter-Kunststoffe AG.

4.2.2. Resin and GFRPs production

4.2.2.1. Resin preparation

The selected polymer matrix is an adaptation of a dual network polymer network reported in previous studies [24, 26] and is composed of six different components. Compared to this previous work Bis[3-(triethoxysilyl)propyl]tetrasulfide (BTS) was replaced by BDS. To facilitate the disulphide cleavage essential in matrix healing TEA was added as a catalyst.

EponTM 828, APTS and BDS were pre-stirred using a magnetic stirrer for 3 hours at room temperature. Ancamine® 2500 was then added and the mixture was manually stirred for 3 minutes until the mixture was fully homogeneous. The resulting mixture

and the tetrathiol were then degassed in a vacuum chamber for 10 minutes. Then, TEA and tetrathiol were added and the final resin was manually stirred for another 5 minutes. The weight ratio of all resin components is depicted in Table 4.1. For characterization of the free standing polymer matrix, the resin was poured into a Teflon mould and was cured for 24 hours at room temperature followed by 60 hours curing at 100°C under ambient conditions.

Table 4.1 Weight ratio of resin components in the self-healing polymer matrix

| Resin component | Weight ratio |
|---|---------------------|
| EponTM 828 | 1 |
| Ancamine® 2500 | 0,646 |
| (3-Aminopropyl)trimethoxysilane | 0,076 |
| Pentaerythritol tetrakis(3-mercaptopropionate) | 0,579 |
| Bis[3-(triethoxysilyl)propyl]disulfide | 0,566 |
| Triethylamine | 0,014 |

4.2.3. Composite processing

A total of 600 gram of resin was prepared per composite plate. In order to increase the pot-life, this amount was divided into two batches of 300 gram resin each. The resin viscosity was found to be below 0.5 Pa.s at room temperature (determined by a rheometer AR 2000 from TA Instruments). The resin was therefore infused at room temperature into a stack of 20 x 30 cm glass fibre reinforcement layers with a $[(+45/-45)/(0/90)]_{45}$ sequence using conventional vacuum assisted resin infusion moulding (VARIM) as described in previous work [18]. To improve the resin impregnation an additional flow mesh was placed at the bottom of the product. Following this procedure a plate thickness of 4.5 mm and a fibre volume fraction of 50 vol.% were targeted. A Teflon film (Cytec, 15 µm, non-perforated) was inserted in between the two central plies to form the notch in the specimens that were prepared for double cantilever beam testing. After infusion the resulting product was first cured for 24 hours at room temperature under vacuum conditions and then for 60 hours at 100°C under ambient conditions. After this final curing step the composite plates were cooled down and cut with a diamond saw to obtain the preferred test specimen geometries.

4.2.4. Characterization methods

4.2.4.1. Matrix characterization

The effect of different curing treatments on the properties of the matrix polymer was investigated with thermal and mechanical testing techniques. The thermo-mechanical properties were measured by dynamic mechanical analysis (DMA) using a TA Instruments DMA Q800 operating in single cantilever bending mode. Rectangular specimens (35 x 12.5 x 2 mm) were heated from -50°C to 150°C with a

heating ramp of 5°C/min. A frequency of 1 Hz and a strain of 0.02% were applied. The tensile behaviour of the matrix was investigated according to ASTM D1708-13 using an Instron Model 3365 universal testing systems equipped with a 1 kN load cell. Dog-bone micro-tensile specimens were loaded until failure at 2 mm/min at room temperature. A total number of 5 samples were tested per test condition.

4.2.4.2. GFRP composite characterization

Three methods of mechanical characterization were selected to investigate the properties of the composites and their self-healing behaviour: 3-point bending, double cantilever beam (DCB) and low-velocity impact testing.

3-point bending experiments were performed according to ASTM D790 to determine the healing of the flexural properties of the composites. A UTM Series LFM-125kN (Walter and Bai), equipped with a 10 kN load cell, was used in compression mode. Specimens were 220 mm long, 15 mm wide and approximately 4.5 mm thick. 1 test condition (85°C healing at 0.2 bar) was repeated 5 times, the remaining test conditions were only performed once. A span-to-depth ratio of 40:1 was used and a crosshead speed of 2 mm/min was applied. As the specimen did not fully fracture, the experiment was terminated after a maximum centre beam deflection of 25 mm was obtained. The flexural stress was calculated using equation (4.1) [39]:

$$\sigma_f = \left(\frac{3PL}{2bd^2} \right) \left[1 + 6 \left(\frac{D}{L} \right)^2 - 4 \left(\frac{d}{L} \right) \left(\frac{D}{L} \right) \right] \quad (4.1)$$

where σ_f is the flexural stress (MPa), L is the support span (mm), d is the depth of beam (mm), P is the measured load at a given point (N), b is the beam thickness (mm), and D is the deflection of the centerline of the specimen at the middle of the support span (mm). The flexural strain was calculated using equation (2) [39]:

$$\varepsilon_f = \frac{6Dd}{L^2} * 100 \quad (4.2)$$

where ε_f is the flexural strain (%). The flexural modulus was calculated using [39]:

$$E_B = \frac{L^3 m}{4bd^3} \quad (4.3)$$

Where E_B is the flexural modulus (MPa) and m is the slope of the linear section of the load-deflection curve between 0 and 0.05 % strain (N/mm). The extent of damage and healing after the 3-point bending experiments was visualized using a digital microscope Keyence VHX2000 with a wide-range zoom lens (100x-1000x

magnification). For the optimal illumination of the surfaces the microscope was equipped with a OP-87229 short ring-light.

Mode I opening of DCB specimens was performed following ASTM D5528. A Zwick mechanical testing machine (model 1455) equipped with a 20 kN load cell was used. A constant crosshead speed of 5 mm/min was applied and the experiment was stopped when a final displacement of 50 mm was achieved. The crack growth was monitored by a camera that was positioned perpendicular to the crack progression. Using the modified beam theory the local fracture toughness (G_I) was determined using [40]:

$$G_I = \frac{3P\delta}{2b(a + |\Delta|)} \quad (4.4)$$

Where δ is the load-point displacement (mm), a is the delamination length (mm) and $|\Delta|$ is the experimental correction factor which is determined by generating a least squares plot of the cube root of the compliance as a function of the delamination length, as is described by ASTM D5528. One sample was tested per test condition.

Low-velocity impact tests were performed according to ASTM D7136 using a free fall impact tower (Rosand IFW) with a 5.5 kg mass and 16 mm diameter hemispherical aluminium impactor. Samples of 80 x 80 mm were used. Three samples were tested per test condition. Samples were impacted with relatively low impact energies of 8, 16 or 30 Joule in order to mainly induce delamination and to minimize fibre breakage. A 60 kN Kistler load cell was used to measure the impact force and light gages were used to measure the inbound and rebound speed of the impactor. The level of dissipated energy (E_d) per impact condition was determined by [41]:

$$E_d = \frac{1}{2}m(v_{in} - v_{out})^2 \quad (4.5)$$

Where m is the mass of the impactor (kg) and v_{in} and v_{out} are the inbound and rebound speed (m/s) respectively. The extent of damage was monitored by taking photographs before and after healing. The photographs before and after healing were further processed using a Matlab code and binarized with a threshold of 0.125 in order to estimate the healed areas per impact energy.

4.2.4.3. Healing treatment

Healing of specimens subjected to bending and impact was performed at room temperature (RT), 70, 85 and 100°C using a hot-air furnace for 16 hours. Contact between the damaged interfaces during healing was ensured by dead weight loading at a constant pressure of 0.2 bar. The specimens tested by Mode I opening

were healed at 85°C and 0.2, 2.0 and 20 bar whereby the higher pressure conditions (2.0 and 20 bar) were applied using a hot-press.

4.3. Results & discussion

4.3.1. Polymer matrix optimisation

To identify the effect of the polymer curing conditions (time and temperature) on the mechanical properties of the composites at room temperature and at the range of intended healing temperatures (70-100°C), Figure 4.2 shows the storage modulus-temperature relation for different curing conditions. At each temperature, the glass transition temperature (T_g) and the storage modulus (E') increase with the curing temperature and time. The increase in E' is most remarkable when $T > T_g$ which indicates an increase in the crosslinking density.

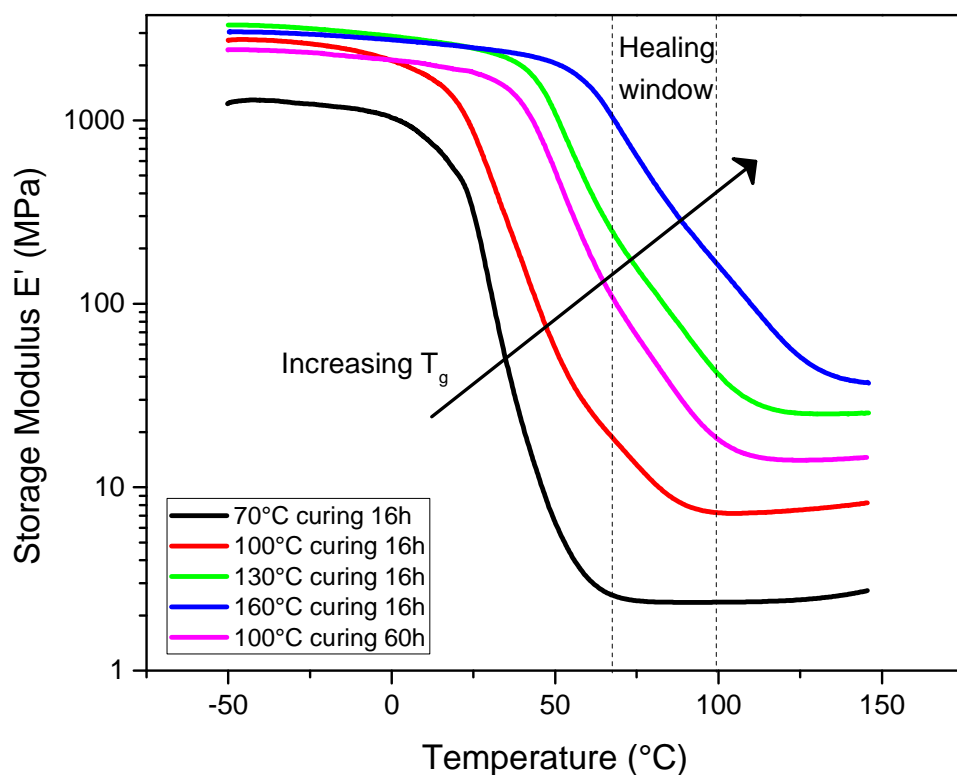


Figure 4.2 Storage modulus vs. temperature of the dual network polymer matrix after different curing conditions.

The general stress-strain relations of the polymer matrix after different curing conditions are given in Supplementary Information S1. Derived from these results, Figure 4.3 shows the variation of the Young's modulus of the polymer matrix after different curing conditions. It is shown that a combination of adequate curing time

and temperature leads to a room temperature stiffness higher than 1000 MPa, which is in the same order of magnitude as that of commercial epoxy matrices. These experiments show that the elastic modulus of the modified matrix after the selected curing treatment is reaching the lower limits of the target region for intrinsic self-healing polymers depicted in Figure 4.1.

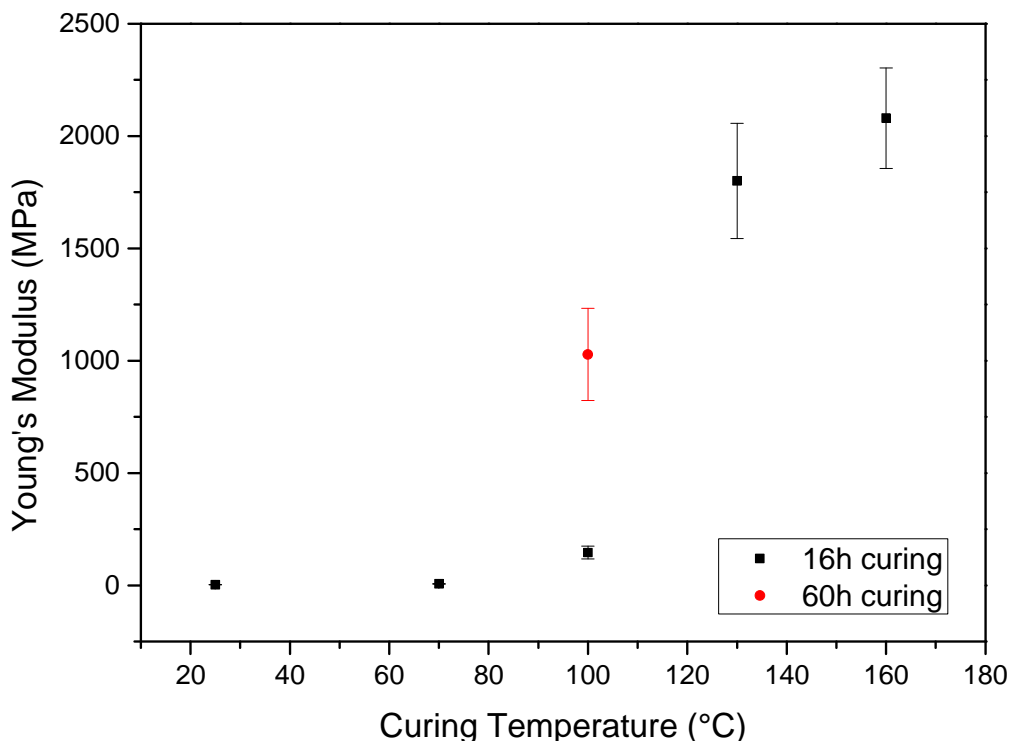


Figure 4.3 Effect of the curing treatment on the resulting Young's modulus of the dual network polymer matrix

Self-healing polymer matrices to be used for structural composites require a modulus that is high at room/service temperature and relatively low at the targeted healing temperatures so the matrix obtains sufficient mobility to heal while retaining its structural integrity [38]. From Figure 4.2 and Figure 4.3 it can be extracted that this combination of properties can be best achieved with a curing process at 100°C for 60 hours amongst all the curing conditions evaluated in this study. Therefore these curing conditions are used throughout the remainder of this study. However, it has to be noted that a more extensive study on these characteristics will most likely lead to a further optimized set of curing parameters.

4.3.2. Composite characterization

Using the curing conditions derived in section 3.1, GFRP laminates were prepared by conventional vacuum infusion processing. As a result, composites with a fibre volume fraction of $51.0 \pm 0.9\%$ were obtained (assuming a negligible porosity). Consecutively, the flexural, interlaminar fracture and impact properties were tested before and after healing with 3-point bending, DCB and low-velocity impact testing respectively.

4.3.2.1. Flexural properties

Figure 4.4 shows the flexural stress-strain relation for different composite beams after multiple healing treatments (always for 16 hours at 0.2 bar) at different healing temperatures. From the curves of the pristine specimen an average flexural modulus of 10.1 ± 0.7 GPa and yield strength of 55.0 ± 3.7 MPa can be derived. These values are approaching those of high-performance composites, although they are not yet at a level where they can fully compete with these materials on a commercial level [21].

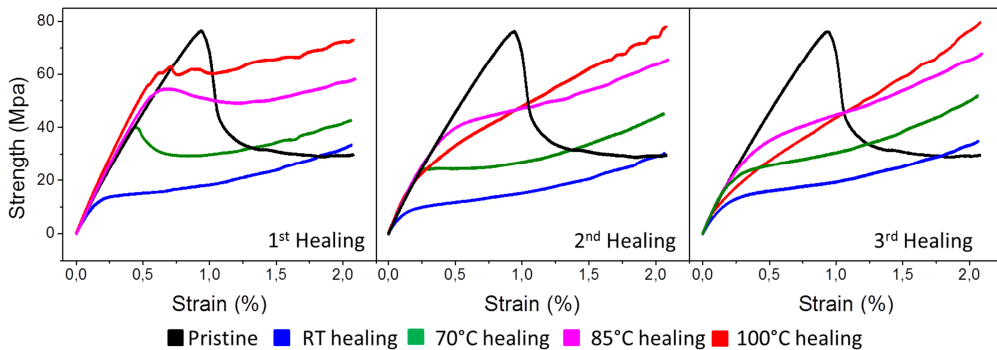


Figure 4.4 Stress-strain curves of the flexural tests performed on composite beams. The figure shows the flexural properties of 3 consecutive runs of healing treatments for 4 different healing temperatures compared to a pristine test. Specimen were healed for 16 hours at a moderate pressure of 0.2 bar.

The results in Figure 4 show that after the first healing treatment, the level of repair depends on the selected healing temperature and that the highest healing temperature (100°C) leads to the highest levels of flexural modulus and yield strength recovery. The development of these mechanical properties is more clearly depicted in Figure 4.5, which reports the 0.1% offset yield strength and flexural modulus versus the number of bending cycles. Figure 4.5 also shows that the flexural modulus slightly increases after the first healing cycle for all healing temperatures applied. This is attributed to the post-curing of the unreacted alkoxysilane groups. The theory that the post-curing effect is the main explanation

for the healing observed is discarded by dedicated further testing as is shown in Supplementary Information S2.

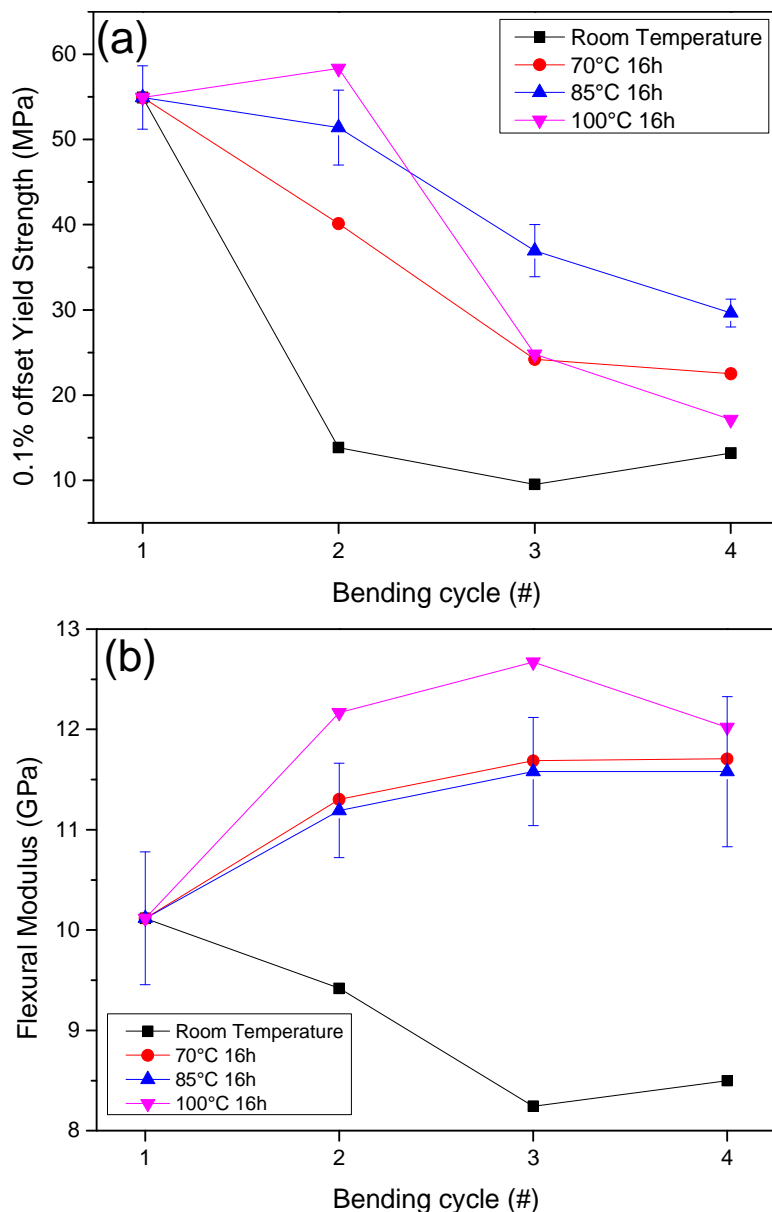


Figure 4.5 Effect of the selected healing temperature on the multiple healing of the yield strength (a) and the flexural modulus (b). Healing is performed for 16 hours at 0.2 bar at different temperatures (70, 85 and 100°C).

When multiple healing is taken into account, it is observed that the yield strength slowly decreases as the number of healing treatments is increased. However, for a

multiple healing treatment of 100°C, the yield strength drops much faster compared to the other healing temperatures. At the fourth bending cycle the resulting yield strength is almost at the level of the non-temperature treated reference specimen, indicating that the healing potential is almost depleted. These results therefore show that for an application with a yield strength design limit of 30 MPa it is better to use a temperature of 85°C as a longer lifetime extension is obtained. A similar trend seems to be present for the calculated flexural modulus although the decay of this property (at a healing temperature of 100°C) sets in later than that of the yield strength. The loss of healing efficiency over time is most likely caused by the slow oxidation of thiol groups which are known to assist the healing via reversible disulfide chemistry [42]. This thiol oxidation is faster when a higher temperature is applied [24]. As a result, the healing potential of these composites is not inexhaustable when low healing pressures are applied. Since healing at 85°C is seemingly most optimal, this temperature is selected as the healing temperature for the other composite healing experiments in the rest of the study.

Another interesting feature observed in Figure 4.4 is that after healing, the stress value at high strain levels is higher than that of a pristine specimen. As it turns out, the modulus at high strain (> 1.0%) of the healed composites is equal to that of the pristine matrix (Supplementary Information S3). At these strain levels it is therefore probable that the stress response is dominated by the polymer matrix which after healing compensates for the broken glass fibres. The flow of the matrix towards the cracks during healing is further illustrated by the OM images in Figure 4.6, which show the cracked regions of the composite before and after healing. The micrographs confirm that the matrix material slightly flows upon a healing treatment, thereby partially filling the crack volume.

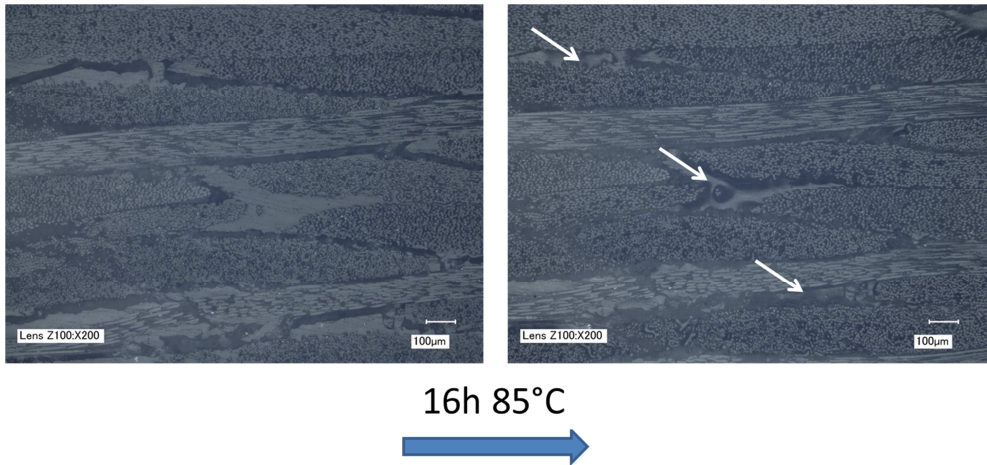


Figure 4.6 Optical microscopy images of a composite that has been subjected to 3-point bending before (left) and after (right) healing. Images are taken perpendicular (z-direction) of the bending direction. White arrows indicate regions of visible matrix flow.

4.3.2.2. *Interlaminar fracture properties*

To investigate the recovery of the interlaminar fracture properties, the composites were tested in Mode I DCB. In doing so, delaminated areas of 10-15 cm² were created. Such damage areas are several orders of magnitude larger than the µm²-mm² damage areas generated in the flexural tests. It was observed that the pressure applied during healing has a profound effect on such macroscale damage and therefore this effect was investigated in more detail by applying healing pressures of 0.2, 2 and 20 bar. Figure 4.7 shows the load-displacement curves of a fractured composite beam healed at 2 bar (for 16 hours at 85°C) for multiple healing cycles. In addition, the crack development during the experiment is shown. The force-displacement curves for the other applied healing pressures are shown in Supplementary Information S4.

From Figure 4.7 it can be observed that after the 1st healing treatment, upon reloading, the crack at the healed region propagates faster and that the measured maximum force is somewhat lower than that for the pristine specimen, indicating only partial damage healing. Upon the application of multiple healing cycles, the onset of crack propagation starts at an increasingly earlier stage for each damage and healing cycle. Still, the rate of crack propagation and the force development are similar for each healing cycle, which indicates that successful multiple healing is obtained.

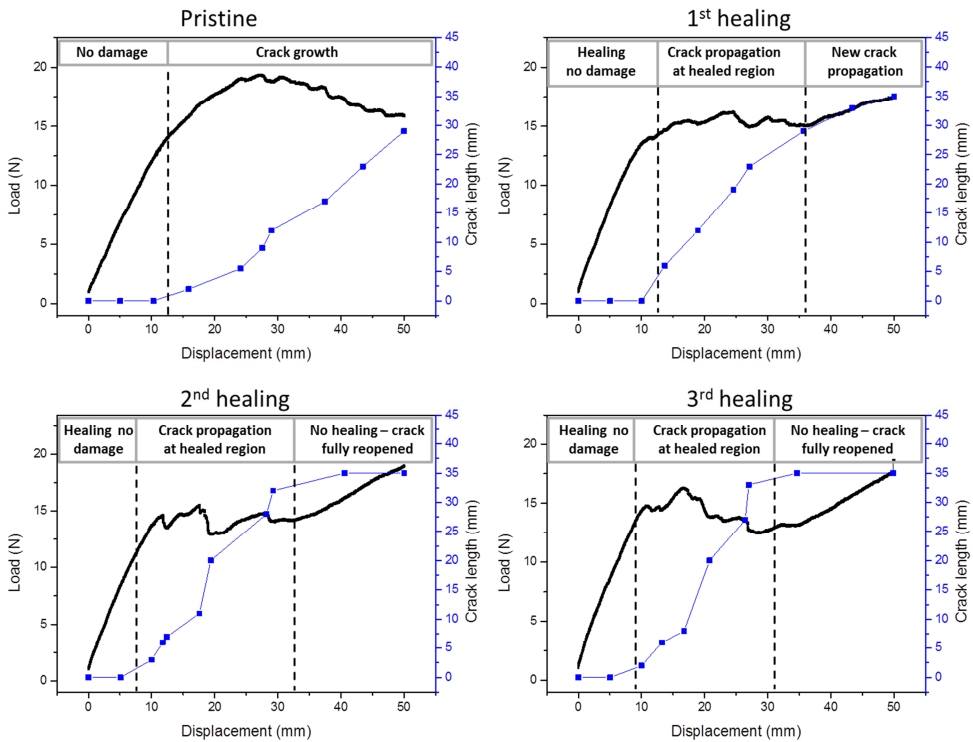


Figure 4.7 Combined load-displacement/crack propagation curves of the Mode I opening of a composite healed three times at 85°C and 2 bar pressure for 16 hours.

Figure 4.8 further explores the effect of healing pressure on the fracture toughness healing by showing the calculated interlaminar fracture toughness (G_I) versus the normalized crack length. From this figure it is observed that the composites have a lower initial fracture toughness than that of commercially available epoxy based thermosets ($>1000 \text{ kJ/m}^2$) [21], which is in line with the comparison of the other identified mechanical properties. Furthermore Figure 4.8 more clearly describes the partial healing observed in Figure 4.7 as the fracture toughness after each healing cycle does not reach the G_I values of the pristine specimen. It is observed that a minimal pressure of 0.2 bar leads to a low level of fracture toughness recovery and that this level almost drops to zero when multiple healing treatments are applied. More interestingly, an applied pressure of 20 bar leads to a near complete recovery of G_I after each applied healing cycle. This indicates that full healing of the fracture toughness can be obtained as long as the damaged interfaces are brought into adequate contact. The interface mismatch will naturally be higher for the large scale delaminations created by Mode I opening compared to the $\mu\text{m}^2\text{-mm}^2$ scale damage caused by flexural tests. Hence, the requirement for a higher external healing pressure can be explained.

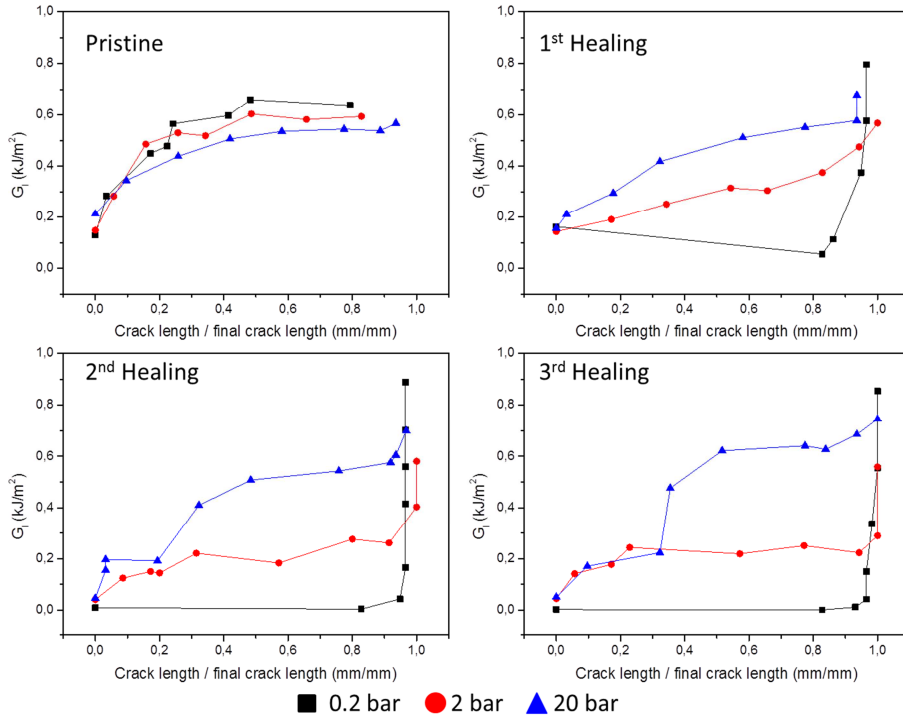


Figure 4.8 Interlaminar fracture toughness plotted versus the normalized crack growth in Mode I opening for 3 consecutive healing treatments at different pressures. Healing is performed at 85°C for 16 hours.

It has to be noted that it is disputable whether the application of high pressure heat treatments (>10 bar) is technologically very relevant since applying such pressures on-site on larger actual composite structures introduces obvious practical problems. However, as smaller de-mounted composite components can still be repaired more easily than with the conventional thermoset repair routes, the proposed strategy is still beneficial to extend the lifetime of composite products. These results also indicate that the focus of composite healing relevant to real applications for the time being should be on the recovery of early stage damage with minimal crack opening (or automated crack closure) as healing in this case can be performed at moderate temperatures and pressures.

4.3.2.3. Low-velocity impact properties

Impact damage is one of the most frequently occurring damage modes in FRPCs. Therefore, the healing of low-velocity impact was selected as the final composite characterization technique in this study. Figure 4.9 shows an example of the image analysis on the healing (16 hours, 85°C, 0.2 bar) of low-velocity impact damage for 3 different levels of impact energy.

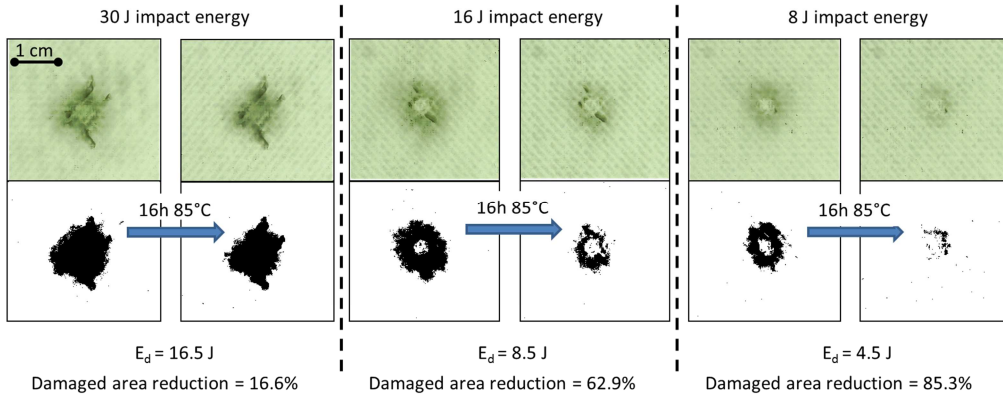


Figure 4.9 Image analysis of the healing of low-velocity impact for 3 different levels of impact energy. Healing is performed at 85°C and 0.2 bar for 16 hours. Top images show the real damaged composite whereas the bottom pictures show the same pictures treated with a binary filter to facilitate the characterization.

The first set of impact studies focussed on an impact energy of 30 J in accordance with ASTM D7136. Figure 4.9 indicates that an impact of 30 J results in a large portion of fibre breakage and consequently only a small reduction of damaged area after healing is observed. Since only damage in the polymer phase can be healed, two additional sets of impact experiments at lower energies (16J and 8J) were performed in which the relative amount of matrix damage versus fibre failure would be higher. Firstly, it is found that the calculated dissipated energy is more than half of the induced energy for all impact conditions. This is an interesting feature for applications that require high damping properties. Secondly, Figure 4.9 shows that as impact energy decreases the amount of visual damage is reduced, but more importantly that the area reduction due to healing increases. This trend is visualized more clearly in Figure 4.10, which shows the percentage of damage area reduction versus the applied impact energy. From this figure a near-linear trend emerges which indicates that only small impact events can be fully healed and that attempts on healing heavy impact event (>30 J energy) will be futile for the current system at a healing pressure of 0.2 bar.

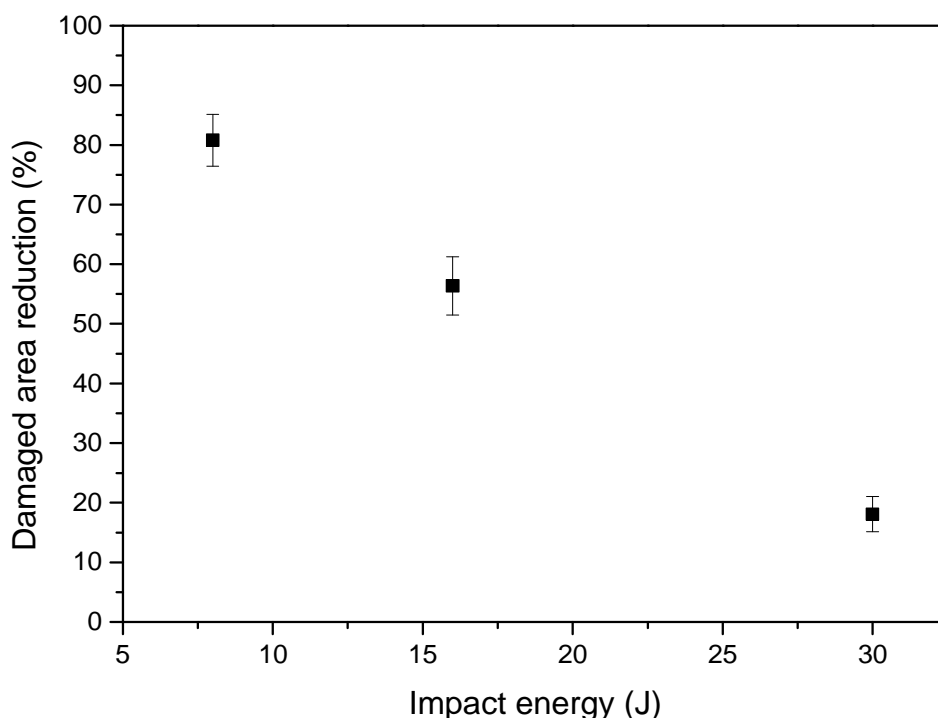


Figure 4.10 Damaged area reduction plotted against the initial impact energy.

4.4. Conclusion

Using a novel epoxy-based thermoset matrix, a GFRP composite with the ability to restore mechanical properties upon a low temperature treatment was developed. This composite has a currently unchallenged combination of a decent stiffness (800-1200 MPa), moderate healing temperatures (70-85°C) below the curing temperature, good damping properties, and the possibility to process by conventional vacuum infusion. Mechanical characterization of the composites demonstrated multiple healing of flexural and interlaminar fracture properties. Additionally the healing of low-energy impact damage was demonstrated. It was found that only minimal pressure is required for the healing of small scale ($< \text{cm}^2$) sized damage. For large scale damage ($> \text{cm}^2$) more healing pressure is required to perfectly align the damaged interfaces and bring back crack faces into contact. However, with high healing pressures full recovery after multiple healing cycles can be obtained provided the damage is concentrated in the matrix phase. Overall, this study shows a self-healing GFRP with mechanical properties that are adequate for medium-tech applications and opens the path towards the development of intrinsic low-temperature self-healing composites with high-end applications.

References

1. Pang, J.W.C. and Bond, I.P., *A hollow fibre reinforced polymer composite encompassing self-healing and enhanced damage visibility*. Composites Science and Technology, 2005. 65(11-12): p. 1791-1799.
2. Williams, H.R., Trask, R.S., and Bond, I.P., *Self-healing sandwich panels: Restoration of compressive strength after impact*. Composites Science and Technology, 2008. 68(15-16): p. 3171-3177.
3. Toohey, K.S., Sottos, N.R., Lewis, J.A., Moore, J.S., and White, S.R., *Self-healing materials with microvascular networks*. Nature Materials, 2007. 6(8): p. 581-585.
4. García, S.J., *Effect of polymer architecture on the intrinsic self-healing character of polymers*. European Polymer Journal, 2014. 53(0): p. 118-125.
5. Blaiszik, B.J., Kramer, S.L.B., Olugebefola, S.C., Moore, J.S., Sottos, N.R., and White, S.R., *Self-healing polymers and composites*, in *Annual Review of Materials Research*. 2010. p. 179-211.
6. Neuser, S., Chen, P.W., Studart, A.R., and Michaud, V., *Fracture toughness healing in epoxy containing both epoxy and amine loaded capsules*. Advanced Engineering Materials, 2014. 16(5): p. 581-587.
7. Prajer, M., Wu, X., García, S.J., and van der Zwaag, S., *Direct and indirect observation of multiple local healing events in successively loaded fibre reinforced polymer model composites using healing agent-filled compartmented fibres*. Composites Science and Technology, 2015. 106(0): p. 127-133.
8. White, S.R., Moore, J.S., Sottos, N.R., Krull, B.P., Santa Cruz, W.A., and Gergely, R.C.R., *Restoration of large damage volumes in polymers*. Science, 2014. 344(6184): p. 620-623.
9. Luterbacher, R., Trask, R.S., and Bond, I.P., *Static and fatigue tensile properties of cross-ply laminates containing vasculs for self-healing applications*. Smart Materials and Structures, 2015. 25(1): p. 015003.
10. Manfredi, E., Cohades, A., Richard, I., and Michaud, V., *Assessment of solvent capsule-based healing for woven E-glass fibre-reinforced polymers*. Smart Materials and Structures, 2015. 24(1).
11. Zhong, N. and Post, W., *Self-repair of structural and functional composites with intrinsically self-healing polymer matrices: A review*. Composites Part A: Applied Science and Manufacturing, 2015. 69(0): p. 226-239.
12. Coope, T.S., Turkenburg, D.H., Fischer, H.R., Luterbacher, R., Van Bracht, H., and Bond, I.P., *Novel Diels-Alder based self-healing epoxies for aerospace composites*. Smart Materials and Structures, 2016. 25(8).
13. Peterson, A.M., Jensen, R.E., and Palmese, G.R., *Room-temperature healing of a thermosetting polymer using the diels-alder reaction*. ACS Applied Materials and Interfaces, 2010. 2(4): p. 1141-1149.
14. Peterson, A.M., Jensen, R.E., and Palmese, G.R., *Kinetic considerations for strength recovery at the fiber-matrix interface based on the Diels-Alder reaction*. ACS Applied Materials and Interfaces, 2013. 5(3): p. 815-821.

15. Bose, R.K., Hohlbein, N., García, S.J., Schmidt, A.M., and van der Zwaag, S., *Connecting supramolecular bond lifetime and network mobility for scratch healing in poly(butyl acrylate) ionomers containing sodium, zinc and cobalt*. Physical Chemistry Chemical Physics, 2015. 17(3): p. 1697-1704.
16. Wang, C.H., Sidhu, K., Yang, T., Zhang, J., and Shanks, R., *Interlayer self-healing and toughening of carbon fibre/epoxy composites using copolymer films*. Composites Part A: Applied Science and Manufacturing, 2012. 43(3): p. 512-518.
17. Post, W., Bose, R., García, S., and van der Zwaag, S., *Healing of Early Stage Fatigue Damage in Ionomer/Fe₃O₄ Nanoparticle Composites*. Polymers, 2016. 8(12): p. 436.
18. Sordo, F. and Michaud, V., *Processing and damage recovery of intrinsic self-healing glass fiber reinforced composites*. Smart Materials and Structures, 2016. 25(8).
19. Cohades, A., Manfredi, E., Plummer, C.J.G., and Michaud, V., *Thermal mending in immiscible poly(ϵ -caprolactone)/epoxy blends*. European Polymer Journal, 2016. 81: p. 114-128.
20. Luo, X., Ou, R., Eberly, D.E., Singhal, A., Viratyaporn, W., and Mather, P.T., *A thermoplastic/thermoset blend exhibiting thermal mending and reversible adhesion*. ACS Applied Materials and Interfaces, 2009. 1(3): p. 612-620.
21. Cohades, A. and Michaud, V., *Thermal mending in E-glass reinforced poly(ϵ -caprolactone)/epoxy blends*. Composites Part A: Applied Science and Manufacturing, 2017. 99: p. 129-138.
22. Canadell, J., Goossens, H., and Klumperman, B., *Self-healing materials based on disulfide links*. Macromolecules, 2011. 44(8): p. 2536-2541.
23. Abdolah Zadeh, M., van der Zwaag, S., and García, S.J., *Self-healing corrosion-protective sol-gel coatings based on extrinsic and intrinsic healing approaches*, in *Advances in Polymer Science*. 2016. p. 185-218.
24. Abdolhazadeh, M., C. Esteves, A.C., van der Zwaag, S., and García, S.J., *Healable dual organic-inorganic crosslinked sol-gel based polymers: Crosslinking density and tetrasulfide content effect*. Journal of Polymer Science, Part A: Polymer Chemistry, 2014. 52(14): p. 1953-1961.
25. Hernández, M., Grande, A.M., Dierkes, W., Bijleveld, J., van der Zwaag, S., and García, S.J., *Turning Vulcanized Natural Rubber into a Self-Healing Polymer: Effect of the Disulfide/Polysulfide Ratio*. ACS Sustainable Chemistry and Engineering, 2016. 4(10): p. 5776-5784.
26. Zhong, N., García, S.J., and van der Zwaag, S., *The effect of filler parameters on the healing of thermal conductivity and mechanical properties of a thermal interface material based on a self-healable organic-inorganic polymer matrix*. Smart Materials and Structures, 2016. 25(8).
27. Ruiz de Luzuriaga, A., Martin, R., Markaide, N., Rekondo, A., Cabanero, G., Rodriguez, J., and Odriozola, I., *Epoxy resin with exchangeable disulfide crosslinks to obtain reprocessable, repairable and recyclable fiber-reinforced thermoset composites*. Materials Horizons, 2016. 3(3): p. 241-247.
28. Susa, A., Bose, R.K., Grande, A.M., van der Zwaag, S., and García, S.J., *Effect of the Dianhydride/Branched Diamine Ratio on the Architecture and*

- Room Temperature Healing Behavior of Polyetherimides*. ACS Applied Materials and Interfaces, 2016. 8(49): p. 34068-34079.
29. Chen, Y., Kushner, A.M., Williams, G.A., and Guan, Z., *Multiphase design of autonomic self-healing thermoplastic elastomers*. Nat Chem, 2012. 4(6): p. 467-472.
 30. Montarnal, D., Cordier, P., Soulié-Ziakovic, C., Tournilhac, F., and Leibler, L., *Synthesis of self-healing supramolecular rubbers from fatty acid derivatives, diethylene triamine, and urea*. Journal of Polymer Science Part A: Polymer Chemistry, 2008. 46(24): p. 7925-7936.
 31. Montarnal, D., Tournilhac, F., Hidalgo, M., Couturier, J.-L., and Leibler, L., *Versatile One-Pot Synthesis of Supramolecular Plastics and Self-Healing Rubbers*. Journal of the American Chemical Society, 2009. 131(23): p. 7966-7967.
 32. Sordo, F., Mougner, S.J., Loureiro, N., Tournilhac, F., and Michaud, V., *Design of Self-Healing Supramolecular Rubbers with a Tunable Number of Chemical Cross-Links*. Macromolecules, 2015. 48(13): p. 4394-4402.
 33. Agache, P.G., Monneur, C., Leveque, J.L., and De Rigal, J., *Mechanical Properties and Young's Modulus of Human Skin in Vivo* Archives of Dermatological Research, 1980. 269: p. 221-232.
 34. Bode, S., Bose, R.K., Matthes, S., Ehrhardt, M., Seifert, A., Schacher, F.H., Paulus, R.M., Stumpf, S., Sandmann, B., Vitz, J., Winter, A., Hoepfner, S., García, S.J., Spange, S., van der Zwaag, S., Hager, M.D., and Schubert, U.S., *Self-healing metallopolymers based on cadmium bis(terpyridine) complex containing polymer networks*. Polymer Chemistry, 2013. 4(18): p. 4966-4973.
 35. Dello Iacono, S., Martone, A., Filippone, G., Acierno, D., Zarrelli, M., Giordano, M., and Amendola, E. *Insight on mendable resin made by combining Diels-Alder epoxy adducts with DGEBA*. in *AIP Conference Proceedings*. 2016.
 36. Bose, R.K., Kötteritzsch, J., García, S.J., Hager, M.D., Schubert, U.S., and van der Zwaag, S., *A rheological and spectroscopic study on the kinetics of self-healing in a single-component diels-alder copolymer and its underlying chemical reaction*. Journal of Polymer Science Part A: Polymer Chemistry, 2014. 52(12): p. 1669-1675.
 37. NETZSCH, *Thermal Properties of Polymers*, NETZSCH, Editor. 2016.
 38. Abdolah Zadeh, M., Grande, A.M., van der Zwaag, S., and García, S.J., *Effect of curing on the mechanical and healing behaviour of a hybrid dual network: A time resolved evaluation*. RSC Advances, 2016. 6(94): p. 91806-91814.
 39. Sordo, F. and Michaud, V., *Adhesion and interfacial healing between supramolecular hybrid networks and glass substrates*. International Journal of Adhesion and Adhesives, 2017. 73: p. 100-108.
 40. *Standard Test Method for Mode I Interlaminar Fracture Toughness of Unidirectional Fiber-Reinforced Polymer Matrix Composites*. 2013, ASTM International.

41. *Standard Test Method for Measuring the Damage Resistance of a Fiber-Reinforced Polymer Matrix Composite to a Drop-Weight Impact Event*. 2015, ASTM International.
42. Pepels, M., Filot, I., Klumperman, B., and Goossens, H., *Self-healing systems based on disulfide-thiol exchange reactions*. *Polymer Chemistry*, 2013. 4(18): p. 4955-4965.

Supplementary Information*S1: Tensile data polymer matrix*

Figure S 4.1 shows the representative stress-strain relations of the polymer matrix for different curing conditions during tensile testing. For comparison, a specimen without a post-curing treatment was tested as well.

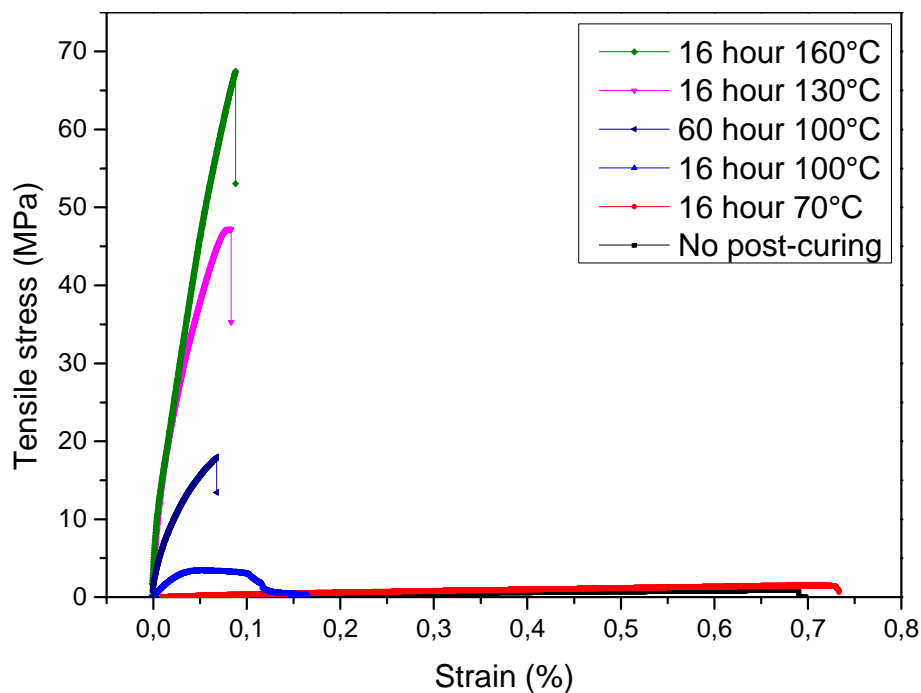


Figure S 4.1 Stress-strain relation of the matrix at different curing conditions

S2: Differentiation between healing and post-curing

To show that the restorative behaviour of the composites developed in this study is not simply due to incomplete curing of the matrix several additional experiments were performed. Firstly, Figure S 4.2 shows the storage modulus evolution of the polymer matrix during a dwell of 16 hours at 85°C. The figure clearly shows an initial drop in modulus upon approaching the dwell temperature. Once this temperature is reached, the storage modulus remains constant, which indicates no further crosslinking of the matrix during healing at this temperature.

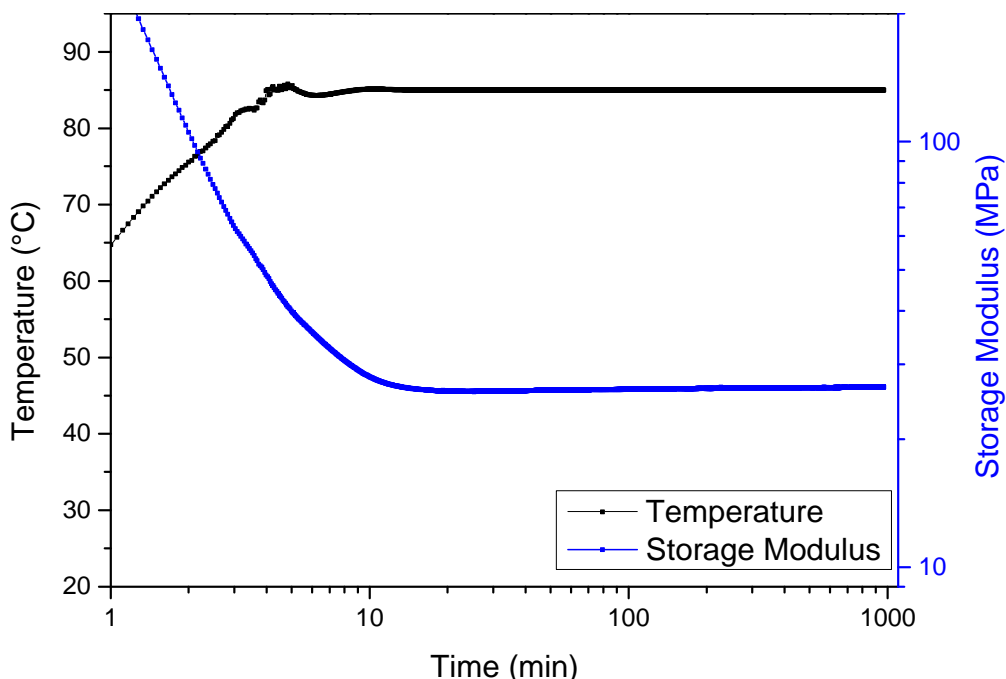


Figure S 4.2 Evolution of the polymer matrix storage modulus during a typical healing treatment of 85°C for 16 hours.

Secondly, Figure S 4.3 shows a repetition of the 3-point bending experiments reported in the main study after treating the test specimens with an additional curing treatment of 100°C and 0.2 bar for 16 hours after sample preparation but prior to testing. These results show a slight stiffness increase for the pristine specimens, which is an indication of minor post-curing at this temperature. Besides, the results show that the reported healing trends in the main study are still valid for these specimen and that the decay of yield strength and stiffness after healing at 100°C is even more profound in this case.

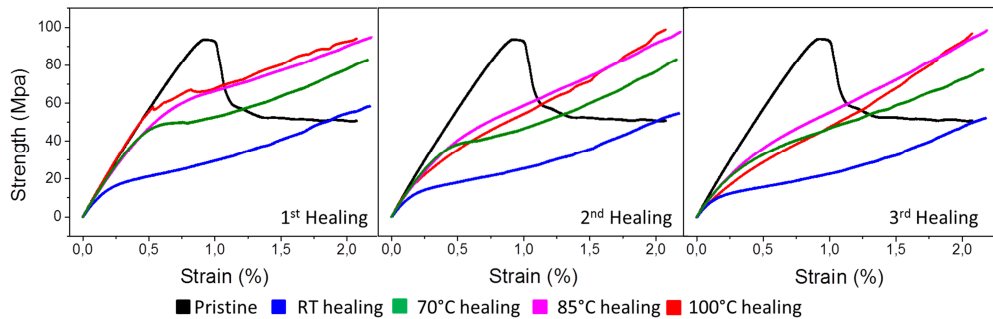


Figure S 4.3 Flexural healing properties of composite beams that were subjected to a 16h, 0.2 bar, 100°C temperature treatment prior to multiple healing tests at different healing conditions.

Finally, Figure S 4.4 shows the infrared spectra of 3 different interfaces of the specimen tested by double cantilever beam testing. Attenuated total reflectance Fourier transform infrared (ATR-FTIR) spectroscopy is performed using a Perkin-Elmer Spectrum 100 series FT-IR spectrophotometer. The IR spectra show that a freshly fractured composite specimen still contains small portions of $\text{Si-OC}_2\text{H}_5$ and Si-OCH_3 and that these peaks are much less profound on a sample, which was healed multiple times and on the undamaged outside of the composite. This shows that, after the first opening of the crack, the polymer is not fully cured, but that this does not greatly affect the healing performance as the healed fractured interface could be healed again for at least two more cycles.

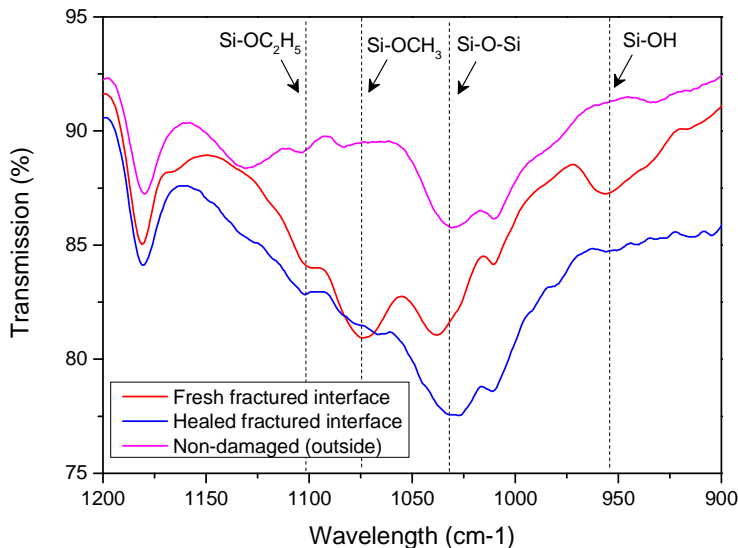


Figure S 4.4 IR spectrum of a fresh fractured interface, healed and re-opened interface and an undamaged interface of a DCB tested composite specimen.

S3: 3-point bending response of matrix material

Figure S 4.5 shows the representative stress-strain curve of the unreinforced polymer matrix that was given a similar curing treatment as prepared composites (60 hours at 100°C, no post-curing). To show that the flexural modulus of the unreinforced matrix at high strain levels is similar to that of the healed specimen, the results of retesting after the 1st healing treatment (Figure 4 in main chapter) at various temperatures were included in this figure as well.

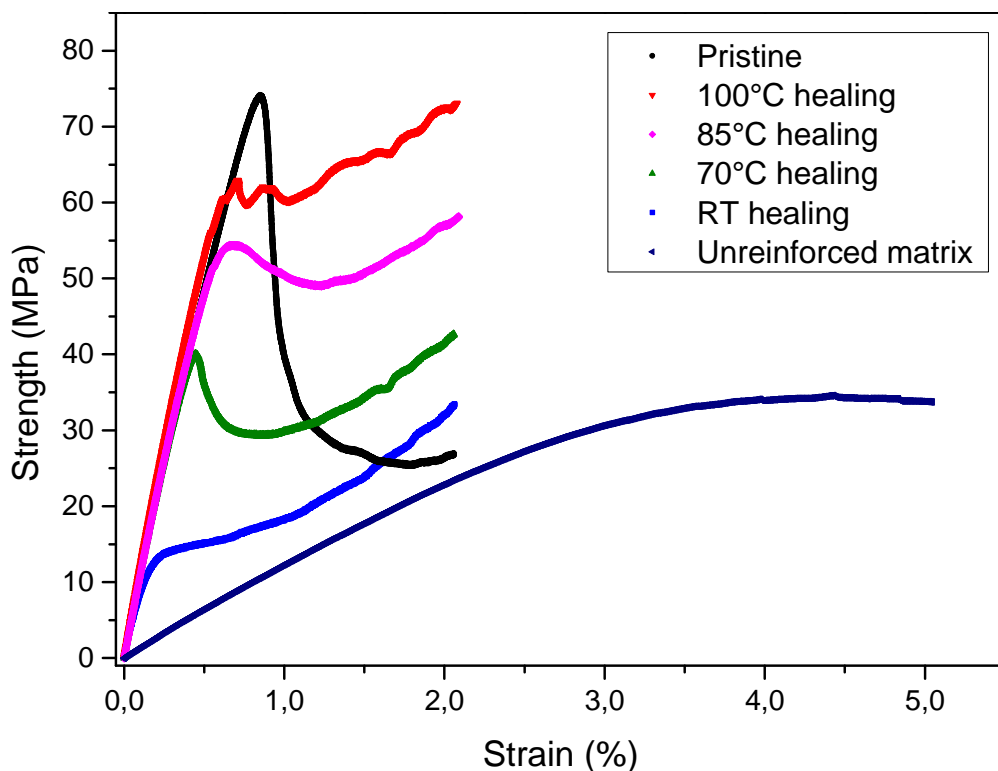


Figure S 4.5 Stress-strain curves of the flexural tests performed on composite beams including that of the unreinforced matrix. Specimens were healed for 16 hours at moderate pressure of 0.2 bar.

S4: Additional data interlaminar fracture testing

The combined load-displacement/crack propagation curves of the Mode I opening of a composite healed three times at 0.2 bar and 20 bar (85°C and 16 hours) are shown in Figure S 4.6 and Figure S 4.7 respectively.

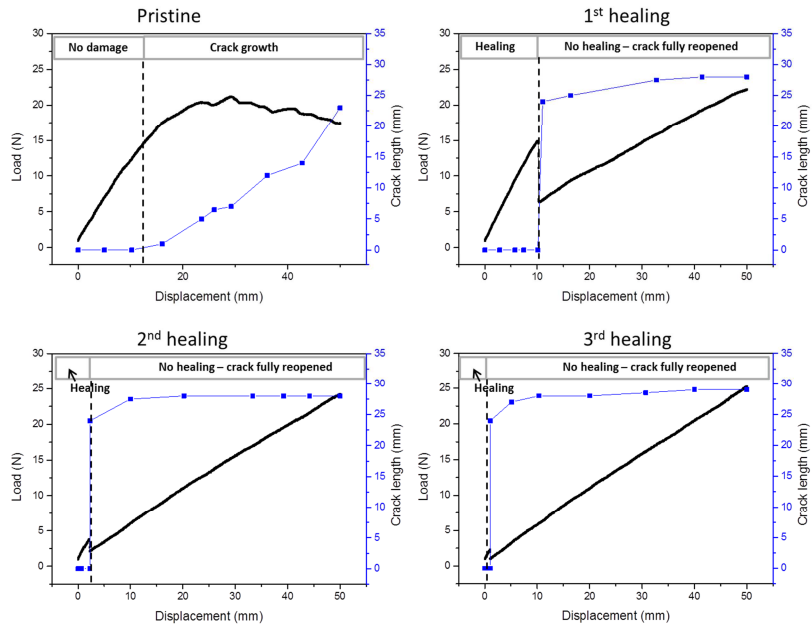


Figure S 4.6 Combined load-displacement/crack propagation curves of the Mode I opening of a composite healed three times at 85°C and 0.2 bar pressure for 16 hours.

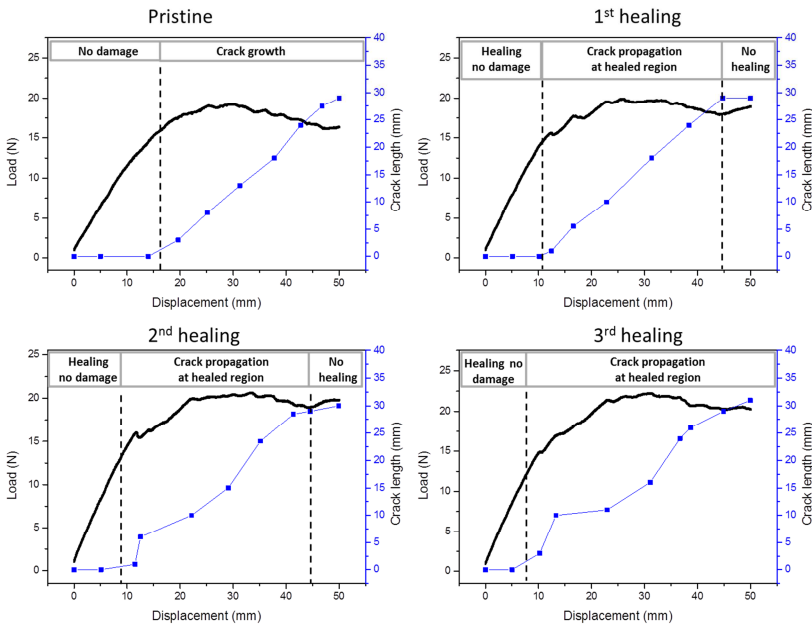


Figure S 4.7 Combined load-displacement/crack propagation curves of the Mode I opening of a composite healed three times at 85°C and 20 bar pressure for 16 hours.

Chapter 5

Healing of Early Stage Fatigue Damage in Ionomer/ Fe_3O_4 Nanoparticle Composites

This chapter has been published as:

W. Post, R.K. Bose, S. J. García, S. van der Zwaag; *Healing of Early Stage Fatigue Damage in Ionomer/ Fe_3O_4 Nanoparticle Composites*, Polymers, volume 8, issue 12, 2016

5.1. Introduction

Polymer based composites are susceptible to many different types of mechanical damages which reduce their reliability and potentially decreases the overall lifetime of the material. By implementation of self-healing technologies the overall lifetime of polymer composites can be prolonged [1, 2]. Within self-healing composites, most attention so far has been on extrinsic healing strategies where an external (liquid) healing agent capable of restoring either the matrix or the filler-matrix interface is encapsulated and embedded in the matrix [3-5]. The mechanism certainly works but there are many issues still to be resolved. Even when solved, the fact remains that the healing reaction locally works only once and this is a major shortcoming [2]. The use of intrinsically healing polymer matrices in such composites is considered to be more optimal because it has the potential of an infinite amount of healing cycles. Additionally, intrinsic healing leaves the optimized macroscopic fiber and ply architecture required for high level mechanical properties unaffected [2, 6, 7].

Ionomers are among the most frequently studied polymer matrices for intrinsic self-healing particulate [8, 9] or fiber reinforced composites [10]. Ionomers have pendant acid groups distributed along the polymer backbone that are neutralized by ionic metal salts. These ionic groups have the tendency to form ionic clusters which create additional physical crosslinks within the polymer network [7]. Ionomers have proven to be capable of restoring mechanical stability by healing of ballistic impact damage using a combination of shape recovery (sometimes called "shape memory") and re-bonding across former damage site surfaces [11-15]. The combination of the shape recovery effect and healing is not exclusive for ionomers but is also found in other polymer systems [16, 17]. Besides healing after ballistic impact, which is investigated in the majority of self-healing ionomer studies, ionomers were also used to heal scratch damage [18] and damage on composite toughening interlayers [19]. The shape restoration of the polymer after puncture is made possible by the heat that is generated upon impact [13, 14]. Strain recovery after deforming a polymer beyond its yield strain and subsequent heating is found to be typical for all semi-crystalline polyethylene-based polymers [20, 21] and is attributed to the dominance of the decrease in the carbon bond angle over the overall carbon-carbon stretching when these polymers are deformed and heated consecutively [22, 23]. Semi-crystalline ionomers were also reported to behave like traditional shape memory polymers by Dolog and Weiss [20]. Since this form of thermal contraction after deformation does not correspond to the definition of shape memory polymers, the phenomenon was more accurately defined as free-shrinkage [21] and we will use this terminology in the present work. Although there seems to be consensus about the mechanisms responsible for the restoration after polymer deformation, there is currently no general agreement on the role that the ionic clusters have on

the healing effect [24], i.e., the reformation of mechanical strength across a former crack.

As is the case for the majority of the intrinsically healing polymers, ionomers need a thermal stimulus to activate their healing behavior. This poses a direct disadvantage in future applications when the intended energy input has to be delivered from the nearby environment to the composite structure (e.g., by using an oven) [25-27]. To overcome this disadvantage the energy input can be delivered locally from within the structure by making the ionomer suitable for inductive heating. In recent years this concept was explored by adding ferromagnetic particles to thermoplastic matrices [28-30]. However, within these studies the thermoplastic material was simply melted and restored to its initial shape and lost all mechanical stability throughout the process. Recently, Hohlbein et al. demonstrated the concept of inductive healing in a new family of ionomers [8]. Although this study showed the great potential of inductive heating for intrinsically self-healing polymers, their experimental ionomers still had rather low tensile properties.

In most studies on self-healing polymer composites, the research focused on the healing of damage after cutting or static overloading [2, 7]. However, when a self-healing polymer is incorporated into a structural composite it is crucial to understand how the material behaves under dynamic fatigue loading and what types of damage are formed during the early stages of this process when the likelihood of complete healing is highest. Multiple studies describe the self-healing of fatigue induced mechanical damage in extrinsic healing composites [31-35]. A recent study focused on the partial restoration of the functional piezoelectric properties in a lead zirconium titanate (PZT) ionomer composite [9]. Nevertheless, to the best of our knowledge, the restoration of mechanical properties after fatigue in intrinsically self-healing polymers has not been investigated.

This study is the first investigation on the self-repair of mechanical properties of intrinsically self-healing polymer particulate composites after fatigue loading conditions. In this work, poly(ethylene-*co*-methacrylic acid) zinc ionomer/Fe₃O₄ nanoparticle composites were developed and subjected to different levels of fatigue loading. The initiated early stage fatigue damage was then healed upon localized heating of the particles by exposure of the composites to an alternating magnetic field. For a proper understanding of the mechanisms involved in the healing process a detailed thermo-mechanical investigation was performed on a set of poly(ethylene-*co*-methacrylic acid) based polymer blends with varying amounts of ionic clusters. Such an approach allowed the identification and separation of the two stages involved in the healing process: (i) the residual strain and network restoration; and (ii) the macroscopic crack sealing. A temperature window for the

different stages of early stage damage healing in ionomer composites was thereby identified.

5.2. Materials and Methods

5.2.1. Materials

In order to evaluate the effect of cluster content, four different poly(ethylene-*co*-methacrylic acid) (EMAA) zinc ionomer blends were prepared based on a previous study that investigated the role of free carboxylic content and cluster state on the healing of surface scratches [18]. The four chosen blends resulted in polymer systems with high (Zn-EMAA), medium (Zn-EMAA/EMAA), no ionic groups (EMAA) and a blend where a relatively high amount of ionic clusters is neutralized (ZnEMAA/AA). In order to make the blends susceptible to inductive heating Fe₃O₄ particles (10 vol.%, 50–100 nm, Sigma Aldrich, Zwijndrecht, The Netherlands) were added to the polymers based on previous healing studies. More information about the nature of the polymers and particles and full characterization can be found elsewhere [8, 14, 20, 21, 29]. The selected blends were prepared with the following materials:

- Zn-EMAA: Surlyn 9520[®](Dupont[™]) containing 3.5 mol% methacrylic acid groups (MAA) out of which 71% were neutralized with Zn²⁺ ions.
- EMAA: Nucrel 960[®] (Dupont[™]) containing 5.4 mol% of MAA groups.
- Zn-EMAA/EMAA: 50/50 wt.% blends of Zn-EMAA and EMAA.
- Zn-EMAA/AA: 90/10 wt.% blend of Zn-EMAA with adipic acid (AA) powder (Sigma Aldrich). In this blend the ionic clusters are destroyed by the adipic acid as is described by Varley et al.[36].

Polymer composites were prepared by mixing all components (polymer pellets, particles and additives) using a twin screw mini-extruder. The extruder volume was 15 mL and a temperature of 200°C and a torque of 50 rpm were applied. The residence time in the extruder was 5 min. After extrusion, the resulting products were compression moulded at 150°C with a pressure of 4 MPa using a hot press resulting in 100 ± 5 µm freestanding films. Teflon films were used to separate the polymer films from the pressing plates. After moulding, the films were given a 15 min heat treatment at 80°C in a preheated convection oven to equilibrate the thermal effects induced due to the rapid cooling after moulding. Films were stored at room temperature for at least 21 days to equilibrate the polymer microstructure prior to further testing. Dog-bone shaped specimens (ASTM D1708) were pressed from the prepared films.

5.2.2. Mechanical Testing

To study the deformation before and after free shrinkage, different levels of quasi-static strain (25–100%) were applied to deform the polymer composites using an Instron Model 3365 universal testing systems equipped with a 1 kN load cell. Dog-bone micro-tensile specimens were stretched at 1 mm/s at room temperature. The average value of 3 experiments was reported.

Fatigue experiments were conducted on dog-bone shaped specimens at room temperature on an MTS 831 Elastomer test system equipped with a 1 kN load cell. The specimens were fatigue tested under different prestrain levels of 25% and 50% from which a sinusoidal waveform with an amplitude of 2.3% and a frequency of 1 Hz was employed. The amount of applied strain cycles ranged from 500 to 50,000. Full fracture tensile tests were performed on different Zn-EMAA specimens at different stages of the fatigue restoration process using the same equipment and conditions as for the deformation experiments. True stress and true strain were calculated from these tests via:

$$\sigma_T = \frac{P}{A_0}(1 + \varepsilon) \quad (5.1)$$

$$\varepsilon_T = \ln(1 + \varepsilon) \quad (5.2)$$

where, σ_T = true stress in MPa; P = measured load in N; A_0 = Area of the cross-section of the dog-bone in mm²; ε = engineering strain in percent; and ε_T = true strain in percent.

The tensile tests were performed 7 days after the fatigue and healing treatments which allows the polymer crystalline phases to fully recover prior to further testing.

5.2.3. Thermomechanical Testing

The effect of cluster content on the deformation that occurs during fatigue and the thermal contraction upon heating was investigated using a Perkin–Elmer Sapphire differential scanning calorimeter (DSC). Samples were heated and cooled between –50°C and 150°C at a rate of 20°C/min under a nitrogen atmosphere.

To obtain a deeper understanding of the effect of the clusters on the self-healing mechanism, the macroscale network mobility of the non-particulate polymer blends was investigated by oscillatory shear rheology. Experiments were performed with a Haake Mars III rheometer. An 8 mm diameter (stainless steel) parallel plate geometry was used throughout. For all the samples, the polymer thickness was between 0.9–1.2 mm, and a constant shear strain γ of 1%, which was within the linear viscoelastic regime of the materials, was applied. Frequency sweep

experiments between 10^2 and 10^{-2} Hz were performed at temperatures of 80 and 110°C, with an isothermal hold for 20 min prior to each temperature step. The supramolecular bond lifetime (τ_b) at different temperatures was then calculated as inverse of the frequency at which the storage and loss moduli crossover in a frequency sweep experiment.

5.2.4. Thermally Induced Healing Process and Evaluation

Induction heating was applied for 15 minutes using a single-turn hairpin induction coil mounted on an Ambrell Easyheat device. The coil and specimen were separated by Teflon foil and the coupling distance was fixed at 1 mm. A frequency of 350 kHz and currents between 200 and 250 A were applied to reach the intended temperatures. Healing temperatures were selected based on the different thermal transitions of the polymer as shown in Figure 5.1 and Figure 5.2. As such, the selected healing temperatures are located below the secondary thermal transition (50°C), in between the secondary transition and the overall melting of the polymer (80°C) and above the overall melting of the polymer (100–110°C). The specimen temperature upon inductive heating was monitored with a FLIR A655sc infrared camera. Since this method only detects the surface temperature of the ionomer composites, a COMSOL Multiphysics model was used to derive a relation between the measured surface temperature and the desired healing temperature within the bulk of the polymer sample. The used model is a stationary heat transfer model that correlates the measured surface temperature to the bulk healing temperature based on the thermal conductivity of the materials used. The model assumes a uniform distribution of particles within in cubic geometry corresponding to the used particle concentration of 10 vol.%. Full information on the applied model (geometry, input parameters and calculations) can be found in Supplementary Materials S1.

The closure and sealing of fatigue induced cracks was monitored with a digital microscope Keyence VHX2000 with a wide-range zoom lens (100×–1000× magnification). For the optimal illumination of the black surfaces the microscope was equipped with a OP-87229 short ring-light. The length of the samples before and after the thermal treatment was measured with a digital caliper and the residual strain was calculated based on this data.

5.3. Results

5.3.1. Thermal and Thermomechanical Analysis

DSC thermograms for all composite grades during heating from 25 to 125°C are shown in Figure 5.1. This temperature region shows a broad melting range which includes a low temperature endotherm that typically appears between 50 and 75°C for all four compositions. Figure 5.2 shows the thermograms of the Zn-EMAA/Fe₃O₄ composite in four different stages of the deformation and thermal treatment

process: (i) material in its pristine state; (ii) after 100% strain deformation; (iii) after 100% strain and 15 min furnace annealing at 80°C ; and (iv) after 100% straining, 80°C annealing and 1 week storage at room temperature.

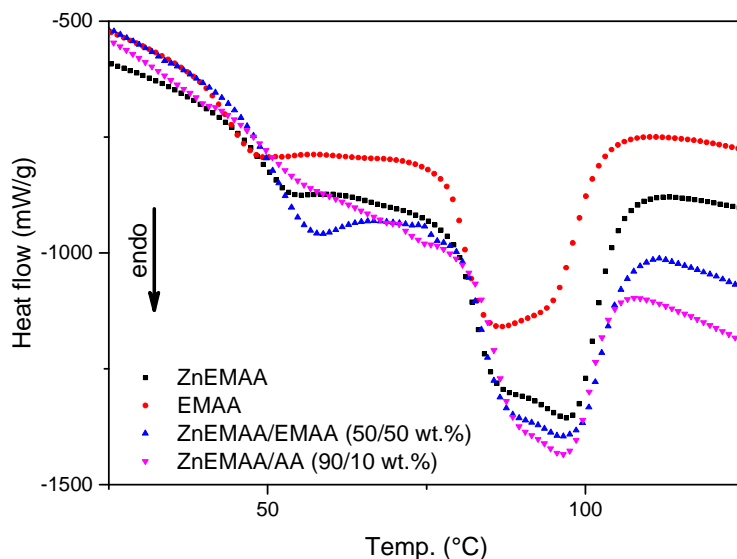


Figure 5.1 DSC thermograms for four particulate polymer blends showing the effect of ionic cluster content on the low-temperature endotherm in the melting range of the polymer composites.

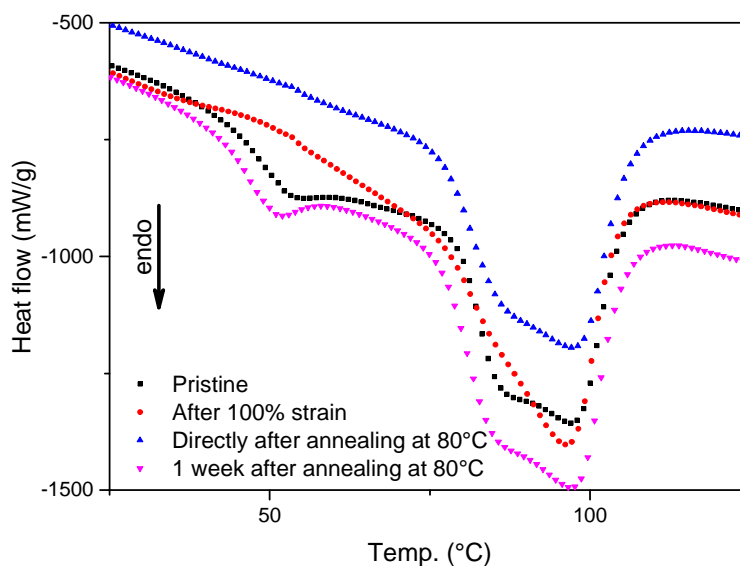


Figure 5.2 DSC thermograms of the Zn-EMAA- Fe_3O_4 composite at different stages of the deformation and thermal treatment process.

Figure 5.1 and 5.2 show the effect the low temperature endotherm upon ionic cluster concentration and during the process of free-shrinkage respectively. In recent literature, the endotherm has often been attributed to a declustering of the ionic clusters which would lead to enough mobility within in the polymer network to support healing [8, 9, 37, 38]. Other studies claim that the endotherm corresponds to the glass transition temperatures of the various phases within the polymer (matrix phase $T_g < 0^\circ\text{C}$) that are linked to the ionic cluster concentration [39, 40]. Figure 5.1 shows that this endotherm also exists in the non-ionic EMAA and is only intensified upon the addition of ionic groups within the polymer grade. The addition of adipic acid results in the diminishing of this endotherm as was reported previously [14]. Figure 5.2 shows that the endotherm disappears upon straining and returns only after one week of annealing at 80°C and is therefore not present during the process of free-shrinkage.

Figure 5.3 shows the storage (G') and loss moduli (G'') of Zn-EMAA in the frequency range of 10^2 – 10^{-2} Hz obtained by frequency sweep rheology. Similar curves were obtained for the other polymer grades. For all polymer grades it is found that at 80°C the storage and loss moduli curves do not intersect and therefore no values of τ_b can be determined. G and G' were found only to intersect at temperatures close to of 110°C which is the overall melting temperature of the polymer grades. The plateau modulus (G_N), which is taken as the high frequency plateau of the G' curve was used to compare the mechanical robustness of each sample. In one of our recent publications we showed the connection between the macroscopic network mobility of ionomers with varying amounts of ionic clusters to the supramolecular bond lifetime (τ_b). It was then proposed that a polymer system with $10\text{ s} < \tau_b < 100\text{ s}$ and $10^5\text{ Pa} < G_N < 10^7\text{ Pa}$ would show good healing behavior combined with strong mechanical properties [41]. The values for G_N and τ_b of the four polymer blends are presented in Table 5.1. Because the final plateau modulus at 110°C was beyond the high frequency range of the rheometer, the G' values for the highest measured frequency are reported instead.

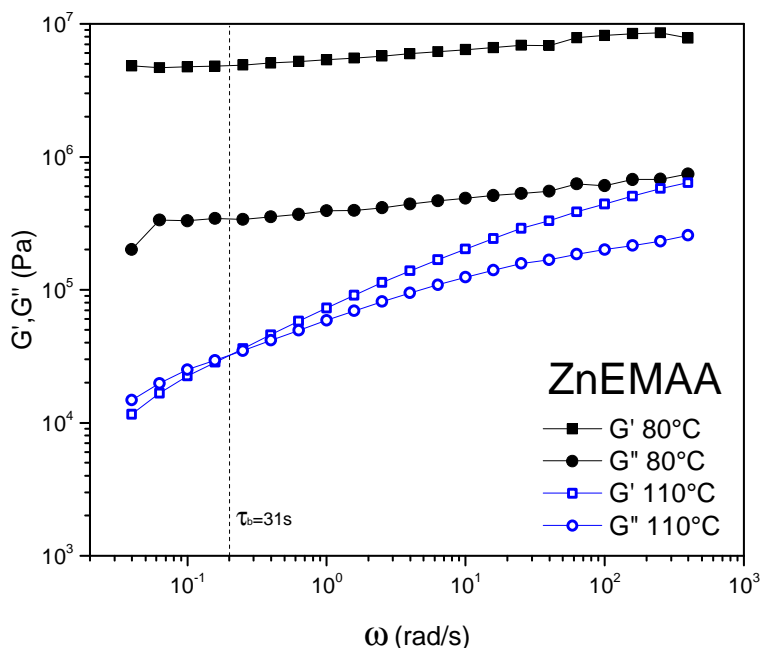


Figure 5.3 Frequency sweep experiment of the Zn-EMAA polymer at 80 and 110°C. The supramolecular bond lifetime τ_b is determined for both polymers at intersection of the G' and G'' at 110°C.

Table 5.1 Overview of the plateau moduli at different temperatures and the supramolecular bond lifetime at 110°C for all polymer matrix blends.

| Parameters | Zn-EMAA | EMAA | Zn-EMAA/EMAA | Zn-EMAA/AA |
|-----------------------|--------------------|--------------------|--------------------|--------------------|
| G_N at 80°C (Pa) | 8.2×10^6 | 3.9×10^4 | 1.2×10^6 | 7.2×10^6 |
| G_N at 110°C (Pa) | $>6.4 \times 10^5$ | $>2.8 \times 10^3$ | $>4.4 \times 10^5$ | $>3.8 \times 10^5$ |
| τ_b at 110°C (s) | 31 | 0.13 | 6.3 | 2.0 |

Table 5.1 shows that at 110°C, the τ_b and G_N values of the Zn-EMAA ionomer meet the demands for good healing ($10 < \tau_b < 100$ s) and good mechanical properties ($G' > 10^5$ Pa and is expected not to exceed 10^7 Pa)[41]. Experiments at higher temperatures ($>130^\circ\text{C}$) move the value of τ_b towards the regime of viscous flow ($\tau_b < 10$ s) indicating that good healing conditions are not met at temperatures well above the overall melting point of the polymer. The values found for the EMMA polymer at a temperature of 110°C are also typical for viscous flow of a molten polymer and therefore the damage recovery cannot be classified as healing. The τ_b and G_N values for the Zn-EMAA/EMAA and Zn-EMAA/AA show that the thermomechanical behavior at the measured temperatures is in between that of Zn-

EMAA and EMAA indicating that the difference in viscoelastic behavior is linked to the presence of ionic clusters.

5.3.2. Effect of Temperature Post-Treatment after Static and Dynamic Loading

All prestrained polymer composites were post treated at different temperatures. As a consequence, a macroscopic shrinkage was observed and quantified. Figure 4 shows the influence of temperature on the free-shrinkage behavior of the Zn-EMAA particulate composite as function of the applied strain. Different levels of initial quasi-static strain levels were applied and the residual strain (at room temperature) after annealing at various temperatures was determined as described.

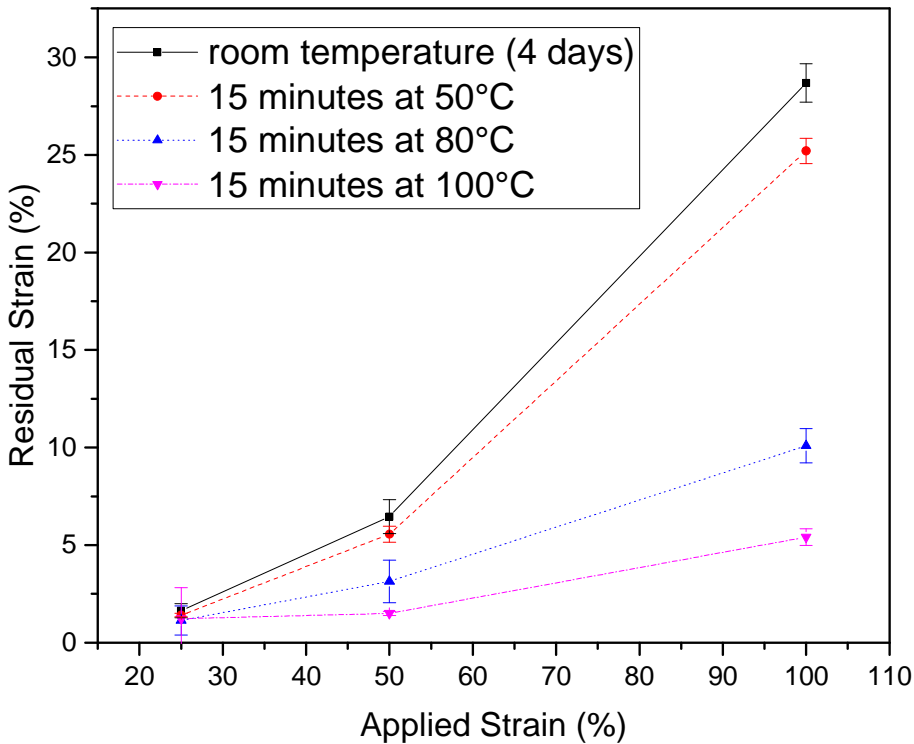


Figure 5.4 Residual contraction behavior in Zn-EMAA/Fe₃O₄ composites as a function of the applied static prestrain and four annealing conditions.

Figure 5.4 shows that, with certain annealing conditions, the residual strain of the Zn-EMAA polymer grade can become near zero up to an applied strain level of about 50%. This upper limit for full strain recovery turns out to be applicable for all polymer composite grades and was therefore used as the maximum prestrain level for the fatigue experiments.

Figure 5.5 shows the residual strain of all polymer grades after different fatigue treatments before and after heating. This figure shows that the residual strain after fatigue increases when the prestrain and the number of cycles are increased. Upon a healing treatment of 15 minutes at 80°C , the residual strain is reduced to levels below 5% for all investigated blends. The EMAA composite without ionic clusters has the lowest levels of residual strain before and after healing. The levels of residual strain for the Zn-EMAA, Zn-EMAA/EMAA and the Zn-EMAA composites are fairly comparable with the exception of the value for the Zn-EMAA/AA blend for which the level of contraction could not be measured after 50,000 strain cycles as complete sample failure occurred at this level of cyclic loading.

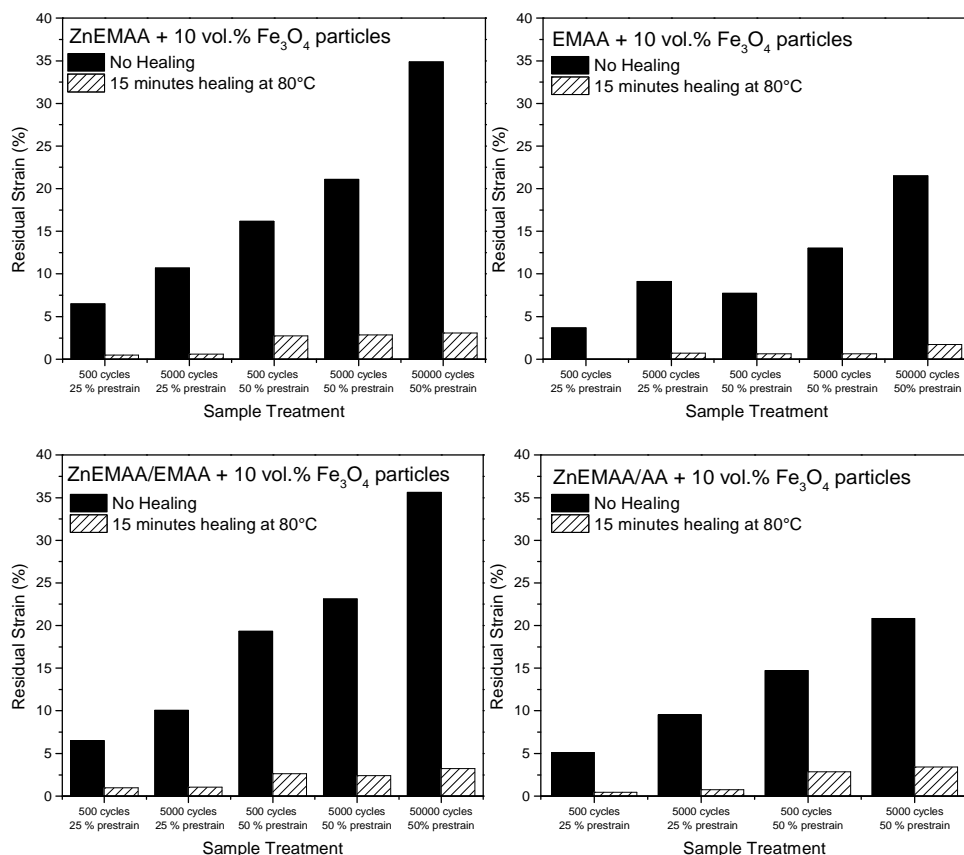


Figure 5.5 Strain restoration after fatigue treatments of Zn-EMAA, EMAA, Zn-EMAA/EMAA and Zn-EMAA/AA composites. Results are shown for different treatments based on the amount of strain cycles and the prestrain that was applied to the composites.

Figure 5.6 shows the stress strain curves of a Zn-EMAA/ Fe_3O_4 composite after several treatments: the quasi-static tensile behavior of a pristine specimen, two fatigued specimens at 1000 and 50,000 strain cycles with a strain amplitude of 2.3% on top of a prior 50% static strain and two specimens that were subjected to

1000 fatigue cycles and subsequently heated to either 80 or 110°C. The obtained results indicate that a fatigued ionomer system shows strain hardening and becomes slightly less ductile. The first effect can be explained by an alignment of polymer chains that were originally packed in the secondary clusters. This explanation is supported by the DSC thermograms in Figure 5.2 that show that this phase disappears upon straining. This effect increases the tensile strength of the polymer composite and can therefore by itself not be seen as a damaging event. However, the second effect is an indication for the loss of mechanical integrity and can be a result of local mechanical damage in the form of random chain scission [42] which could potentially occur upon the application of multiple fatigue cycles. The figure shows that the strain hardening increases when the number of applied fatigue cycles is increased from 1000 to 50,000. Figure 5.6 also shows that the original stress–strain relation can be restored when a suitable heat treatment is applied. A heat treatment of 80°C already shows a big reduction of the strain hardening effect and after a 110°C treatment the initial tensile behavior is almost completely restored.

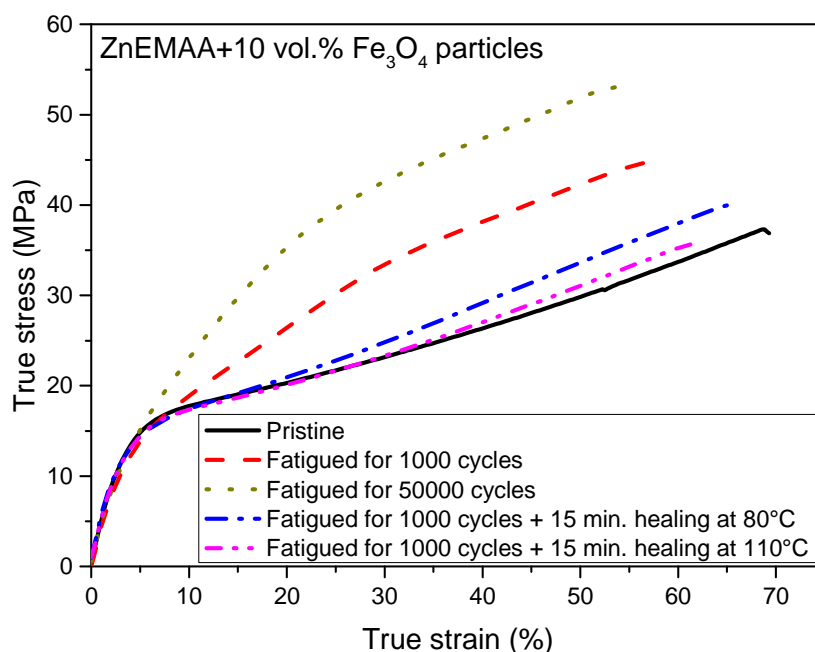


Figure 5.6 Stress–strain curves taken during the several stages of the fatigue damage-recovery process. It shows that the strain hardening increases when the number of applied fatigue cycles is increased from 1000 to 50,000 and that the original stress–strain relation can be restored when a heat treatment is applied.

Optical microscopy images of the surface of a fatigued Zn-EMAA specimen (1000 strain cycles, 50% prestrain) before and after inductive heating are shown in Figure

5.7. The analysis showed that some of the nanoparticles formed micron-sized agglomerates rather than being homogeneously distributed which suggests that the results currently obtained are not fully optimal. The agglomerates promote the crack initiation upon straining and fatigue loading, but their presence does not disturb the mechanism of fatigue healing to be demonstrated in this work. The images show that fatigue loading led to the formation of microcracks close to clusters of Fe_3O_4 particles which act as stress concentrators in the composite. A similar fatigue treatment on a Zn-EMAA specimen without particles did not show any microcracks. The images also show that inductive heating at 80°C closes the cracks but does not seal the edges of the crack back together. Upon a second fatigue treatment of 1000 cycles, it is shown that these cracks propagate into larger cracks. On the other hand, inductive annealing at 110°C shows a complete sealing of the crack edges and results in the effective disappearance of the crack. In this case, a follow-up fatigue treatment only leads to reopening of these cracks. This is expected since the crack locations remain the weak spots of the composite. However, after a 110°C induction treatment the cracks have not propagated as is seen for the specimens that are only healed at 80°C . These observations are in line with the results of the frequency sweep experiments obtained in Figure 5.3.

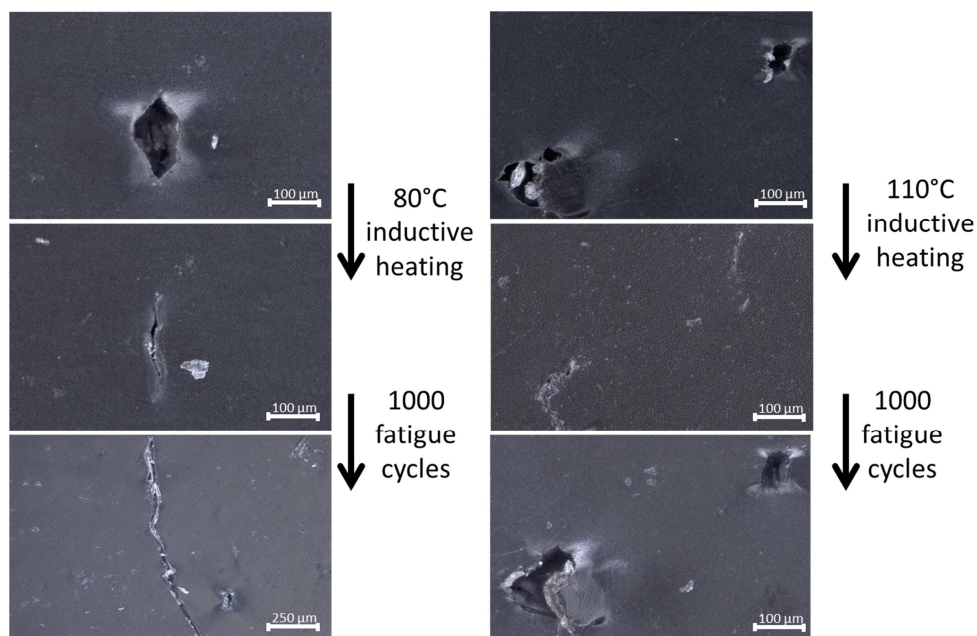


Figure 5.7 OM images showing the difference between crack closure and crack sealing which is achieved by inductive at different temperatures: (left) the crack closure at 80°C and the further crack propagation upon a second treatment of 1000 fatigue cycles; and (right) a series of cracks that are sealed at 110°C and reopened upon a second fatigue treatment of 1000 fatigue cycles.

Figure 5.8 shows the decay in maximal stress during 1000 fatigue cycles for Zn-EMAA preloaded to an initial strain of 50%. Figure 5.8a shows an ionomer composite specimen that was tested twice without any healing treatment in between. In this figure the strain hardening effect that is also visible in Figure 5.6 can be observed. Figure 5.8b and 5.8c show a similar set of experiments, however, with an inductive heat treatment at 80 or 110°C, respectively, in between cyclic loading. The figures show that both heat treatments restore the initial fatigue response and delete the strain hardening effect as a result of the recovery of the original network properties.

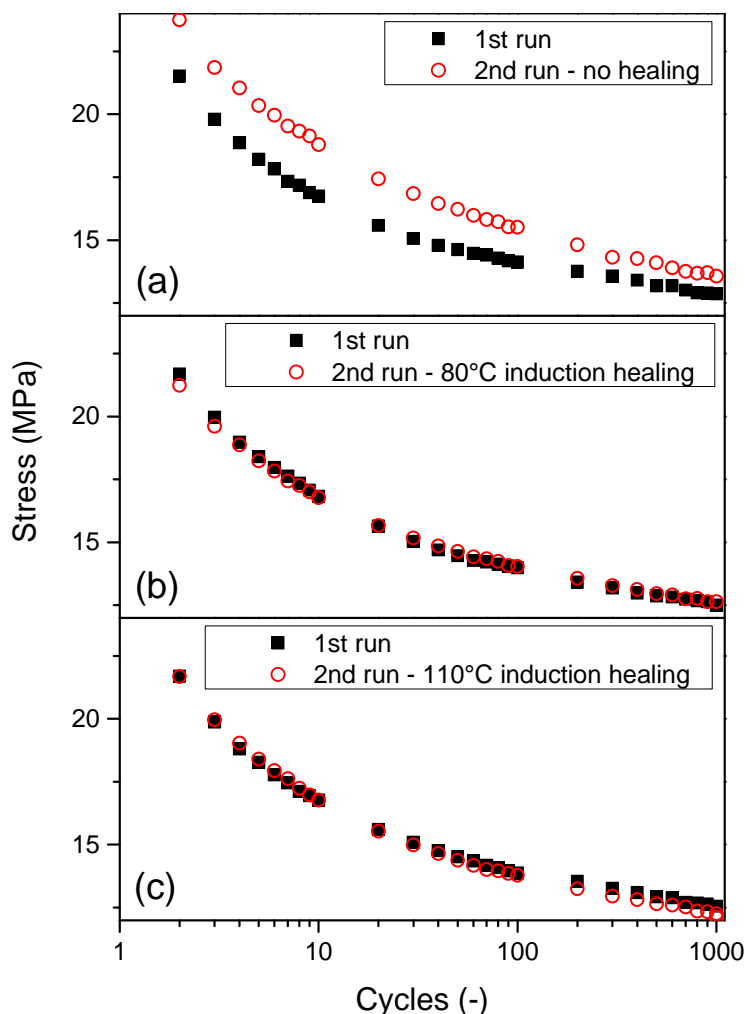


Figure 5.8 Fatigue response of three Zn-EMAA/Fe₃O₄ composites after two consecutive experiments. The first run in all three graphs is performed on a pristine specimen and the second run shows the response: (a) after one week without additional treatments; or after 15 min of inductive heating at: (b) 80°C; and (c) 110°C.

5.4. Discussion

The optical microscopy images in Figure 5.7 show a clear distinction between the closure and the sealing of fatigue induced cracks at the two healing temperatures. Although there seems to be an agreement on the mechanisms that are responsible for the contraction/closure [20, 21], there is still an ongoing debate on the mechanism that is responsible for the crack sealing behavior of ionomers. The main discussion revolves around the low-temperature endotherm that is visualized by DSC in Figure 5.2. The majority of studies on self-healing ionomers attribute this endotherm to a declustering of the ionic multiplets that are formed within the polymer microstructure as was described by Tadano et al. [38]. It is reported that the declustering of these multiplets would create sufficient mobility for the polymer to heal at temperatures below the melting point [8, 9, 14, 18, 37]. Another theory, posed by Eisenberg, describes the clusters of multiplets as a thermally stable phase with its own T_g that is higher than that of the surrounding non-ionic polymer phases. In their work, the origin of the low temperature endotherm is attributed to the crystallization of secondary crystals which form in between the primary crystal lattices over time [39, 40]. In a recent publication by Kalista et al., it is reviewed that the most experimental evidence points towards the latter explanation for the thermomechanical behavior of ionomers. However, the precise mechanism responsible for the self-healing of ionomers is still under discussion [24].

The results that are depicted in this work support the theory of Eisenberg over that of Tadano. A first indication is the fact that the DSC spectrum in Figure 5.2 shows a low temperature endotherm for the EMAA polymer. Since there are no ionic clusters present in this polymer, the endotherm in this spectrum cannot be attributed to ionic multiplet formation within the structure. The presence of ionic clusters does, however, affect the formation of the low temperature endotherm and the secondary crystalline phase as is described by Loo et al. [40]. In a similar fashion, the addition of adipic acid restricts the formation of this secondary crystalline phase as the corresponding endotherm peak around 50°C in Figure 5.1 flattens out completely. The results depicted in Figure 5.3 also contradict the declustering concept since no crossover point between G and G' can be found at 80°C [8, 9, 37].

The fact that the low temperature endotherm disappears upon straining (Figure 5.2) indicates that the molecular origin of this endotherm is not the sole explanation of the ionomer healing characteristics. The free-shrinkage behavior that is observed in this temperature range is most likely a result from the overall melting peak in the polymer which is very broad and starts at the onset of the low temperature endotherm. This statement is supported by the temperature dependency of the residual strain shown in Figure 5.4. The smaller crystals melt at lower temperatures

while the larger crystals remain crystallized and serve as a rigid internal structural entity as is also common in shape memory polymers [20].

The thermal contraction is shown to be independent of the presence of clusters and the low-temperature endotherm, since Figure 5.5 shows that the strain restoration after fatigue is clearly present for all compositions. As a matter of fact, these diagrams show that the contraction is highest in the non-ionic EMAA material as only in this material 100% restoration is observed after an applied strain of 50%. This is an indication that the presence of clusters might even restrict the mobility of the reforming secondary crystal phases of the polymer and thereby hindering the free-shrinkage capacity which is supported by the studies of Loo et al. [40].

The optical microscopy images show that sealing of the fatigue induced microcracks only occurs when the ionomer is heated above 110°C. This is in line with rheological data obtained in Figure 5.3 and Table 5.1. Here it is shown that the viscous component of the polymer does not get dominant over the elastic component before the overall melting point is reached. However, both thermal treatments lead to a full restoration of the original tensile behavior and fatigue response. This indicates that the polymer network is effectively repaired at temperatures below the melt temperature and that the formation and presence of microcracks does not directly affect the mechanical properties in the early stages of the damage formation. Nevertheless, the healing of the early stage damage will be necessary to extend the lifetime of the ionomer composites since these unsealed microcracks will eventually propagate into larger cracks, as was shown in Figure 5.7. These propagated cracks will ultimately induce the destructive failure of the material as was observed for the 50,000-cycle fatigue treatment of the Zn-EMAA/AA blend.

The addition of the nanoparticles (10 vol.%) was found to barely affect the overall tensile properties of the polymer. Full information on the impact of the nanoparticles on the tensile properties can be found in Supplementary Materials S2. Besides a slight increase in yield strength and Young's modulus, the main effect was an increased brittleness which is considered to have no effect on the applicability of the polymers since a tensile strain of at least 100% can still be achieved for the composites, as is depicted in Figure 5.4. Nevertheless, it was found that the Fe₃O₄ particles induce microcracks that are not observed in the pure polymer films. Based on this, it could be reasoned that the particles only weaken the material and no additional mechanical benefits are obtained. However, since the microcracks do not affect the overall tensile properties and fatigue response of the polymer composite and can be fully healed by heating at 110°C there is a zero net negative effect of the particles on the polymer behavior. On the other hand, the ferromagnetic particles allow the polymer to be healed by inductive heating which is crucial for

larger composite structures that cannot be heated by external contact heating and therefore require internal heating.

Although the thermal behavior below the overall melting temperature is comparable for all investigated blends and therefore independent of cluster content, there is a clear difference in the region above the melt. Table 5.1 shows different values for τ_b and G_N for the four polymer systems which can be explained by the presence of the ionic clusters. These create an additional phase in the polymer microstructure which has higher thermomechanical stability than the surrounding polymer phase. As a result, the non-ionic phase can flow in between the ionic clusters and thereby heal cracks and interfaces at a temperature above its melting point, while the overall polymer system maintains its required level of mechanical stability. When the cluster concentration is not high enough, the polymer will show melt flow and is therefore not considered to be a self-healing polymer. Based on the current observations it is possible to propose an ionomer healing temperature dependency scheme. Figure 5.9 shows a two-step healing mechanism in which the thermally induced free-shrinkage is independent of cluster content and can be triggered by applying a temperature between the two main melting points of the polymer. At this temperature, the residual strain and the strain hardening that occur upon deformation are fully restored. Early stage damage in the form of fatigue induced microcracks can be subsequently healed by melting the polymer while the ionic clusters act as a stable phase providing sufficient mechanical properties for good healing conditions.

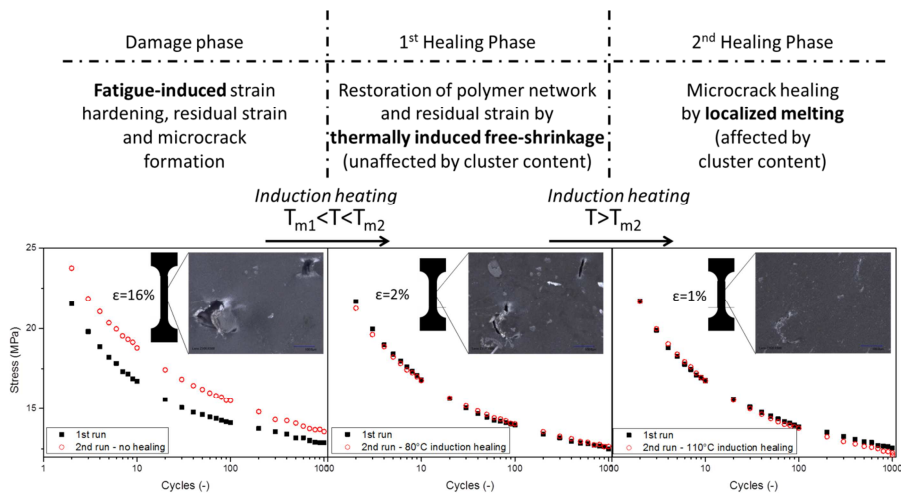


Figure 5.9 Ionomer healing temperature dependency scheme. In the 1st healing phase, the thermally induced free-shrinkage restores the residual strain and the polymer network at temperatures in between the melting point of the secondary crystal phase (T_{m1}) and the overall melting point (T_{m2}). In the 2nd healing phase, microcracks are closed due to localized melting above T_m in which the ionic clusters act as a stable phase providing sufficient mechanical properties for good healing conditions.

5.5. Conclusions

This work reports on the healing of early stage fatigue damage in poly(ethylene-*co*-methacrylic acid) based nanoparticulate composites upon localized inductive heating. It is found that there are three main damage modes that occur in the early stage of the fatigue process: residual strain, strain hardening and the formation of microcracks. Although the residual strain and strain hardening are a result of the nature of the polymer phase, the formation of microcracks is only observed upon the addition of the particulate phase.

It is demonstrated that healing of this early stage fatigue damage occurs in two different steps. Firstly, the deformation is restored by the free-shrinkage of the polymer. At temperatures below the melt temperature, the polymer network is healed and the fatigue induced strain hardening is reset. Secondly, only at temperatures above the melting point of the polymer phase, microcracks are sealed. It is shown that the thermally induced free-shrinkage in these polymers does not depend on the presence of ionic clusters, but that the ability to heal cracks in composite structures is reserved for ionomers that contain a sufficient amount of ionic clusters which guarantees an acceptable level of mechanical stability during healing. This implies that ionomers need to be thermally treated at above-the-melt temperatures in order to heal all the early stage damage that is induced upon fatigue loading.

References

1. van der Zwaag, S., *An Introduction to Material Design Principles: Damage Prevention versus Damage Management*, in *Self-Healing Materials an Alternative Approach to 20 Centuries of Materials Science*, S. van der Zwaag, Editor. 2007, Springer Netherlands: Dordrecht.
2. van der Zwaag, S., Grande, A.M., Post, W., García, S.J., and Bor, T.C., *Review of current strategies to induce self-healing behaviour in fibre reinforced polymer based composites*. Materials Science and Technology 2014. 30(13): p. 1633-1641.
3. Toohey, K.S., Hansen, C.J., Lewis, J.A., White, S.R., and Sottos, N.R., *Delivery of two-part self-healing chemistry via microvascular networks*. Advanced Functional Materials, 2009. 19(9): p. 1399-1405.
4. White, S.R., Moore, J.S., Sottos, N.R., Krull, B.P., Santa Cruz, W.A., and Gergely, R.C.R., *Restoration of large damage volumes in polymers*. Science, 2014. 344(6184): p. 620-623.
5. Billiet, S., Hillewaere, X.K.D., Teixeira, R.F.A., and Du Prez, F.E., *Chemistry of crosslinking processes for self-healing polymers*. Macromolecular Rapid Communications, 2013. 34(4): p. 290-309.
6. García, S.J., *Effect of polymer architecture on the intrinsic self-healing character of polymers*. European Polymer Journal, 2014. 53(0): p. 118-125.
7. Zhong, N. and Post, W., *Self-repair of structural and functional composites with intrinsically self-healing polymer matrices: A review*. Composites Part A: Applied Science and Manufacturing, 2015. 69: p. 226-239.
8. Hohlbein, N., Shaaban, A., and Schmidt, A.M., *Remote-controlled activation of self-healing behavior in magneto-responsive ionomeric composites*. Polymer (United Kingdom), 2015. 69: p. 301-309.
9. James, N.K., Lafont, U., van der Zwaag, S., and Groen, W.A., *Piezoelectric and mechanical properties of fatigue resistant, self healing PZT-ionomer composites*. Smart Materials and Structures, 2014. 23(5): p. 055001
10. Sundaresan, V.B., Morgan, A., and Castellucci, M. *Self-Healing of Ionomeric Polymers with Carbon Fibers from Medium-Velocity Impact and Resistive Heating*. Smart Materials Research, 2013. 2013, 12 DOI: 10.1155/2013/271546.
11. Grande, A.M., Castelnovo, L., Landro, L.D., Giacomuzzo, C., Francesconi, A., and Rahman, M.A., *Rate-dependent self-healing behavior of an ethylene-co-methacrylic acid ionomer under high-energy impact conditions*. Journal of Applied Polymer Science, 2013. 130(3): p. 1949-1958.
12. Grande, A.M., Coppi, S., Di Landro, L., Sala, G., Giacomuzzo, C., Francesconi, A., and Rahman, M.A. *An experimental study of the self-healing behavior of ionomeric systems under ballistic impact tests*. in *Proceedings of SPIE*. 2012. San Diego.
13. Kalista Jr, S.J., Ward, T.C., and Oyetunji, Z., *Self-healing of poly(ethylene-co-methacrylic acid) copolymers following projectile puncture*. Mechanics of Advanced Materials and Structures, 2007. 14(5): p. 391-397.

14. Varley, R.J. and van der Zwaag, S., *Towards an understanding of thermally activated self-healing of an ionomer system during ballistic penetration*. Acta Materialia, 2008. 56(19): p. 5737-5750.
15. Varley, R.J. and van der Zwaag, S., *Autonomous damage initiated healing in a thermo-responsive ionomer*. Polymer International, 2010. 59(8): p. 1031-1038.
16. Luo, X. and Mather, P.T., *Shape memory assisted self-healing coating*. ACS Macro Letters, 2013. 2(2): p. 152-156.
17. Rodriguez, E.D., Luo, X., and Mather, P.T., *Linear/network poly(ϵ -caprolactone) blends exhibiting shape memory assisted self-healing (SMASH)*. ACS Applied Materials and Interfaces, 2011. 3(2): p. 152-161.
18. Vega, J.M., Grande, A.M., van der Zwaag, S., and García, S.J., *On the role of free carboxylic groups and cluster conformation on the surface scratch healing behaviour of ionomers*. European Polymer Journal, 2014. 57(0): p. 121-126.
19. Wang, C.H., Sidhu, K., Yang, T., Zhang, J., and Shanks, R., *Interlayer self-healing and toughening of carbon fibre/epoxy composites using copolymer films*. Composites Part A: Applied Science and Manufacturing, 2012. 43(3): p. 512-518.
20. Dolog, R. and Weiss, R.A., *Shape memory behavior of a polyethylene-based carboxylate ionomer*. Macromolecules, 2013. 46(19): p. 7845-7852.
21. Scogna, R.C. and Register, R.A., *Plastic deformation of ethylene/methacrylic acid copolymers and ionomers*. Journal of Polymer Science, Part B: Polymer Physics, 2009. 47(16): p. 1588-1598.
22. Slutsker, A.I., Vettegren', V.I., Kulik, V.B., Hilarov, V.L., Polikarpov, Y.I., and Karov, D.D., *Detailed of deformation processes in polymeric crystals*. Physics of the Solid State, 2015. 57(11): p. 2305-2313.
23. Lacks, D.J. and Rutledge, G.C., *Mechanisms for axial thermal contraction in polymer crystals: polyethylene vs isotactic polypropylene*. Chemical Engineering Science, 1994. 49(17): p. 2881-2888.
24. Kalista, S.J., Pflug, J.R., and Varley, R.J., *Effect of ionic content on ballistic self-healing in EMAA copolymers and ionomers*. Polymer Chemistry, 2013. 4(18): p. 4910-4926.
25. Amamoto, Y., Otsuka, H., Takahara, A., and Matyjaszewski, K., *Self-healing of covalently cross-linked polymers by reshuffling thiuram disulfide moieties in air under visible light*. Advanced Materials, 2012. 24(29): p. 3975-3980.
26. Canadell, J., Goossens, H., and Klumperman, B., *Self-healing materials based on disulfide links*. Macromolecules, 2011. 44(8): p. 2536-2541.
27. Lafont, U., Van Zeijl, H., and van der Zwaag, S., *Influence of cross-linkers on the cohesive and adhesive self-healing ability of polysulfide-based thermosets*. ACS Applied Materials and Interfaces, 2012. 4(11): p. 6280-6288.
28. Adzima, B.J., Kloxin, C.J., and Bowman, C.N., *Externally triggered healing of a thermoreversible covalent network via self-limited hysteresis heating*. Advanced Materials, 2010. 22(25): p. 2784-2787.

29. Corten, C.C., Urban, M.W., and Shelby, F., *Repairing polymers using an oscillating magnetic field*. Advanced Materials, 2009. 21(48): p. 5011-5015.
30. Duenas, T., Enke, A., Chai, K., Castellucci, M., Sundaresan, V.B., Wudl, F., Murphy, E.B., Mal, A., Alexandar, J.R., Corder, A., and Ooi, T.K., *Smart self-healing material systems using inductive and resistive heating*, in *ACS Symposium Series*. 2010. p. 45-60.
31. Brown, E.N., White, S.R., and Sottos, N.R., *Retardation and repair of fatigue cracks in a microcapsule toughened epoxy composite - Part II: In situ self-healing*. Composites Science and Technology, 2005. 65(15-16 SPEC. ISS.): p. 2474-2480.
32. Jones, A.S., Rule, J.D., Moore, J.S., Sottos, N.R., and White, S.R., *Life extension of self-healing polymers with rapidly growing fatigue cracks*. Journal of the Royal Society Interface, 2007. 4(13): p. 395-403.
33. Neuser, S. and Michaud, V., *Fatigue Response of Solvent-Based Self-Healing Smart Materials*. Experimental Mechanics, 2014. 54(2): p. 293-304.
34. Yuan, Y.C., Rong, M.Z., Zhang, M.Q., Yang, G.C., and Zhao, J.Q., *Self-healing of fatigue crack in epoxy materials with epoxy/mercaptan system*. Express Polymer Letters, 2011. 5(1): p. 47-59.
35. Luterbacher, R., Trask, R.S., and Bond, I.P., *Static and fatigue tensile properties of cross-ply laminates containing vasculs for self-healing applications*. Smart Materials and Structures, 2015. 25(1): p. 015003.
36. Varley, R.J., Shen, S., and van der Zwaag, S., *The effect of cluster plasticisation on the self healing behaviour of ionomers*. Polymer, 2010. 51(3): p. 679-686.
37. Hohlbein, N., von Tapavicza, M., Nellesen, A., and Schmidt, A.M., *Self-Healing Ionomers*, in *Self-Healing Polymers*, W.H. Binder, Editor. 2013, Wiley-VCH Verlag GmbH & Co.: Weinheim. p. 315-334.
38. Tadano, K., Hirasawa, E., Yamamoto, H., and Yano, S., *Order-disorder transition of ionic clusters in ionomers*. Macromolecules, 1989. 22(1): p. 226-233.
39. Eisenberg, A., Hird, B., and Moore, R.B., *A new multiplet-cluster model for the morphology of random ionomers*. Macromolecules, 1990. 23(18): p. 4098-4107.
40. Loo, Y.L., Wakabayashi, K., Huang, Y.E., Register, R.A., and Hsiao, B.S., *Thin crystal melting produces the low-temperature endotherm in ethylene/methacrylic acid ionomers*. Polymer, 2005. 46(14): p. 5118-5124.
41. Bose, R.K., Hohlbein, N., García, S.J., Schmidt, A.M., and van der Zwaag, S., *Connecting supramolecular bond lifetime and network mobility for scratch healing in poly(butyl acrylate) ionomers containing sodium, zinc and cobalt*. Physical Chemistry Chemical Physics, 2015. 17(3): p. 1697-1704.
42. Fayolle, B., Richaud, E., Colin, X., and Verdu, J., *Review: Degradation-induced embrittlement in semi-crystalline polymers having their amorphous phase in rubbery state*. Journal of Materials Science, 2008. 43(22): p. 6999-7012.

Supplementary Information

S1: Model description

The temperature of the tested specimen upon inductive heating was monitored with a FLIR A655sc infrared camera. Since this method only detects the surface temperature of the ionomer composites, a COMSOL Multiphysics 5.2 model was used to derive a relation between the measured surface temperature and the desired healing temperature within the bulk of the polymer sample. The used model is a stationary heat transfer model that correlates the measured surface temperature to the bulk healing temperature based on the thermal conductivity of the materials used.

The base of the model is a unit cell that consists of a cube containing a sphere in its centre that occupies 10 vol.% of the cubic shape. This unit cell was then used to construct a $3 \times 3 \times 3$ matrix resulting in a cubic structure with 27 equally divided spheres in its body. This cubic structure was placed in another cubic shape with a volume that is 159% larger than the matrix. In the model, the matrix represents the polymer composite and the spheres act as the iron oxide fillers. The surrounding cube represents the air that cools the specimen during heating. The "heat transfer in solids" physics module, available in COMSOL Multiphysics 5.2, was then applied to the developed geometry. The input data used for the polymer and particle phase are depicted in Table S 5.1:

Table S 5.1 Input parameters for heat transfer model used to correlate measured surface temperature to the overall bulk temperature.

| Parameters | Surlyn 9520 | Iron Oxide |
|--|-------------|------------|
| Thermal conductivity (W/(m·K)) | 0.246 | 50 |
| Density (kg/m³) | 950 | 5.1 |
| Heat Capacity at constant pressure J/(kg·K) | 2100 | 450 |

The surrounding layer of air was given the pre-programmed input parameters that are available in COMSOL Multiphysics 5.2. It is experimentally observed that, upon the application of a specific inductive field, the temperature of the particulate composite reaches a steady state within 5 min. Therefore a temperature profile is created by setting temperature boundary conditions on both the filler material and the surrounding air. The temperature of air was set at 293.15 K whereas the temperature of the spheres was varied from 343.15 to 473.15 K. Based on these input parameters the temperature gradient along the edge of the matrix structure is

calculated as it represents the composite surface that is measured with the IR camera. The edge values (corner points of the matrix) of these temperature gradients are then considered to represent the surface temperature and are plotted versus the set boundary temperature of the particles, which is found to correspond to the uniform bulk temperature of the material. The resulting plot is shown in Figure S5.1.

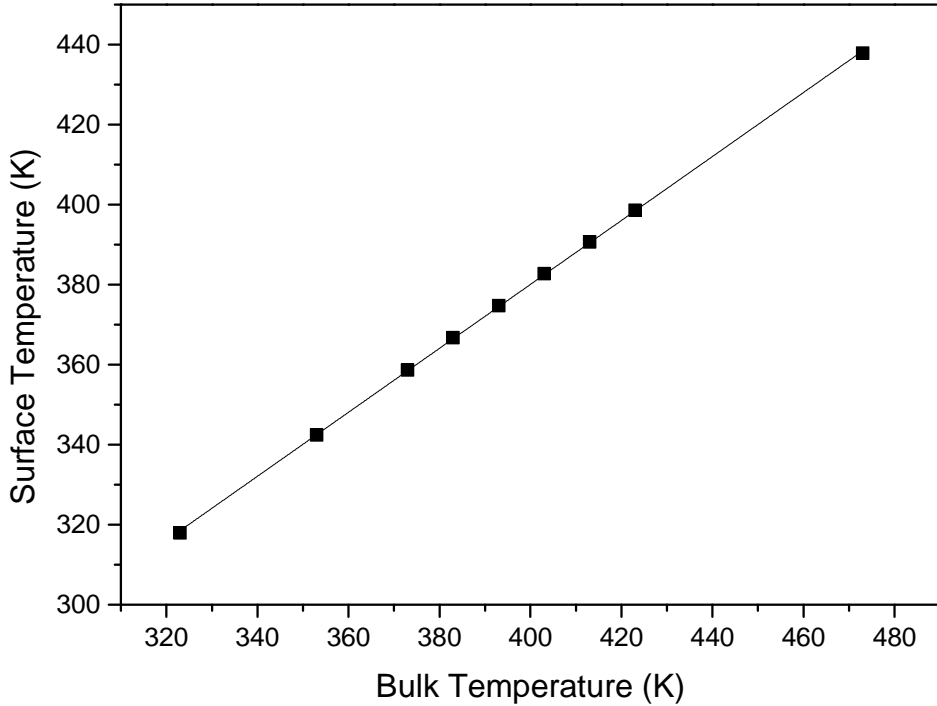


Figure S5.1 Calculated surface temperature versus bulk temperature.

From the calculated data the following linear relation was derived:

$$\text{Surface Temperature} = 0.80 * \text{Bulk Temperature} + 60.33 \quad (\text{S5.1})$$

The empirical Equation (S5.1) relates the measured surface temperature (in K) to the bulk temperature of the polymer and is used to determine the experimental healing temperatures.

S2. Effect of Fe_3O_4 Particles on Matrix Properties

The effect of the Fe_3O_4 particles on the ionomer matrix was investigated by tensile testing using an Instron Model 3365 universal testing systems equipped with a 1 kN load cell. Dog-bone micro-tensile specimens were stretched at 1 mm/s at room temperature. The tensile curves of a Zn-EMAA specimen with and without particle loading are shown in Figure S5.2.

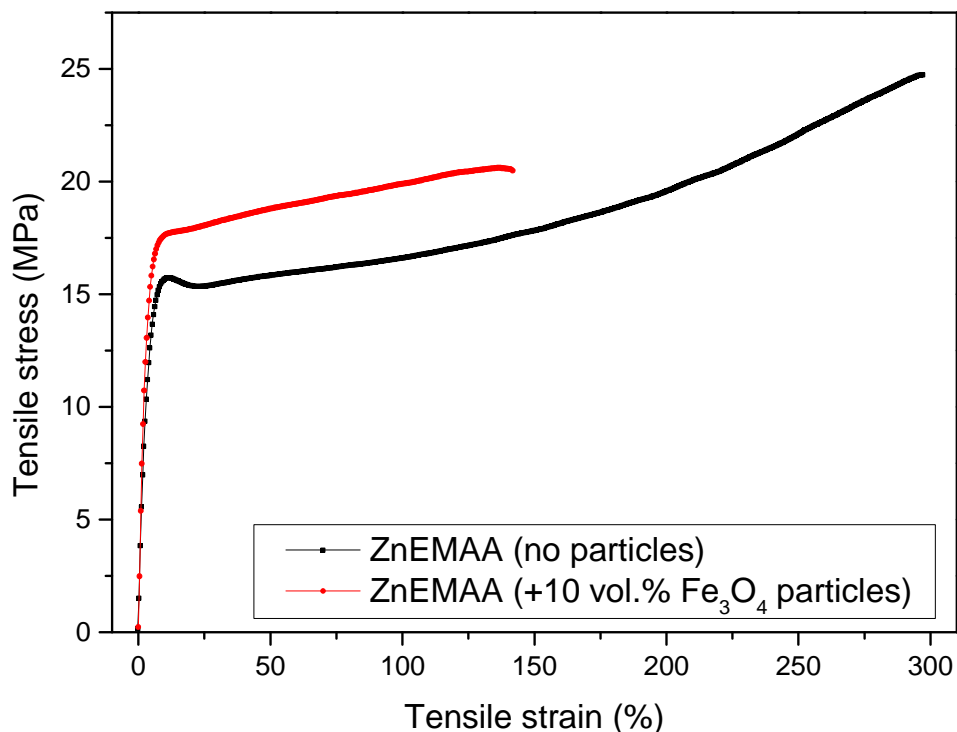


Figure S5.2 Stress-strain curves of the Zn-EMAA ionomer with and without the addition of particles.

Based on the tensile response in Figure S5.2 the yield strength, ultimate strength, Young's modulus and strain at break were determined. These values are determined for all four polymer blends and their values are depicted in Table S 5.2.

Table S 5.2 Overview of mechanical properties of the ionomer nanoparticle composites and their non-particle counterparts.

| Polymer | Filler | Yield Strength (MPa) | Ultimate Strength (MPa) | Young's Modulus (MPa) | Strain at Break (%) |
|--------------|---|----------------------|-------------------------|-----------------------|---------------------|
| Zn-EMAA | No filler | 15.7 | 24.7 | 365 | 297 |
| | 10 vol.% Fe ₃ O ₄ | 17.6 | 20.6 | 431 | 142 |
| EMAA | No filler | 8.7 | 23.5 | 108 | 455 |
| | 10 vol.% Fe ₃ O ₄ | 11.1 | 18.4 | 250 | 195 |
| Zn-EMAA/EMAA | No filler | 12.4 | 22.5 | 252 | 331 |
| | 10 vol.% Fe ₃ O ₄ | 13.6 | 19.5 | 324 | 179 |
| Zn-EMAA/AA | No filler | 10.3 | 14.2 | 222 | 267 |
| | 10 vol.% Fe ₃ O ₄ | 14.0 | 15.7 | 327 | 45 |

Chapter 6

Non-destructive monitoring of delamination healing of a CFRP composite with a thermoplastic ionomer interlayer

This chapter has been published as:

W. Post, M. Kersemans, I. Solodov, K. Van Den Abeele, S. J. García, S. van der Zwaag; *Non-destructive monitoring of delamination healing of a CFRP composite with a thermoplastic ionomer interlayer*, Composites Part A: Applied Science and Manufacturing, Volume 101, October 2017, Pages 243-253

6.1. Introduction

For more than two decades fibre reinforced polymer composites (FRPCs) have emerged in many engineering constructions, and now have become an indispensable option in modern design strategies for advanced load bearing light weight products because of their low relative density, high strength and high stiffness [1, 2]. However, a major disadvantage of FRPCs is that they are sensitive to impact, leading to barely visible impact damage, matrix cracking and delaminations which can ultimately result in catastrophic failure of the component without much prior notification [3, 4]. In order to prevent such a failure mode, FRPCs are often over-dimensioned or subjected to periodic non-destructive testing (NDT). Alternatively, to raise the impact resistance and interlaminar fracture toughness of FRPC's, thermoplastic interlayers in between the composite plies have been proposed [5, 6]. The interlayers lower the overall mechanical properties but prevent wide spreading of the impact damage as they 'contain' the damage by delamination at the interlayer-FRPC interface or by internal damage [7]. A further and as-yet barely explored advantage of such thermoplastic interlayers is that they can be made out of self-healing polymers, i.e. polymers which can restore their adhesive and internal strength autonomously or by a simple in-situ thermal treatment.

Within the field of self-healing polymer composites the majority of early studies focussed on extrinsic healing strategies in which an 'external' healing agent is added to the matrix prior to consolidation. The healing agent can be included via capsules, hollow fibres or vascular systems and is released upon fracture of the matrix [8-10]. The major drawback of these systems is that they only lead to single healing events and multiple healing (at a specific location) is not possible. In intrinsic healing polymer systems the restorative behaviour is embedded within the polymer structure itself and only needs an external trigger in the form of a modest temperature raise. Such polymers are theoretically capable of an infinite number of healing cycles [11, 12], provided the healing conditions are such that the separated crack surfaces can come into contact again.

Ionomers are a class of thermoplastic polymers that are capable of intrinsic self-healing upon thermal activation as shown for scratch, ballistic impact and fatigue damage [13-17]. This healing takes place at modest temperatures, i.e. at around 100-120°C which is well below the overall melt flow temperature of the material. Hence, while being a thermoplastic, ionomers offer major advantages over conventional thermoplastic interlayer materials as damage repair does not require reheating to a high temperature at which massive flow occurs everywhere in the structure. In the case of healing of ionomers the macroscopic flow is restricted to local areas around the damage or delamination site. Moreover, ionomers have also

been employed as interlayer material in conventional carbon fibre/epoxy composites due to their good adhesive properties [5, 18]. These two characteristics make ionomers ideal candidates to be used as self-healing interlaminar systems for CFRP structures.

However, as long as self-healing interface layers for CFRPs are in their development stage and the conditions of guaranteed quasi-autonomous repair are yet to be defined, there will be a need for NDT of delaminations and internal damage in a quantitative or at least semi-quantitative manner. The appropriate NDT techniques to monitor such damage should at least provide information on the areal extent of the damage and if possible on the location and height of the internal cavity. Although the requirement for non-destructive healing evaluation seems evident, the majority of studies that investigate the self-healing behaviour of composite materials focus on destructive testing of damaged and healed samples and the involvement of NDT is limited to a couple of studies only [19-24].

One of the most powerful NDT techniques for the detection of meso- and macroscopic damage in composite materials is the use of broad-band ultrasound, i.e. elastic waves with frequencies above 20 kHz. By appropriate analysis of the reflection or transmission of ultrasonic waves, several types of damage, such as voids, cracks and delaminations, can be detected and localized [25-29]. This approach has been thoroughly developed in the past, and is currently adapted for NDT in a number of industrial applications. A recent development in the field of ultrasonics is based on the occurrence of local defect resonance (LDR) [30, 31]. In this testing mode, an internally damaged component is excited at such a frequency that the damage region is forced into a resonance vibration mode with local displacements being several times higher than its surroundings. This resonance signal is then detected and used to reconstruct and visualise the location and dimension of the damage site. Since the LDR vibration is constrained exclusively in the defect area, the spatial resolution of the resonant imaging is comparable with conventional ultrasonic NDT techniques despite the lower frequencies used.

In this work, a comparative study is performed on carbon fibre reinforced polymer (CFRP) composites with an ionomer interlayer in which artificial delaminations of various sizes and at different locations were introduced during production. The dimensions of the defects prior and after thermal healing are measured by conventional ultrasonics and LDR. In addition, the compressive strength of the as-produced and healed samples is measured and the data are correlated to the various NDT results.

6.2. Material and methods

6.2.1. Materials

Prior to composite production, CFRP laminates of 1 mm were produced by infusing two layers of satin woven carbon fibre fabrics (285 g/m², Haufler composites) with Epikote™ 04908 resin (HEXION). The CFRP layers were cured for 16 hours at room temperature and post-cured for 8 hours at 80°C, as prescribed by the resin supplier, resulting in laminates with a T_g of approximately 90°C. PV5414 ionomer films (500 μ m thickness) were obtained from DuPont®.

6.2.2. Ionomer-CFRP laminate production

Ionomer-CFRP laminates of 10x10 cm² were produced by stacking and two-step pressing the CFRP and ionomer components for 1 minute at 100°C with a pressure of 1 MPa using a hot press. The overall stacking sequence consists of 2 layers of CFRP and 2 layers of ionomer film. Artificial delaminations (i.e. non-fused regions) were introduced by placing two aluminium plates containing a circular hole of either 2 or 5 cm in between the heated dies of the hot press and the outer CFRP layers prior to the last pressing step. The size of the resulting non-fused areas, the delaminations, corresponds to the size of the hole within the aluminium plate. A schematic overview of the ionomer-CFRP laminate production is shown in Figure 6.1. For the CFRP-ionomer laminate configuration shown in Figure 6.1a, two identical pre-pressed and perfectly bonded substructures each consisting of 1 layer CFRP and one layer ionomer film (5 minutes at 100°C and 1 MPa of pressure) were used. Using this protocol a delamination was created within the thermoplastic interlayer (called the 'soft-soft delamination' hereafter). This type of delamination is to be regarded as an internal defect in the thermoplastic interlayer itself. For the CFRP-ionomer laminate shown in Figure 6.1b, the final pressing was done with a single CFRP plate on the one hand and a perfectly bonded CFRP plate-ionomer substructure consisting of 1 layer CFRP and two layers of ionomer film on the other hand. This way, a delamination is introduced at the interface of the CFRP and the ionomer interlayer (called the 'rigid-soft delamination' hereafter). This type of delamination is to be regarded as a proper delamination between layers of different properties, being the thermoplastic interlayer and the CFRP face plate.

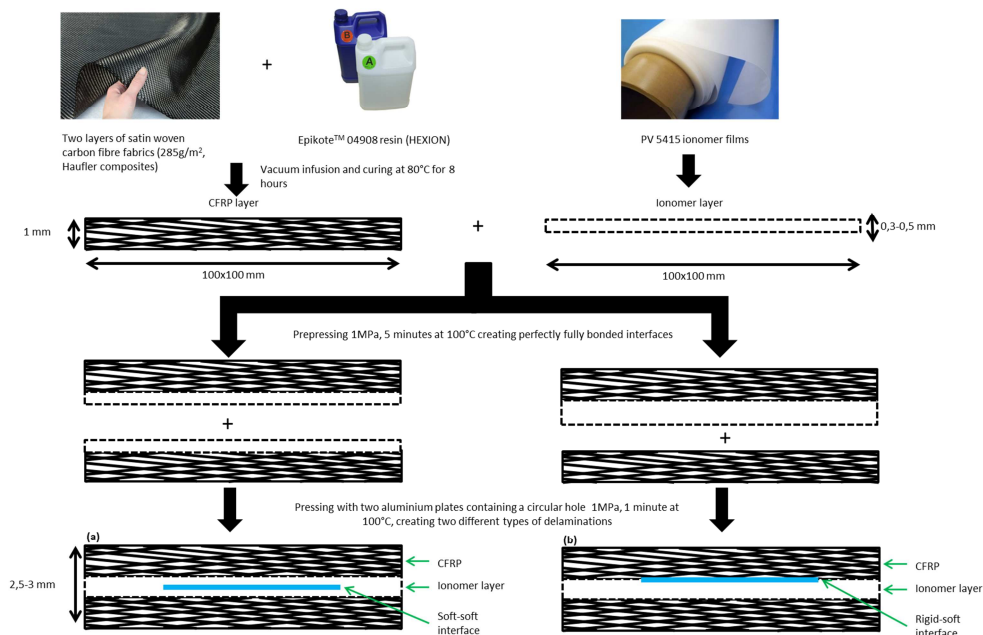


Figure 6.1 Schematic overview of the production process of the artificially induced delaminations in CFRP-ionomer laminates. Both the soft-soft (a) and rigid-soft (b) delamination production are shown.

6.2.3. Healing treatment

Healing was performed by pressure-less annealing of the laminates at a temperature of 100°C in a hot-air furnace. The specimens were healed for a total time up to 40 hours. However, to allow ultrasonic monitoring of the actual delaminated area during the annealing treatment, the specimens were taken out of the oven after 1, 2, 3, 4, 5, 6, 7, 8, 9, 10, 11, 12, 14, 16, 18, 20, 22, 24, 26, 28 and 40 hours for the water-coupled C-scan measurements and after 1, 2, 3, 5, 9, 11, 13, 15, 17, 20, 25 and 40 hours for air-coupled C-scan and LDR measurements. The NDT measurements were conducted at room temperature and typically took 30 minutes for the water-coupled C-scan measurements and 1 hour for the air-coupled C-scan and LDR measurements. No efforts were made to rapidly cool the samples from the oven temperature to room temperature. Although healing was performed above the T_g of both the epoxy and the ionomer, no thermal degradation of the polymeric phase was observed as is described in Supplementary information S1.

6.2.4. Characterization

6.2.4.1. Thermomechanical analysis of the ionomer film

The optimal healing temperature of the PV5414 ionomer film from a molecular mobility perspective was determined using a Perkin-Elmer Sapphire differential

scanning calorimeter (DSC). Samples were heated and cooled between -50°C and 150°C at a rate of $20^{\circ}\text{C}/\text{min}$ under a nitrogen atmosphere.

In order to obtain information on the flow characteristics of the PV5414 ionomer, the macroscale network mobility of the $500\text{ }\mu\text{m}$ film was investigated by small amplitude oscillatory shear rheology. The experiment was performed using a Haake Mars III rheometer, employing an 8 mm diameter (stainless steel) parallel plate geometry. A constant shear strain γ of 1% was applied, which is within the linear viscoelastic regime of the material. Frequency sweep experiments between 10^2 – 10^{-2} Hz were performed at temperatures of 70 and 100°C , with isothermal hold periods of 20 minutes in between temperature steps. The supramolecular bond lifetime (τ_b) at these temperatures was then calculated as the inverse of the frequency at which the storage and loss moduli crossover in a frequency sweep experiment [32].

6.2.4.2. Ultrasonic NDT analysis

Water-coupled ultrasonic C-scan experiments

Water-coupled C-scans, both in reflection and transmission, were made on the different samples and their various healing stages, in order to extract the remaining delaminated area and to quantify the progression of healing. Water temperature was measured to be $22^{\circ}\text{C} \pm 1^{\circ}\text{C}$. Dynamic time-gating, based on the pulse echo of the front surface, was applied for the C-scans in reflection. In this way, non-horizontality of the samples is compensated for and the imaging depth is kept constant. An ultrasonic pulse with a centre frequency $f_c = 5\text{ MHz}$ was used (H5K transducer with diameter 13 mm, General Electric). The distance between transducer(s) and inspected sample was approximately 70 mm. The pulser/receiver apparatus operates at a sampling frequency of 400 MHz (USIP40, General Electric), and the maximum pulse amplitude is evaluated in the selected time gate. For both x-direction (index axis) and y-direction (scanning axis), a scan range of 0-120 mm was applied with a grid step of 1 mm and 0.1 mm respectively. The actual scanning speed was set at 50 mm/s.

Air-coupled ultrasonic C-scan experiments

Air-coupled C-scans were carried out after each heating step described in the healing protocol. The applied frequency was 200 kHz. The Ultrason focused transducers (focus distance 38 mm, size of focus spot $\sim 2\text{ mm}$) were positioned in a normal transmission mode. The transducers were powered with rectangular bursts of 200 V amplitude and 10 periods of carrier frequency. The data acquisition unit included 14-bit A/D converter with 5 MHz sampling frequency and 40 dB maximum amplification. In the C-scans, scanning steps of 1 mm along the x and the y-axes were combined with scanning speed of 20 mm/s along the x-axis.

Local defect resonance

Local Defect Resonance (LDR) is caused by a local decrease in stiffness for a certain mass of the material in direct contact with the area of delamination being in local resonance [31]. A frequency match between the input and the defect natural frequency results in a substantial increase in local vibrations which can be used for identification of the position and the size of the defect. The vibrations in the specimen were excited by piezo-actuators SI Scientific Instruments GmbH with a frequency response extended into high kHz range to comprise an expected value of LDR frequency of the delamination. To identify the LDR frequency the transducers are driven in chirp modes (bandwidth 200 kHz, input voltage 1-2 V) generated by the HP 33120A arbitrary waveform generator. The C-scan of the specimen surface was implemented with the laser vibrometer Polytec PSV 300 and colour coded images of the distributions of vibration amplitudes over the specimen surface were obtained for all resonance peaks in the vibration spectrum. The image with maximum vibrations localised inside the delamination area corresponds to its local resonance whose frequency and frequency response (amplitude vs. frequency) were identified from the spectrum data.

6.2.4.3. Mechanical characterization of the pristine and healed composites

In order to determine the effect of the delamination healing in the CFRP-ionomer composites on the in-plane compression strength the composites were mechanically loaded. Compression tests were performed using a well-aligned Zwick/Roell 250 kN universal testing machine with a crosshead speed of 1 mm/min. Samples were clamped on every side of the panel based on conditions as prescribed in ASTM D7137(M)-07. However, several amendments to the standard were made for practical reasons. As such, the dimensions of the specimen are selected differently, the clamping side plates have dimensions of 105 x 80 mm, a thickness of 5 mm and bolts were used per 30 mm clamping length. The non-delaminated specimen was tested 4 times. However, as all delaminated and healed specimen had to be characterized by the various NDT techniques prior to mechanical testing, per condition only one sample was tested.

6.3. Results

6.3.1. Thermomechanical properties of the ionomer interlayer

Thermal characterization of the ionomer film was performed in order to obtain a good understanding of the healing characteristics of the ionomer interlayer prior to mechanical testing and non-destructive evaluation. The DSC curve in Figure 6.2 clearly shows the two main thermal transitions which are typical for ionomer based polymers. Both transitions play a specific role in the healing process [17].

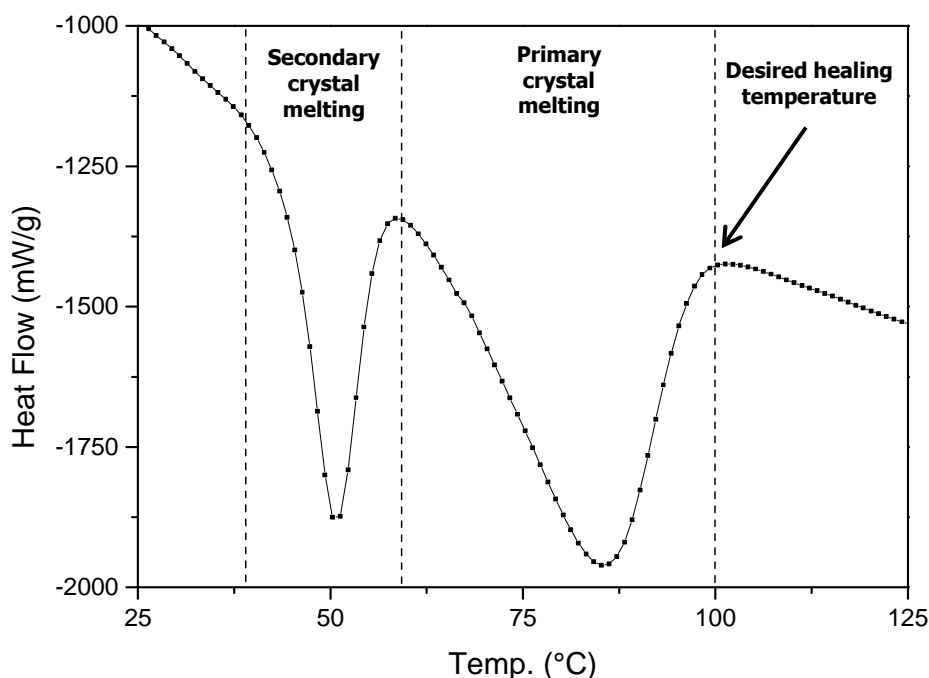


Figure 6.2 DSC curve of the heating of the ionomer interlayer. During heating, two healing stages can be identified, during which secondary and primary crystal melting occurs between 40-60°C and 60-100°C respectively.

Figure 6.2 shows that the primary polymer crystals melt at a temperature above 100°C. Previous work showed that full healing of the ionomer interlayers will only occur when annealed at or slightly above this temperature [17]. At these temperatures the polymer phase has enough mobility to flow locally while the ionic clusters maintain its rigidity preventing the polymer to flow at a macroscopic level. The critical temperature for healing based on DSC measurements is confirmed by the rheological data displayed in Figure 6.3 which show that the storage modulus G' and the loss modulus G'' do not intersect at temperatures below 100°C. Hence, below this temperature, there is no macroscale mobility and therefore no healing.

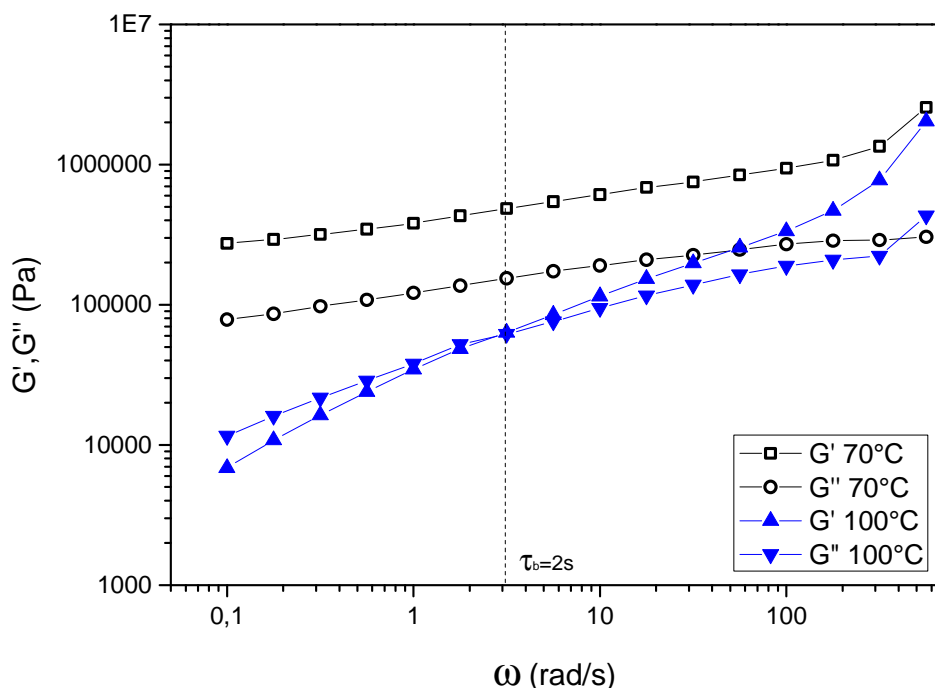


Figure 6.3 Frequency sweep experiment of the ionomer film at 70°C and 100°C. The supramolecular bond lifetime τ_b can be determined at the temperature where the storage and loss modulus intersect.

From the data in Figure 6.3, the supramolecular bond lifetime can be derived at the temperature where G' and G'' intersect. For a healing temperature of 100°C, a τ_b of 2 seconds is determined ($\tau_b = 2\pi/\omega$). Since the plateau modulus that could be derived at this temperature exceeds 10^5 Pa, the used ionomer meets the semi-quantitative requirements for an intrinsic self-healing polymer combining good healing with decent mechanical properties [32].

6.3.2. Non-destructive characterization

6.3.2.1. C-scanning techniques

All delaminated CFRP-ionomer laminates prepared in this study were inspected before and after the full healing treatment by means of two implementations of C-scanning techniques: water-coupled (WCU) and air-coupled (ACU). The corresponding transmission images for the various laminated structures with a 5 cm and 2 cm delamination are displayed in Figure 6.4 and Figure 6.5 respectively. Using the WCU technique it is also possible to visualize the delaminations and healing using the reflection output. The reflection WCU scans are shown in the supplementary information (S1), where one can easily verify the complementarity between transmission and reflection WCU C-scans. Although the use of reflection over transmission is favourable from an application point of view, the transmission

output is mainly analysed throughout this study in order to compare to the comparable transmission signal obtained in the ACU C-scans.

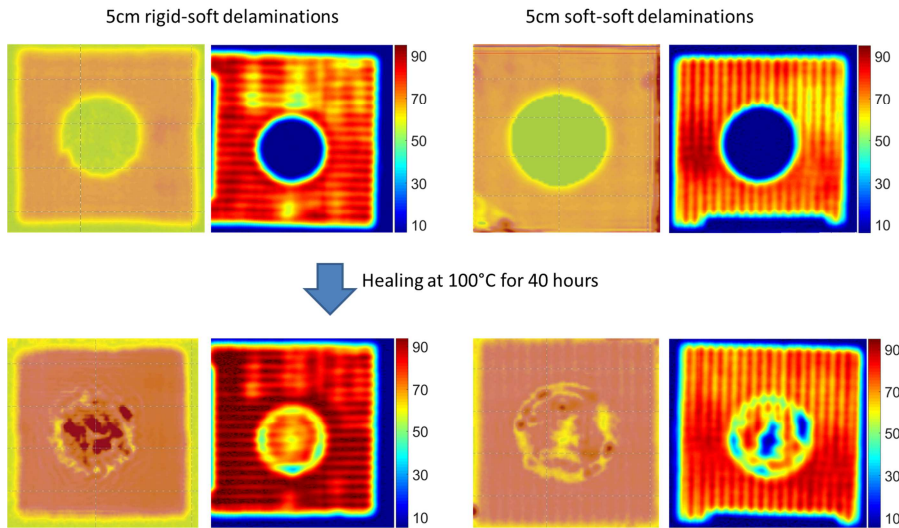


Figure 6.4 Overview of the C-scan transmission amplitude images for laminates with rigid-soft and soft-soft delamination with an initial radius of 5 cm scanned with ACU (left column) and WCU (right column). The top images clearly visualize the circular unhealed delaminations whereas the bottom images correspond to the scan results for the same specimen after a healing treatment at 100°C for 40 hours. Colour bar indicates percentage for WCU transmission.

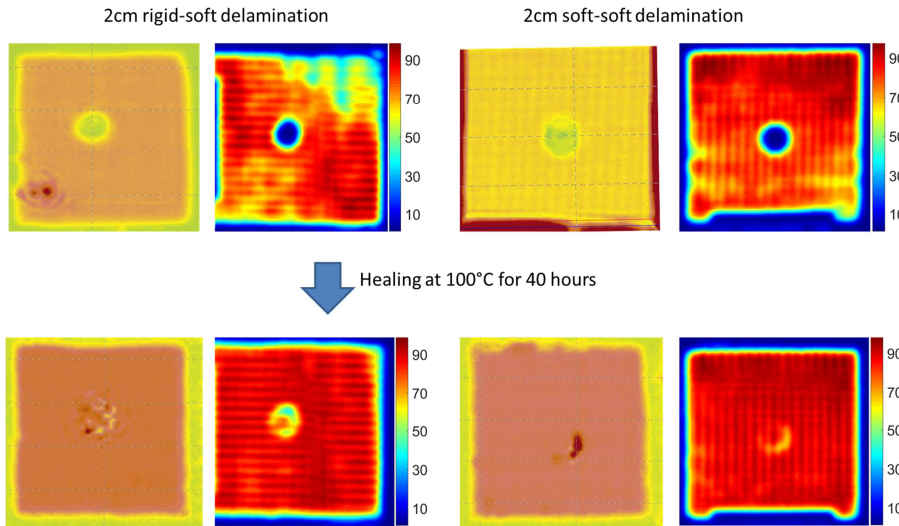


Figure 6.5 Overview of the C-scan transmission amplitude images for laminates with rigid-soft and soft-soft delaminations with an initial radius of 2 cm scanned with ACU (left column) and WCU (right column). The top images clearly visualize the circular unhealed delaminations whereas the bottom images correspond to the scan results for the same specimen after a healing treatment at 100°C for 40 hours. Colour bar indicates percentage for WCU transmission.

From the figures 6.4 and 6.5, it can be seen that both C-scanning techniques are equally capable of detecting the soft-soft and the rigid-soft delaminations. However, based on the scans, no distinction can be made between the two different types of delaminations. In addition, the scans also visualize the almost complete healing of the delaminations after healing for 40 hours at 100°C. Clearly, even in extensively healed specimens, traces of the original delaminated area can be detected.

For the 5 cm delaminations these traces are mainly located at the edges and in the middle of the original delaminations. The healed region in the rigid-soft specimen is more evenly distributed than that of the soft-soft specimen in which a more random distribution of the healed area is present. The unhealed zones at the edge of the delamination are believed to be caused by volumes of air that are trapped within the specimen upon production. In delaminations induced by low-velocity impact, pockets of trapped air will not be present, and therefore it is expected that such unhealed regions will not exist in actual applications. The unhealed zone in the middle of the specimen could be of similar origin but might also be caused by the fact that the delaminated interfaces were too far apart initially and did not make contact during the non-pressurized healing treatment. The C-scan images for the 2 cm delamination specimen also show unhealed regions at the edge of the delamination. However, the middle regions seem to be fully healed in these specimens.

When comparing the WCU and ACU scans, it can be observed that the WCU scans clearly reveal the primary orientation of the carbon fibre fabric that is used whereas this hidden feature is less obvious in the ACU scans, which is a logical effect of the substantially lower frequency of the ACU scans (200 kHz vs 5 MHz). More interestingly, the ACU scans show a couple of darker regions within the healed areas which are not readily observed in the WCU scans. These regions indicate that the amplitudes of the transmitted waves through the healed areas are larger than those transmitted through the pristine areas. The higher transmission indicates additional acoustic matching in those areas which apparently caused by variation of local thickness of the ionomer layer and/or acoustic impedance of the healed interface. This implies that the nature of the healed region is somewhat different from that of the pristine regions.

In order to obtain further information on the healing mechanism of these delaminations, the specimens were monitored at intermediate steps during the entire healing process using WCU (soft-soft delaminations) and ACU/LDR (rigid-soft) delaminations. As an example, the healing of the 5 cm soft-soft delamination and of the 5cm rigid-soft delamination is shown in Figure 6.6 and Figure 6.7 respectively.

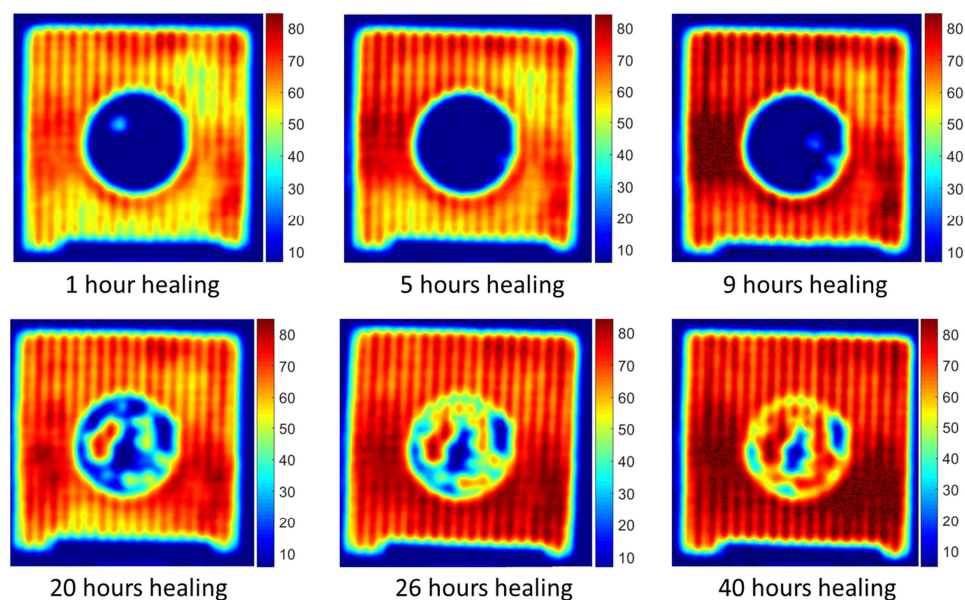


Figure 6.6 Healing of the 5cm soft-soft delaminated CFRP-ionomer laminate over time, monitored with WCU transmission C-scan. Healing is performed at 100°C. Accumulated healing time is indicated below each image. Colour scales indicate level of WCU transmission.

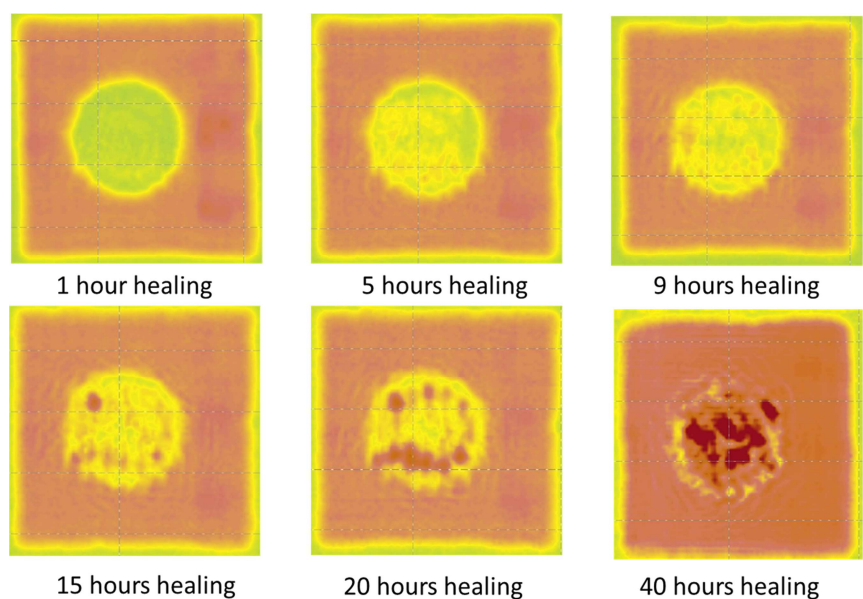


Figure 6.7 Healing of the 5cm rigid-soft delaminated CFRP-ionomer laminate over time, monitored with ACU scanning. Healing is performed at 100°C. Accumulated healing time is indicated below each image.

Figure 6.6 and Figure 6.7 show that the healing in the soft-soft and rigid-soft specimens becomes visible after 9 and 5 hours respectively. However, these relatively long onset times are mainly attributed to the fact that in the initial stages of the experiment, the specimen has more frequently been scanned and therefore removed from the oven. For this reason, it can be expected that in a continuous healing scan the onset of perceptible healing would occur at an earlier stage. Furthermore, it is observed that the healing process within the delamination starts from small nucleation points which then grow into bigger regions that ultimately merge together into the healed areas presented in Figure 6.4. Similar nucleation and growth events were also observed for all other delamination types covered in this study.

In Figure 6.8 we plot the normalised delaminated area as a function of the accumulated healing time at 100°C for both the 5 cm and the 2 cm diameter initial delaminations for the soft-soft composites, as determined by the WCU transmission C-scanning. To quantify the healing, after each healing step, the total area in the delaminated zone was determined for which the transmission amplitude was larger than 60% (relative to the intact region). The figure shows that there is a certain minimal healing time before the healing becomes detectable and that this minimal time is longer for the larger diameter delamination. Furthermore, the figure shows that in both cases the healing at the longest annealing times has not led to complete disappearance of the delamination as some ultrasonic scattering centres remain at the delamination site. It should be pointed that, given the manner in which the delaminations were introduced, these scattering centres are unlikely to be due to filament fracture but rather correspond to remaining imperfections at the healed interfaces.

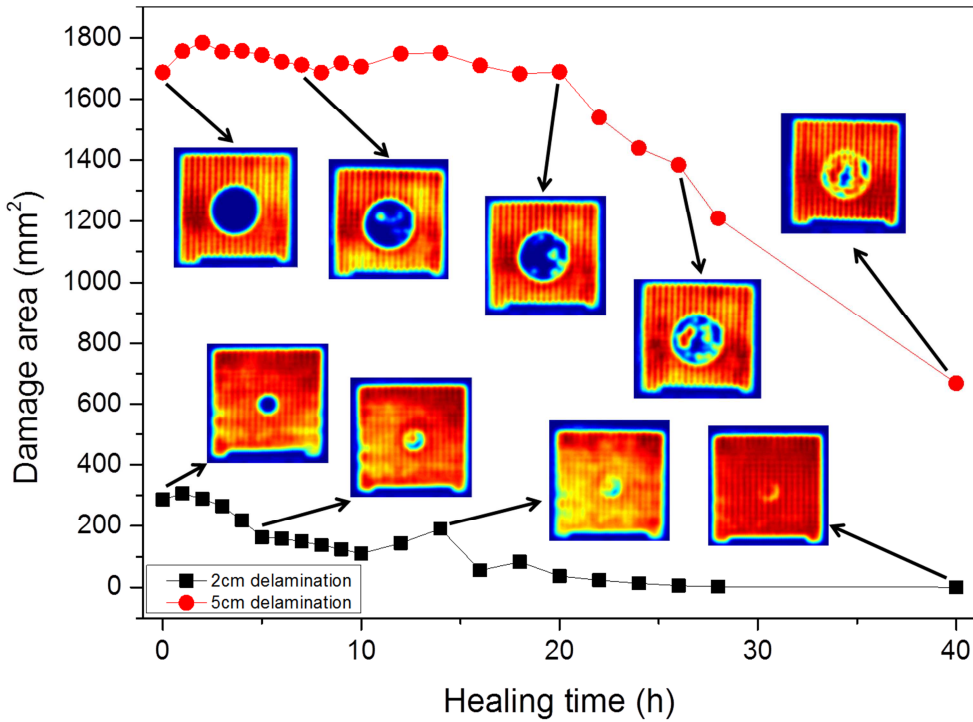


Figure 6.8 Delaminated area as function of the accumulated healing time at 100°C for both the 5 cm and the 2 cm diameter initial delaminations for the soft-soft composites, as determined by WCU.

6.3.2.2. Local defect resonance scanning

Figure 6.9 shows the evolution of the local defect resonance (LDR) of a composite with a 5 cm delamination induced at the rigid-soft interface during several stages of the healing treatment. Clearly, both the frequency response and the amplitude of the LDR signal change as healing progresses.

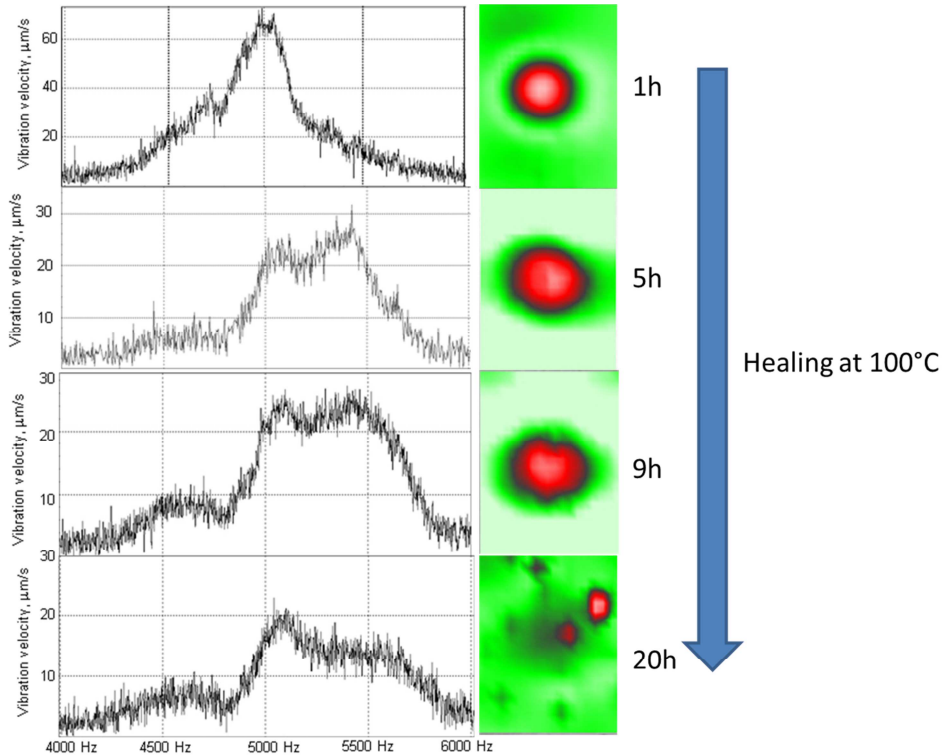


Figure 6.9 Evolution of the LDR response of a CFRP-ionomer composite with a 5cm delaminations induced in the rigid-soft interface over a 20 hour healing treatment at 100°C.

Figure 6.9 shows that the centre of the delamination frequency response shifts to the higher values as a function of healing time. This frequency variation is plotted in Figure 6.10 and exhibits a dramatic shift in the first few hours of the heating. The data in this figure enable to clarify the structure of the delamination resonance and some features of the healing process. The LDR frequency value for circular delaminations (and the defects like flat-bottomed holes (FBH)) is described by the following formula [31]:

$$f_0 \approx \frac{1.6h}{R^2} \sqrt{\frac{E}{12\rho(1-\nu^2)}} \quad (6.1)$$

where h is the thickness of the vibrating component in the composite and R is the radius of the defect. For an isotropic CFRP fabric, an in-plane Young's modulus E of 60 GPa, a material density ρ of $6 \cdot 10^3 \text{ kg/m}^3$ and a Poisson's ratio ν of 0.1 can be estimated. By using $h = 1 \text{ mm}$ for the CFRP layer and $R = 2.5 \text{ cm}$ for the delaminated area in the above relation a f_0 of approximately 4500 Hz is obtained for the unhealed situation which is in very close agreement with the measurement in

Figure 6.10, even though the properties of the tested laminates are not fully isotropic. The agreement indicates that the LDR signal is due to resonant vibrations of the unloaded (delaminated) part of upper CFRP layer in the rigid-soft configuration (Figure 6.1).

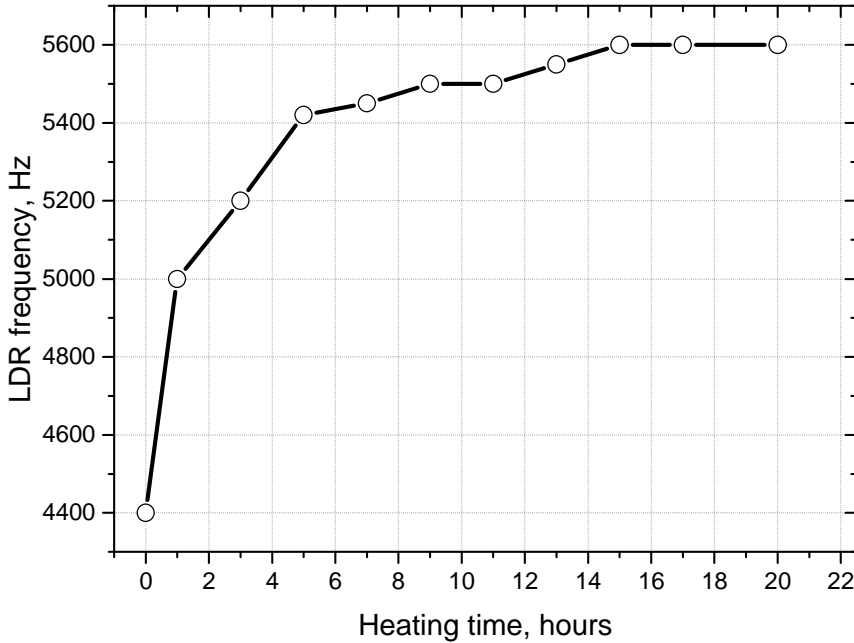


Figure 6.10 Evolution of the LDR frequency of the 5cm rigid-soft delaminated specimen as function of the healing time

Another feature seen in the plots of Figure 6.9 is related to the decrease in amplitude and widening of the LDR response. This is an indication of the increase in damping of the resonant vibrations in the delamination area. Like in the case of a classical resonance, the quality factor Q of LDR is reciprocal to the energy loss of vibrations. An obvious decrease in Q on the course of self-healing in Figure 6.9 delivers the information on the reduced delaminated area and the through thickness gap closure at the delamination interface which must clearly cause the observed increase in vibration damping.

Despite the fact that the determination of LDR characteristics seems to be a good approach for quantification of the healing of the soft-rigid delamination, it appeared that no distinctive resonant behaviour could be detected for soft-soft delaminated specimens. The absence of a LDR response for these specimens follows from the mechanism of the delamination resonance clarified above: the internal surface of the CFRP layer which used to vibrate freely (like in a FBH) and resonate for the

rigid-soft interface is clamped by an ionomer layer that prevents development of LDR in soft-soft interface.

6.3.3. Destructive characterization by compression testing

Compression test experiments were performed on pristine, delaminated and healed specimen (see section 2.2) to show the effect of damage and healing on the mechanical properties of the composites. As an example of the typical outcome of these tests, the resulting compression test curves for the soft-soft 5 cm delaminated specimen are shown in Figure 6.11. In this particular case, the healed sample had received an un-interrupted healing treatment at 100°C up to 40 hours.

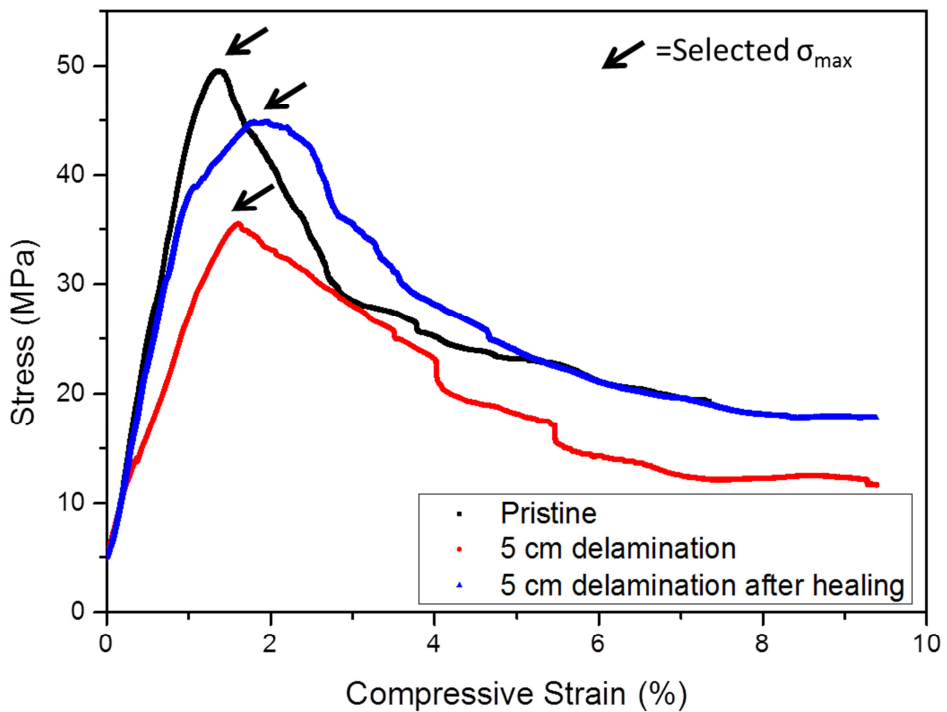


Figure 6.11 Compression test curves for the 5 cm soft-soft CFRP-ionomer composite. Partial restoration of the compressive strength is shown after 40 hours of healing.

From Figure 6.11, it is clear that the introduction of a delamination within the thermoplastic layer leads to a definite lowering of the compressive strength. After healing, an increase in the ultimate compressive strength is observed although the value of the undamaged specimen is not fully recovered. Similar trends were observed for all other laminated composites, and their compressive strengths are listed in Table 6.1.

Table 6.1 Overview of the ultimate compressive strengths of delaminated and healed CFRP-ionomer laminates (40 hours of healing with intermittent stops)

| Initial delamination size | Ultimate Compressive Strength (MPa) | | | |
|---------------------------|-------------------------------------|---------------|-------------------|---------------|
| | <i>Soft-soft</i> | | <i>Rigid-soft</i> | |
| | <i>Non-healed</i> | <i>Healed</i> | <i>Non-healed</i> | <i>Healed</i> |
| 2cm | 48.0 | 47.2 | 42.2 | 45.5 |
| 5cm | 35.5 | 44.8 | 41.1 | 47.1 |

6.4. Discussion

While the healing of damage (cracks and delaminations) in bulk ionomer samples [13, 15, 33] and particulate composites with ionomers as the matrix polymer [16, 17, 34] has been reported extensively in the literature, the current observations show for the first time the healing of delamination damage in CFRP composites with ionomer as the thermoplastic interlayer. The reduction of the delamination sites has been monitored using three non-destructive inspection techniques and the post-healing compression experiments demonstrated that the reduction of the delamination zone was accompanied by an increase in the compression strength, i.e. by restoration of the local adhesion and hence the overall load bearing capability.

We will now look in more detail into the actual reduction of the delamination sites as a result of the intrinsic self-healing nature of the ionomer. In many self-healing polymer systems the so called ‘zipper mechanism’, in which a local healing event automatically creates the surface contact for the subsequent healing step, is found to be the key factor to facilitate healing [35-37]. It is reasonable to expect that such a mechanism, starting from the edges of the delaminations, also might hold for the closure of the artificial delaminations. Figure 6.6 and 6.7 show that the healing grows not only from the edges but also from any point of cross-interface contact created during the annealing. It is likely that an assumed discontinuous curvature in the ionomer layer as a result of the compression stress that is applied on the edges of the polymer film during the laminate production process, is responsible for the slower healing from the edges and the presence of a weak residual ‘rim’ in the ultrasonic images for the samples healed for the longest healing time is due to this effect. The discontinuous curvature of the ionomer at the edges of the delamination would also explain the observed incubation time for healing (Figure 6.8). If this explanation is valid, it may imply that ‘real’ delaminated surfaces (e.g. from low-velocity impact loading) would not suffer from this effect, and that such delaminations might follow the expected healing direction from the edges towards the middle. Another explanation for the incomplete healing as observed in Figures 6.5-6.10 might be related to the thermal method used to create the delamination

area leading to the presence of entrapped air in the zone of controlled non-fusion. As after production the delamination is surrounded by fully dense material and ionomers are almost impermeable to air, the contraction of the delamination would lead to 'bubbles of slightly compressed trapped air' which would prevent full healing as the opposing sites of such bubbles would never get in contact and hence such bubbles would never heal (certainly not in the case of healing in the absence of an external contact reinforcing pressure). An indirect indication for the role of trapped air in determining the final state after complete healing comes from an additional experiment that was performed on an 'open' soft-soft delamination for which the resulting WCU scan images are displayed in Figure 6.12.

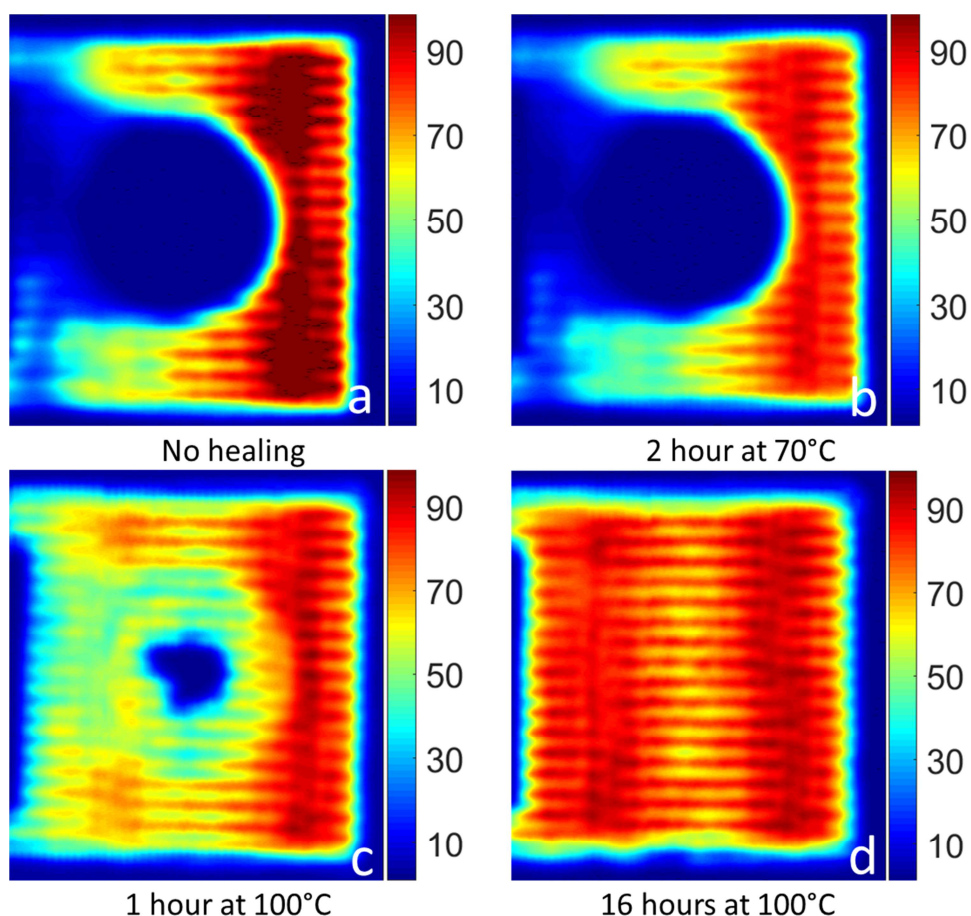


Figure 6.12 WCU scan of a soft-soft delamination that is open on one side. The specimen was scanned using WCU during different stages of the healing process. Color scale indicates the level of transmission.

The WCU scans initially show one open side of the delamination which is in contact with the surrounding environment (Figure 6.12a). Subfigure 6.12b supports the

thermomechanical conditions for effective healing discussed above and confirms the absence of healing after a treatment at 70°C, i.e. below the minimal healing temperature as defined from DSC and rheometry. More interestingly, Figure 6.12c shows very progressive healing after only 1 hour of healing at 100°C compared to the closed delamination in Figure 6.6. Additionally, the delamination seems to close from the edges towards the middle following the zipper mechanism, and the delamination appears to be fully closed after 16 hours of healing. Hence full interfacial healing might be obtainable for ionomer interlayers in CFRP composites under the right conditions.

While the three ultrasonic techniques (ACU, WCU and LDR) give more or less the same type of information regarding the healing of the delaminations there are also some interesting differences. The plot of the LDR frequency during healing clearly demonstrates the growth of multiple zones within the delaminated zone as the LDR spectrum changes from a single frequency peak to a wider spectral frequency response as is shown in Figure 6.9. However, the LDR analysis does not provide the all-inclusive information on the shape of the delamination as the employed C-scanning techniques do. On the other hand, Figure 6.10 and 6.11 clearly show that both the drop of the vibration amplitude and the shift of the LDR frequency undergo the largest transition during the onset of the healing, as opposed to the C-scanning techniques in which the healing effect becomes most prominent at the end of the process as explained previously. Neither WCU nor ACU showed noticeable sensitivity to these nucleation points which implies that the LDR based non-destructive technique is capable of monitoring healing events at an earlier stage than the ultrasonic C-scanning techniques, provided the mechanical quality factor of at least on the damaged interfaces is high enough to be detected.

Finally, we like to demonstrate that the observed reduction of the delamination area as determined by ultrasound techniques is not because the delamination area has dropped below the resolution limit for ultrasound but indeed is accompanied by a recovery of the adhesion force and hence the mechanical strength as determined in in-plane compression tests. To this aim we plot in Figure 6.13 the compression strength (i.e. the maximum load in the compression test) against the delaminated area as determined by WCU. The plot contains data points for defect free composites, as-produced composites with small and large delaminations and composites healed for 40 hours at 100°C, i.e. fully or partially healed samples. The data plotted in Figure 6.13 clearly demonstrate that healing not only leads to a reduction in delaminated area but also to an increase in compression strength. Furthermore, within experimental uncertainty all data points seem to lie more or less on a single line connecting compression strength to delaminated area, i.e. there is not much difference between the strength of a pristine composite with an artificial as-produced delaminated area and that of a composite with a healed delamination

of the same area. The observed trend is in accordance with the well-known strength to delaminated area after impact relation [38-41]. Finally, the extrapolated strength for a fully healed delaminated sample corresponds to that of the perfect pristine sample, which indicated that the remaining interfacial imperfections as determined by the ultrasonic tests are relatively harmless from a mechanical point of view.

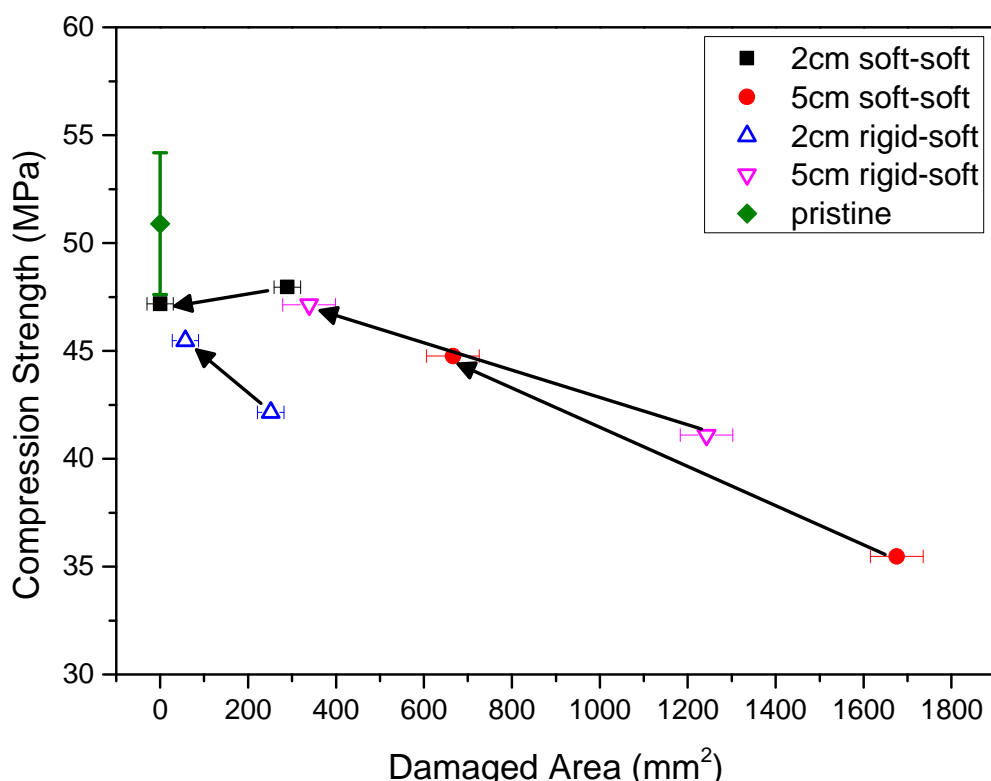


Figure 6.13 Relation between the compression strength and the delaminated area for the CFRP-ionomer composites tested. Results prior to thermal healing and after the full sequence of healing steps are shown for two different types of delaminations and two different initial sizes. Arrows indicate the effect of the thermal healing treatment (40 hours at 100°C, with intermittent stops). Error bars for delaminated area were estimated based on the error found in the WCU scans before the onset of healing.

6.5. Conclusion

The healing of artificial delaminations in CFRP composites with an ionomer interlayer is demonstrated by both air-coupled ultrasonic (ACU) and water-coupled ultrasonic (WCU) C-scan methods. Delaminations were introduced either within the ionomer layer (soft-soft interface) or at the CFRP-ionomer interface (rigid-soft interface). Both ACU and WCU show that healing starts from local nucleation points which then grow into larger zones of healed area. The ACU and WCU images were more informative at the final stages of the healing process. Using a Local Defect

Resonance (LDR) approach early stages of healing could also be detected and monitored. For the ACU and the WCU method, no differences were detected between the soft-soft and rigid-soft delaminations, whereas LDR analysis distinguished between rigid-soft delaminations (detectable) and soft-soft delaminations (undetectable). Finally, it was shown that for large delaminations, a quasi-linear relation was found between the delaminated area measured with C-scanning and the failure strength in compression for both pristine and partially healed samples. The communality in the correlation indicates that the contribution of the healed delamination to the compression strength equals that of the pristine interlayer.

References

1. Chung, D.D.L., *Composite Materials*. 2nd ed. Engineering Materials and Processes. 2010: Springer London.
2. Agarwal, B.D., Broutman, L.J., and Chandrashekhara, K., *Analysis And Performance Of Fiber Composites*. Third Edition ed. 2006: John Wiley & Sons.
3. Agrawal, S., Singh, K.K., and Sarkar, P.K., *Impact damage on fibre-reinforced polymer matrix composite - A review*. Journal of Composite Materials, 2014. 48(3): p. 317-332.
4. Norris, C.J., Bond, I.P., and Trask, R.S., *The role of embedded bioinspired vasculature on damage formation in self-healing carbon fibre reinforced composites*. Composites Part A: Applied Science and Manufacturing, 2011. 42(6): p. 639-648.
5. Hojo, M., Matsuda, S., Tanaka, M., Ochiai, S., and Murakami, A., *Mode I delamination fatigue properties of interlayer-toughened CF/epoxy laminates*. Composites Science and Technology, 2006. 66(5): p. 665-675.
6. Greenhalgh, E. and Hiley, M., *The assessment of novel materials and processes for the impact tolerant design of stiffened composite aerospace structures*. Composites Part A: Applied Science and Manufacturing, 2003. 34(2): p. 151-161.
7. Yasaee, M., Killock, C., Hartley, J., and Bond, I.P., *Control of Compressive Fatigue Delamination Propagation of Impact Damaged Composites Using Discrete Thermoplastic Interleaves*. Applied Composite Materials, 2015. 22(5): p. 559-572.
8. White, S.R., Moore, J.S., Sottos, N.R., Krull, B.P., Santa Cruz, W.A., and Gergely, R.C.R., *Restoration of large damage volumes in polymers*. Science, 2014. 344(6184): p. 620-623.
9. Luterbacher, R., Trask, R.S., and Bond, I.P., *Static and fatigue tensile properties of cross-ply laminates containing vasculs for self-healing applications*. Smart Materials and Structures, 2015. 25(1): p. 015003.

10. Toohey, K.S., Hansen, C.J., Lewis, J.A., White, S.R., and Sottos, N.R., *Delivery of two-part self-healing chemistry via microvascular networks*. Advanced Functional Materials, 2009. 19(9): p. 1399-1405.
11. Zhong, N. and Post, W., *Self-repair of structural and functional composites with intrinsically self-healing polymer matrices: A review*. Composites Part A: Applied Science and Manufacturing, 2015. 69: p. 226-239.
12. García, S.J., *Effect of polymer architecture on the intrinsic self-healing character of polymers*. European Polymer Journal, 2014. 53(0): p. 118-125.
13. Kalista, S.J., Pflug, J.R., and Varley, R.J., *Effect of ionic content on ballistic self-healing in EMAA copolymers and ionomers*. Polymer Chemistry, 2013. 4(18): p. 4910-4926.
14. Varley, R.J., Shen, S., and van der Zwaag, S., *The effect of cluster plasticisation on the self healing behaviour of ionomers*. Polymer, 2010. 51(3): p. 679-686.
15. Vega, J.M., Grande, A.M., van der Zwaag, S., and García, S.J., *On the role of free carboxylic groups and cluster conformation on the surface scratch healing behaviour of ionomers*. European Polymer Journal, 2014. 57(0): p. 121-126.
16. James, N.K., Lafont, U., van der Zwaag, S., and Groen, W.A., *Piezoelectric and mechanical properties of fatigue resistant, self healing PZT-ionomer composites*. Smart Materials and Structures, 2014. 23(5): p. 055001
17. Post, W., Bose, R., García, S., and van der Zwaag, S., *Healing of Early Stage Fatigue Damage in Ionomer/Fe₃O₄ Nanoparticle Composites*. Polymers, 2016. 8(12): p. 436.
18. Wang, C.H., Sidhu, K., Yang, T., Zhang, J., and Shanks, R., *Interlayer self-healing and toughening of carbon fibre/epoxy composites using copolymer films*. Composites Part A: Applied Science and Manufacturing, 2012. 43(3): p. 512-518.
19. Prajer, M., Wu, X., García, S.J., and van der Zwaag, S., *Direct and indirect observation of multiple local healing events in successively loaded fibre reinforced polymer model composites using healing agent-filled compartmented fibres*. Composites Science and Technology, 2015. 106: p. 127-133.
20. Norris, C.J., Meadway, G.J., O'Sullivan, M.J., Bond, I.P., and Trask, R.S., *Self-healing fibre reinforced composites via a bioinspired vasculature*. Advanced Functional Materials, 2011. 21(19): p. 3624-3633.
21. Tabaković, A., Post, W., Cantero, D., Copuroglu, O., Garcia, S.J., and Schlangen, E., *The reinforcement and healing of asphalt mastic mixtures by rejuvenator encapsulation in alginate compartmented fibres*. Smart Materials and Structures, 2016. 25(8).
22. Van Stappen, J., Bultreys, T., Gilabert, F.A., Hillewaere, X.K.D., Gómez, D.G., Van Tittelboom, K., Dhaene, J., De Belie, N., Van Paepegem, W., Du Prez, F.E., and Cnudde, V., *The microstructure of capsule containing self-healing materials: A micro-computed tomography study*. Materials Characterization, 2016. 119: p. 99-109.

23. Bekas, D.G., Baltzis, D., Tsirka, K., Exarchos, D., Matikas, T., Meristoudi, A., Pispas, S., and Paipetis, A.S., *Self-healing polymers: Evaluation of self-healing process via non-destructive techniques*. *Plastics, Rubber and Composites*, 2016. 45(4): p. 147-156.
24. Pang, J.W.C. and Bond, I.P., *A hollow fibre reinforced polymer composite encompassing self-healing and enhanced damage visibility*. *Composites Science and Technology*, 2005. 65(11-12): p. 1791-1799.
25. Kersemans, M., De Baere, I., Degrieck, J., Van Den Abeele, K., Pyl, L., Zastavnik, F., Sol, H., and Van Paepegem, W., *Nondestructive damage assessment in fiber reinforced composites with the pulsed ultrasonic polar scan*. *Polymer Testing*, 2014. 34: p. 85-96.
26. Kersemans, M., De Baere, I., Degrieck, J., Van Den Abeele, K., Pyl, L., Zastavnik, F., Sol, H., and Van Paepegem, W., *Damage Signature of Fatigued Fabric Reinforced Plastics in the Pulsed Ultrasonic Polar Scan*. *Experimental Mechanics*, 2014. 54(8): p. 1467-1477.
27. Solodov, I., Pfeleiderer, K., Gerhard, H., Predak, S., and Busse, G., *New opportunities for NDE with air-coupled ultrasound*. *NDT and E International*, 2006. 39(3): p. 176-183.
28. Solodov, I.Y., Stoessel, R., and Busse, G., *Material characterization and NDE using focused slanted transmission mode of air-coupled ultrasound*. *Research in Nondestructive Evaluation*, 2004. 15(2): p. 65-85.
29. Neuenschwander, J., Furrer, R., and Roemmeler, A., *Application of air-coupled ultrasonics for the characterization of polymer and polymer-matrix composite samples*. *Polymer Testing*, 2016. 56: p. 379-386.
30. Solodov, I., *Resonant acoustic nonlinearity of defects for highly-efficient nonlinear NDE*. *Journal of Nondestructive Evaluation*, 2014. 33(2): p. 252-262.
31. Solodov, I., Bai, J., Bekgulyan, S., and Busse, G., *A local defect resonance to enhance acoustic wave-defect interaction in ultrasonic nondestructive evaluation*. *Applied Physics Letters*, 2011. 99(21).
32. Bose, R.K., Hohlbein, N., García, S.J., Schmidt, A.M., and van der Zwaag, S., *Connecting supramolecular bond lifetime and network mobility for scratch healing in poly(butyl acrylate) ionomers containing sodium, zinc and cobalt*. *Physical Chemistry Chemical Physics*, 2015. 17(3): p. 1697-1704.
33. Varley, R.J. and van der Zwaag, S., *Towards an understanding of thermally activated self-healing of an ionomer system during ballistic penetration*. *Acta Materialia*, 2008. 56(19): p. 5737-5750.
34. Hohlbein, N., Shaaban, A., and Schmidt, A.M., *Remote-controlled activation of self-healing behavior in magneto-responsive ionomeric composites*. *Polymer (United Kingdom)*, 2015. 69: p. 301-309.
35. Dong, J., Ding, J., Weng, J., and Dai, L., *Graphene enhances the shape memory of poly (acrylamide-co-acrylic acid) grafted on graphene*. *Macromolecular Rapid Communications*, 2013. 34(8): p. 659-664.
36. Zhang, Z., Hu, Y., Liu, Z., and Guo, T., *Synthesis and evaluation of a moisture-promoted healing copolymer*. *Polymer*, 2012. 53(14): p. 2979-2990.

37. Rodriguez, E.D., Luo, X., and Mather, P.T., *Linear/network poly(ϵ -caprolactone) blends exhibiting shape memory assisted self-healing (SMASH)*. ACS Applied Materials and Interfaces, 2011. 3(2): p. 152-161.
38. Kumar, R.L.V., Jawali, N.D., Srikanth, L., Kumar, C.R., Prakash, M.R., and Rao, R.M.V.G.K., *Post Impact Compression Strength (PICS) Evaluation of Glass/Epoxy Composite Using a Novel Approach — Effect of Delamination Area*. Journal of Reinforced Plastics and Composites, 2007. 26(11): p. 1101-1109.
39. Tan, K.T., Watanabe, N., Iwahori, Y., and Ishikawa, T., *Effect of stitch density and stitch thread thickness on compression after impact strength and response of stitched composites*. Composites Science and Technology, 2012. 72(5): p. 587-598.
40. Wu, K.-W., Lee, C.-L., Chang, Y.-C., and Ong, C.-L., *Compressive strength of delaminated and repaired composite plates*. Materials Chemistry and Physics, 1996. 43(2): p. 173-177.
41. Zhou, G., *Effect of impact damage on residual compressive strength of glass-fibre reinforced polyester (GFRP) laminates*. Composite Structures, 1996. 35(2): p. 171-181.

Supplementary Information

S1: Thermogravimetric analysis of laminate components

Thermogravimetric analysis was performed to investigate the thermal stability of the composite components using a TG/DTA-7 Pyris Diamond (PerkinElmer). Figure S 6.1a shows a temperature ramp of 10°C/min for the ionomer-CFRP laminate components. From this figure it is clear that all laminate components have a degradation temperature (2% weight loss) well above 300°C thereby indicating the thermal stability at the applied healing temperature (100°C). To add to this statement, Figure S 6.1b shows an isothermal treatment of the CFRP laminate at 100°C for 60 hours without any measurable thermal degradation. In addition, differential scanning calorimetry (DSC) was performed using a Perkin–Elmer Sapphire differential DSC. Samples were heated and cooled between -50°C and 200°C at a rate of 10°C/min under a nitrogen atmosphere. Figure S 6.2 shows the two thermograms of the CFRP interlayer before and after a thermal treatment of 60 hours at 100°C. No distinct differences that could indicate any form of thermal degradation were observed in these thermograms.

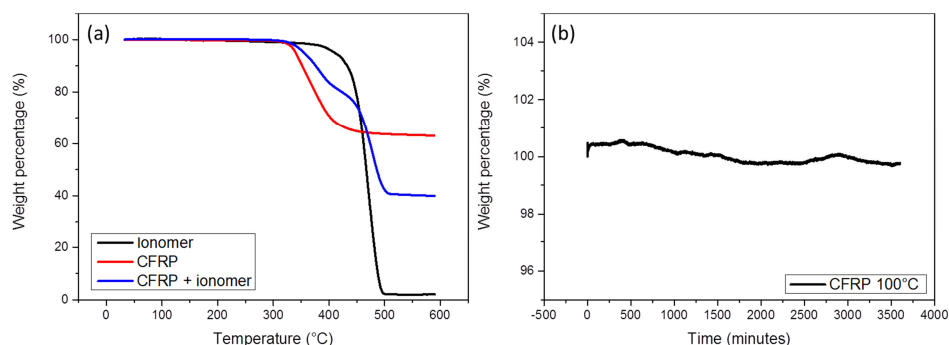


Figure S 6.1 TGA temperature ramp of the individual components of the CFRP-ionomer composite (a) and the residual weight of the CFRP during an isothermal treatment of 100°C.

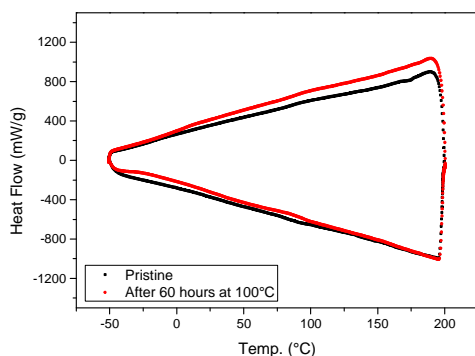


Figure S 6.2 DSC thermogram of the CFRP laminate layer before and after a thermal treatment of 60 hours at 100°C.

S2: WCU reflection scans

Figure S 6.3 shows the healing of both rigid-soft and soft-soft delaminations with an initial radius of 5cm visualized by WCU reflections scans.

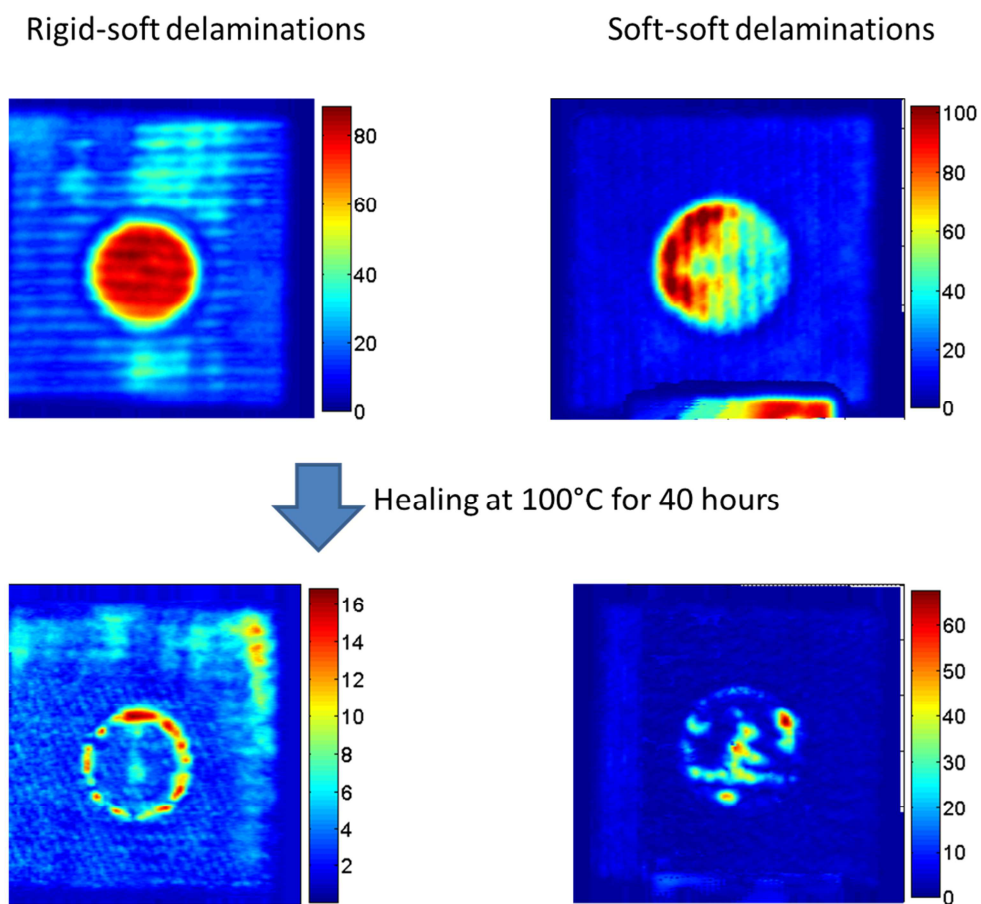


Figure S 6.3 Overview of the WCU-scan reflection amplitude images for laminates with rigid-soft and soft-soft delaminations with an initial radius of 5 cm). The top images clearly visualize the circular unhealed delaminations whereas the bottom images correspond to the scan results for the same specimen after a healing treatment at 100°C for more than 40 hours. Colour scales indicate level of WCU reflection.

S3: Healing efficiencies

The healing efficiency for the ultimate tensile strength (UTS) was determined by comparing the healed strength values to those of the largest damaged site measured (in this case the 5 cm soft-soft specimen) by:

$$UTS\ efficiency = \frac{\sigma_{healed} - \sigma_{largest\ damage}}{\sigma_{pristine} - \sigma_{largest\ damage}} \quad (S6.1)$$

The NDT healing efficiency of the area (A) measured by water coupled ultrasound (WCU) C-scanning measurement was calculated by:

$$NDT\ efficiency = 1 - \frac{A_{healed}}{A_{damaged}} \quad (S6.2)$$

The UTS and NDT healing efficiencies are plotted versus each other for the four specimen investigated in this study in Figure S 6.4

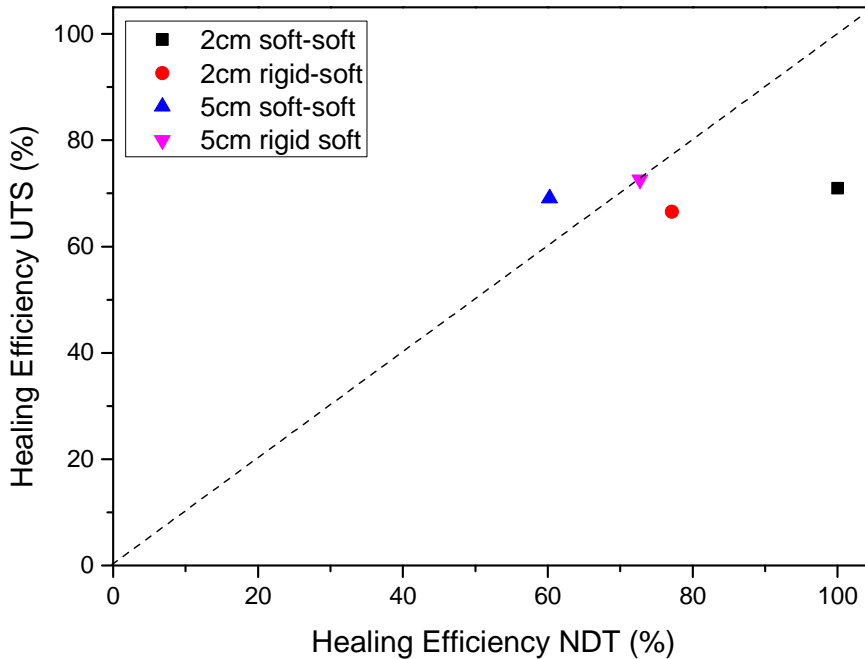


Figure S 6.4 Calculated healing efficiency of the ultimate tensile strength vs. the healing efficiency determined by non-destructive WCU testing.

Summary

Self-healing polymer composites

Over the past decade, many different strategies were developed to introduce self-healing properties in structural polymer composite materials. Although many of the investigated routes show promising results on an academic scale, the first commercially feasible self-healing structural polymer composite has yet to be developed. The main objective of this thesis is to contribute to the gap closure between the academic concept of structural self-healing composites and its fully implemented industrial applications. As such, each chapter targeted one of the existing scientific issues, within some of the most promising healing strategies available, that are currently preventing the industrial acceptance of self-healing polymer composites.

Chapter 2 shows the feasibility of compartmented fibres as healing agent carriers for the autonomous extrinsic healing of glass fibre reinforced polymer (GFRP) composites. The compartmented fibre concept is considered to be a potential solution for distribution issues that arise in microcapsule- and continuous network based extrinsic healing concepts. The concept had yet to be demonstrated for healing of thermoset polymer matrices. Aim of the work was to reduce the mismatch in mechanical response of the alginate fibres and the fibre reinforced polymer composites and to show that the concept can be employed to partially heal GFRP composites. First, the effect of montmorillonite (MMT) clay on the fibre tensile and vacuole lateral compression properties is reported. It is found that the fibre tensile properties are enhanced with increasing MMT concentration, while the effects on the vacuole lateral compression properties were seemingly negligible. Second, the proof of concept of healing by compartmented fibres in GFRP composites is shown. A single- and a double healing agent configuration, both based on epoxy-thiol chemistry, are compared in these model GFRP composites. The healing phenomena are quantified by mechanical characterization (interlaminar fracture and flexural testing) and non-destructive testing techniques (x-ray micro-tomography and air-coupled ultrasonic C-scanning). It is found that a configuration with one healing agent performs better than a system with two separate agents and that further exploitation of the compartmented fibre concept should focus on the healing of

matrix damage as the loss of mechanical integrity due to glass fibre fracture cannot be overcome.

Chapter 3 gives an overview of the different approaches for intrinsic healing in structural and functional polymer composites that have been reported in the literature in recent years. Firstly, the effect and potential of various healing stimuli (i.e. thermal, photochemical, electrical and moisture triggered healing) are discussed. Secondly, both structural properties (i.e. stiffness and strength) and functional properties (i.e. electrical conductive, electromagnetic, thermomechanical, magnetic and thermal conductive functionality) of particle- and fibre reinforced polymer composite materials are analysed. Finally, the potential of healing structural and functional properties within these polymer composites is evaluated. As such, it is concluded that in the case of both classes of polymer matrix composites, very often mechanical damage in the polymer matrix or debonding at the matrix-filler interface is responsible for the decrease in intended properties. Furthermore, it is derived that the crucial factors for successful self-repair are similar for both structural and functional polymer composites. This realization can ultimately lead to the design of polymer composites that autonomously restore multiple properties using the same intrinsic self-healing mechanism.

A general trend for thermo-reversible intrinsic healing polymer matrices is that upon improving the polymer stiffness, the required minimum healing temperature increases to temperatures well above room temperature. As such, *Chapter 4* focusses on the challenge to develop a thermoset matrix polymer that possesses both good mechanical properties and a moderate healing temperature. The development of a novel intrinsic healing GFRP composite based on a disulphide-containing organic-inorganic thermoset matrix is reported. Thermomechanical experiments show that the newly developed matrix has a currently unchallenged combination of a decent Young's modulus (800-1200 MPa) and the ability for multiple healing at moderate temperatures (70-85°C). On top of that, the developed resin can be used for the processing of GFRP composites by conventional vacuum infusion. The mechanical properties and the extent of healing are determined by flexural, fracture and low-velocity impact testing. Small sized (<cm²) damage could be partially healed multiple times using a minimal healing pressure to ensure a good alignment of the damaged interfaces. The level of healing could be enhanced, even for large (>cm²) damage, by increasing the healing pressure provided the location of the primary damage is concentrated within the matrix phase. The polymer matrix composite introduced here represents a significant step forward from the often mechanically inferior intrinsically self-healing composites towards structural self-healing composites.

Chapter 5 investigated the recovery of mechanical properties after fatigue in intrinsically self-healing polymers. While the majority of studies on self-healing polymer composites focus on the healing of damage after manual cutting or static overloading, it is important for industrial acceptance of intrinsic healing polymers to understand the polymer response under dynamic fatigue loading. Therefore, this chapter reports on the healing of early stage fatigue damage in ionomer/nanoparticulate composites. A series of poly(ethylene-co-methacrylic acid) zinc ionomer/ Fe_3O_4 nanoparticle composites with varying amounts of ionic clusters is developed and subjected to different levels of fatigue loading. The initiated damage is healed via localized inductive heating of the embedded nanoparticles by exposure to an alternating magnetic field. It is demonstrated that healing of early stage damage in ionomer particulate composites occurs in two different steps. First, the deformation is restored by the free-shrinkage of the polymer at temperatures below the melt temperature. At such temperatures, the polymer network is recovered; thereby resetting the fatigue induced strain hardening. Then, at temperatures above the melting point of the polymer phase, fatigue-induced microcracks are sealed, hereby preventing crack propagation upon further loading. It is shown that the thermally induced free-shrinkage of these polymers does not depend on the presence of ionic clusters, but that the ability to heal cracks by localized melting is reserved for ionomers that contain a sufficient amount of ionic clusters guaranteeing an acceptable level of mechanical stability during healing.

Within the field of self-healing polymer composites (and within this thesis) destructive testing is the most conventional approach to quantify healing behaviour. However, for the acceptance of self-healing structural composites for real life applications, it is crucial that the effects of healing can be identified by non-destructive testing techniques. *Chapter 6* reports on a comparative study on monitoring of delamination healing in carbon fibre reinforced polymer (CFRP) - ionomer sandwich composites by non-destructive techniques and destructive compression testing. Artificial delaminations of various areal dimensions and nature are introduced during production of the composites. The extent of the delamination and the healing thereof is monitored in both air and water-coupled ultrasonic C-scan experiments as well as by the frequency shift of the local defect resonance (LDR). It is shown that the LDR approach can be used to detect the early stage healing of the delaminations while ultrasonic C-scanning techniques are very effective to determine the extent of healing in the final stages of the repair process. A quasi-linear relation is observed between the delaminated area measured with ultrasonic C-scan and the compressive failure strength in destructive testing. Hence, on demand local heating of delaminated thermoplastic interlayers can really recover the properties of technical quality CFRP composites, provided the damage is located within the interlayer or at the CFRP-ionomer interface.

Samenvatting

Zelfherstellende polymeer composieten

Gedurende de afgelopen decennia zijn diverse strategieën ontwikkeld om zelfherstellende eigenschappen te introduceren in vezelversterkte polymeer matrix composieten voor constructieve toepassingen. Ondanks dat veel van de onderzochte technologieën veelbelovend lijken vanuit academisch oogpunt, moet het eerste commerciële zelfherstellende composiet nog op de markt verschijnen. De voornaamste reden hiervoor is dat men er tot op heden nog niet in geslaagd is om zelfherstellende eigenschappen én hoogwaardige mechanische eigenschappen in één composiet materiaal te verenigen. Het onderzoek zoals beschreven in dit proefschrift had als doel om het gat tussen het academisch concept en de industriële realisatie van zelfherstellende vezelversterkte composieten te verkleinen. Elk hoofdstuk richt zich zodoende op één van de afzonderlijke uitdagingen die er nu nog voor zorgen dat industriële toepassing van zelfherstellende composieten nog geen werkelijkheid is.

Hoofdstuk 2 beschrijft de haalbaarheid van het gebruik van gecompartmenteerde vezels gevuld met reactieve vloeibare 'healing agents' voor het autonome en extrinsieke zelfherstel van glasvezelversterkte polymeer composieten. Het gecompartmenteerde vezel concept biedt een mogelijke oplossing voor de vloeistof distributieproblemen die zich voordoen in de langer bestaande concepten op basis van microcapsules en continue vezelnetwerken. Tot op heden is de succesvolle werking van het concept nog niet aangetoond voor thermoharder polymeermatrixen. In dit hoofdstuk beschrijven we twee relevante deelonderzoeken. Het eerste komt voort uit het feit dat de mechanische eigenschappen van de gecompartmenteerde alginaatvezels en die van composieten te zeer van elkaar verschillen. Er is daarom gekeken naar het verstevigende effect van montmorilloniet (MMT) klei op de mechanische eigenschappen van de alginaatvezels. Het blijkt dat de treksterkte van de vezels verbetert naarmate er meer MMT wordt toegevoegd, terwijl het effect op de laterale compressie-eigenschappen van de vacuolen verwaarloosbaar is. Het tweede doel van dit hoofdstuk is om aan te tonen dat gecompartmenteerde vezels daadwerkelijk gebruikt kunnen worden om glasvezel epoxy composieten te herstellen. Daartoe zijn enkelvoudige en tweevoudige configuraties onderzocht. Het herstelmechanisme is in beide gevallen gebaseerd op

epoxy-thiol chemie. Het herstelgedrag van de composieten is bepaald via mechanische testen (interlaminaire breuk- en buigproeven) en niet-destructieve testmethoden (röntgen-microtomografie en ultrasone C-scans). Vastgesteld is dat een configuratie met een enkele vloeibare reactant beter werkt dan een configuratie met twee verschillende reactanten. We stellen vast dat verder onderzoek naar gecompartmenteerde vezels voor het zelfherstel in composieten gericht moet worden op het repareren van microschade in de polymeer matrix, gezien het verlies in mechanische eigenschappen door glasvezelbreuk via deze weg niet gecompenseerd kan worden.

In *Hoofdstuk 3* wordt een overzicht gegeven van de in de literatuur bekende methodes om intrinsiek zelfherstellend vermogen te introduceren in composieten voor functionele en constructieve toepassingen. Eerst worden de meest gangbare stimuli om het herstelproces in gang te zetten (i.e. warmte, licht, elektriciteit en vocht) voor intrinsiek zelfherstellende polymeren omschreven. Daarna worden zowel de diverse eigenschappen (sterkte en stijfheid, maar ook elektrische geleidbaarheid, elektromagnetisch, thermo-mechanisch en, magnetisch gedrag en thermische geleiding) die van belang zijn voor polymeer composieten beschreven. Tot slot worden de mechanismen besproken die vereist zijn om elk van de afzonderlijke polymeer eigenschappen te laten herstellen. De conclusie van het hoofdstuk is dat het verlies van zowel structurele als functionele eigenschappen voornamelijk veroorzaakt wordt door mechanische schade in de matrix of aan het matrix-vulmateriaal grensvlak. Daarnaast is er afgeleid dat de cruciale factoren die verantwoordelijk zijn voor succesvol herstel van het materiaal gelijk zijn voor beide typen polymeer composieten. Dit besef kan uiteindelijk leiden tot polymeer composieten die meerdere structurele en functionele eigenschappen kunnen herstellen middels hetzelfde intrinsieke herstelmechanisme.

De algemene trend in thermo-reversibele intrinsiek herstellende polymeren is dat dat een hogere stijfheid of mechanische sterkte meestal gepaard gaat met toename van de hersteltemperatuur tot waarden ver boven kamertemperatuur. *Hoofdstuk 4* richt zich dan ook op de uitdaging om een thermoharder matrix te ontwikkelen met hoogwaardige mechanische eigenschappen die zichzelf kan repareren bij relatieve lage temperaturen. Het hoofdstuk beschrijft de ontwikkeling van een nieuw zelfherstellend composiet met een disulfide bevattende organisch-anorganische matrix. Thermo-mechanische experimenten tonen aan dat het ontwikkelde matrixpolymeer een momenteel onovertroffen combinatie van een hoge stijfheid (een elasticiteitsmodulus van 800-1200 MPa) en een lage hersteltemperatuur (70-85°C) herbergt. Daarbovenop kan deze matrix gebruikt worden voor de productie van vezelversterkte composieten via de conventionele vacuüminfusie methode. De mechanische eigenschappen en de mate van zelfherstel van de geproduceerde composieten zijn vastgesteld middels buig-, interlaminaire breuk- en lage-snelheid

botsproeven. Op basis van de verkregen resultaten wordt geconcludeerd dat kleine schadeniveaus ($< \text{cm}^2$) meerdere keren gedeeltelijk hersteld kunnen worden door de beschadigde composieten licht te verhitten bij een minimale druk. De druk moet worden aangebracht om een goed contact tussen de beschadigde grensvlakken te waarborgen. Daarnaast laten de resultaten zien dat grotere schadeniveaus volledig hersteld kunnen worden wanneer de druk verhoogd wordt, mits de primaire schade zich concentreert in de matrixfase. Het hier gerapporteerde polymeer-matrix composiet is zodoende een grote stap voorwaarts in de ontwikkeling van technisch relevante zelfherstellende composieten voor constructieve toepassingen.

In *Hoofdstuk 5* wordt het herstel van de mechanische eigenschappen na vermoeiing van intrinsiek zelfherstellende polymeren omschreven. Voor de industriële acceptatie van zelfherstellende polymeren in constructieve toepassingen is het vaak belangrijker dat door vermoeiing geïnduceerde schade zich herstelt dan dat schade door eenmalige overbelasting quasi-spontaan verdwijnt. Het hoofdstuk beschrijft het herstel van de initiële vermoeiingsschade die ontstaat tijdens de vermoeiing van nanodeeltjes gevulde ionomeren. Om dit te bereiken, is een reeks poly(ethyleen-co-methacrylzuur) zink-ionomeer/ Fe_3O_4 nanocomposieten met verschillende hoeveelheden ionische clusters vervaardigd en blootgesteld aan verschillende niveaus van vermoeiing. De ontstane schade is vervolgens lokaal hersteld middels inductieverwarming door het aanbrengen van een altemnerend magnetisch veld. Er wordt aangetoond dat de vermoeiingsschade in deze composieten herstelt via een tweetraps proces. In de eerste fase, bij een temperatuur onder het smeltpunt van het ionomeer, wordt de polymeerdeformatie en de door vermoeiing geïnduceerde versteviging van het ionomeer ongedaan gemaakt door vrije-krimp en het herstel van het polymeer netwerk. Bij een temperatuur boven het smeltpunt van de polymeerfase worden ook de door vermoeiing ontstane microscheurtjes gedicht. Hierdoor wordt verdere scheurpropagatie en de vorming van macroscheuren voorkomen. Er is aangetoond dat thermisch geïnduceerde vrije-krimp in deze polymeren onafhankelijk is van de fractie ionische clusters. Daarentegen is de capaciteit om scheurtjes te dichten middels lokaal smeltgedrag voorbehouden aan ionomeren met een afdoende fractie ionische clusters aangezien deze er voor zorgen dat de mechanische integriteit van het composiet tijdens de herstelbehandeling gewaarborgd blijft.

De meest gangbare methode om het herstelgedrag van zelfherstellende composieten te kwantificeren is die van destructief testen. Dit geldt voor het gros van de gepubliceerde artikelen op het gebied van zelfherstellende composieten alsmede het werk dat in deze thesis wordt gerapporteerd. Echter, voordat zelfherstellende composieten daadwerkelijk kunnen worden toegepast is het van cruciaal belang dat de mate van zelfherstel bepaald kan worden door middel van non-destructieve testmethodes (NDTs). In *Hoofdstuk 6* worden verschillende NDTs

gebruikt om het herstel over tijd van delaminaties in koolstofvezel versterkte polymeer – ionomeer sandwichcomposieten te volgen. De verschillende NDTs worden zowel met elkaar alsmede met destructieve compressietesten vergeleken. Om dit te realiseren zijn er tijdens het productieproces kunstmatige delaminaties (met verschillende afmetingen en gelegen aan verschillende grensvlakken) in de composieten geïntroduceerd. Vervolgens wordt het herstelgedrag van deze delaminaties gevolgd door lucht- en water-gekoppelde ultrasone C-scans alsmede door de bepaling van de verschuiving van de lokale defect resonantiefrequenties (LDR). Er is aangetoond dat de LDR methode met name effectief is tijdens de initiële fases van het herstelproces, terwijl ultrasoon C-scannen meer informatie verschaft naarmate het herstel verder gevorderd is. Daarnaast is er aangetoond dat er een quasilineaire afhankelijkheid bestaat tussen het resterende delaminatieoppervlak en de 'in-plane' compressiesterkte. Dit toont aan dat het lokaal verwarmen van gedelamineerde thermoplastische tussenlagen daadwerkelijk kan leiden tot het herstel van mechanische eigenschappen in hoogwaardige composieten mits de ontstane schade zich bevindt in de tussenlaag of aan het grensvlak van de ionomere tussenlaag en de koolstof-composietlagen.

Acknowledgements

A PhD is often considered an individual achievement. However, within the past four years I had the pleasure of meeting and collaborating with many different people. Without them the work in this thesis would not have been possible.

I would like to start by thanking my promotor Sybrand van der Zwaag for giving me the opportunity to pursue my PhD degree within the Novel Aerospace Materials group. Your honest and critical feedback helped to bring the work to a higher level and to develop myself as a better researcher. I highly appreciate the fact that you were always approachable for questions regardless of the location and time zone you were currently in. Special thanks for the adequate and fast feedback during the final stages of the project.

I also owe a lot of gratitude to my daily supervisor Santiago García. Thank you for encouraging me to keep exploring new research routes and for your inexhaustible input of new creative ideas to increase the quality of my work. I really appreciate that your door was always open for questions and that you showed that you had a lot of faith in me during these four years. Besides the professional aspects, I also enjoyed the good times during the many Alamsa trips, conferences and other meetings.

I would like to thank Veronique Michaud for hosting me for three months in their group at EPFL. I really enjoyed the work in the group and the life in Switzerland. Amael, thank you for making my stay in Lausanne a great success from both a professional and a personal point of view. I highly appreciate the time you took to assist me in the lab and to show me around your beautiful country. Many thanks to all other LPAC colleagues for the good times, great memories and nice (but very expensive) beers.

During my PhD I had the pleasure of collaborating with many different researchers from all over Europe. I would like to thank Mathias Kersemans, Koen van den Abeele and Igor Solodov for the great collaboration and the many non-destructive tests on my composite materials. I would also like to acknowledge all the other consortium members within the Alamsa project for the fruitful discussions and the nice meetings. Thanks to Etienne Jeoffroy from ETH Zürich for the many hours spent on the vacuole compression tests.

In Delft I was also involved in various joint-projects. Nuria, 'muchas gracias' for the nice work we performed during your stay and for all the (very distinctive) laughs. Tommaso, 'grazie' for the many in-depth discussions and for not consuming all my time by always asking just 'one thing'. I would like to thank my MSc. student Petter for the great teamwork on his project and his attempts to push the self-healing concept to the next level.

Within the Delft Aerospace Structures and Materials laboratory there have been many people throughout the years that helped me with setting up and performing my experiments. A special thanks to Gertjan Mulder, who was open to every (on forehand) crazy experiment I wanted to perform and helped me on my quest to use every possible piece of equipment that is available in the aircraft hall. Furthermore I would like to thank Berthil, Misja, Bob, Fred, Bart, Victor, Frans, Cees and Johan for assisting me with my work. Also I would like to express my gratitude to Rob, Ed and Peter from the DEMO workshop for the fabrication of and assistance with various pieces of equipment, and the fibre spinning line in particular.

For the past four years, I had the honour to be part of a truly magnificent research group. The NovAM group is known, even outside the Netherlands, for its amazing people and I highly enjoyed working in such a high quality but also very social environment. First, I would like to thank Shanta for resolving all the administrative mess that the TU Delft tends to create. Arijana, Wouter, Daniella and Nan, it has been a pleasure to go through this PhD process together. As we all more or less started around the same time, we had the opportunity to share many experiences and help each other along the way and that really meant a lot to me. Special thanks to Ranjita, Hamideh and Michael for making our office the coolest office in the hallway (also literally). Furthermore I would like to thank Christian, Kevin, Michiel, Željka, Martino, Hussein, Paul, Vincenzo, Casper, Niels, Maruti, Srikanth, Nadine, Marianella, Renee, Marlies, Johan, Hongli, Jimmy, Hao, Mariana, Vincent, Taylor, Silvia, Clara and all the other NovAM colleagues and students for all the coffee breaks, cake baking and extensive Atmosfeer sessions.

During my time in Delft I had the pleasure to be part of two great hockey teams. Therefore I would really like to thank the guys of Scoop H2 and Rijswijk H3 for taking my mind off my thesis work during the many training sessions and Sunday matches and for the many nice moments outside the hockey field. The frequent reunions with my friends from Heeren Zeeven, Heren 5, Kwakkie, Villa Gammel en We Zijn Er Bijna! were always memorable and very helpful in realizing that my PhD is not all there is. Kjell, thanks for being there on all those occasions when I really needed a beer. Pui, thanks for putting a constant smile on my face during the last year of my PhD. Although it is often described as being the toughest and most

stressful year of the project, I think that meeting you was one of the main reasons that made it so that this was not the case for me.

Finally, I would like to thank my brother Erik, my sister Marleen, and my parents for all the support during the past four years and all the years before. I honestly don't know how I would have managed to finish this project without your constant patience, confidence, care, love and extra meatballs. Thanks for everything.

Curriculum Vitae

Wouter Post was born on the 22nd of December 1987 in Heemskerk. In 2006 He obtained his 'Gymnasium' degree at Het Zaanlands Lyceum in Zaandam. He started his academic career at the University of Twente where he obtained his BSc. degree in Chemical Engineering by the end of 2010. As part of the BSc. programme he performed his final assignment on the development of oxygen permeating perovskite materials at the University of Queensland in Brisbane, Australia.

After finishing the bachelor degree, he enrolled into the Molecules & Materials track of the Chemical Engineering MSc. programme at the University of Twente. He received his MSc. degree, cum laude, in June 2013. During the MSc. programme he performed an internship at Teijin Aramid BV on surface modification of aramid pulp. In June 2013, he graduated, cum laude, on the gas-liquid interfacial polymerization of hybrid thin films at the Inorganic Membranes research group within the Mesa+ Institute of the University of Twente.

In August 2013, he started his Ph.D. programme at Delft University of Technology on the development of self-healing polymer composites for structural applications within the Novel Aerospace Materials group where he was supervised by professor Sybrand van der Zwaag and dr. Santiago García. As a part of his Ph.D. programme he published multiple peer-reviewed papers and he obtained the title of *Accredited Polymer Scientist* (RPK) from the National Dutch Graduate School of Polymer Science and Technology (PTN). In the last year of his Ph.D. he spent 3 months as a visiting researcher at École Polytechnique Fédérale de Lausanne in Switzerland within the Laboratory for Processing of Advanced Composites (LPAC) chaired by professor Veronique Michaud. After his Ph.D. he continued his work within the Novel Aerospace Materials group as a post-doctoral researcher.

List of publications

Journal publications

W. Post, E. Jeoffroy, S. J. García, S. van der Zwaag

Self-healing glass fibre-reinforced polymer composites based on montmorillonite reinforced compartmented alginate fibres

Polymer Composites, under review

N. García-Huete , **W. Post**, J. M. Laza, J. L. Vilas, L. M. León, S. J. García

Effect of the blend ratio on the shape memory and self-healing behaviour of ionomer-polycyclooctene crosslinked polymer blends

European Polymer Journal, under review

W. Post, A. Cohades, V. Michaud, S. van der Zwaag, S. J. García

Healing of a glass fibre reinforced composite with a disulphide containing organic-inorganic epoxy matrix

Composites, Science and Technology, volume 152, November 2017, pages 85-93

W. Post, M. Kersemans, I. Solodov, K. Van Den Abeele, S. J. García, S. van der Zwaag

Non-destructive monitoring of delamination healing of a CFRP composite with a thermoplastic ionomer interlayer

Composites Part A: Applied Science and Manufacturing, volume 101, October 2017, pages 243-253

W. Post, R.K. Bose, S.J. García, S. van der Zwaag

Healing of early stage fatigue damage in ionomer/ Fe_3O_4 nanoparticle composites

Polymers, volume 8, 2016, page 436

A. Tabaković, **W. Post**, D. Cantero, O. Copuroglu, S. J. García and E. Schlangen

The reinforcement and healing of asphalt mastic mixtures by rejuvenator encapsulation in alginate compartmented fibres

Smart Materials and Structures, Volume 25, Issue 8, 15 July 2016, 084003

N. Zhong and **W. Post**

Self-repair of structural and functional composites with intrinsically self-healing polymer matrices: A review

Composites Part A: Applied Science and Manufacturing, Volume 69, 2015, pages 226–239

S. van der Zwaag, A.M. Grande, **W. Post**, S.J. García, T.C. Bor
Review of current strategies to induce self-healing behaviour in fibre reinforced polymer based composites
Material Science & Technology, volume 30, 2014, Pages. 1633–1641

Book chapter

S. Mookhoek, M. Prajer, **W. Post**, H. Fischer, S.J. García, S. van der Zwaag
Compartmented fibres: a local and multiple healing events approach for self-healing fibre reinforced composites
Self-Healing Materials: Pioneering research in the Netherlands pp. 61-68

Selected conference contributions

W. Post, A. Cohades, S.J. García, S. van der Zwaag, V. Michaud
Oral Presentation: *Low temperature healing of bending, Mode I and impact-induced damage of a disulphide containing polymer - glass fibre reinforced composite*
6th International conference on self-healing materials, Friedrichshafen, Germany, June 2017

W. Post, I. Solodov, S.J. García, S. van der Zwaag
Poster Presentation: *Self-healing of fracture damage in model thermoset composites containing alginate-based compartmented fibres*
16th European conference on composite materials, Munich, Germany, 28 June 2016

W. Post, S.J. García, S. van der Zwaag
Oral Presentation: *Healing of early stage fatigue damage in ionomer/Fe₃O₄ nanoparticle composites by inductive heating*
Dutch Polymer Days, 7 March 2016, Lunteren

W. Post, S.J. García, S. van der Zwaag
Oral Presentation: *Healing of fatigue damage of ionomer composite interlayers by localized heating upon magnetic induction*
20th International conference on composite materials, Copenhagen, Denmark, 23 July 2015

W. Post, S.J. García, S. van der Zwaag
Oral Presentation: *Healing of early stage damage in ionomer composite interlayers by localized heating upon magnetic induction*
5th International conference on self-healing materials, Durham, USA, 24 June 2015

W. Post, S.J. García, S. van der Zwaag
Oral Presentation: *Self-healing of fibre reinforced thermoset composites based on compartmented fibres containing liquid healing agents*
15th European conference on composite materials, Sevilla, Spain, 26 June 2014